Patterns and dynamics of sedimentation and biogeochemical processes in the Skagerrak

DISSERTATION

zur Erlangung des Doktorgrades

an der Mathematisch-Naturwissenschaftlichen Fakultät

der Christian-Albrechts-Universität zu Kiel

vorgelegt von

Timo Spiegel

Kiel, 2024

Erster Gutachter: Prof. Dr. Klaus Wallmann (GEOMAR)

Zweiter Gutachter:

Tag der mündlichen Prüfung:

Zum Druck freigegeben:

_____

Dekan

Eidesstattliche Erklärung

Hiermit erkläre ich, dass die beigefügte Arbeit, abgesehen von der Beratung durch meine Betreuer und die Zuhilfenahme der angegebenen Mittel, nach Inhalt und Form selbständig verfasst wurde. Ich versichere, dass ich die beigefügte Arbeit ausschließlich in diesem und keinem anderen Promotionsverfahren vorgelegt habe. Diesem Promotionsverfahren ist kein gescheitertes Promotionsverfahren vorausgegangen und mir ist noch kein akademischer Grad entzogen worden. Die Arbeit wurde weder veröffentlicht noch zur Veröffentlichung eingereicht. Die Arbeit ist im Rahmen der Regeln guter wissenschaftlicher Praxis der Deutschen Forschungsgemeinschaft entstanden.

Kiel, 27.03.2024

Timo Spiegel — Ort, Datum

Abstract

The North Sea represents a major sink for atmospheric carbon dioxide (CO_2) from anthropogenic emissions. However, the North Sea sediment and carbon cycles have been heavily affected by human activities during the last century. In particular, frequent resuspension of sedimentary particulate organic carbon (POC) by bottom trawling, dredging or wind farm constructions might reduce POC burial and, consequently, reduce the CO_2 sequestration potential of the North Sea.

The Skagerrak serves as the largest depocenter for sediments and POC in the North Sea. Hence, Skagerrak deposits provide a historical record of how the North Sea ecosystem has changed over time. This thesis revisits sedimentation and biogeochemical processes in the Skagerrak based on a combination of solid phase and porewater geochemistry, in-situ measurements and modeling. Highly resolved temporal and spatial data are used to better characterize the benthic sediment, POC and biogenic silica (bSi) cycles in the Skagerrak and to track the impact of human and natural processes in the North Sea over the past ~100 years. A major finding of this thesis reveals that average sedimentation rates and POC burial fluxes substantially decreased from before to after the year 1963 in the Skagerrak. Possible explanations involve a shift in the North Sea circulation pattern and increasing POC settling in other depocenters of the North Sea, such as the Wadden Sea. Hence, deposition rates in the Skagerrak are likely dominated by these processes rather than by the effect of sediment resuspension caused by human activities on deposition rates in the Skagerrak. In order to assess the spatial variability of sedimentation processes in the Skagerrak, a machine learning model is used to upscale compiled datasets to areawide spatial distributions of porosities, mass accumulation rates (MAR) and lead-210 (^{210}Pb) rain rates in the Skagerrak. The spatial distributions reveal areas of elevated ^{210}Pb rain rates and MAR at intermediate water depths following the shape of the general water circulation pattern. A tentative North Sea sediment budget including the updated MAR estimate highlights the Skagerrak as the primary sink for material in the North Sea. The benthic cycles of POC and bSi show that roughly 50 % of the POC and bSi raining onto the seafloor are recycled during early diagenesis and reintroduced to bottom waters. The other half is permanently buried in the sediment. In a global context, comparably high POC and bSi burial efficiencies as well as low sedimentary bSi:POC ratios reflect the influence of the large lateral sediment input from the North Sea. The ^{210}Pb and bSi rain rates are further used to estimate the contributions of locally produced and laterally transported POC to the total sedimentary POC pool. They are included in a compilation of different approaches, which show that 19±6 % of the deposited POC are derived from local primary production, whereas 81±6 % are transported laterally into the Skagerrak. The results of this thesis extend our knowledge of sedimentation and biogeochemical processes in the Skagerrak under changing environmental conditions. However, further work is recommended for a detailed understanding of how the Skagerrak and the North Sea have been affected by human activities. In

particular, large-scale and temporally resolved particle transport models and provenance studies could help to identify the major drivers behind the decline in sedimentation rates and POC burial in the Skagerrak.

Kurzfassung

Die Nordsee ist eine wichtige Senke für anthropogenes Kohlendioxid (CO_2) . Im letzten Jahrhundert wurden der Sediment- und Kohlenstoffkreislauf jedoch stark durch menschliche Eingriffe beeinflusst. Insbesondere durch Grundschleppnetzfischerei oder den Ausbau von Windparks wird der am Meeresboden abgelagerte partikulärer organischer Kohlenstoff (POC) aufgewirbelt und in die Wassersäule zurückgeführt. Durch solche und andere menschliche Prozesse verlieren die Nordseesedimente möglicherweise POC, wodurch das Potential für die Aufnahme von CO_2 durch die Nordsee gemindert wird.

Der Skagerrak ist der größte Ablagerungsraum für Sedimente und POC in der Nordsee. Die Ablagerungen im Skagerrak können daher Aufschluss darüber geben, wie sich das Ökosystem der Nordsee im Laufe der Zeit durch menschliche Einflüsse verändert hat. Diese Dissertation untersucht Sedimentations- und biogeochemische Prozesse mit Hilfe von Festphasen- und Porenwasserdaten, in-situ Messungen und durch Modellierung. Zeitlich und räumlich hochaufgelöste Daten werden dabei genutzt, um die benthischen Sediment-, POC- und biogenen Silikat (bSi) Kreisläufe besser zu verstehen und darüber die natürlichen und menschlichen Einflüsse auf die Nordsee über die letzten 100 Jahre zu bestimmen. Ein wichtiges Ergebnis dieser Arbeit ist, dass sich die durchschnittlichen Sedimentations- und POC Vergrabungsraten vor und nach dem Jahr 1963 stark verringert haben. Mögliche Gründe könnten eine Veränderung des dominanten Strömungsmusters der Nordsee oder erhöhte Vergrabungsraten in anderen Ablagerungsräumen in der Nordsee, wie zum Beispiel dem Wattenmeer, sein. Vermutlich haben diese Prozesse das Signal der menschengemachten Sedimentaufwirbelung auf die Ablagerungsraten im Skagerrak überprägt. Ein Machine Learning Modell wird genutzt, um die räumliche Verteilung der Porosität, und Massenakkumulationsraten (MAR) und Ablagerungsraten von Blei-210 (^{210}Pb) im gesamten Skagerrak darzustellen. Die räumliche Verteilung zeigt erhöhte MAR und ^{210}Pb Ablagerungsraten in mittleren Wassertiefen entlang des dominanten Strömungsmusters. Mit Hilfe der MAR wird ein vorläufiges Sedimentbudget für die gesamte Nordsee aufgestellt, welches den Skagerrak als größten Ablagerungsort für Sedimente im Nordseeraum bestätigt. Die Untersuchung der benthischen POC und bSi Kreisläufe zeigt, dass ca. 50% des abgelagerten POC und bSi im Meeresboden remineralisiert oder aufgelöst und zurück in die Wassersäule geführt werden. Die andere Hälfte wird permanent im Skagerrak vergraben. Vergleichsweise hohe Vergrabungseffizienzen von POC und bSi und geringe bSi:POC Verhältnisse in Sedimenten des Skagerraks im Vergleich zu globalen Daten können vermutlich auf den hohen lateralen Transport von Nordseesedimenten in den Skagerrak zurückgeführt werden. Die ^{210}Pb und bSi Ablagerungsraten werden zudem genutzt, um die Anteile von lokal produziertem und lateral herantransportierten POC an den Gesamtablagerungsraten von POC zu bestimmen. Zusammen mit anderen Ansätzen wird der Beitrag von lokal produzierten POC auf 19±6 %geschätzt,

während der lateral herantransportierte POC den größeren Anteil mit 81±6 % ausmacht. Die Ergebnisse dieser Arbeit tragen zu einem verbesserten Verständnis der Sedimentationsprozesse und benthischen Kreisläufe im Skagerrak bei. Es wird weitere Forschung an den menschlichen Einflüssen auf die Ökosysteme des Skagerraks und der Nordsee empfohlen. Insbesondere können großskalige und zeitlich aufgelöste Partikel-Transportmodelle und eine Provinienzanalyse dabei helfen die verschiedenen Prozesse aufzuschlüsseln, die zu der Verringerung von Sediment- und POC Ablagerungsraten im Skagerrak führen.

Table of contents

I. General introduction

I.1 Climate change and the marine carbon cycle

Anthropogenic carbon dioxide (CO_2) emissions cause global warming with various consequences for global ecosystems (IPCC, 2023). The ocean acts as a major CO_2 sink, absorbing around 25% of global anthropogenic CO_2 emissions (DeVries, 2022; Friedlingstein et al., 2023). The CO_2 is cycled through the ocean by physical transport and the biological, carbonate and solubility pumps (Longhurst and Glen Harrison, 1989; Longhurst, 1991; Duan and Sun, 2003; Millero, 2007; Emerson and Hedges, 2008; Volk and Hoffert, 2013; De La Rocha and Passow, 2014; Turner, 2015; Middelburg, 2019; DeVries, 2022). Phytoplankton take up CO_2 in surface waters to synthesize particulate organic carbon (POC), while calcifying organisms produce particulate inorganic carbon (PIC), such as carbonate minerals ($CaCO_3$). The POC and PIC sink through the water column where they are partly remineralised or dissolved and recycled back to surface waters. However, a fraction of the particulates reaches the seafloor and is embedded into marine sediments. Upon sedimentation, the POC and PIC are subject to early diagenesis and dissolution processes and a proportion of the carbon is released back into the water column as a benthic flux. The remaining carbon is permanently buried in marine sediments and is effectively removed from the marine carbon cycle on geological timescales (Berner, 1980, 1982; Holland, 1984). Hence, ocean sciences have become a focal point in current scientific research to mitigate the rise of atmospheric CO_2.

I.2 APOC project

The work for this thesis was carried out in the framework of the project APOC - "Anthropogenic impacts on particulate organic carbon cycling in the North Sea" funded by the Federal Ministry of Education and Research, Germany (BMBF).

I.2.1 Motivation behind APOC

The North Sea region represents a substantial carbon sink with estimated total CO_2 uptake rates of 1.38 mol C m^{-2} yr^{-1} (Thomas et al., 2005). Approximately 1.43 Tg of POC accumulate annually at the seafloor and 230 Tg POC are stored in the upper 10 cm of North Sea surface sediments (Diesing et al., 2021). This accounts for 0.9 - 2.4% of global shelf POC storage (LaRowe et al., 2020; Diesing et al., 2021). However, the North Sea POC system has been increasingly affected by human activities since industrial times (ICES, 2018, 2019, 2020; OSPAR, 2023). Human activities in the North Sea include bottom trawling (Eigaard et al., 2017; Rijnsdorp et al., 2020), offshore wind farm construction (Baeye and Fettweis, 2015; Slavik et al., 2019; Daewel et al., 2022; Heinatz and

Scheffold, 2023), dredging (De Groot, 1986; Mielck et al., 2019), coastal protection means (Kelletat, 1992; Hoeksema, 2007; Hofstede, 2008), eutrophication (Pätsch et al., 2010; Skogen et al., 2014; Axe et al., 2017) and river damming (IKSE, 2005, 2012; Lange et al., 2008; Hübner and Schwandt, 2018). These human pressures directly or indirectly affect the seafloor ecosystem and biogeochemistry. For instance, frequent resuspension of seafloor sediments and POC may result in less POC burial and consequently reduced CO_2 sequestration in the North Sea region (Bradshaw et al., 2021; Sala et al., 2021; Hiddink et al., 2023). Hence, the main goal of the APOC project was to quantify the contribution of POC burial to atmospheric CO_2 drawdown in the North Sea and how the ecosystem has been affected by anthropogenic interventions. The project further aimed to identify regions that are particularly vulnerable and could benefit from being converted into marine protected areas to maintain their stability against human pressures (Zarate-Barrera and Maldonado, 2015). Finally, the gained knowledge should be communicated with policymakers to support the development of appropriate strategies for the future economic utilization of the North Sea region.

I.2.2 Structure of APOC

Four research institutes and one non-governmental organization collaborated to achieve the project's goals. The research institutes included the Alfred Wegener Institute Helmholtz Centre for Polar and Marine Research (AWI), Helmholtz Centre Hereon (HZG), University of Hamburg (UHH) and the GEOMAR Helmholtz Centre for Ocean Research Kiel (GEOMAR). The main task of AWI, HZG and GEOMAR involved the biogeochemical characterization of POC deposition and benthic turnover by field data and modeling in the major sedimentary depocenters of the North Sea. The regional data was used by colleagues at HZG and UHH to validate large-scale models across the entire North Sea including deposition, burial and resuspension at the seafloor, transport pathways and atmospheric CO_2 uptake by the ocean. In addition, the research institutes worked closely together with colleagues from the German Federation for the Environment and Nature Conservation (BUND). The BUND functioned as the interface between scientists and the wider public and guaranteed the knowledge transfer of the APOC results to stakeholders and policymakers on national and EU levels.

I.3 GEOMAR team's contribution

The research institute GEOMAR hosted the PhD students Nina Lenz and Timo Spiegel, who collaboratively worked on GEOMAR's contribution to the APOC project. At GEOMAR, our team focused on the research area of the Skagerrak, which is located between Denmark, Norway and Sweden. The Skagerrak is notable for being the largest depocenter for sediments and POC from the North Sea. Mass accumulation rates (MAR) in the Skagerrak yield 28 - 46 Mt yr^{-1} (van Weering et

al., 1993; De Haas and van Weering, 1997; Spiegel et al., 2024), which represents ~45 - 80% of the annual suspended sediment input into the North Sea (Oost et al., 2021; Spiegel et al., 2024). Consequently, a substantial portion of the Skagerrak deposits (50 - 90%) is delivered by lateral transport from the North Sea into the Skagerrak (Liebezeit, 1988; Anton et al., 1993; Meyenburg and Liebezeit, 1993; De Haas and van Weering, 1997). Based on these premises, the GEOMAR's team fundamental idea developed:

If there has been any variability in the sediment and POC system of the North Sea over time, it should be evident in the sedimentary record of the Skagerrak.

Following this concept, we reconstructed the deposition history in the Skagerrak to estimate the impact of human activities on the North Sea ecosystem over the past ~100 years. To achieve that, GEOMAR's team investigated (1) the temporal variability of the lateral sediment and POC transport from the North Sea into the Skagerrak and (2) how sediment contributions from different source areas to the Skagerrak have developed over time.

I.4 Objectives of this thesis

Within the framework of the APOC project, the main objective of this thesis is to determine the temporal variability of the lateral POC transport into the Skagerrak. The lateral POC input can be estimated by the amount of POC settling onto the Skagerrak seafloor (POC rain rate). However, POC rain rates are not solely derived from lateral inputs, but are also sourced from local primary production in Skagerrak surface waters (Fig. I1). Hence, another objective of this study is to differentiate between these two carbon pools in Skagerrak deposits. Ultimately, the temporal evolution of POC rain rates and the quantification of local and lateral sources to the POC pool were studied to trace the impact of human activities on the POC cycle in the North Sea.

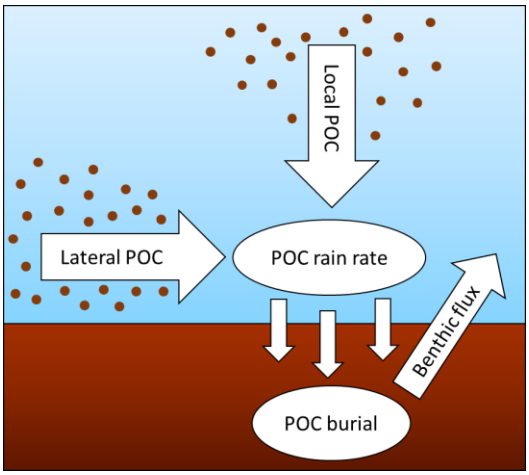

Figure I1. Schematic diagram of particulate organic carbon (POC) cycling in the water column (blue) and seafloor sediments (brown) in the Skagerrak. POC that rains onto the seafloor (POC rain rate) is derived from locally produced POC in the surface ocean (Local POC) and laterally transported POC from the North Sea (Lateral POC). In the sediment, POC is partly remineralized and recycled to bottom waters as a benthic flux. The remaining POC is permanently buried in Skagerrak sediments.

I.4.1 Temporal variability of POC rain rates

POC rain rates are determined by the sum of POC that is recycled within the sediment and released back to the bottom water as DIC (benthic DIC flux) and the POC that escapes remineralization and is permanently buried (POC burial flux) in Skagerrak sediments (Fig. I1). The POC burial flux can be calculated based on sedimentation rate reconstructions and measured POC contents. In order to reconstruct sedimentation rates, we set up an age-depth model using the radioisotope lead-210 (^{210}Pb) and the three time markers Caesium-137 (^{137}Cs), fraction modern carbon-14 (F^{14}C) and mercury (Hg). Due to its radioactive properties, ^{210}Pb continuously decays during burial in sediments. As the half-life of ^{210}Pb is well known (22.3 years), the depths in sediment cores can be attributed to certain ages. The time markers, on the other hand, allow for the resolution of an individual year or a short period in the sediment cores. Activity peaks of ^{137}Cs and F^{14}C are a result of atmospheric nuclear weapon tests in 1963 (van Weering et al., 1993; Deng et al., 2020). Additionally, a peak in Hg concentrations can be attributed to legal regulations on the economic usage of Hg between 1960 and 1970 (Leipe et al., 2013; Moros et al., 2017; Polovodova Asteman et al., 2018). The age-depth relationships derived from ^{210}Pb and the time markers are then combined to reconstruct sedimentation rates over time.

Benthic DIC fluxes at the sediment-water interface are determined by in-situ benthic chamber measurements. To obtain a comprehensive understanding of how POC rain rates have changed over time, it would be necessary to also temporally resolve benthic DIC fluxes. However, the benthic chamber measurements carried out in this study only provided a 28 - 35 hour snapshot of the benthic efflux from seafloor sediments. Considering that the required data gathering for a temporal analysis would involve extensive field studies that are both time- and resource-consuming, this study assumes benthic DIC fluxes to be steady-state.

I.4.2 Local and lateral contributions to POC rain rates

POC rain rates in the Skagerrak are a mixture of locally produced POC from primary production in surface waters and laterally transported material from the North Sea. Hence, an integral part of this work is to differentiate between these two POC pools. Previous studies estimated the lateral POC input to account for 50 - 90% of sedimentary POC (Liebezeit, 1988; Anton et al., 1993; Meyenburg and Liebezeit, 1993; De Haas and van Weering, 1997) based on carbohydrate data and comparisons between primary production rates and total POC deposition in the Skagerrak. This thesis revisits the characterization of the POC pools by investigating biogenic silica (bSi) and ^{210}Pb rain rates. Local primary production is seasonally dominated by siliceous organisms such as diatoms (Gran-Stadniczeñko et al., 2019). Hence, one approach involved using bSi rain rates in the Skagerrak as an

indicator for locally produced POC raining onto the seafloor. Secondly, the local atmospheric ^{210}Pb flux and total ^{210}Pb rain rates are compared to determine the local and lateral contributions to the bulk particle settling in the Skagerrak.

I.4.3 Extending the scientific knowledge and database

In addition to addressing the specific goals of APOC, this thesis aims to extend the current knowledge basis on marine benthic sediment, POC and bSi cycling as well as the coupling of POC and bSi in the ocean. Studying the cycling and budgets of these constituents is essential for understanding the oceanic drawdown of atmospheric CO2, the distribution, transport and participation of these constituents in biogeochemical reactions and how they interact with the food web and the cycling of other compounds in the marine environment. In turn, detailed regional investigations are a prerequisite to improve global marine sediment, POC and bSi cycling and budget estimates. Particularly in the Skagerrak, the interplay between dynamic natural and human processes results in significant temporal variability and spatial heterogeneity. Hence, the Skagerrak offers an ideal setting to investigate sedimentation and biogeochemical patterns over time and space. This thesis revisits, updates and extends the Skagerrak database to improve its spatial and temporal resolution. High-resolution age-depth modeling is used to determine average sedimentation rates and POC burial fluxes before and after 1963. Contemporarily, this represents the first attempt to describe the changes in benthic cycling in the Skagerrak over the past century. Compiled data of individual stations are spatially upscaled using a machine learning approach to present areawide and highly resolved spatial distributions of porosities, MAR and 210Pb rain rates across the Skagerrak. Furthermore, there is currently no comprehensive study on bSi cycling in the Skagerrak. To fill this knowledge gap, we describe benthic bSi recycling and burial and discuss the Skagerrak results in comparison to other environmental settings.

I.5 Additional work at GEOMAR

The temporal variability of lateral POC transport into the Skagerrak reflects the net trend of the entire North Sea system. Since the North Sea is affected by a combination of human and natural processes with variable temporal and spatial distributions, no comprehensive reasoning behind potential North Sea shifts can be derived solely based on the deposition history in the Skagerrak. Hence, the reconstructions of sediment and POC depositions are combined with a provenance analysis carried out by Nina Lenz at GEOMAR. The provenance study aims to determine the proportional contributions of different source areas to the Skagerrak deposits. Based on the clay mineral composition and the radiogenic isotopes strontium (Sr), neodymium (Nd) and hafnium (Hf) in

surface sediment across the North Sea, characteristic end-member areas are identified. Subsequently, the downcore variabilities of clay mineral and radiogenic isotope distribution are determined in sediment cores from the Skagerrak. Finally, the contributions of the different end-members to Skagerrak sediments are quantified over time based on mixing equations. The sediment provenance results are used to identify potential reasons behind the temporal variability in the lateral POC input into the Skagerrak.

I.6 Study area and research cruise AL561

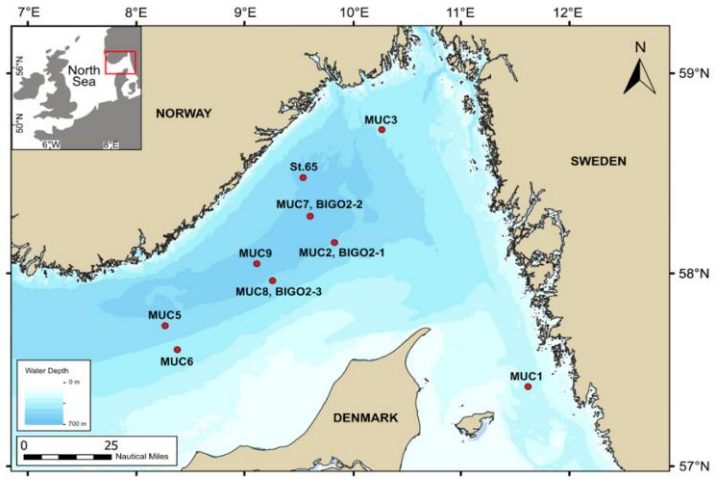

Figure I2. Study area and locations of multiple corer (MUC) and Biogeochemical Observatory (BIGO) stations.

The Skagerrak is a continental margin sea located in the northeastern part of the North Sea between Denmark, Norway and Sweden (Fig. I2). It connects waters transported from the North Sea and the Baltic Sea. With maximum water depths of ~700 meters in the central basin, the Skagerrak represents the deepest part of the wider North Sea region. In this area, current velocities decrease, which supports the sinking of particles transported from the North Sea. The resulting MAR of 28 - 46 Mt yr^{-1} (van Weering et al., 1993; De Haas and van Weering, 1997; Spiegel et al., 2024) make the Skagerrak the largest depocenter for sediment from the North Sea.

To accomplish the aims of this thesis and the APOC project, a research cruise AL561 with the RV Alkor was carried out from Aug. 2nd to Aug. 13th 2021 (Schmidt, 2021). Sediment, porewater and bottom water samples were taken by recovery of short (<50cm) multiple corers (MUC). Considering previous sedimentation rate estimates of up to 1.0 cm yr^{-1} (Ståhl et al., 2004), additional sediment samples were obtained from greater sediment depths using gravity corers (GC) up to 5 meters in length to ensure complete data coverage over the last century. To describe solute fluxes across the sediment-water interface, Biogeochemical Observatories (BIGO) were deployed at three stations.

Benthic chambers were placed onto the seafloor and partly driven into the upper sediment. Benthic fluxes were then determined from the variability of solute concentrations in the bottom water enclosed by the chambers. Frequent bottom trawling, waves, currents and storms can disturb the seafloor at water depths shallower than 200 meters (Sköld et al., 2018). Hence, the majority of the sampling focused on the undisturbed Skagerrak basin below 400 meters water depth. Three MUCs and two GCs were taken at shallower water depths as reference stations to characterize deposition under disturbed conditions. The data gathered from cruise AL561 were complemented by sediment and porewater samples from cruise AL557 (Thomas et al., 2022).

I.7 Manuscript outline

The following chapters II - V contain published, submitted and prepared manuscripts in scientific journals resulting from this thesis. They revisit various topics that have been introduced in chapter I.

Chapter II investigates the temporal variability of sedimentation rates in the Skagerrak. Average sedimentation rates before and after 1963 show a consistent and substantial decrease across the stations, indicating that the North Sea sediment system has changed over time. Based on their respective contributions to the total North Sea sediment budget, the study qualitatively discusses responsible processes behind the decline in sedimentation rates in the Skagerrak. The observed trend might be explained by a shift in the North Sea circulation pattern and increasing sediment deposition in other North Sea regions, such as the Wadden Sea.

Chapter II has been submitted to the Journal Frontiers in Marine Sciences and is currently in the review process as:

Spiegel, T., Dale, A.W., Lenz, N., Schmidt, M., Moros, M., Lindhorst, S., Wolschke, H., Müller, D., Butzin, M., Fuhr, M., Kalapurakkal, H.T., Kasten, S., Wallmann, K., 2024. A look into the temporal variability of sedimentation rates in the Skagerrak to track human and natural impacts in the North Sea - In review.

Author contributions:

TS, AWD, and KW designed the study. TS wrote the original draft and all co-authors reviewed and edited the manuscript. NL and MS helped with the sampling during the research cruise. MM and HW provided data from ^{210}Pb and ^{137}Cs measurements. MM additionally measured Hg concentrations. SL provided grain size data and helped with their interpretation. DM and SK provided F^{14}C data and helped with their interpretation. MB provided F^{14}C model data and helped with their interpretation. HTK helped with ^{210}Pb measurements at GEOMAR. KW acquired the funding.

Chapter III presents spatial distributions of porosities, ^{210}Pb rain rates and MAR across the entire Skagerrak region. Spatial upscaling of individual data points is done using machine learning. In short, machine learning uses spatial data of parameters that are available in high resolution (e.g. water depth or current velocities) to spatially upscale the desired variables at the same resolution. The spatial distributions are used to revisit previous estimates on areawide MAR in the Skagerrak. Total ^{210}Pb rain rates are compared to atmospheric ^{210}Pb fluxes to estimate proportions of local and lateral ^{210}Pb and sediment inputs. Furthermore, the study presents a tentative North Sea sediment budget including the updated MAR, which verifies the Skagerrak to be the largest depocenter for sediments in the North Sea.

Chapter III has been published as:

Spiegel, T., Diesing, M., Dale, A.W., Lenz, N., Schmidt, M., Sommer, S., Böttner, C., Fuhr, M., Kalapurakkal, H.T., Wallmann, K., 2024. Modelling mass accumulation rates and 210Pb rain rates in the Skagerrak: lateral sediment transport dominates the sediment input. Front. Mar. Sci. 11. https://doi.org/10.3389/fmars.2023.1141448.

Author contributions: TS: Writing – original draft. MD: Data curation, Methodology, Writing – review & editing. AD: Supervision, Writing – review & editing. NL: Writing – review & editing. MS: Writing – review & editing. SS: Writing – review & editing. CB: Writing – review & editing. MF: Writing – review & editing. HK: Writing – review & editing, Software, Visualization. CS: Writing – review & editing. KW: Funding acquisition, Project administration, Supervision, Writing – review & editing.

Chapter IV describes the benthic bSi cycle in the Skagerrak. About 50% of the bSi raining onto the seafloor dissolves in the sediment and is reintroduced into the water column. The remaining bSi is permanently buried in the sediment. In a global context, bSi cycling in the Skagerrak extends the dataset towards shelf areas with high bSi burial efficiencies. The high burial efficiencies are likely the result of the large lateral input of sediments bearing recalcitrant bSi from the North Sea. Low bSi:POC ratios in Skagerrak sediments compared to other shelf environments are hypothesized to be a result of the long transit times for the sediments, where bSi dissolution might outcompete POC degradation.

Chapter IV has been published as:

Spiegel, T., Dale, A.W., Lenz, N., Schmidt, M., Sommer, S., Kalapurakkal, H.T., Przibilla, A., Lindhorst, S., Wallmann, K., 2023. Biogenic silica cycling in the Skagerrak. Front. Mar. Sci. 10, 1141448. https://doi.org/10.3389/fmars.2023.1141448.

Author contributions: TS processed most of the samples in the laboratory and wrote the manuscript. TS, KW and AD developed the numerical model used in the study and contributed with discussions.

NL helped with cruise planning, sample preparation in the laboratory and contributed with discussions. MS coordinated the research cruise Al561 and contributed with discussions. SS coordinated the biogeochemical observatory (BIGO) deployments and helped with evaluating the BIGO data. HTK helped with the ^{210}Pb analyses and contributed with discussions. AP provided the porewater data for station 65. SL provided the grain-size data and helped with the interpretation. All authors contributed to the paper by drafting, reading, finalizing, and approving the text. All authors contributed to the article and approved the submitted version.

Chapter V combines the individual results of chapters II - IV to describe the temporal and spatial patterns of benthic POC cycling in the Skagerrak. The temporal variability of POC burial fluxes is quantified based on the sedimentation rate reconstruction presented in Chapter II. Average POC burial fluxes decreased significantly from before to after 1963. Additionally, the thesis compiles different approaches to quantify local and lateral POC sources to Skagerrak sediments. They include the ^{210}Pb rain rate and bSi rain rate data presented in chapters III and IV. The compilation shows that 50 - 90 % of the POC originates from lateral transport.

Chapter V represents a preliminary draft as further data is currently collected to constrain the presented results. In particular, chlorophyll-a and lipid measurements of suspended and sedimentary material as well as POC transport modeling in the water column will be considered to improve our understanding of the quality and different sources of the POC deposited in the Skagerrak.

In addition to the above manuscripts, I contributed to the following articles as a Co-Author during the three-year PhD period:

Fuhr, M., Wallmann, K., Dale, A.W., Kalapurakkal, H.T., Schmidt, M., Sommer, S., Deusner, C., **Spiegel, T.**, Kowalski, J., Geilert, S., 2024. Alkaline mineral addition to anoxic to hypoxic Baltic Sea sediments as a potentially efficient CO2-removal technique. Front. Clim. 6, 1338556. https://doi.org/10.3389/fclim.2024.1338556.

Von Jackowski, A., Walter, M., **Spiegel, T.**, Buttigieg, P.L., Molari, M., 2023. Drivers of pelagic and benthic microbial communities on Central Arctic seamounts. Front. Mar. Sci. 10, 1216442. https://doi.org/10.3389/fmars.2023.1216442.

Zhang, W., Porz, L., Yilmaz, R., Wallmann, K., **Spiegel, T.**, Neumann, A., Holtappels, M., Kasten, S., Kuhlmann, J., Ziebarth, N., Taylor, B., Ha Ho-Hagemann1, Daewel, U., Schrum, C., 2023. Intense and persistent bottom trawling impairs long-term carbon storage in shelf sea sediments (preprint). Under review at Nature Communications Earth & Environment. https://doi.org/10.21203/rs.3.rs-3313118/v.

Vosteen, P., **Spiegel, T.**, Gledhill, M., Frank, M., Zabel, M., Scholz, F., 2022. The Fate of Sedimentary Reactive Iron at the Land-Ocean Interface: A Case Study from the Amazon Shelf. Geochem. Geophys. Geosystems 23, e2022GC010543. https://doi.org/10.1029/2022GC010543.

Literature

Anton, K.K., Liebezeit, G., Rudolph, C., Wirth, H., 1993. Origin, distribution and accumulation of organic carbon in the Skagerrak. Mar. Geol. 111, 287–297. https://doi.org/10.1016/0025-3227(93)90136-J

Axe, P., Clausen, U., Leujak, W., Malcolm, S., Ruiter, H., Prins, T., Harvey, E.T., 2017. Eutrophication Status of the OSPAR Maritime Area. Third Integrated Report on the Eutrophication Status of the OSPAR Maritime Area.

Baeye, M., Fettweis, M., 2015. In situ observations of suspended particulate matter plumes at an offshore wind farm, southern North Sea. Geo-Mar. Lett. 35, 247–255. https://doi.org/10.1007/s00367-015-0404-8

Berner, R.A., 1982. Burial of organic carbon and pyrite sulfur in the modern ocean; its geochemical and environmental significance. Am. J. Sci. 282, 451–473. https://doi.org/10.2475/ajs.282.4.451

Berner, R.A., 1980. Early diagenesis: a theoret. approach, Princeton series in geochemistry. Princeton University Press, Princeton, N.J.

Bradshaw, C., Jakobsson, M., Brüchert, V., Bonaglia, S., Mörth, C.-M., Muchowski, J., Stranne, C., Sköld, M., 2021. Physical Disturbance by Bottom Trawling Suspends Particulate Matter and Alters Biogeochemical Processes on and Near the Seafloor. Front. Mar. Sci. 8, 683331. https://doi.org/10.3389/fmars.2021.683331

Daewel, U., Akhtar, N., Christiansen, N., Schrum, C., 2022. Offshore wind farms are projected to impact primary production and bottom water deoxygenation in the North Sea. Commun. Earth Environ. 3, 292. https://doi.org/10.1038/s43247-022-00625-0

De Groot, S.J., 1986. Marine sand and gravel extraction in the North Atlantic and its potential environmental impact, with emphasis on the North Sea. Ocean Manag. 10, 21–36. https://doi.org/10.1016/0302-184X(86)90004-1

De Haas, H., van Weering, T.C.E., 1997. Recent sediment accumulation, organic carbon burial and transport in the northeastern North Sea. Mar. Geol. 136, 173–187. https://doi.org/10.1016/S0025-3227(96)00072-2

De La Rocha, C.L., Passow, U., 2014. The Biological Pump, in: Treatise on Geochemistry. Elsevier, pp. 93–122. https://doi.org/10.1016/B978-0-08-095975-7.00604-5

Deng, L., Bölsterli, D., Kristensen, E., Meile, C., Su, C.-C., Bernasconi, S.M., Seidenkrantz, M.-S., Glombitza, C., Lagostina, L., Han, X., Jørgensen, B.B., Røy, H., Lever, M.A., 2020. Macrofaunal control of microbial community structure in continental margin sediments. Proc. Natl. Acad. Sci. 117, 15911–15922. https://doi.org/10.1073/pnas.1917494117

DeVries, T., 2022. The Ocean Carbon Cycle. Annu. Rev. Environ. Resour. 47, 317–341. https://doi.org/10.1146/annurev-environ-120920-111307

Diesing, M., Thorsnes, T., Bjarnadóttir, L.R., 2021. Organic carbon densities and accumulation rates in surface sediments of the North Sea and Skagerrak. Biogeosciences 18, 2139–2160. https://doi.org/10.5194/bg-18-2139-2021

Duan, Z., Sun, R., 2003. An improved model calculating CO2 solubility in pure water and aqueous NaCl solutions from 273 to 533 K and from 0 to 2000 bar. Chem. Geol. 193, 257–271. https://doi.org/10.1016/S0009-2541(02)00263-2

Eigaard, O.R., Bastardie, F., Hintzen, N.T., Buhl-Mortensen, L., Buhl-Mortensen, P., Catarino, R., Dinesen, G.E., Egekvist, J., Fock, H.O., Geitner, K., Gerritsen, H.D., González, M.M., Jonsson, P., Kavadas, S., Laffargue, P., Lundy, M., Gonzalez-Mirelis, G., Nielsen, J.R., Papadopoulou, N., Posen, P.E., Pulcinella, J., Russo, T., Sala, A., Silva, C., Smith, C.J., Vanelslander, B., Rijnsdorp, A.D., 2017. The footprint of bottom trawling in European waters: distribution, intensity, and seabed integrity. ICES J. Mar. Sci. 74, 847–865. https://doi.org/10.1093/icesjms/fsw194

Emerson, S., Hedges, J., 2008. Chemical Oceanography and the Marine Carbon Cycle, 1st ed. Cambridge University Press. https://doi.org/10.1017/CBO9780511793202

Friedlingstein et al., 2023. Global Carbon Budget 2023. Earth Syst. Sci. Data 15, 5301–5369. https://doi.org/10.5194/essd-15-5301-2023

Gran-Stadniczeñko, S., Egge, E., Hostyeva, V., Logares, R., Eikrem, W., Edvardsen, B., 2019. Protist Diversity and Seasonal Dynamics in Skagerrak Plankton Communities as Revealed by Metabarcoding and Microscopy. J. Eukaryot. Microbiol. 66, 494–513. https://doi.org/10.1111/jeu.12700

Heinatz, K., Scheffold, M.I.E., 2023. A first estimate of the effect of offshore wind farms on sedimentary organic carbon stocks in the Southern North Sea. Front. Mar. Sci. 9, 1068967. https://doi.org/10.3389/fmars.2022.1068967

Hiddink, J.G., Van De Velde, S.J., McConnaughey, R.A., De Borger, E., Tiano, J., Kaiser, M.J., Sweetman, A.K., Sciberras, M., 2023. Quantifying the carbon benefits of ending bottom trawling. Nature 617, E1–E2. https://doi.org/10.1038/s41586-023-06014-7

Hoeksema, R.J., 2007. Three stages in the history of land reclamation in the Netherlands. Irrig. Drain. 56, S113–S126. https://doi.org/10.1002/ird.340

Hofstede, J., 2008. Coastal Flood Defence and Coastal Protection along the North Sea Coast of Schleswig-Holstein. Küste 134–142.

Holland, H.D., 1984. The chemical evolution of the atmosphere and oceans, Princeton series in geochemistry. Princeton University Press, Princeton, N.J.

Hübner, G., Schwandt, D., 2018. EXTREME LOW FLOW AND WATER QUALITY – A LONG-TERM VIEW ON THE RIVER ELBE. Erdkunde 72, 235–252.

ICES, 2020. Greater North Sea ecoregion ? Fisheries overview, including mixed-fisheries considerations. https://doi.org/10.17895/ICES.ADVICE.7605

ICES, 2019. Working Group on the Effects of Extraction of Marine Sediments on the Marine Ecosystem (WGEXT). https://doi.org/10.17895/ICES.PUB.5733

ICES, 2018. Greater North Sea Ecoregion ? Ecosystem overview. https://doi.org/10.17895/ICES.PUB.4670

IKSE, 2012. Abschlussbericht über die Erfüllung des „Aktionsplans Hochwasserschutz Elbe“ im Zeitraum 2003–2011.

IKSE, 2005. Die Elbe und ihr Einzugsgebiet – Ein geographisch-hydrologischer und wasserwirtschaftlicher Überblick.

IPCC, 2023. Sections. In: Climate Change 2023: Synthesis Report. Contribution of Working Groups I, II and III to the Sixth Assessment Report of the Intergovernmental Panel on Climate Change [Core Writing Team, H. Lee and J. Romero (eds.)]. IPCC, Geneva, Switzerland, pp. 35-115, doi: 10.59327/IPCC/AR6-9789291691647.

Kelletat, D., 1992. Coastal Erosion and Protection Measures at the German North Sea Coast. J. Coast. Res. 8, 699–711.

Lange, D., Müller, H., Piechotta, F., Schubert, R., 2008. The Weser Estuary. Küste 275–287.

LaRowe, D.E., Arndt, S., Bradley, J.A., Burwicz, E., Dale, A.W., Amend, J.P., 2020. Organic carbon and microbial activity in marine sediments on a global scale throughout the Quaternary. Geochim. Cosmochim. Acta 286, 227–247. https://doi.org/10.1016/j.gca.2020.07.017

Leipe, T., Moros, M., Kotilainen, A., Vallius, H., Kabel, K., Endler, M., Kowalski, N., 2013. Mercury in Baltic Sea sediments—Natural background and anthropogenic impact. Geochemistry 73, 249–259. https://doi.org/10.1016/j.chemer.2013.06.005

Liebezeit, G., 1988. Early diagenesis of carbohydrates in the marine environment—II. Composition and origin of carbohydrates in Skagerrak sediments, in: Organic Geochemistry In Petroleum Exploration. Elsevier, pp. 387–391. https://doi.org/10.1016/B978-0-08-037236-5.50046-4

Longhurst, A.R., 1991. Role of the marine biosphere in the global carbon cycle. Limnol. Oceanogr. 36, 1507–1526. https://doi.org/10.4319/lo.1991.36.8.1507

Longhurst, A.R., Glen Harrison, W., 1989. The biological pump: Profiles of plankton production and consumption in the upper ocean. Prog. Oceanogr. 22, 47–123. https://doi.org/10.1016/0079-6611(89)90010-4

Meyenburg, G., Liebezeit, G., 1993. Mineralogy and geochemistry of a core from the Skagerrak/Kattegat boundary. Mar. Geol. 111, 337–344. https://doi.org/10.1016/0025-3227(93)90139-M

Middelburg, J.J., 2019. Marine Carbon Biogeochemistry: A Primer for Earth System Scientists, SpringerBriefs in Earth System Sciences. Springer International Publishing, Cham. https://doi.org/10.1007/978-3-030-10822-9

Mielck, F., Hass, H.C., Michaelis, R., Sander, L., Papenmeier, S., Wiltshire, K.H., 2019. Morphological changes due to marine aggregate extraction for beach nourishment in the German Bight (SE North Sea). Geo-Mar. Lett. 39, 47–58. https://doi.org/10.1007/s00367-018-0556-4

Millero, F.J., 2007. The Marine Inorganic Carbon Cycle. Chem. Rev. 107, 308–341. https://doi.org/10.1021/cr0503557

Moros, M., Andersen, T.J., Schulz-Bull, D., Häusler, K., Bunke, D., Snowball, I., Kotilainen, A., Zillén, L., Jensen, J.B., Kabel, K., Hand, I., Leipe, T., Lougheed, B.C., Wagner, B., Arz, H.W., 2017. Towards an event stratigraphy for Baltic Sea sediments deposited since AD 1900: approaches and challenges. Boreas 46, 129–142. https://doi.org/10.1111/bor.12193

Oost, A., Colina Alonso, A., Esselink, P., Wang, Z.B., Kessel, T. van, Maren, B. van, 2021. Where mud matters: towards a mud balance for the trilateral Wadden Sea Area: mud supply, transport and deposition. Wadden Academy, Leeuwarden.

OSPAR, 2023. OSPAR Quality Status Synthesis Report 2023. oap.ospar.org.

Pätsch, J., Lorkowski, I., Kühn, W., Moll, A., Serna, A., 2010. 150 years of ecosystem evolution in the North Sea-from pristine conditions to acidification. Eur. Geophys. Union Gen. Assem. 2010 Vienna Austria 2010 12291.

Polovodova Asteman, I., Risebrobakken, B., Moros, M., Binczewska, A., Dobosz, S., Jansen, E., Sławińska, J., Bąk, M., 2018. Late Holocene palaeoproductivity changes: a multi-proxy study in the Norwegian Trench and the Skagerrak, North Sea. Boreas 47, 238–255. https://doi.org/10.1111/bor.12264

Rijnsdorp, A.D., Boute, P., Tiano, J., Lankheet, M., Soetaert, K., Beier, U., de Borger, E., Hintzen, N.T., Molenaar, P., Polet, H., Poos, J.J., Schram, E., Soetaert, M., van Overzee, H., van De Wolfshaar, K., van Kooten, T., 2020. The implications of a transition from tickler chain beam trawl to electric pulse trawl on the sustainability and ecosystem effects of the fishery for North Sea sole: an impact assessment. Wageningen Marine Research, IJmuiden,. https://doi.org/10.18174/519729

Sala, E., Mayorga, J., Bradley, D., Cabral, R.B., Atwood, T.B., Auber, A., Cheung, W., Costello, C., Ferretti, F., Friedlander, A.M., Gaines, S.D., Garilao, C., Goodell, W., Halpern, B.S., Hinson, A., Kaschner, K., Kesner-Reyes, K., Leprieur, F., McGowan, J., Morgan, L.E., Mouillot, D., Palacios-Abrantes, J., Possingham, H.P., Rechberger, K.D., Worm, B., Lubchenco, J., 2021. Protecting the global ocean for biodiversity, food and climate. Nature 592, 397–402. https://doi.org/10.1038/s41586-021-03371-z

Schmidt, M., 2021. Dynamics and variability of POC burial in depocenters of the North Sea (Skagerrak), Cruise No. AL561, 2.08.2021 – 13.08.2021, Kiel – Kiel, APOC. GEOMAR Helmholtz Centre for Ocean Research Kiel. https://doi.org/10.3289/CR_AL561

Skogen, M.D., Eilola, K., Hansen, J.L.S., Meier, H.E.M., Molchanov, M.S., Ryabchenko, V.A., 2014. Eutrophication status of the North Sea, Skagerrak, Kattegat and the Baltic Sea in present and future climates: A model study. J. Mar. Syst. 132, 174–184. https://doi.org/10.1016/j.jmarsys.2014.02.004

Sköld, M., Göransson, P., Jonsson, P., Bastardie, F., Blomqvist, M., Agrenius, S., Hiddink, J., Nilsson, H., Bartolino, V., 2018. Effects of chronic bottom trawling on soft-seafloor macrofauna in the Kattegat. Mar. Ecol. Prog. Ser. 586, 41–55. https://doi.org/10.3354/meps12434

Slavik, K., Lemmen, C., Zhang, W., Kerimoglu, O., Klingbeil, K., Wirtz, K.W., 2019. The large-scale impact of offshore wind farm structures on pelagic primary productivity in the southern North Sea. Hydrobiologia 845, 35–53. https://doi.org/10.1007/s10750-018-3653-5

Spiegel, T., Diesing, M., Dale, A.W., Lenz, N., Schmidt, M., Sommer, S., Böttner, C., Fuhr, M., Kalapurakkal, H.T., Wallmann, K., 2024. Modelling mass accumulation rates and 210 Pb rain rates

in the Skagerrak: lateral sediment transport dominates the sediment input. Front. Mar. Sci. 11. https://doi.org/10.3389/fmars.2023.1141448

Ståhl, H., Tengberg, A., Brunnegård, J., Bjørnbom, E., Forbes, T.L., Josefson, A.B., Kaberi, H.G., Hassellöv, I.M.K., Olsgard, F., Roos, P., Hall, P.O.J., 2004. Factors influencing organic carbon recycling and burial in Skagerrak sediments. J. Mar. Res. 62, 867–907. https://doi.org/10.1357/0022240042880873

Thomas, H., Bozec, Y., De Baar, H.J.W., Elkalay, K., Frankignoulle, M., Schiettecatte, L.-S., Kattner, G., Borges, A.V., 2005. The carbon budget of the North Sea. Biogeosciences 2, 87–96. https://doi.org/10.5194/bg-2-87-2005

Thomas, H., Freund, W., Mears, C., Meckel, E., Minutolo, F., Nantke, C., Neumann, A., Seidel, M., Van Dam, B., 2022. ALKOR Scientific Cruise Report. The Ocean's Alkalinity - Connecting geological and metabolic processes and time-scales: mechanisms and magnitude of metabolic alkalinity generation in the North Sea Cruise No. AL557. Open Access. Alkor-Berichte, AL557. GEOMAR Helmholtz-Zentrum für Ozeanforschung Kiel, Kiel, Germany, 22 pp.

Turner, J.T., 2015. Zooplankton fecal pellets, marine snow, phytodetritus and the ocean's biological pump. Prog. Oceanogr. 130, 205–248. https://doi.org/10.1016/j.pocean.2014.08.005

van Weering, T.C.E., Berger, G.W., Okkels, E., 1993. Sediment transport, resuspension and accumulation rates in the northeastern Skagerrak. Mar. Geol. 111, 269–285. https://doi.org/10.1016/0025-3227(93)90135-I

Volk, T., Hoffert, M.I., 2013. Ocean Carbon Pumps: Analysis of Relative Strengths and Efficiencies in Ocean-Driven Atmospheric CO_2 Changes, in: Sundquist, E.T., Broecker, W.S. (Eds.), Geophysical Monograph Series. American Geophysical Union, Washington, D. C., pp. 99–110. https://doi.org/10.1029/GM032p0099

Zarate-Barrera, T.G., Maldonado, J.H., 2015. Valuing Blue Carbon: Carbon Sequestration Benefits Provided by the Marine Protected Areas in Colombia. PLOS ONE 10, e0126627. https://doi.org/10.1371/journal.pone.0126627

A look into the temporal variability of sedimentation rates in the Skagerrak to track human and natural impacts in the North Sea

Timo Spiegel[1*], Andrew W. Dale[1], Nina Lenz[1], Mark Schmidt[1], Matthias Moros[2], Sebastian Lindhorst[3], Hendrik Wolschke[4], Daniel Müller[5,6], Martin Butzin[7], Michael Fuhr[1], Habeeb Thanveer Kalapurakkal[1], Sabine Kasten[5,6,7], Klaus Wallmann[1]

[1] GEOMAR Helmholtz Centre for Ocean Research Kiel, Wischhofstraße 1–3, 24148 Kiel, Germany

[2] Leibniz Institute for Baltic Sea Research Warnemünde, Seestraße 15, DE-18119 Rostock, Germany

[3] Universität Hamburg, Bundesstraße 55, 20146 Hamburg, Germany

[4] Helmholtz-Zentrum Hereon, Institute of Coastal Environmental Chemistry, Max-Planck Str. 1, 21502, Geesthacht, Germany

[5] Alfred Wegener Institute Helmholtz Centre for Polar and Marine Research, Am Handelshafen 12, 27570 Bremerhaven, Germany

[6] University of Bremen, Faculty of Geosciences, Klagenfurter Straße 4, 28359 Bremen, Germany

[7] MARUM - Center for Marine Environmental Sciences University of Bremen, Leobener Straße 8 28359 Bremen, Germany

***Correspondence:**
Timo Spiegel
tspiegel@geomar.de

Keywords: Sedimentation rate, Temporal variability, Age-depth model, Skagerrak, North Sea, ^{210}Pb, ^{137}Cs, ^{14}C.

Abstract

Since industrial times, the North Sea sediment system has been subject to a dynamic hydrographic regime and intense human alteration. The Skagerrak serves as the largest depocenter for suspended sediment originating from the North Sea. Thus, deposits in the Skagerrak provide a historical record of potential shifts in the sediment cycle of the North Sea. Despite the availability of sedimentation rate data in the Skagerrak, previous studies focused on steady-state reconstructions and little is known about how these rates may have changed over time. To address this knowledge gap, we present high-resolution age-depth models based on the natural radionuclide ^{210}Pb in combination with the anthropogenic time markers ^{137}Cs, fraction modern ^{14}C ($F^{14}C$) and mercury (Hg) to determine average sedimentation rates before and after the year 1963 at six stations in the Skagerrak. We applied 1963 as the boundary since this year is constrained by ^{137}Cs and $F^{14}C$ due to atomic weapons testing and by changes in sedimentary Hg contents. Our primary result reveals a consistent decrease in sedimentation rates at all stations. On average, sedimentation rates decreased from 0.36 to 0.15 cm yr^{-1}, indicating that the sediment system of the North Sea substantially changed. Possible reasons

for the decreasing sedimentation rates in the Skagerrak include a shift in the North Sea circulation pattern, enhanced sediment trapping in the Wadden Sea and reduced sediment inputs due to river damming and coastal protection. These processes have likely outweighed the impacts of temperature, humidity, sea level rise and sediment resuspension triggered by human activities and storm events. However, we stress that our data do not allow for a quantitative analysis demonstrating the need for a more comprehensive understanding of the major driving factors behind the temporal variability of sediment cycling in the North Sea. We recommend integrating the Skagerrak data into larger-scale physical models that consider non-steady state particle transport in the North Sea. Furthermore, our insight could be improved by combining the sedimentation rate data with information on the provenance of the Skagerrak deposits to better determine the temporal evolution of sediment transport pathways in the North Sea.

II.1 Introduction

Multiple human activities that impact the sedimentary system of the North Sea include bottom trawling (Eigaard et al., 2017; ICES, 2020; Rijnsdorp et al., 2020), dredging and sediment extraction (De Groot, 1986; ICES, 2019; Mielck et al., 2019), the construction of offshore wind farms (Baeye and Fettweis, 2015; Slavik et al., 2019; Daewel et al., 2022; Heinatz and Scheffold, 2023), coastal protection and land reclamation (Kelletat, 1992; Hoeksema, 2007; Hofstede, 2008), river damming (IKSE, 2005; Lange et al., 2008; IKSE, 2012; Hübner and Schwandt, 2018) and eutrophication (Pätsch et al., 2010; Skogen et al., 2014; Axe et al., 2017). Since 1900, these human activities and their environmental impact notably increased in the North Sea region (ICES, 2018, 2019, 2020; OSPAR, 2023). The sediment cycle is regulated not just by human activities but also by natural processes such as circulation patterns, waves, tides, storms, riverine discharge, and coastal erosion (Stride, 1982; Eisma and Irion, 1988; Green et al., 1995; Elliott et al., 1998; Holland and Elmore, 2008; Stanev et al., 2009; Fettweis et al., 2010; Dangendorf et al., 2014). Hence, the sediment system of the North Sea may have undergone changes over time due to human and natural processes, considering the economic pressure, the region's dynamic environment and the impact of climate change.

The bulk sediment cycle governs the cycling of elements and compounds in the ocean, such as organic carbon (OC), nutrients and pollutants. Hence, both human and natural impacts may also affect the biogeochemistry of the North Sea. For instance, disturbance of the seafloor reintroduces sedimentary OC into the oxygenated water column, which can enhance OC respiration rates. The degree of sedimentary OC loss due to bottom trawling (Bradshaw et al., 2021; Sala et al., 2021; Hiddink et al., 2023) and the balance between OC loss and OC trapping in wind park areas (Heinatz and Scheffold, 2023) are currently debated. Hence, it is crucial to assess how the sedimentary system

of the North Sea may have changed over time to safeguard its ecological value and establish a baseline for resource management plans.

Approximately 45 - 80 % of the total suspended sediment input to the North Sea accumulates in the Skagerrak (Oost et al., 2021; Spiegel et al., 2024). Hence, the sedimentary archives of the Skagerrak mirror the sediment system of the entire North Sea region under changing environmental conditions. Despite the large amount of available sedimentary records for the Skagerrak (i.e. Erlenkeuser and Pederstad, 1984; van Weering et al., 1987, 1993; Paetzel et al., 1994; Ståhl et al., 2004; Deng et al., 2020), little is known about the temporal variability of sediment transport into the Skagerrak. In this study, we investigate how sedimentation rates at six stations in the Skagerrak have changed over time using high-resolution age-depth modeling. Age-depth relationships were obtained from the continuous decay of excess lead-210 ($^{210}Pb_{ex}$) in sediments (Krishnaswamy et al., 1971; Sanchez-Cabeza and Ruiz-Fernández, 2012) and data on caesium-137 (^{137}Cs), fraction modern carbon-14 ($F^{14}C$) and mercury (Hg), which serve as time markers in the sediment cores. The activity peaks of ^{137}Cs and $F^{14}C$ reflect the atmospheric nuclear weapon tests that were most prevalent in 1963 (van Weering et al., 1993; Deng et al., 2020), while the peaks in Hg concentrations result from its economic utilization prior to regulations between 1960 and 1970 (Leipe et al., 2013; Moros et al., 2017; Polovodova Asteman et al., 2018). The $^{210}Pb_{ex}$ and time marker data are then combined to determine average sedimentation rates before and after the year 1963 to derive a general temporal trend for the Skagerrak. Subsequently, we discuss the sedimentation rate variability within the Skagerrak in relation to potential driving factors that could have altered the sediment system of the North Sea.

II.2 Study area

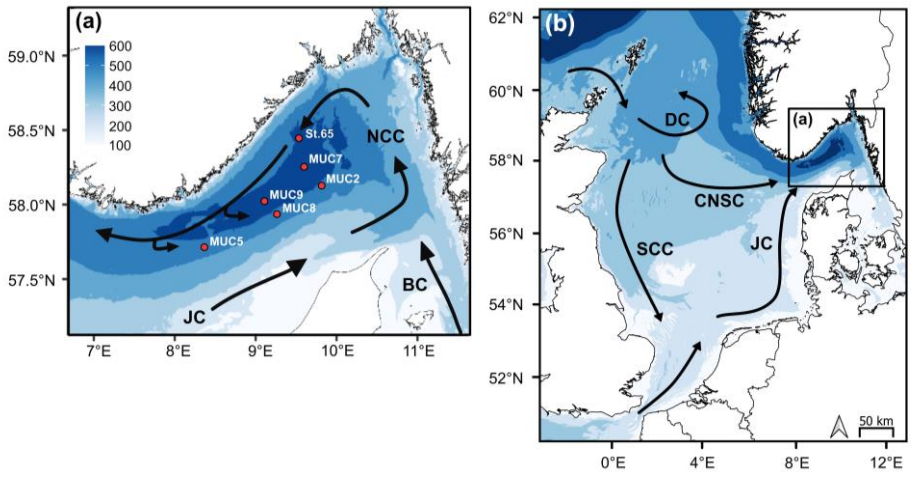

Figure II1. Study area with information on water depth for (a) the Skagerrak and (b) the North Sea. Black arrows indicate the surface water circulation of the Jutland Current (JC), the Baltic Current (BC), the

Norwegian Coastal Current (NCC), the Dooley Current (DC), the Central North Sea Current (CNSC) and the Scottish Coastal Current (SCC).

The Skagerrak strait is located between Denmark, Norway and Sweden and links the North Sea and the Kattegat with a maximum water depth of approximately 700 m (Fig. II1a). Surface waters in the Skagerrak circulate anticlockwise. Water from the North Sea enters the Skagerrak through the Jutland Current from the south, which, together with the Baltic Current, results in the outflowing Norwegian Coastal Current leaving the Skagerrak to the north (Rodhe, 1987, 1996; van Weering et al., 1987; Otto et al., 1990). Annual total sediment deposition in the Skagerrak is 35 Mt yr^{-1} (Spiegel et al., 2024). Skagerrak sediments are characterized by a large lateral input of mostly lithogenic material from the North Sea (van Weering et al., 1993; De Haas and van Weering, 1997; Spiegel et al., 2023, 2024). The sediment composition comprises fine-grained silt and clay sediments in the deeper parts of the Skagerrak and sandy material (<40% clay) near the coastlines (Stevens et al., 1996). Sediments at the stations presented in this study were dominated by fine-grained material (Tab. II1). On a larger scale, the Skagerrak is connected to the currents in the North Sea (Fig. II1b). Water that is transported into the North Sea through the northern Atlantic entrance is split into two currents. The first one, the Dooley Current, flows eastwards and supplies the Central North Sea Current, which carries the water further into the Skagerrak. The second current, the Scottish Coastal Current, moves southwards until it converges with the inflow of Atlantic water from the English Channel in the southern North Sea. The resulting water mass is transported northwards via the Jutland Current to the Skagerrak (Otto et al., 1990; Rodhe, 1998; Winther and Johannessen, 2006).

II.3 Material and methods

II.3.1 Sampling

We present data from six stations (65 to 677 m water depth) in the Skagerrak. Sampling was performed during two research cruises with R/V Alkor, AL557 in June and AL561 in August 2021, respectively (Schmidt, 2021; Thomas et al., 2022). At each station, a short sediment core was recovered (<50cm) using a multiple-corer (MUC). Sediment samples for porosity and solid phase analysis were taken at every centimetre of the MUCs and were stored refrigerated at 4°C until further home-based processing.

Table II1. Summary of sampling sites.

Station	Latitude N	Longitude E	Water depth (m)	Porosity [a]	Grain-sizes [a] D_{50} (µm)	Sediment type
MUC2	58° 10.884'	09° 47.624'	500	0.78	9	Silt, clay

MUC5	57º 45.191'	08º 17.173'	434	0.77	9	Silt, clay
MUC7	58º 18.785'	09º 34.335'	677	0.82	7	Silt, clay
MUC8	57º 59.286'	09º 14.305'	490	0.77	14	Silt, clay
MUC9	58º 04.352'	09º 05.736'	604	0.80	8	Silt, clay
St.65	58° 30.068'	09° 29.887'	530	0.79		

[a] Porosity and D_{50} (50% of particles are smaller than the given value) are means of the whole core. Detailed grain-size distributions are shown in the supplement (Fig. IIS4a, b).

II.3.2 Analytical techniques

Porosity in the sediment samples was determined from the loss of water after freeze-drying and assuming a density of dry solids of 2.5 g cm^{-3}. For the analysis of ^{210}Pb and ^{137}Cs, freeze-dried and homogenized sediment was embedded into containers that were sealed with a two-component epoxy resin. Steady-state equilibration between ^{226}Ra and ^{214}Bi was achieved by storing the samples for two weeks. Analysis of total ^{210}Pb and ^{137}Cs activities was carried out by gamma spectrometry on n-type planar or coaxial Ge-detectors at GEOMAR (MUC5), IOW Warnemünde (MUC2, MUC7 and MUC8), Göttingen (St.65) and IAF Dresden (MUC9). The natural background decay of ^{226}Ra (295 keV) in marine sediments was subtracted from the total ^{210}Pb activities to obtain the excess ^{210}Pb ($^{210}Pb_{ex}$) values.

Radiocarbon analyses were performed on benthic infaunal foraminiferal assemblages at stations MUC2, MUC7 and MUC8. Sediment samples were gently washed through a 63 µm sieve and subsequently dried at 40°C. Only well-stained and preserved individuals were collected and subsequently sorted by species. The foraminiferal species used in this study have been described in detail in the literature and included *Bolivina skagerrakensis*, *Bulimina marginata*, *Uvigerina mediterranea*, *Ammonia beccaria Batavus*, *Melonis barleeanum Williamson* and *N. Labradoricum* (Van Weering and Qvale, 1983; Qvale and Nigam, 1985; Nordberg and Bergsten, 1988; Heier-Nielsen et al., 1995; Hass, 1996; Gyllencreutz et al., 2006). Radiocarbon analyses were performed using a MICADAS micro-scale AMS and followed standard procedures as described in Mollenhauer et al. (2021). Samples were processed by acid hydrolysis of foraminifera tests containing between 59 and 96 µg carbon in a CHS system directly connected to the MICADAS via the Gas Interface System (Wacker et al., 2013). Results were reported as fraction modern ($F^{14}C$) expressed relative to the atmospheric ^{14}C content in 1950 (Reimer et al., 2004).

Contents of Hg were measured in 20 - 100 mg of dried sediment at every centimeter using a DMA-80 Analyser from MLS Company, following the method described in Leipe et al. (2013). The certified reference material CRM (BCR) 142R and the soil standard SRM 2709 were used for calibration. For further details on the method and data quality see Leipe et al. (2013).

Bulk sediment grain-size distributions were determined for each station except St.65. A volume of 1.5 cm^3 was sampled equidistantly, each centimeter from the sediment cores. Samples were treated with 10% - 30% hydrogen peroxide and 60% acetic acid to dissolve organic and carbonate compounds. Subsequently, samples were dispersed in water using tetra-sodium diphosphate decahydrate. Grain-size distributions were determined at the CEN, University of Hamburg, with a laser-diffraction particle-sizer (Sympatec HELOS/KF Magic; range 0.5/18 to 3200 3500 µm). Accuracy of measurements and absence of a long-term instrumental drift was ensured by regular analysis of an in-house standard (standard deviation for mean grain size and D50 over the analysis period was < 1.1 µm). Statistical evaluation of grain-size distributions was based on the graphical method (Folk and Ward, 1957), calculated using Gradistat (Blott and Pye, 2001).

II.3.3 Age-depth model description

Age-depth relationships in the sediment cores were established using $^{210}Pb_{ex}$ activity profiles and activity or concentration peaks of ^{137}Cs, $F^{14}C$ and Hg, which represented time markers of the year 1963. In order to determine sedimentation rates, we applied a numerical transport reaction model to simulate the down-core distributions of $^{210}Pb_{ex}$, ^{137}Cs, $F^{14}C$ and Hg with the following one-dimensional partial differential equation:

$$ds(1-\phi)\frac{\partial C}{\partial t} = \frac{\partial}{\partial x}\left(ds\,(1-\phi)\,D_B\frac{\partial C}{\partial x} - ds\,(1-\phi)\,us\,C\right) - ds(1-\phi)\,\lambda_C\,C \quad \text{(II1)}$$

where C is the activity or concentration, ds is the density of dry solids (2.5 g cm^{-3}), ϕ is porosity, D_B is the bioturbation coefficient, us is the burial velocity and λ_C is the decay constant of ^{210}Pb (0.031 yr^{-1}), ^{137}Cs (0.023 yr^{-1}) and $F^{14}C$ (0.00012 yr^{-1}), respectively. No post-depositional migration of the elements within the sediment or through interstitial water at the sediment water interface was assumed to occur. In case of the radionuclides, we further assumed that the activities of the parent nuclides, i.e. ^{226}Ra for ^{210}Pb, were independent of depth (Koide et al., 1973; Robbins and Edgington, 1975; Appleby and Oldfieldz, 1983).

Steady-state sediment compaction was considered in the model by using the following function to fit the porosity data (Berner, 1980):

$$\phi = \phi_c + (\phi_0 - \phi_c)^{\left(-\frac{x}{px}\right)} \quad \text{(II2)}$$

where ϕ_0 is the porosity at the sediment surface, ϕ_c is the porosity in compacted sediment and px is the attenuation coefficient. Burial velocities were described as:

$$us = \frac{SR \cdot (1-\phi_c)}{(1-\phi)} \quad \text{(II3)}$$

where SR is the sedimentation rate after compaction. Temporal variability of SR was implemented using a sigmoid function:

$$SR = \frac{SR_1\text{-}SR_2}{1 + e^{\frac{t_{max} - (2021 - 1963) - t}{z}}} \quad (II4)$$

where SR_1 is the sedimentation rate before 1963, SR_2 determines the change in sedimentation rates in 1963 and SR_1 - SR_2 is the sedimentation rate after 1963. The value 2021 corresponds to the time of sampling, t_{max} denotes the maximum simulation time (years before present), t is the simulation time, and z controls the smoothing of the transition between different sedimentation rates. In the model runs, t_{max} was set to 500 years to ensure steady-state conditions prior to 1963. The parameter z was set to 6 to provide a sharp transition between sedimentation rates. In order to minimize the number of variable parameters in the model, we opted to set the timing of the change in sedimentation rates to 1963 in each core. The year 1963 was selected as sedimentation rates after 1963 can be constrained by fitting the peaks of the time marker data ^{137}Cs, $F^{14}C$ and Hg. Hence, the presented model setup did not compute and evaluate every possible configuration of sedimentation rate variation in the Skagerrak. Instead, a single sedimentation rate change in 1963 was specified to derive a general trend across stations by comparing average sedimentation rates before and after 1963.

The distribution of the solid phase parameters in surface sediments was used to constrain bioturbation rates:

$$D_B = D_{B0} \cdot \exp\left(-\frac{x^2}{2 \cdot {x_B}^2}\right) \quad (II5)$$

where D_{B0} is the bioturbation coefficient at the sediment-water interface and x_B controls the bioturbation mixing depth.

Upper boundary conditions were set as temporally variable fluxes to the seafloor:

$$FC(t) = SR(t) \cdot ds\ (1\text{-}\phi_0) \cdot C_0(t) \quad (II6)$$

where FC(t) is the flux to the seafloor and $C_0(t)$ is the activity or concentration in settling particles. With regards to $^{210}Pb_{ex}$, a common approach for age-depth reconstruction is the constant initial concentration (CIC) method (Appleby and Oldfieldz, 1983; Sanchez-Cabeza and Ruiz-Fernández, 2012), which assumes a constant ^{210}Pb activity in particles settling to the seafloor irrespective of sedimentation rate variability. Following this method, $C_0(t)$ in Eq. II6 was set temporally constant and we refer to it as Pb_0 in the following. The value of Pb_0 is typically determined by extrapolating the $^{210}Pb_{ex}$ data towards the sediment surface using exponential regression (Sanchez-Cabeza and Ruiz-Fernández, 2012). However, sediment mixing occurred within the top 5 - 15 cm of our cores, which can lead to uncertainty in such extrapolations. Hence, Pb_0 was chosen to be a fitting parameter for $^{210}Pb_{ex}$ in the model simulations. For the time markers ^{137}Cs and Hg, $C_0(t)$ was determined using

an interpolation function that was fitted to time series data presented in previous studies for atmospheric deposition of ^{137}Cs in the northern hemisphere (Garcia Agudo, 1998) and global Hg emissions into the atmosphere (Hylander and Meili, 2003; Streets et al., 2011). The period of enhanced Hg input corresponding to the extensive American gold mining period between 1860 and 1920 was not considered in our model, as it was not reflected by the Hg data in the sediment cores. For $F^{14}C$, we approximated $C_0(t)$ with dissolved inorganic radiocarbon concentrations of surface water ($F^{14}C_{DIC}$) simulated using the ocean general circulation model FESOM2 (Danilov et al., 2017; for the implementation of $F^{14}C_{DIC}$ see Lohmann et al., 2020; Butzin et al., 2023). The model considered $F^{14}C_{DIC}$ as a single abiotic tracer which was connected with the carbon cycle only through $^{14}CO_2$ air-sea exchange calculated according to Wanninkhof (2014) and assuming a homogeneous concentration of 2000 mmol m^{-3} of DIC in surface water following Toggweiler et al. (1989). FESOM2 was run from 1850 CE to 2015 CE with prescribed periodic climate forcing (Large and Yeager, 2009) as well as with transient values of atmospheric CO_2 (Meinshausen et al., 2017) and $F^{14}C$ (Graven et al., 2017), starting from preindustrial conditions determined in a previous study (Lohmann et al., 2020). Overall, the simulated anthropogenic $F^{14}C_{DIC}$ distribution was in line with global observations (Key et al., 2004; Butzin et al., 2021). FESOM2 employs unstructured meshes with variable horizontal metric resolution. Here, the resolution was about 127 000 surface nodes in the horizontal and 47 layers in the vertical. The model results were remapped to regular geographical coordinates and evaluated nearest to the core sites. The temporal variability of $C_0(t)$ for ^{137}Cs, $F^{14}C$ and Hg that were used to calculate upper boundary fluxes and the calculated upper boundary fluxes for all parameters are shown in the supplement (Fig. IIS1, IIS2). At the lower model boundary (50 cm), a zero gradient condition was imposed for all model variables.

In total, eight parameters (SR_1, SR_2, Pb_0, ϕ_0, ϕ_c, px, D_{B0}, x_B) were adjusted to fit the porosity, $^{210}Pb_{ex}$, ^{137}Cs, $F^{14}C$ and Hg data. The parameters ϕ_0, ϕ_c and px were determined by visually fitting the measured porosity data (Fig. IIS3). The parameters SR_1, SR_2, Pb_0, DB_0 and x_B were first evaluated by a Monte Carlo-type approach (3000 runs) after Dale et al. (2021). For each Monte Carlo run, a random configuration of the five parameters was selected within the ranges of 0.1 to 0.8 cm yr^{-1} for SR_1 and SR_2, 10 to 45 dpm g^{-1} for Pb_0, 2 to 30 cm^2 yr^{-1} for DB_0 and 1 to 6 cm for x_B. In order to prevent negative sedimentation rates, SR_2 was restricted to select smaller values than SR_1. The ranges were chosen based on initial test runs, literature values and visual identification of the bioturbation layer in the $^{210}Pb_{ex}$ data. The goodness of fit of each configuration was evaluated by the sum of least square regressions between modeled and measured data of ^{210}Pb and ^{137}Cs data. The average of the ten configurations with the minimum sum of least square regressions was used as an approximation for SR_1, SR_2, Pb_0, DB_0 and x_B. In a second step, this configuration was further fine-tuned by visually fitting the measured data, with an emphasis on fitting the exact position of the ^{137}Cs peak. The parameterisation of the adjustable variables is summarized in Table II2. The model simulations were

run using the partial differential equation solver implemented in Mathematica 12.2. Mass conservation was > 99 % in all model runs.

Table II2. Model results for the temporal variability of sedimentation rates.

Model data	MUC2 500m	MUC5 434m	MUC7 677m	MUC8 490m	MUC9 604m	St.65 530m
Sedimentation rate before 1963, SR_1 (cm yr^{-1}) [a]	0.42	0.28	0.26	0.72	0.25	0.24
Sedimentation rate decrease in 1963, SR_2 (cm yr^{-1}) [a]	0.24	0.15	0.11	0.50	0.14	0.12
Sedimentation rate after 1963, SR_1 - SR_2 (cm yr^{-1}) [a]	0.18	0.13	0.15	0.22	0.11	0.12
Initial $^{210}Pb_{ex}$ activity, Pb_0 (dpm g^{-1})	32	24	44	29	29	30
Bioturbation coefficient at sediment-water interface, D_{B0} (cm^2 yr^{-1})	7.0	7.0	6.0	9.5	4.0	4.0
Attenuation coefficient for bioturbation, x_B (cm)	4.0	3.0	3.5	5.0	3.0	3.5
Porosity at sediment-water interface, ϕ_0 (-)	0.89	0.87	0.89	0.89	0.88	0.90
Porosity in compacted sediment, ϕ_c (-)	0.77	0.74	0.80	0.75	0.78	0.76
Porosity attenuation coefficient, px (cm)	0.17	0.10	0.11	0.14	0.13	0.15

[a] SR_1 and SR_2 determine the sedimentation rates before and after the pre-selected year 1963.

II.4 Results

II.4.1 Measured and modeled sediment geochemistry

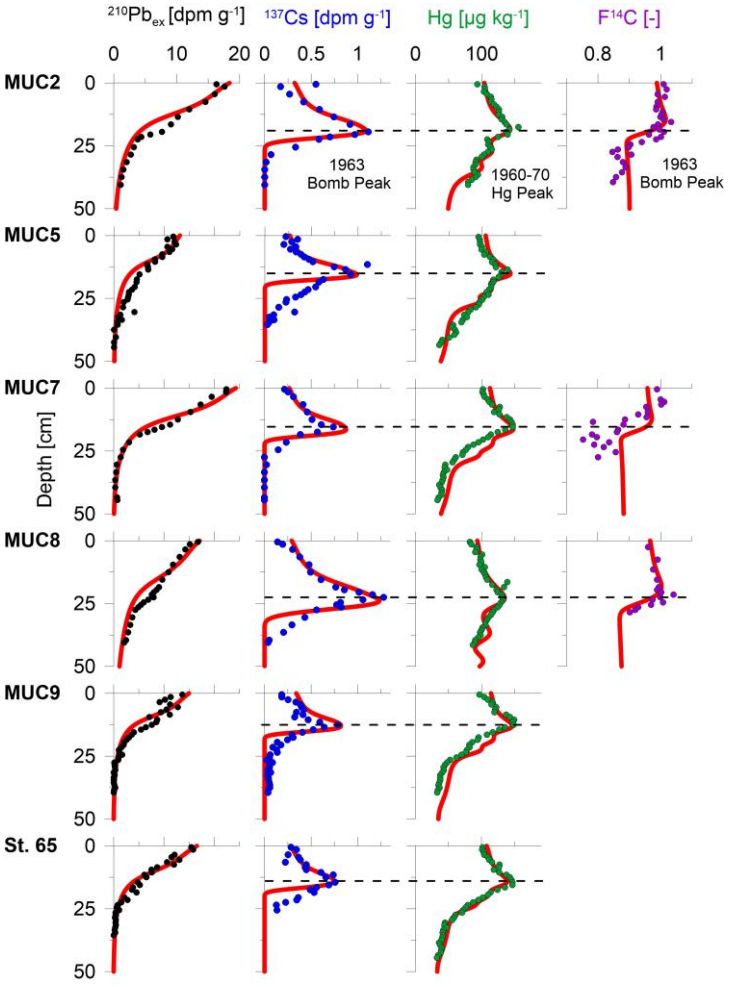

Figure II2. Measured data (symbols) and model simulations (curves) of $^{210}Pb_{ex}$ (black), ^{137}Cs (blue), Hg (green) and $F^{14}C$ (purple). The dashed lines indicate the sediment depth of the time markers of the bomb tests in 1963 and the Hg regulations in 1960 - 1970.

Sediments consisted of fine-grained material with mean D_{50} values ranging from 7 to 14 µm (Tab. II1), with near-constant grain size distributions with sediment depth and time in MUC2 and MUC8 (Fig. IIS4a, b). In MUC5, MUC7 and MUC9, multiple grain size peaks were observed with D_{50} values between 20 and 40 µm.

Activities of $^{210}Pb_{ex}$ generally decreased exponentially with sediment depth (Fig. II2). In the upper 5 - 10 cm, the activities tended to be more constant. In depth intervals between 10 and 25 cm, the profiles did not follow the expected exponential decline with sediment depth but showed slightly elevated values. In this horizon, the model data deviated notably from the measured data. The average root mean square error (RMSE) between the measured and model data was 1.1 dpm g^{-1}.

The time markers ^{137}Cs, Hg and $F^{14}C$ showed coinciding peaks situated between 10 and 25 cm sediment depth. Below the ^{137}Cs activity peak, measured data extended deeper into the sediment compared to the model simulation. At certain stations, the Hg data showed two additional peaks at sediment depths below the main peak, most pronounced at station MUC2. Mean RMSEs between modeled and measured data for ^{137}Cs, Hg and $F^{14}C$ were 0.11 dpm g^{-1}, 8.92 µg kg^{-1} and 0.04, respectively.

II.4.2 Modeled sedimentation rates and mixing

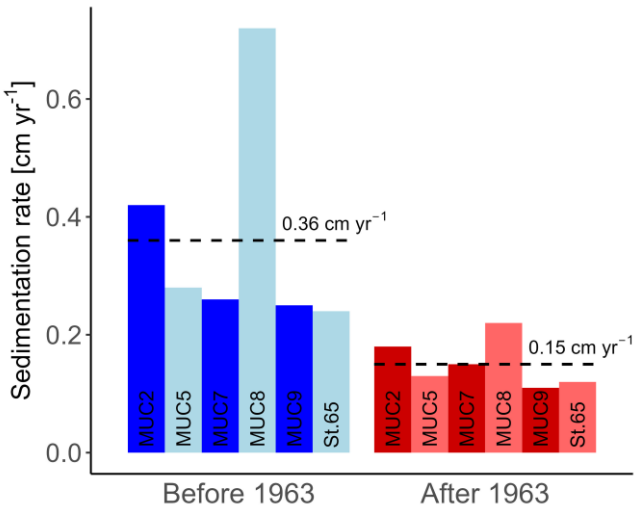

Figure II3. Modeled sedimentation rates before (blue) and after 1963 (red) at each station. The dashed lines indicate average sedimentation rates before and after 1963.

Sedimentation rates determined by the model ranged from 0.24 to 0.72 cm yr^{-1} before and from 0.11 to 0.22 cm yr^{-1} after 1963 (Tab. II2, Fig. II3). On average, sedimentation rates decreased from 0.36 to 0.15 cm yr^{-1}. Station MUC8 showed a remarkably higher sedimentation rate of 0.72 cm yr^{-1} before 1963 compared to the other stations. Sediment mixing by bioturbation was limited to the upper 5 - 15 cm with bioturbation coefficients (D_{B0}) and mixing coefficients (x_B) of 4.0 - 9.5 cm^2 yr^{-1} and 3.0 - 5.0 cm, respectively (Tab. II2, Fig. IIS5). The resulting age models are shown in the supplement (Fig. IIS6).

II.5 Discussion

II.5.1 Data and model evaluation

Applying a steady-state sedimentation rate was not sufficient to simultaneously fit the $^{210}Pb_{ex}$ and time marker data. Hence, we simulated temporally variable sedimentation rates in the model by implementing a single sedimentation rate change in 1963 (Eq. II4). It is important to note that the actual timing, magnitude and number of changes in the natural system may differ from our model results. We therefore recommend verifying the presented general trend by considering further age-depth parameters, such as time markers for different years. Nevertheless, the specified model set-up produced satisfactory fits to the measured data suggesting that the derived general trend of net decreasing sedimentation rates over the last 110 years is reasonable.

II.5.1.1 Modeling approach for $^{210}Pb_{ex}$

Currently, several methods exist to determine the age-depth relationship based on $^{210}Pb_{ex}$ (Krishnaswamy et al., 1971; Robbins and Edgington, 1975; Appleby and Oldfieldz, 1983; Sanchez-Cabeza and Ruiz-Fernández, 2012; Foucher et al., 2021). Among them, the CIC and constant rate of supply (CRS) models are the most commonly applied methods in the Skagerrak (van Weering et al., 1987, 1993; Paetzel et al., 1994) and worldwide (Foucher et al., 2021). In principle, CRS assumes a constant flux of $^{210}Pb_{ex}$ to the seafloor whereas CIC assumes constant activity of $^{210}Pb_{ex}$ in particles settling to the seafloor (Pb_0). The applicable model is usually determined by relationships between sedimentation rates, down-core integrated $^{210}Pb_{ex}$ values and $^{210}Pb_{ex}$ activities in settling particles (Appleby and Oldfieldz, 1983; Sanchez-Cabeza and Ruiz-Fernández, 2012). Although the amount of data presented in this study only allowed a limited evaluation, the averaged sedimentation rates (Tab. II2) are roughly proportional to the integrated $^{210}Pb_{ex}$ activities (Spiegel et al., 2024) at the different sites. In addition, the presented $^{210}Pb_{ex}$ data roughly follow a monotonic decline with

sediment depth outside the bioturbated zone, both of which are indicators of the applicability of the CIC method (Appleby and Oldfieldz, 1983). Furthermore, the CIC method is generally recommended when variable sources of $^{210}Pb_{ex}$ are present (Sanchez-Cabeza and Ruiz-Fernández, 2012) and sediment focusing occurs (Appleby and Oldfieldz, 1983). This is the case in the Skagerrak marked by a significant lateral input of $^{210}Pb_{ex}$ and high sedimentation rates along the deeper basin where our stations are located (De Haas and van Weering, 1997; Spiegel et al., 2024). In addition, testing both methods through the Monte Carlo analysis and subsequent visual fine-tuning procedure revealed slightly better fits of the CIC model to the measured data. For the reasons above, the CIC method was chosen to determine age-depth relationships. Knowledge of the activity in settling particles is necessary for the CIC method, which is usually determined by extrapolating the measured data in sediment cores towards the surface sediment. However, sediment mixing occurred in the upper sediment layer (5 - 15 cm) of the presented cores, which can lead to uncertainty in such extrapolations (Sanchez-Cabeza and Ruiz-Fernández, 2012). In addition, elevated activities between 10 - 25 cm in the $^{210}Pb_{ex}$ profiles did not follow an exponential shape, further complicating extrapolations to the surface. The excess ^{210}Pb in this depth interval may be attributed to the production of ^{210}Pb in the atmosphere during nuclear bomb testing in 1963 (Jaworowski, 1966; Jaworowski et al., 1978). However, this relation is controversial, as other studies did not observe elevated ^{210}Pb values in samples measured during that period (Bhandari et al., 1966; Crozaz, 1966). If nuclear weapon tests did introduce ^{210}Pb into the atmosphere, this additional ^{210}Pb input was not considered in the model, which may explain the observed deviation between the measured and modeled data in this specific depth interval. Since sediment mixing and the intermediate non-exponential shape complicated extrapolations to the sediment surface, we opted to implement Pb_0 as a fitting parameter in the model (Eq. II6) instead of determining it by extrapolation. In order to evaluate this approach, we compared the values of Pb_0 resulting from the Monte Carlo and visual fine-tuning to values obtained using an exponential regression function from below the bioturbated zone (bioturbation rate < 0.2 $cm^2\ yr^{-1}$), which revealed similar values and trends between stations (Tab. II2, Tab. IIS1). However, it is important to note that the results obtained using exponential regression varied substantially depending on where the boundary of the bioturbation zone was set, suggesting that the use of Pb_0 as a fitting parameter might be more accurate in bioturbated sediments.

II.5.1.2 Time marker triplet of the year 1963

Measured $^{210}Pb_{ex}$ is often used as the only fitting parameter in published studies, such that sediment mixing and variable atmospheric ^{210}Pb inputs may cause substantial uncertainty in the sedimentation rate estimates. However, this study was able to verify the results derived from $^{210}Pb_{ex}$ by utilizing the activity or concentration peaks of ^{137}Cs, $F^{14}C$ and Hg as time markers to constrain age-depth

relationships. The peaks in Hg concentrations were likely the result of its intense usage and production during industrialization, which were progressively regulated from 1960 to 1970 (Leipe et al., 2013; Moros et al., 2017; Polovodova Asteman et al., 2018). Two events, the nuclear bomb tests in 1963 and the Chernobyl reactor accident in 1986, released substantial amounts of ^{137}Cs and $F^{14}C$ into the atmosphere that can eventually be traced in marine sediments. Given the age-depth reconstructions based on $^{210}Pb_{ex}$ and the correlation with the Hg peaks, the ^{137}Cs and $F^{14}C$ peaks detected in our sediment cores were attributed to the bomb tests in 1963. This is consistent with previous studies in the Skagerrak (van Weering et al., 1993; Deng et al., 2020) and in the Baltic Sea (Moros et al., 2017). Hence, the time marker triplet allowed for a robust depth relation to the year 1963 in all sediment cores, which was used to constrain the presented sedimentation rates. Since the peak positions between the time markers slightly differed in the same core, we focused on fitting the ^{137}Cs data, because this parameter has often been presented alongside $^{210}Pb_{ex}$ in previous studies in the Skagerrak (van Weering et al., 1993; Paetzel et al., 1994; Beks, 2000; Deng et al., 2020). Considering only slight differences in the peak position, the general trend of decreasing sedimentation rates is independent of which parameter is focused on. Most pronounced at stations MUC5, MUC8 and St.65, the model inaccurately predicted the ^{137}Cs data in sediment depths below the bomb peak. Solid phase mixing was excluded to be the reason as other solid phase data exhibited reasonable model fits at the same sediment depths. Previous studies indicated that ^{137}Cs can desorb from particles and migrate downwards through solute diffusion processes in marine (Bakunov et al., 2023), lacustrine (Krishnaswamy et al., 1971; Klaminder et al., 2012; Bakunov et al., 2019) and soil sediments (Almgren and Isaksson, 2006). As the model does not consider ^{137}Cs diffusion, the observed misfit may be explained by molecular diffusion of ^{137}Cs to deeper sediment layers.

II.5.1.3 Bioturbation parameterisation

The elevated $^{210}Pb_{ex}$ values between 10 - 25 cm and the ^{137}Cs data below the bomb peak might indicate a more complex bioturbation layer than assumed in the model. Trying to fit the data with time-dependant bioturbation rates and constant sedimentation rates led to either poor fits or extreme bioturbation parameters that were not in line with previous studies (Rosenberg et al., 1996; Dauwe et al., 1998; Kristensen et al., 2018). We further tested setting non-steady state sedimentation rates and two separate bioturbation layers, one at the surface and another one at the depth interval of the elevated $^{210}Pb_{ex}$ and ^{137}Cs values. Although there is no indication of a second bioturbation layer in our dataset, it was possible to reduce the pronounced model deviations in the specific depth layers with this setup, as shown exemplarily for MUC5 in the supplement (Fig. IIS7). In this example, the sedimentation rate decrease was set to 0.32 cm yr^{-1} before and 0.18 cm yr^{-1} after 1963. Hence, the change in sedimentation rates only slightly differed from the results obtained without a second

bioturbation layer (Tab. II2), indicating that the general trend of decreasing sedimentation rates in the Skagerrak remains valid. However, sedimentation rates and bioturbation rates were partly interchangeable in this setup as they similarly affected the solid phase distributions and no conclusive parameterisation could be derived. Based on the available data, it was not possible to determine the depth distribution of bioturbation intensities independently to constrain our model results, i.e. by direct or further particle tracer methods (Maire et al., 2008). Furthermore, no visible signs of bioturbation, such as macrofauna or burrow structures, were observed below 10 cm in the sediment cores during sampling (Spiegel et al., 2023). Although the data may suggest a more complex bioturbation zone, we opted for steady-state bioturbation rates to maintain the simplicity of the model.

II.5.2 Change in sedimentation rates in 1963

The major finding of this study was a consistent decrease in sedimentation rates across all stations, with sedimentation rates decreasing on average by a factor of two after 1963 (Tab. II2, Fig. II3). The presented sedimentation rates were of similar magnitude to previous studies in the Skagerrak region (Erlenkeuser and Pederstad, 1984; van Weering et al., 1987, 1993; Ståhl et al., 2004; Diesing et al., 2021). Higher sedimentation rates at MUC8 might be the result of spatial inhomogeneities between the different stations. Comparably high sedimentation rates of 0.6 - 1.1 cm yr^{-1} have been reported in the northeastern part of the Skagerrak (Erlenkeuser and Pederstad, 1984; van Weering et al., 1993). A previous study determined steady-state sedimentation rates for MUC5 (0.32 cm yr^{-1}), MUC9 (0.19 cm yr^{-1}) and St.65 (0.26 cm yr^{-1}) based on the same dataset, but only using $^{210}Pb_{ex}$ for age-depth reconstruction (Spiegel et al., 2023). The differences compared to the temporally variable sedimentation rates in this study can be attributed to the different modeling approaches and the application of multiple parameters for age-depth reconstructions. The comparison indicates the potential degree of uncertainty in some of the existing literature in the Skagerrak that relied on a single parameter for sedimentation rate reconstructions.

Previous studies estimated sediment deposition in the Skagerrak to account for 45 - 80 % of the total sediment inputs into the North Sea (Oost et al., 2021; Spiegel et al., 2024). Furthermore, a substantial proportion of the Skagerrak deposits (~76 %) likely originates from the North Sea (De Haas and van Weering, 1997; Spiegel et al., 2024). Considering that sedimentation rates halved on average at the six stations, it is reasonable to infer that the North sediment system has been subject to significant change in the period from 1900 to 2021.

II.5.3 Driving factors for the temporal variability of sedimentation rates in the Skagerrak

In this section, we discuss how major human and natural processes in the North Sea may have affected the sedimentation rates in the Skagerrak. It should be noted that our dataset only allowed for a qualitative assessment of the drivers of changes in sedimentation, which can serve as a basis for future quantitative analysis of the sediment cycle in the North Sea. We recommend integrating the data and different impacts into non-steady state particle transport models to comprehend the temporal evolution of the sediment cycle. To validate such models, additional field data on the provenance, transport pathways and deposition of sediments in the North Sea are necessary.

II.5.3.1 Exploring processes contradictory to a decrease in sedimentation rates

Bottom trawling, sediment extraction and other human activities disturb the seabed and resuspend surface sediments (De Groot, 1986; Baeye and Fettweis, 2015; Eigaard et al., 2017; ICES, 2019; Mielck et al., 2019; Slavik et al., 2019; ICES, 2020; Rijnsdorp et al., 2020; Daewel et al., 2022; Heinatz and Scheffold, 2023), increasing the particle load in the water column. Similarly, climate change-related changes in temperature, precipitation and sea level rise in the North Sea region (Wahl et al., 2013) likely enhanced sediment inputs by elevated coastal erosion rates. Since part of the additional suspended material is transported to the Skagerrak, such human and natural processes should theoretically lead to an increase in sedimentation rates in the Skagerrak and thus contradict our observations.

Storm events occur frequently in the North Sea (Dangendorf et al., 2014) and redistribute sediments (Green et al., 1995; Stanev et al., 2009; Fettweis et al., 2010). Since particle settling is dependent on the energetic conditions in the water column (Hjulstrom, 1939; McCAVE and Swift, 1976), grain size records have been used as proxies for past storm activity in the Skagerrak (Hass, 1996). Accordingly, sharp layers with notably coarser grain sizes at MUC5, MUC7 and MUC9 (Fig IIS4a, b) were likely the result of certain storm events. However, no clear trends in the frequency or shape of the grain size peaks with sediment depth or time were observed across the stations. To further test the correlation between grain sizes and sediment deposition in the Skagerrak, we set multiple short periods of high sedimentation rates in the model according to the grain size distributions. This approach generally led to insufficient model fits to the ^{210}Pb and time marker data (data not shown), further suggesting that the grain size distribution does not reliably correlate with sedimentation rates in the Skagerrak. Hence, although storm events can be traced by the grain size in the Skagerrak, they were likely not responsible for the general long-term trend in sedimentation rate.

II.5.3.2 Potential contributors to the decrease in sedimentation rates

Although the above human and natural processes affect the North Sea, other factors that outweigh these processes are required to explain the observed decrease in sedimentation rates in the Skagerrak. River dams have been progressively constructed in the major North Sea rivers and their tributaries, that is, the Elbe, Weser and Ems rivers (IKSE, 2005; Lange et al., 2008; IKSE, 2012; Hübner and Schwandt, 2018). River damming typically leads to a reduction in the riverine particle discharge into the ocean (Syvitski et al., 2005; Ericson et al., 2006; Graf, 2006). Considering that ~ 5 - 11 % of the total sediment inputs into the North Sea originate from rivers (Eisma and Irion, 1988; Oost et al., 2021), river damming may have substantially reduced the suspended sediment budget of the North Sea. However, this factor alone may not fully explain the considerable decline in sedimentation rates in the Skagerrak.

Extensive parts of the North Sea coastline have been protected against erosion by dykes, wave breaks, land reclamation and other coastal protection means (Kelletat, 1992; Hoeksema, 2007; Hofstede, 2008). Coastal erosion has been estimated to contribute ~ 3 - 9 % of the total sediment inputs in the North Sea (Eisma and Irion, 1988; Puls et al., 1997; Oost et al., 2021). However, recent studies suggested that current coastal erosion rates might be underestimated in the North Atlantic (Regard et al., 2022) and in the Baltic Sea (Wallmann et al., 2022). Therefore, coastal protection and subsequent mitigation of erosional sediment inputs might be a major driving factor for the decrease in sedimentation rates in the Skagerrak.

Approximately 14 - 25 % of the total suspended solids entering the North Sea are deposited in the Wadden Sea, making it a major sink for sediments (Oost et al., 2021). Previous studies have suggested that a combination of relative sea level rise, circulation patterns and redistribution of sediments may have increased accretion rates in the Wadden Sea (Cahoon et al., 2000; van Wijnen and Bakker, 2001; Flemming, 2002; Madsen et al., 2007; Bartholdy et al., 2010; Lodder et al., 2019), while other observations indicated a loss of sediments in certain areas (Flemming and Nyandwi, 1994; Mai and Bartholomä, 2000; van Wijnen and Bakker, 2001; Flemming, 2002; Lodder et al., 2019). Ultimately, it remains unclear how the sediment input across the entirety of the Wadden Sea region has changed over time. Given the substantial deposition, it is feasible that the suspended sediment load of the North Sea would decline significantly if accretion rates in the Wadden Sea gradually increased over time. Consequently, less material would have been available for transportation into the Skagerrak, potentially leading to the observed decrease in sedimentation rates.

The hydrography of the North Sea reveals two major transportation pathways for water and sediment from the northern Atlantic to the Skagerrak (Fig. II1b). Previous studies demonstrated that the variability in the circulation system of the North Sea correlates with the North Atlantic Oscillation (NAO) and wind conditions (Mathis et al., 2015; Daewel and Schrum, 2017). They show that before

1960, weaker westerly wind conditions likely diminished the water inflow through the northern entrance, thereby enhancing the Dooley Current and Central North Sea Current. These currents transport sediment on a direct pathway to the Skagerrak, which could explain higher sedimentation rates in the Skagerrak prior to 1963. Between 1970 and 2000 a positive NAO phase and strong westerly winds fostered the southward transport along the British coastline. During this period, a larger proportion of the sediment was likely transported along the elongated pathway through the southern North Sea and across the depocenter of the Wadden Sea where the sediment could settle before reaching the Skagerrak. Given that 13 - 30 % of the total sediment input is delivered through the northern entrance, the temporal variability in the hydrography and its effect on the amount of sediment that reaches the Skagerrak may have partly resulted in the decline of sedimentation rates in the Skagerrak.

II.6 Conclusion

Based on high-resolution age-depth modeling using $^{210}Pb_{ex}$, ^{137}Cs, $F^{14}C$ and Hg at six sediment cores in the Skagerrak, we determined that sedimentation rates on average decreased from 0.36 before to 0.15 cm yr^{-1} after 1963. Although a single sedimentation rate change in 1963 may not reflect the actual number and timings of sedimentation rate variations in the natural system, the specified model setup produced satisfactory fits to the measured data. In order to verify our model results, we recommend examining additional age-depth parameters, particularly time markers for years other than 1963. The model could further benefit from an independent determination of bioturbation parameters. Considering that the Skagerrak represents the largest depocenter for sediments from the North Sea, the decline in sedimentation rates suggests that the sediment system of the North Sea has been subject to substantial change in the last 110 years. We summarized major processes that potentially shifted the sediment cycle of the North Sea leading to a decrease in sedimentation rates in the Skagerrak:

- A change in the North Sea circulation pattern reduced the amount of sediment transported to the Skagerrak
- Increased sediment deposition in the Wadden Sea
- Coastal protection and river damming

These factors are likely to have outweighed processes that should theoretically increase Skagerrak sedimentation, such as resuspension triggered by human activities and storm events, temperature, humidity and sea level rise. However, a quantitative evaluation of the different contributors to

sediment deposition in the Skagerrak is necessary to better describe the temporal change in the sediment system of the North Sea.

Acknowledgements

We wish to thank the captain and the crew of RV Alkor for their support onboard the RV Alkor during the cruise AL561, as well as our colleagues Bettina Domeyer, Anke Bleyer, Regina Surberg, Matthias Türk and Asmus Petersen for their help onboard and in the GEOMAR laboratories. We also thank Andreas Neumann from the Helmholtz-Zentrum Hereon for providing sediment samples of St.65 from the RV Alkor cruise AL557. We would further like to acknowledge Bernd Kopka and Marvin Blaue from the Laboratory for Radioisotopes at the University of Göttingen and Christian Kunze and Robert Arndt from the IAF Dresden for the ^{210}Pb and ^{137}Cs analyses. We are further thankful for ^{14}C measurements performed by Gesine Mollenhauer and her team at Alfred Wegener Institute Helmholtz Centre for Polar and Marine Research. Funding for this study was provided by the Federal Ministry of Education and Research, Germany, via the APOC project (03F0874B) – "Anthropogenic impacts on particulate organic carbon cycling in the North Sea".

Literature

Almgren, S., Isaksson, M., 2006. Vertical migration studies of 137Cs from nuclear weapons fallout and the Chernobyl accident. J. Environ. Radioact. 91, 90–102. https://doi.org/10.1016/j.jenvrad.2006.08.008

Appleby, P.G., Oldfieldz, F., 1983. The assessment of 210Pb data from sites with varying sediment accumulation rates. Hydrobiologia 103, 29–35. https://doi.org/10.1007/BF00028424

Axe, P., Clausen, U., Leujak, W., Malcolm, S., Ruiter, H., Prins, T., Harvey, E.T., 2017. Eutrophication Status of the OSPAR Maritime Area. Third Integrated Report on the Eutrophication Status of the OSPAR Maritime Area.

Baeye, M., Fettweis, M., 2015. In situ observations of suspended particulate matter plumes at an offshore wind farm, southern North Sea. Geo-Mar. Lett. 35, 247–255. https://doi.org/10.1007/s00367-015-0404-8

Bakunov, N.A., Bolshiyanov, D.Yu., Aksenov, A.O., Makarov, A.S., 2023. On Global 137Cs Diffusion in Bottom Sediments of Northern Seas. Radiochemistry 65, 485–492. https://doi.org/10.1134/S1066362223040100

Bakunov, N.A., Bol'shiyanov, D.Yu., Pravkin, S.A., 2019. 137Cs in Bottom Sediments of Oligotrophic Lakes: Migration Mechanism. Radiochemistry 61, 122–128. https://doi.org/10.1134/S1066362219010181

Bartholdy, A.T., Bartholdy, J., Kroon, A., 2010. Salt marsh stability and patterns of sedimentation across a backbarrier platform. Mar. Geol. 278, 31–42. https://doi.org/10.1016/j.margeo.2010.09.001

Beks, J.P., 2000. Storage and distribution of plutonium, 241Am, 137Cs and 210Pbxs in North Sea sediments. Cont. Shelf Res. 20, 1941–1964. https://doi.org/10.1016/S0278-4343(00)00057-1

Berner, R.A., 1980. Early diagenesis: a theoretical approach, Princeton series in geochemistry. Princeton University Press, Princeton, N.J.

Bhandari, N., Lal, D., Rama, D., 1966. Stratospheric circulation studies based on natural and artificial radioactive tracer elements. Tellus 18 (2–3), 391–406.

Blott, S.J., Pye, K., 2001. GRADISTAT: a grain size distribution and statistics package for the analysis of unconsolidated sediments. Earth Surf. Process. Landf. 26, 1237–1248. https://doi.org/10.1002/esp.261

Bradshaw, C., Jakobsson, M., Brüchert, V., Bonaglia, S., Mörth, C.-M., Muchowski, J., Stranne, C., Sköld, M., 2021. Physical Disturbance by Bottom Trawling Suspends Particulate Matter and Alters Biogeochemical Processes on and Near the Seafloor. Front. Mar. Sci. 8, 683331. https://doi.org/10.3389/fmars.2021.683331

Butzin, M., Sidorenko, D., Köhler, P., 2021. A multi-resolution ocean simulation of the anthropogenic radiocarbon transient (other). pico. https://doi.org/10.5194/egusphere-egu21-3118

Butzin, M., Ye, Y., Völker, C., Gürses, Ö., Hauck, J., Köhler, P., 2023. Carbon isotopes in the marine biogeochemistry model FESOM2.1-REcoM3 (preprint). Climate and Earth system modeling. https://doi.org/10.5194/egusphere-2023-1718

Cahoon, D.R., French, J.R., Spencer, T., Reed, D., Möller, I., 2000. Vertical accretion versus elevational adjustment in UK saltmarshes: an evaluation of alternative methodologies. Geol. Soc. Lond. Spec. Publ. 175, 223–238. https://doi.org/10.1144/GSL.SP.2000.175.01.17

Crozaz, G., 1966. Dating of Glaciers by Lead-210. Symp Radioact. Dating Methods Low-Level Count. 385.

Daewel, U., Akhtar, N., Christiansen, N., Schrum, C., 2022. Offshore wind farms are projected to impact primary production and bottom water deoxygenation in the North Sea. Commun. Earth Environ. 3, 292. https://doi.org/10.1038/s43247-022-00625-0

Daewel, U., Schrum, C., 2017. Low-frequency variability in North Sea and Baltic Sea identified through simulations with the 3-D coupled physical–biogeochemical model ECOSMO. Earth Syst. Dyn. 8, 801–815. https://doi.org/10.5194/esd-8-801-2017

Dangendorf, S., Müller-Navarra, S., Jensen, J., Schenk, F., Wahl, T., Weisse, R., 2014. North Sea Storminess from a Novel Storm Surge Record since AD 1843*. J. Clim. 27, 3582–3595. https://doi.org/10.1175/JCLI-D-13-00427.1

Danilov, S., Sidorenko, D., Wang, Q., Jung, T., 2017. The Finite-volumE Sea ice–Ocean Model (FESOM2). Geosci. Model Dev. 10, 765–789. https://doi.org/10.5194/gmd-10-765-2017

Dauwe, B., Herman, P., Heip, C., 1998. Community structure and bioturbation potential of macrofauna at four North Sea stations with contrasting food supply. Mar. Ecol. Prog. Ser. 173, 67–83. https://doi.org/10.3354/meps173067

De Groot, S.J., 1986. Marine sand and gravel extraction in the North Atlantic and its potential environmental impact, with emphasis on the North Sea. Ocean Manag. 10, 21–36. https://doi.org/10.1016/0302-184X(86)90004-1

De Haas, H., van Weering, T.C.E., 1997. Recent sediment accumulation, organic carbon burial and transport in the northeastern North Sea. Mar. Geol. 136, 173–187. https://doi.org/10.1016/S0025-3227(96)00072-2

Deng, L., Bölsterli, D., Kristensen, E., Meile, C., Su, C.-C., Bernasconi, S.M., Seidenkrantz, M.-S., Glombitza, C., Lagostina, L., Han, X., Jørgensen, B.B., Røy, H., Lever, M.A., 2020. Macrofaunal control of microbial community structure in continental margin sediments. Proc. Natl. Acad. Sci. 117, 15911–15922. https://doi.org/10.1073/pnas.1917494117

Diesing, M., Thorsnes, T., Bjarnadóttir, L.R., 2021. Organic carbon densities and accumulation rates in surface sediments of the North Sea and Skagerrak. Biogeosciences 18, 2139–2160. https://doi.org/10.5194/bg-18-2139-2021

Eigaard, O.R., Bastardie, F., Hintzen, N.T., Buhl-Mortensen, L., Buhl-Mortensen, P., Catarino, R., Dinesen, G.E., Egekvist, J., Fock, H.O., Geitner, K., Gerritsen, H.D., González, M.M., Jonsson, P., Kavadas, S., Laffargue, P., Lundy, M., Gonzalez-Mirelis, G., Nielsen, J.R., Papadopoulou, N., Posen, P.E., Pulcinella, J., Russo, T., Sala, A., Silva, C., Smith, C.J., Vanelslander, B., Rijnsdorp, A.D., 2017. The footprint of bottom trawling in European waters: distribution, intensity, and seabed integrity. ICES J. Mar. Sci. 74, 847–865. https://doi.org/10.1093/icesjms/fsw194

Eisma, D., Irion, G., 1988. Suspended Matter and Sediment Transport, in: Salomons, W., Bayne, B.L., Duursma, E.K., Förstner, U. (Eds.), Pollution of the North Sea. Springer Berlin Heidelberg, Berlin, Heidelberg, pp. 20–35. https://doi.org/10.1007/978-3-642-73709-1_2

Elliott, M., Nedwell, S., Jones, N.V., Read, S.J., Cutts, N.D., Hemingway, K.L., 1998. Intertidal Sand and Mudflats & Subtidal Mobile Sandbanks (volume II). An overview of dynamic and sensitivity characteristics for conservation management of marine SACs. Scott. Assoc. Mar. Sci. UK Mar. SACs Proj.

Ericson, J., Vorosmarty, C., Dingman, S., Ward, L., Meybeck, M., 2006. Effective sea-level rise and deltas: Causes of change and human dimension implications. Glob. Planet. Change 50, 63–82. https://doi.org/10.1016/j.gloplacha.2005.07.004

Erlenkeuser, H., Pederstad, K., 1984. Recent sediment accumulation in Skagerrak as depicted by 210pb-dating. Nor. Geol. Tidsskr. 18.

Fettweis, M., Francken, F., Van Den Eynde, D., Verwaest, T., Janssens, J., Van Lancker, V., 2010. Storm influence on SPM concentrations in a coastal turbidity maximum area with high anthropogenic impact (southern North Sea). Cont. Shelf Res. 30, 1417–1427. https://doi.org/10.1016/j.csr.2010.05.001

Feyling-Hanssen, R.W., n.d. in Late Quaternary deposits from the Oslofjord area 426.

Flemming, B.W., 2002. Effects of Climate and Human Interventions on the Evolution of the Wadden Sea Depositional System (Southern North Sea), in: Wefer, G., Berger, W.H., Behre, K.-E., Jansen, E. (Eds.), Climate Development and History of the North Atlantic Realm. Springer Berlin Heidelberg, Berlin, Heidelberg, pp. 399–413. https://doi.org/10.1007/978-3-662-04965-5_26

Flemming, B.W., Nyandwi, N., 1994. Land reclamation as a cause of fine-grained sediment depletion in backbarrier tidal flats (Southern North Sea). Neth. J. Aquat. Ecol. 28, 299–307. https://doi.org/10.1007/BF02334198

Folk, R.L., Ward, W.C., 1957. Brazos River bar [Texas]; a study in the significance of grain size parameters. J. Sediment. Res. 27, 3–26. https://doi.org/10.1306/74D70646-2B21-11D7-8648000102C1865D

Foucher, A., Chaboche, P.-A., Sabatier, P., Evrard, O., 2021. A worldwide meta-analysis (1977–2020) of sediment core dating using fallout radionuclides including ¹³⁷Cs and ²¹⁰Pb_{xs} Earth Syst. Sci. Data 13, 4951–4966. https://doi.org/10.5194/essd-13-4951-2021

Garcia Agudo, E., 1998. Global distribution of 137Cs inputs for soil erosion and sedimentation studies, in: International Atomic Energy Agency (Ed.), Use of 137Cs in the Study of Soil Erosion and Sedimentation. IAEA-TECDOC-1028 117–121.

Graf, W.L., 2006. Downstream hydrologic and geomorphic effects of large dams on American rivers. Geomorphology 79, 336–360. https://doi.org/10.1016/j.geomorph.2006.06.022

Graven, H., Allison, C.E., Etheridge, D.M., Hammer, S., Keeling, R.F., Levin, I., Meijer, H.A.J.J., Rubino, M., Tans, P.P., Trudinger, C.M., Vaughn, B.H., White, J.W.C., 2017. Compiled records of carbon isotopes in atmospheric CO 2 for historical simulations in CMIP6. Geosci. Model Dev. 10, 4405–4417. https://doi.org/10.5194/GMD-10-4405-2017

Green, M.O., Vincent, C.E., McCave, I.N., Dickson, R.R., Rees, J.M., Pearsons, N.D., 1995. Storm sediment transport: observations from the British North Sea shelf. Cont. Shelf Res. 15, 889–912. https://doi.org/10.1016/0278-4343(95)80001-T

Gyllencreutz, R., Backman, J., Jakobsson, M., Kissel, C., Arnold, E., 2006. Postglacial palaeoceanography in the Skagerrak. The Holocene 16, 975–985. https://doi.org/10.1177/0959683606hl988rp

Hass, H.C., 1996. Northern Europe climate variations during late Holocene: evidence from marine Skagerrak. Palaeogeogr. Palaeoclimatol. Palaeoecol. 123, 121–145. https://doi.org/10.1016/0031-0182(95)00114-X

Heier-Nielsen, S., Conradsen, K., Heinemeier, J., Knudsen, K.L., Nielsen, H.L., Rud, N., Sveinbjörnsdóttir, Á.E., 1995. Radiocarbon Dating of Shells and Foraminifera from the Skagen Core, Denmark: Evidence of Reworking. Radiocarbon 37, 119–130. https://doi.org/10.1017/S0033822200030551

Heinatz, K., Scheffold, M.I.E., 2023. A first estimate of the effect of offshore wind farms on sedimentary organic carbon stocks in the Southern North Sea. Front. Mar. Sci. 9, 1068967. https://doi.org/10.3389/fmars.2022.1068967

Hiddink, J.G., Van De Velde, S.J., McConnaughey, R.A., De Borger, E., Tiano, J., Kaiser, M.J., Sweetman, A.K., Sciberras, M., 2023. Quantifying the carbon benefits of ending bottom trawling. Nature 617, E1–E2. https://doi.org/10.1038/s41586-023-06014-7

Hjulstrom, F., 1939. Transportation of detritus by moving water. PD Trask Ed Recent Mar. Sediments Am Assoc Pet. Geol. Tulsa 5–31.

Hoeksema, R.J., 2007. Three stages in the history of land reclamation in the Netherlands. Irrig. Drain. 56, S113–S126. https://doi.org/10.1002/ird.340

Hofstede, J., 2008. Coastal Flood Defence and Coastal Protection along the North Sea Coast of Schleswig-Holstein. Küste 134–142.

Holland, K.T., Elmore, P.A., 2008. A review of heterogeneous sediments in coastal environments. Earth-Sci. Rev. 89, 116–134. https://doi.org/10.1016/j.earscirev.2008.03.003

Hübner, G., Schwandt, D., 2018. EXTREME LOW FLOW AND WATER QUALITY – A LONG-TERM VIEW ON THE RIVER ELBE. Erdkunde 72, 235–252.

Hylander, L.D., Meili, M., 2003. 500 years of mercury production: global annual inventory by region until 2000 and associated emissions. Sci. Total Environ. 304, 13–27. https://doi.org/10.1016/S0048-9697(02)00553-3

ICES, 2020. Greater North Sea ecoregion ? Fisheries overview, including mixed-fisheries considerations. https://doi.org/10.17895/ICES.ADVICE.7605

ICES, 2019. Working Group on the Effects of Extraction of Marine Sediments on the Marine Ecosystem (WGEXT). https://doi.org/10.17895/ICES.PUB.5733

ICES, 2018. Greater North Sea Ecoregion ? Ecosystem overview. https://doi.org/10.17895/ICES.PUB.4670

IKSE, 2012. Abschlussbericht über die Erfüllung des „Aktionsplans Hochwasserschutz Elbe“ im Zeitraum 2003–2011.

IKSE, 2005. Die Elbe und ihr Einzugsgebiet – Ein geographisch-hydrologischer und wasserwirtschaftlicher Überblick.

Jaworowski, Z., 1966. Temporal and Geographical Distribution of Radium D (Lead-210). Nature 212, 886–889. https://doi.org/10.1038/212886a0

Jaworowski, Z., Kownacka, L., Grotowski, K., Kwiatkowski, K., 1978. Lead-210 from nuclear explosions in the environment. Nucl. Technol. 37, 159–166.

Kelletat, D., 1992. Coastal Erosion and Protection Measures at the German North Sea Coast. J. Coast. Res. 8, 699–711.

Key, R.M., Kozyr, A., Sabine, C.L., Lee, K., Wanninkhof, R., Bullister, J.L., Feely, R.A., Millero, F.J., Mordy, C., Peng, T. -H., 2004. A global ocean carbon climatology: Results from Global Data Analysis Project (GLODAP). Glob. Biogeochem. Cycles 18, 2004GB002247. https://doi.org/10.1029/2004GB002247

Klaminder, J., Appleby, P., Crook, P., Renberg, I., 2012. Post-deposition diffusion of ^{137}Cs in lake sediment: Implications for radiocaesium dating. Sedimentology 59, 2259–2267. https://doi.org/10.1111/j.1365-3091.2012.01343.x

Koide, M., Bruland, K.W., Goldberg, E.D., 1973. Th-228/Th-232 and Pb-210 geochronologies in marine and lake sediments. Geochim. Cosmochim. Acta 37, 1171–1187. https://doi.org/10.1016/0016-7037(73)90054-9

Krishnaswamy, S., Lal, D., Martin, J.M., Meybeck, M., 1971. Geochronology of lake sediments. Earth Planet. Sci. Lett. 11, 407–414. https://doi.org/10.1016/0012-821X(71)90202-0

Kristensen, E., Røy, H., Debrabant, K., Valdemarsen, T., 2018. Carbon oxidation and bioirrigation in sediments along a Skagerrak-Kattegat-Belt Sea depth transect. Mar. Ecol. Prog. Ser. 604, 33–50. https://doi.org/10.3354/meps12734

Lange, D., Müller, H., Piechotta, F., Schubert, R., 2008. The Weser Estuary. Küste 275–287.

Large, W.G., Yeager, S.G., 2009. The global climatology of an interannually varying air–sea flux data set. Clim. Dyn. 33, 341–364. https://doi.org/10.1007/s00382-008-0441-3

Leipe, T., Moros, M., Kotilainen, A., Vallius, H., Kabel, K., Endler, M., Kowalski, N., 2013. Mercury in Baltic Sea sediments—Natural background and anthropogenic impact. Geochemistry 73, 249–259. https://doi.org/10.1016/j.chemer.2013.06.005

Lodder, Wang, Elias, Van Der Spek, De Looff, Townend, 2019. Future Response of the Wadden Sea Tidal Basins to Relative Sea-Level rise—An Aggregated Modelling Approach. Water 11, 2198. https://doi.org/10.3390/w11102198

Lohmann, G., Butzin, M., Eissner, N., Shi, X., Stepanek, C., 2020. Abrupt Climate and Weather Changes Across Time Scales. Paleoceanogr. Paleoclimatology 35, e2019PA003782. https://doi.org/10.1029/2019PA003782

Madsen, A.T., Murray, A.S., Andersen, T.J., Pejrup, M., 2007. Temporal changes of accretion rates on an estuarine salt marsh during the late Holocene — Reflection of local sea level changes? The Wadden Sea, Denmark. Mar. Geol. 242, 221–233. https://doi.org/10.1016/j.margeo.2007.03.001

Mai, S., Bartholomä, A., 2000. The missing mud flats of the Wadden Sea: a reconstruction of sediments and accommodation space lost in the wake of land reclamation, in: Proceedings in Marine Science. Elsevier, pp. 257–272. https://doi.org/10.1016/S1568-2692(00)80021-2

Maire, O., Lecroart, P., Meysman, F., Rosenberg, R., Duchêne, J., Grémare, A., 2008. Quantification of sediment reworking rates in bioturbation research: a review. Aquat. Biol. 2, 219–238. https://doi.org/10.3354/ab00053

Mathis, M., Elizalde, A., Mikolajewicz, U., Pohlmann, T., 2015. Variability patterns of the general circulation and sea water temperature in the North Sea. Prog. Oceanogr. 135, 91–112. https://doi.org/10.1016/j.pocean.2015.04.009

McCAVE, I.N., Swift, S.A., 1976. A physical model for the rate of deposition of fine-grained sediments in the deep sea. Geol. Soc. Am. Bull. 87, 541. https://doi.org/10.1130/0016-7606(1976)87<541:APMFTR>2.0.CO;2

Meinshausen, M., Vogel, E., Nauels, A., Lorbacher, K., Meinshausen, N., Etheridge, D.M., Fraser, P.J., Montzka, S.A., Rayner, P.J., Trudinger, C.M., Krummel, P.B., Beyerle, U., Canadell, J.G., Daniel, J.S., Enting, I.G., Law, R.M., Lunder, C.R., O'Doherty, S., Prinn, R.G., Reimann, S., Rubino, M., Velders, G.J.M., Vollmer, M.K., Wang, R.H.J., Weiss, R., 2017. Historical greenhouse gas concentrations for climate modelling (CMIP6). Geosci. Model Dev. 10, 2057–2116. https://doi.org/10.5194/gmd-10-2057-2017

Mielck, F., Hass, H.C., Michaelis, R., Sander, L., Papenmeier, S., Wiltshire, K.H., 2019. Morphological changes due to marine aggregate extraction for beach nourishment in the German Bight (SE North Sea). Geo-Mar. Lett. 39, 47–58. https://doi.org/10.1007/s00367-018-0556-4

Mollenhauer, G., Grotheer, H., Gentz, T., Bonk, E., Hefter, J., 2021. Standard operation procedures and performance of the MICADAS radiocarbon laboratory at Alfred Wegener Institute (AWI), Germany. Nucl. Instrum. Methods Phys. Res. Sect. B Beam Interact. Mater. At. 496, 45–51. https://doi.org/10.1016/j.nimb.2021.03.016

Moros, M., Andersen, T.J., Schulz-Bull, D., Häusler, K., Bunke, D., Snowball, I., Kotilainen, A., Zillén, L., Jensen, J.B., Kabel, K., Hand, I., Leipe, T., Lougheed, B.C., Wagner, B., Arz, H.W., 2017. Towards an event stratigraphy for Baltic Sea sediments deposited since AD 1900: approaches and challenges. Boreas 46, 129–142. https://doi.org/10.1111/bor.12193

Nordberg, K., Bergsten, H., 1988. Biostratigraphic and sedimentological evidence of hydrographic changes in the Kattegat during the later part of the Holocene. Mar. Geol. 83, 135–158. https://doi.org/10.1016/0025-3227(88)90056-4

Oost, A., Colina Alonso, A., Esselink, P., Wang, Z.B., Kessel, T. van, Maren, B. van, 2021. Where mud matters: towards a mud balance for the trilateral Wadden Sea Area: mud supply, transport and deposition. Wadden Academy, Leeuwarden.

OSPAR, 2023. OSPAR Quality Status Synthesis Report 2023. oap.ospar.org.

Otto, L., Zimmerman, J.T.F., Furnes, G.K., Mork, M., Saetre, R., Becker, G., 1990. Review of the physical oceanography of the North Sea. Neth. J. Sea Res. 26, 161–238. https://doi.org/10.1016/0077-7579(90)90091-T

Paetzel, M., Schrader, H., Bjerkli, K., 1994. Do decreased trace metal concentrations in surficial skagerrak sediments over the last 15–30 years indicate decreased pollution? Environ. Pollut. 84, 213–226. https://doi.org/10.1016/0269-7491(94)90132-5

Pätsch, J., Lorkowski, I., Kühn, W., Moll, A., Serna, A., 2010. 150 years of ecosystem evolution in the North Sea-from pristine conditions to acidification. Eur. Geophys. Union Gen. Assem. 2010 Vienna Austria 2010 12291.

Polovodova Asteman, I., Risebrobakken, B., Moros, M., Binczewska, A., Dobosz, S., Jansen, E., Sławińska, J., Bąk, M., 2018. Late Holocene palaeoproductivity changes: a multi-proxy study in the Norwegian Trench and the Skagerrak, North Sea. Boreas 47, 238–255. https://doi.org/10.1111/bor.12264

Puls, W., Heinrich, H., Mayer, B., 1997. Suspended particulate matter budget for the German Bight. Mar. Pollut. Bull. 34, 398–409. https://doi.org/10.1016/S0025-326X(96)00161-0

Qvale, G., Nigam, R., 1985. Bolivina skagerrakensis, a new name for Bolivina cf. B. robusta, with notes on its ecology and distribution. J. Foraminifer. Res. 15, 6–12. https://doi.org/10.2113/gsjfr.15.1.6

Regard, V., Prémaillon, M., Dewez, T.J.B., Carretier, S., Jeandel, C., Godderis, Y., Bonnet, S., Schott, J., Pedoja, K., Martinod, J., Viers, J., Fabre, S., 2022. Rock coast erosion: An overlooked source of sediments to the ocean. Europe as an example. Earth Planet. Sci. Lett. 579, 117356. https://doi.org/10.1016/j.epsl.2021.117356

Reimer, P.J., Brown, T.A., Reimer, R.W., 2004. Discussion: Reporting and Calibration of Post-Bomb 14C Data. Radiocarbon 46, 1299–1304. https://doi.org/10.1017/S0033822200033154

Rijnsdorp, A.D., Boute, P., Tiano, J., Lankheet, M., Soetaert, K., Beier, U., de Borger, E., Hintzen, N.T., Molenaar, P., Polet, H., Poos, J.J., Schram, E., Soetaert, M., van Overzee, H., van De Wolfshaar, K., van Kooten, T., 2020. The implications of a transition from tickler chain beam trawl to electric pulse trawl on the sustainability and ecosystem effects of the fishery for North Sea sole: an impact assessment. Wageningen Marine Research, IJmuiden,. https://doi.org/10.18174/519729

Robbins, J.A., Edgington, D.N., 1975. Determination of recent sedimentation rates in Lake Michigan using Pb-210 and Cs-137. Geochim. Cosmochim. Acta 39, 285–304. https://doi.org/10.1016/0016-7037(75)90198-2

Rodhe, J., 1998. The Baltic and North Seas: a process-oriented review of the physical oceanography. The sea 11, 699–732.

Rodhe, J., 1996. On the dynamics of the large-scale circulation of the skagerrak. J. Sea Res. 35, 9–21. https://doi.org/10.1016/S1385-1101(96)90731-5

Rodhe, J., 1987. The large-scale circulation in the Skagerrak; interpretation of some observations. Tellus A 39A, 245–253. https://doi.org/10.1111/j.1600-0870.1987.tb00305.x

Rosenberg, R., Hellman, B., Lundberg, A., 1996. Benthic macrofaunal community structure in the Norwegian Trench, deep skagerrak. J. Sea Res. 35, 181–188. https://doi.org/10.1016/S1385-1101(96)90745-5

Sala, E., Mayorga, J., Bradley, D., Cabral, R.B., Atwood, T.B., Auber, A., Cheung, W., Costello, C., Ferretti, F., Friedlander, A.M., Gaines, S.D., Garilao, C., Goodell, W., Halpern, B.S., Hinson, A., Kaschner, K., Kesner-Reyes, K., Leprieur, F., McGowan, J., Morgan, L.E., Mouillot, D., Palacios-Abrantes, J., Possingham, H.P., Rechberger, K.D., Worm, B., Lubchenco, J., 2021. Protecting the global ocean for biodiversity, food and climate. Nature 592, 397–402. https://doi.org/10.1038/s41586-021-03371-z

Sanchez-Cabeza, J.A., Ruiz-Fernández, A.C., 2012. 210Pb sediment radiochronology: An integrated formulation and classification of dating models. Geochim. Cosmochim. Acta 82, 183–200. https://doi.org/10.1016/j.gca.2010.12.024

Schmidt, M., 2021. Dynamics and variability of POC burial in depocenters of the North Sea (Skagerrak), Cruise No. AL561, 2.08.2021 – 13.08.2021, Kiel – Kiel, APOC. GEOMAR Helmholtz Centre for Ocean Research Kiel. https://doi.org/10.3289/CR_AL561

Skogen, M.D., Eilola, K., Hansen, J.L.S., Meier, H.E.M., Molchanov, M.S., Ryabchenko, V.A., 2014. Eutrophication status of the North Sea, Skagerrak, Kattegat and the Baltic Sea in present and future climates: A model study. J. Mar. Syst. 132, 174–184. https://doi.org/10.1016/j.jmarsys.2014.02.004

Slavik, K., Lemmen, C., Zhang, W., Kerimoglu, O., Klingbeil, K., Wirtz, K.W., 2019. The large-scale impact of offshore wind farm structures on pelagic primary productivity in the southern North Sea. Hydrobiologia 845, 35–53. https://doi.org/10.1007/s10750-018-3653-5

Spiegel, T., Dale, A.W., Lenz, N., Schmidt, M., Sommer, S., Kalapurakkal, H.T., Przibilla, A., Lindhorst, S., Wallmann, K., 2023. Biogenic silica cycling in the Skagerrak. Front. Mar. Sci. 10. https://doi.org/10.3389/fmars.2023.1141448

Spiegel, T., Diesing, M., Dale, A.W., Lenz, N., Schmidt, M., Sommer, S., Böttner, C., Fuhr, M., Kalapurakkal, H.T., Wallmann, K., 2024. Modelling mass accumulation rates and 210 Pb rain rates in the Skagerrak: lateral sediment transport dominates the sediment input. Front. Mar. Sci. 11. https://doi.org/10.3389/fmars.2023.1141448

Ståhl, H., Tengberg, A., Brunnegård, J., Bjørnbom, E., Forbes, T.L., Josefson, A.B., Kaberi, H.G., Hassellöv, I.M.K., Olsgard, F., Roos, P., Hall, P.O.J., 2004. Factors influencing organic carbon recycling and burial in Skagerrak sediments. J. Mar. Res. 62, 867–907. https://doi.org/10.1357/0022240042880873

Stanev, E.V., Dobrynin, M., Pleskachevsky, A., Grayek, S., Günther, H., 2009. Bed shear stress in the southern North Sea as an important driver for suspended sediment dynamics. Ocean Dyn. 59, 183–194. https://doi.org/10.1007/s10236-008-0171-4

Stevens, R.L., Bengtsson, H., Lepland, A., 1996. Textural provinces and transport interpretations with fine-grained sediments in the Skagerrak. J. Sea Res. 35, 99–110. https://doi.org/10.1016/S1385-1101(96)90739-X

Streets, D.G., Devane, M.K., Lu, Z., Bond, T.C., Sunderland, E.M., Jacob, D.J., 2011. All-Time Releases of Mercury to the Atmosphere from Human Activities. Environ. Sci. Technol. 45, 10485–10491. https://doi.org/10.1021/es202765m

Stride, A.H. (Ed.), 1982. Offshore tidal sands: processes and deposits. Chapman and Hall, London ; New York.

Syvitski, J.P.M., Vörösmarty, C.J., Kettner, A.J., Green, P., 2005. Impact of Humans on the Flux of Terrestrial Sediment to the Global Coastal Ocean. Science 308, 376–380. https://doi.org/10.1126/science.1109454

Thomas, H., Freund, W., Mears, C., Meckel, E., Minutolo, F., Nantke, C., Neumann, A., Seidel, M., Van Dam, B., 2022. ALKOR Scientific Cruise Report. The Ocean's Alkalinity - Connecting geological and metabolic processes and time-scales: mechanisms and magnitude of metabolic alkalinity generation in the North Sea Cruise No. AL557. Open Access. Alkor-Berichte, AL557. GEOMAR Helmholtz-Zentrum für Ozeanforschung Kiel, Kiel, Germany, 22 pp.

Toggweiler, J.R., Dixon, K., Bryan, K., 1989. Simulations of radiocarbon in a coarse-resolution world ocean model: 1. Steady state prebomb distributions. J. Geophys. Res. Oceans 94, 8217–8242. https://doi.org/10.1029/JC094iC06p08217

van Weering, T.C.E., Berger, G.W., Kalf, J., 1987. Recent sediment accumulation in the Skagerrak, Northeastern North Sea. Neth. J. Sea Res. 21, 177–189. https://doi.org/10.1016/0077-7579(87)90011-1

van Weering, T.C.E., Berger, G.W., Okkels, E., 1993. Sediment transport, resuspension and accumulation rates in the northeastern Skagerrak. Mar. Geol. 111, 269–285. https://doi.org/10.1016/0025-3227(93)90135-I

van Weering, T.C.E., Qvale, G., 1983. Recent sediments and foraminiferal distribution in the Skagerrak, northeastern North Sea. Mar. Geol. 52, 75–99. https://doi.org/10.1016/0025-3227(83)90022-1

van Wijnen, H.J., Bakker, J.P., 2001. Long-term Surface Elevation Change in Salt Marshes: a Prediction of Marsh Response to Future Sea-Level Rise. Estuar. Coast. Shelf Sci. 52, 381–390. https://doi.org/10.1006/ecss.2000.0744

Wacker, L., Fahrni, S.M., Hajdas, I., Molnar, M., Synal, H.-A., Szidat, S., Zhang, Y.L., 2013. A versatile gas interface for routine radiocarbon analysis with a gas ion source. Nucl. Instrum. Methods Phys. Res. Sect. B Beam Interact. Mater. At. 294, 315–319. https://doi.org/10.1016/j.nimb.2012.02.009

Wahl, T., Haigh, I.D., Woodworth, P.L., Albrecht, F., Dillingh, D., Jensen, J., Nicholls, R.J., Weisse, R., Wöppelmann, G., 2013. Observed mean sea level changes around the North Sea coastline from 1800 to present. Earth-Sci. Rev. 124, 51–67. https://doi.org/10.1016/j.earscirev.2013.05.003

Wallmann, K., Diesing, M., Scholz, F., Rehder, G., Dale, A.W., Fuhr, M., Suess, E., 2022. Erosion of carbonate-bearing sedimentary rocks may close the alkalinity budget of the Baltic Sea and support atmospheric CO2 uptake in coastal seas. Front. Mar. Sci. 9, 968069. https://doi.org/10.3389/fmars.2022.968069

Wanninkhof, R., 2014. Relationship between wind speed and gas exchange over the ocean revisited. Limnol. Oceanogr. Methods 12, 351–362. https://doi.org/10.4319/lom.2014.12.351

Winther, N.G., Johannessen, J.A., 2006. North Sea circulation: Atlantic inflow and its destination. J. Geophys. Res. Oceans 111, 2005JC003310. https://doi.org/10.1029/2005JC003310

Modeling mass accumulation rates and ^{210}Pb rain rates in the Skagerrak: Lateral sediment transport dominates the sediment input

Timo Spiegel[1*], Markus Diesing[2], Andrew W. Dale[1], Nina Lenz[1], Mark Schmidt[1], Stefan Sommer[1], Christoph Böttner[3], Michael Fuhr[1], Habeeb Thanveer Kalapurakkal[1], Cosima-S. Schulze[4], Klaus Wallmann[1]

[1] GEOMAR Helmholtz Centre for Ocean Research Kiel, Wischhofstraße 1–3, 24148 Kiel, Germany

[2] Geological Survey of Norway, P.O. Box 6315, Torgarden, 7491 Trondheim, Norway

[3] Aarhus University, Institute for Geoscience, Høegh-Guldbergs Gade 2, 8000, Aarhus, Denmark

[4] Albert-Ludwigs-Universität Freiburg, Institute of Earth and Environmental Sciences, Tennenbacher Str. 4, 79106 Freiburg, Germany

***Correspondence:**
Timo Spiegel
tspiegel@geomar.de

Keywords: Machine learning, Mass accumulation rate, Sedimentation rate, Porosity, Spatial distribution, ^{210}Pb, Skagerrak, North Sea.

Abstract

Sediment fluxes to the seafloor govern the fate of elements and compounds in the ocean and serve as a prerequisite for research on elemental cycling, benthic processes and sediment management strategies. To quantify these fluxes over seafloor areas, it is necessary to scale up sediment mass accumulation rates (MAR) obtained from multiple sample stations. Conventional methods for spatial upscaling involve averaging of data or spatial interpolation. However, these approaches may not be sufficiently precise to account for spatial variations of MAR, leading to poorly constrained regional sediment budgets. Here, we utilize a machine learning approach to scale up porosity and ^{210}Pb data from 145 and 65 stations, respectively, in the Skagerrak. The models predict the spatial distributions by considering several predictor variables that are assumed to control porosity and ^{210}Pb rain rates. The spatial distribution of MAR is based on the predicted porosity and existing sedimentation rate data. Our findings reveal highest MAR and ^{210}Pb rain rates to occur in two parallel belt structures that align with the general circulation pattern in the Skagerrak. While high ^{210}Pb rain rates occur in intermediate water depths, the belt of high MAR is situated closer to the coastlines due to lower porosities at shallow water depths. Based on the spatial distributions, we calculate a total MAR of 34.7 Mt yr^{-1} and a ^{210}Pb rain rate of $4.7 \cdot 10^{14}$ dpm yr^{-1}. By comparing atmospheric to total ^{210}Pb rain

rates, we further estimate that 24% of the ^{210}Pb originates from the local atmospheric input, with the remaining 76% being transported laterally into the Skagerrak. The updated MAR in the Skagerrak is combined with literature data on other major sediment sources and sinks to present a tentative sediment budget for the North Sea, which reveals an imbalance with sediment outputs exceeding the inputs. Substantial uncertainties in the revised Skagerrak MAR and the literature data might close this imbalance. However, we further hypothesize that previous estimates of suspended sediment inputs into the North Sea might have been underestimated, considering recently revised and elevated estimates on coastal erosion rates in the surrounding region of the North Sea.

III.1 Introduction

Bulk sediment fluxes control the transport and distribution of many substances in the water and sediment column, such as organic carbon and pollutants. Furthermore, in coastal and shelf regions that are used economically, sediment budgets are crucial to assess the anthropogenic pressure on the natural systems, such as the disturbance of surface sediments and redistribution of sedimentary material, and to set up management plans for seafloor resources (Walling and Collins, 2008; Morang et al., 2012). An integral part of the sediment cycle is the accumulation and subsequent burial of particles at the seafloor, which acts as the ultimate sink in many marine geochemical mass balances. In regional sediment budgets, estimates of area-wide sediment mass accumulation rates (MAR) are often obtained by averaging and subsequent upscaling of the average MAR to the study area extent. This approach has been applied in previous studies to estimate sediment budgets in the North Sea and Skagerrak (van Weering et al., 1987; Bøe et al., 1996; De Haas et al., 1996; De Haas and van Weering, 1997). However, the traditional upscaling technique is unable to resolve non-linear spatial heterogeneities between individual data sites, which is particularly important in such dynamic regions. As a result, current area-wide quantifications derived using the averaging technique are likely associated with high uncertainties.

The Skagerrak represents the largest depocenter for sediments from the North Sea. With the dynamic hydrography, complex seabed topography and high data density, the Skagerrak offers an ideal setting to examine MAR in an environment with various sedimentation patterns. Furthermore, the Skagerrak and North Sea sedimentary systems have been increasingly impacted by anthropogenic activities such as bottom trawling (ICES, 2020), sediment extraction (De Groot, 1986; ICES, 2019; Mielck et al., 2019) or offshore wind park constructions (Heinatz and Scheffold, 2023) since industrial times. Hence, sediment budgeting in this area may improve our understanding of sediment redistribution in a changing environment. In this study, a machine learning approach was applied to upscale the gathered data from literature studies and own sampling campaigns and predict the spatial distributions of sediment water content (porosity) and ^{210}Pb rain rates in the Skagerrak. Based on the

modeled porosity and published spatial data on sedimentation rates (Diesing et al., 2021), we present an area-wide MAR and compare it to previous estimates. The radionuclide ^{210}Pb is known to be readily scavenged by particles in the water column and to settle alongside sediments (e.g. Krishnaswamy et al., 1971; Nittrouer et al., 1979; Nozaki et al., 1991). Hence, the spatial distribution of ^{210}Pb rain rates serves as an indicator of sedimentation rates and is compared to the sedimentation patterns previously presented in Diesing et al. (2021). Furthermore, area-wide ^{210}Pb rain rates are utilized to estimate the contributions of local and lateral inputs in the Skagerrak. Finally, we compare the machine learning approach with previous estimates based on upscaling that used the averaging approach.

III.2 Study area

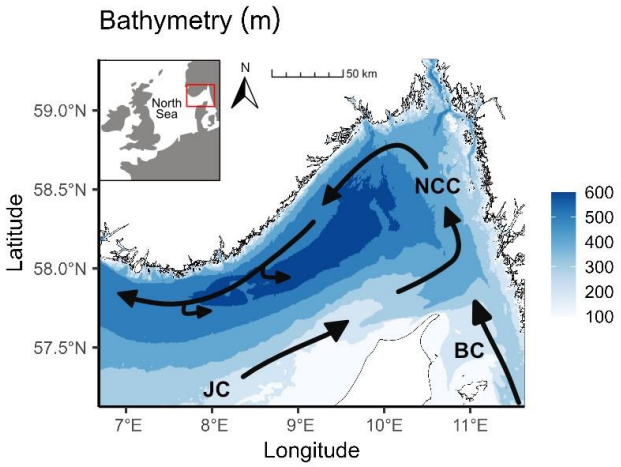

Figure III1. Study area with information on water depth. Black arrows indicate the current regime. The Jutland Current (JC) originates from the south and merges with the Baltic Current (BC) to form the Norwegian Coastal Current (NCC), which leaves the Skagerrak northwards.

The Skagerrak is located between Denmark, Norway, and Sweden and connects the North Sea and the Kattegat, with water depths reaching about 700 meters (Fig. III1). The Jutland current carries water and suspended particles from the central and southern North Sea to the Skagerrak, where it meets the Baltic current and continues to circulate anticlockwise before leaving the Skagerrak northward through the Norwegian Coastal Current (van Weering et al., 1987; Otto et al., 1990). Towards the northeastern Skagerrak, current velocities decrease and the particles transported into the Skagerrak settle. As a result, the Skagerrak sediments are characterized by a large lateral input primarily consisting of lithogenic material from the North Sea (van Weering et al., 1993; De Haas and van Weering, 1997). The sediment composition varies throughout the region, with sand (< 40% clay) being common along the Danish coast while fine-grained silt and clay sediments dominate the Skagerrak basin at water depth below ~150 m (Stevens et al., 1996; P. J. Mitchell et al., 2019). The

sediment column is potentially subject to substantial reworking due to bottom trawling by fisheries at water depths shallower than approximately 300-500 m (ICES, 2020).

III.3 Material and Methods

A machine learning model was employed to scale up the data of individual stations and determine the spatial distributions of the desired variables porosity and ^{210}Pb rain rate (response variables). In principle, high-resolution spatial data of parameters that were assumed to correlate with the response variables, e.g. bathymetry or grain size (predictor variables), were sourced from the available literature in the study area. These predictor variables were leveraged by the model to predict the spatial distribution of the response variables at the same resolution as the predictors using a quantile regression forest (QRF) algorithm (Meinshausen, 2006).

III.3.1 Data collection

III.3.1.1 Response variables

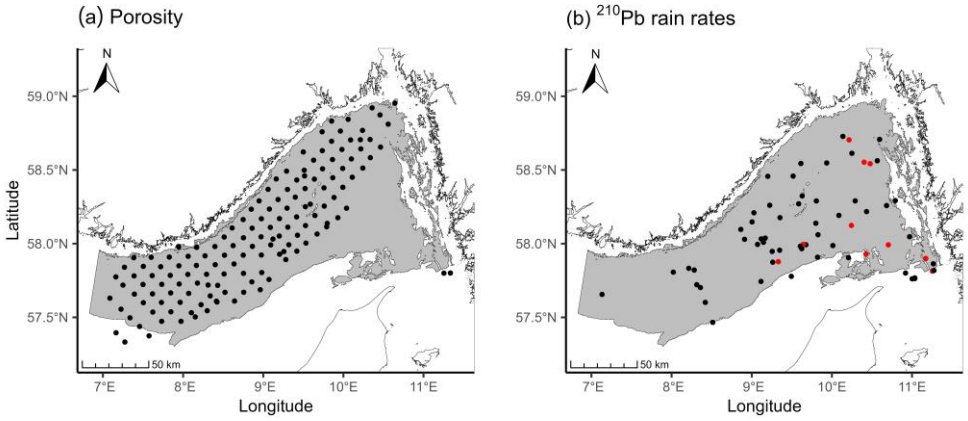

Figure III2. Stations where data was available for (a) porosity and (b) ^{210}Pb rain rates that were utilized for spatial predictions. The gray area refers to the area of applicability (AOA) of the model. Stations marked in red indicate disturbed ^{210}Pb profiles that do not reach natural background levels at the bottom of the sediment core, likely due to physical mixing by currents and waves or bottom trawling.

Most of the data used to determine the spatial distribution of porosity were sourced from the PANGAEA database by applying a data warehouse search over the area of interest. The downloaded data were filtered to retain records with realistic porosity values between 20% and 100%, as the range of typical values of porosity is 50 - 90% for unconsolidated muddy sediments and 25 - 50% for sandy sediments (Richardson and Jackson, 2017). Additionally, we limited the dataset to the upper 0.1 m of sediment depth. Data on ^{210}Pb were collected from various publications (Erlenkeuser and

Pederstad, 1984; Erlenkeuser, 1985; van Weering et al., 1987; Wilken et al., 1990; van Weering et al., 1993; Paetzel et al., 1994; Beks, 2000; Ståhl et al., 2004; Ferdelman, 2005a, 2005b, 2005c; Deng et al., 2020). A full summary of the porosity and ^{210}Pb data is given in the supplement (Tab. IIIS1, IIIS2). The literature data were complemented with data from nine short sediment cores (< 50 cm) recovered over two sampling campaigns in the Skagerrak, AL557 and AL561, with R/V Alkor in June and August 2021, respectively (Schmidt, 2021; Thomas et al., 2022; Spiegel et al., 2023). Porosity was determined by weighting sediment samples before and after conventional drying in an oven or freeze-drying. The porosity was then calculated from the difference between the two weights and the density of dry solids of the sediment, which was either measured or assumed (2.3 - 2.6 g cm^{-3}). Measurements of ^{210}Pb were carried out by alpha or gamma spectrometry. In marine sediments, the term excess ^{210}Pb (^{210}Pb$_{ex}$) refers to the ^{210}Pb content that is introduced by sinking particles and excludes the ^{210}Pb resulting from the natural background decay of ^{226}Ra within the sediment column. ^{210}Pb$_{ex}$ values were obtained either by subtracting the natural background activities of ^{226}Ra or by subtracting the steady-state ^{210}Pb activity in sediment depths below the profile of exponential ^{210}Pb decay. In some studies, the raw ^{210}Pb values were not explicitly provided but were depicted either as linear or double logarithmic plots. In those cases, the activity data were carefully extracted from the figures by graphical evaluation. In total, the dataset consists of porosity and ^{210}Pb data gathered from 194 and 65 locations, respectively (Fig. III2, Tab. IIIS1, IIIS2). Averaging porosity values in the same grid cell of the model resulted in 145 porosity values for the machine learning procedure (see section III3.2).

To determine total ^{210}Pb rain rates to the seafloor (FPb), the ^{210}Pb$_{ex}$ activity data were integrated over the sediment column ranging from the surface (0) to the depth where the ^{210}Pb activities reached natural background levels (max) and multiplied by the decay constant (Cochran et al., 1990; Alperin et al., 2002):

$$\mathrm{FPb} = \int_0^{\max} \mathrm{Pb} \cdot \lambda \cdot \rho_{\mathrm{DB}}\, \mathrm{dx} \quad \text{(III1)}$$

$$\rho_{\mathrm{DB}} = \mathrm{ds} \cdot (1\text{-}\phi) \quad \text{(III2)}$$

where Pb is the ^{210}Pb$_{ex}$ activity, λ is the ^{210}Pb decay constant (0.031 yr^{-1}), ρ_{DB} is the dry bulk density, ds is the density of dry solids that was assumed to be 2.5 g cm^{-3} and ϕ is depth-dependent porosity. An interpolation function was fitted through the downcore ^{210}Pb$_{ex}$ data using the program Mathematica 12.2. This function was integrated over the entire sediment core to determine the depth-integrated ^{210}Pb$_{ex}$ activity. At 10 stations, ^{210}Pb$_{ex}$ at the bottom of the sediment core did not reach natural background levels. Hence, the ^{210}Pb$_{ex}$ inventories were underestimated at these sites to an uncertain extent (highlighted in red in Fig. III2b). Considering the exponential decline of ^{210}Pb$_{ex}$

activities with sediment depth, and generally low $^{210}Pb_{ex}$ activities observed at these sites, a relatively minor error was expected by including these stations.

For a comparison between atmospheric ^{210}Pb input rates and total ^{210}Pb rain rates, it is usually necessary to consider the production of ^{210}Pb by the in-situ decay of ^{226}Ra in the water column (Cochran et al., 1990). However, given the long half-life of ^{226}Ra (1600 yr), along with the large sedimentary inventory of ^{210}Pb and relatively shallow water depths in the Skagerrak, the decay of ^{226}Ra in the water column contributes < 1% to the sedimentary ^{210}Pb pool. Thus, a correction for this fraction was not performed.

III.3.1.2 Predictor variables

Initially, a wide range of potential predictor variables was selected considering their data availability at a sufficient spatial resolution and full area coverage in the Skagerrak, including topographic, sedimentological, hydrodynamic, and oceanographic variables. Porosity and ^{210}Pb rain rates were expected to be controlled by particle transport and the characteristics of the transported particles in the Skagerrak. Hence, bathymetry, current velocity, distance to the shoreline and suspended particulate matter concentrations were chosen as predictor variables as they directly or indirectly reflect particle transport and distribution (Tab. III1). Since the particle size has been shown to be closely related to porosity (Wilson et al., 2018), the content of silt and clay in surface sediments was also chosen as a predictor variable. Furthermore, the ratio of the tidal benthic boundary layer thickness to water depth is important for sediment transport dynamics near the seabed (Williams et al., 2019) and was deemed an important environmental control on sediment fluxes in a previous study (Diesing et al., 2021). Temperature and salinity were also included as predictor variables as they have been shown to reflect the contributions of different water masses to the Skagerrak, i.e. from the North Sea, Baltic Sea and local riverine input (Kristiansen and Aas, 2015) that carry the sediment and ^{210}Pb into the Skagerrak. Despite ^{210}Pb being closely related to bulk sediment fluxes, we opted to exclude the spatial distribution of sedimentation rates (Diesing et al., 2021) from the list of predictor variables. This decision was made to avoid circularity arguments, as the presented sedimentation rate data in the literature itself is derived from ^{210}Pb measurements.

The predictor variables were gathered from various sources with unequal spatial extent, projection, and resolution. To create a stack of predictor layers, the predictor raster data were separately cropped to the area of interest depending on the initial resolution and projection. Subsequently, the predictors were reprojected to a common projection (Lambert azimuthal equal-area) and a resolution of 500 m by 500 m). The grid cells were aligned prior to modeling. The response data were averaged in those cases where more than one value fell into a grid cell of the predictor stack.

Table III1. List of predictor variables used in the ^{210}Pb rain rate and porosity models.

Predictor variable	Model	Source	Resolution (arcmin)[a]
Bathymetry (m)	^{210}Pb	EMODnet Bathymetry Consortium (2018), Mitchell et al. (2019a)	0.125
Ratio of tidal boundary layer thickness to water depth (-)	^{210}Pb	Williams et al. (2019)	1.5 · 1.0
Mean tidal current speed at the seafloor (m s^{-1})	^{210}Pb	Mitchell et al. (2019a, c)	0.125
Maximum surface current speed (m s^{-1})	^{210}Pb	https://bio-oracle.org, Tyberghein et al. (2012), Assis et al. (2018)	5.0
Minimum surface current speed (m s^{-1})	^{210}Pb	https://bio-oracle.org, Tyberghein et al. (2012), Assis et al. (2018)	5.0
Maximum surface water temperature (°C)	^{210}Pb	https://bio-oracle.org, Tyberghein et al. (2012), Assis et al. (2018)	5.0
Minimum surface water temperature (°C)	^{210}Pb	https://bio-oracle.org, Tyberghein et al. (2012), Assis et al. (2018)	5.0
Mean bottom water salinity	^{210}Pb	https://bio-oracle.org, Tyberghein et al. (2012), Assis et al. (2018)	5.0
Mean surface water salinity	^{210}Pb	https://bio-oracle.org, Tyberghein et al. (2012), Assis et al. (2018)	5.0
Minimum bottom water salinity	^{210}Pb	https://bio-oracle.org, Tyberghein et al. (2012), Assis et al. (2018)	5.0
Maximum surface water salinity	^{210}Pb	https://bio-oracle.org, Tyberghein et al. (2012), Assis et al. (2018)	5.0
Content of silt and clay in surface sediments (%)	Porosity	Mitchell et al. (2019a, b)	0.125
Summer suspended particulate matter (g m^{-3})	Porosity	Mitchell et al. (2019a, c)	0.125
Euclidean distance to shoreline (m)	Porosity	Calculated	0.125
Mean bottom water temperature (°C)	Porosity	https://bio-oracle.org, Tyberghein et al. (2012), Assis et al. (2018)	5.0

[a] 0.125 arcmin are ~ 116m · 230m, 1.5 · 1.0 arcmin are ~ 1.5km · 1.0 km and 5 arcmin are ~ 4.9km · 9.2 km (x · y) at a latitude of 58°N, representative of the research area.

III.3.2 Machine learning models

The complete analysis was carried out in the free software environment for statistical computing and graphics R 4.2.3 (R Core Team, 2022) and RStudio 2023.03.0. This section provides an overview of the methodology used to spatially predict porosity and ^{210}Pb rain rates. We first give an overview of the workflow and its key features. The subsequent sections give more detailed information on the algorithms and R packages that were used.

III.3.2.1 Overview

The goal of this study is to determine the spatial distribution of a variable in a specific area. However, only a limited number of precise measurements of this variable is at our disposal. The task is therefore to estimate the variable at unsampled locations. This can be achieved by spatial prediction, which is the estimation of unknown quantities based on sample data and assumptions regarding the form of the trend and its variance and spatial correlation (Bivand et al., 2008). There are different types of spatial prediction models such as deterministic (e.g., inverse distance weighted interpolation) and

stochastic methods (e.g., kriging). Here, we opted for a data-driven machine learning approach, because such models are flexible, can fit nonlinear and complex relationships, and do not need to satisfy strict statistical assumptions as opposed to stochastic models. In addition, such approaches allow users to quantify the uncertainty in the predictions.

Machine learning spatial models make predictions based on learned relationships between the variable to be predicted (response variable) and predictor variables, which exist with better coverage over the area of interest. Initially, it might be prudent to select a wide range of potentially relevant predictor variables, ideally based on a conceptual model (Guisan and Zimmermann, 2000) of the environmental system to be modeled. It is, however, generally recommended to limit the number of predictor variables that are finally used for modeling, as the predictive power decreases with an increase in the number of predictor variables given a fixed number of response data points (Hughes, 1968). The aims of variable selection are threefold: (1) to improve the prediction performance, (2) to enable faster predictions, and (3) to increase the interpretability of the model (Guyon and Elisseeff, 2003). Here, we use a forward selection approach whereby the model performance of various combinations of predictors is determined. Starting with combinations of two predictors, the number of predictors is increased until the model performance increases no longer.

Cross-validation is usually employed for model tuning and predictor variable selection. A frequently used scheme is k-fold cross-validation, whereby the dataset is randomly partitioned into k parts (folds) of approximately equal size. A single fold is retained for validating the model, while the remaining k - 1 folds are used to train the model. This is repeated k times, such that every fold serves as validation data once. The performance of a trained model can then be tested based on independent data not used for model building. However, truly independent test data are rarely available due to the costs of collecting sample data offshore. Holding back a fraction (usually 20-50%) of the data from model building and using this dataset for model testing might sometimes be an alternative. However, this requires a sufficiently large dataset. Additionally, a single split into training and test data might be unrepresentative and may provide misleading information about estimates and their uncertainty (Lyons et al., 2018). Because of these limitations, k-fold cross-validation is frequently used for model validation.

The use of machine learning algorithms in spatial prediction has strongly increased in recent years due to the advantages mentioned above and the seemingly high performance that is frequently achieved. However, it has been shown that model performance indicators might be inflated when spatial autocorrelation in the data is ignored (Ploton et al., 2020). To account for this, spatially separated folds can be generated for cross-validation. This is achieved by separating the sample data into spatial blocks of a size that accounts for spatial autocorrelation in the data. The blocks are subsequently randomly assigned to folds (Valavi et al., 2019).

Sampling design should be an integral part of spatial prediction and modeling to ensure good coverage of the environmental and geographic space (Biswas and Zhang, 2018). However, due to the costs of obtaining new sample data, making use of existing data stored in databases is crucial. This does mean that the set of sampling stations used for modeling rarely constitutes an optimal sampling design. Tools exist to gain insights to what extent the existing sample data deviates from an optimal design. Diesing (2020) provided plots that allow to assess to what extent the selected samples cover the environmental space of the predictor variables. Meyer and Pebesma (2022) compared the distributions of the spatial distances of sample data to their nearest neighbor with the distribution of distances from all points of prediction locations within an area of interest to the nearest sample data point. They showed that in the case of a spatially random sample dataset, which is a preferred design for spatial prediction, the two distribution curves overlap to a large extent. Model performance can be estimated with a random cross-validation in such a case. Conversely, clustered sample datasets show nearest neighbor distances between samples that are shorter than the distances from the prediction locations to the nearest sample data point. Spatial cross-validation is advised to derive realistic estimates of model performance.

Another way of accounting for limitations in the distribution of the sample data is to estimate the area in which the predictive model is valid. This area of applicability (AOA) of a model is defined as the area where the model was enabled to learn about relationships based on the training data, and where the estimated cross-validation performance holds. To delineate the AOA, a dissimilarity index (DI) is initially calculated. The DI is based on distances to the training data in the multidimensional predictor variable space. To account for the relevance of predictor variables responsible for prediction patterns variables are weighted by the model-derived variable importance scores prior to distance calculation. The AOA is then derived by applying a threshold based on the DI observed in the training data using cross-validation (Meyer and Pebesma, 2021).

III.3.2.2 Quantile regression forests

The QRF algorithm (Meinshausen, 2006) was selected to generate spatial predictions of porosity and ^{210}Pb rain rates. QRF can be seen as an extension of the random forest (RF) algorithm (Breiman, 2001), which has shown high predictive accuracy in several studies across various research domains (Prasad et al., 2006; Mutanga et al., 2012; Oliveira et al., 2012; Huang et al., 2014). The RF is an ensemble technique that creates regression trees using the predictor and response data. Each tree is constructed from a bootstrapped sample and a random subset of the predictor variables is used at each split in the tree-building process, making every tree in the forest unique. Individually, each tree in the forest may be a poor predictor and any combination of two trees can give different predictions. However, by aggregating the predictions over many uncorrelated trees, prediction variance is

reduced, and accuracy is improved (James et al., 2013). RF can handle a large number of predictor variables, is insensitive to the inclusion of noisy predictors, can be used without extensive parameter tuning, and makes no assumptions regarding the shape of distributions of the response or predictor variables (Cutler et al., 2007). While RF outputs the mean over many regression trees to make an ensemble prediction, the QRF algorithm also returns the whole distribution of the response variable, based on which other measures of central tendency (e.g. median) and prediction uncertainty can be obtained. Following common practice in the global soil mapping community (Arrouays et al., 2014; Heuvelink, 2014), we used the 90% prediction interval (PI90) as a measure of spatially explicit uncertainty. PI90 gives the range of values within which the true value is expected to occur nine times out of ten, with a one in twenty probability for each of the two tails (Arrouays et al., 2014). It is defined as:

$$PI90 = q_{0.95} - q_{0.05} \quad \text{(III3)}$$

with $q_{0.95}$ and $q_{0.05}$ being the 0.95 and 0.05 quantiles of the distribution, respectively. We chose the median as a measure of central tendency, as the conditional distributions were expected to be non-normal, and the median was not affected by extreme outliers.

As RF, and by extension QRF, has been shown to perform well without extensive parameter tuning (Cutler et al., 2007), we only carried out limited parameter tuning. The number of variables to consider at any given split (m_{try}) was tuned as part of the forward feature selection (see below). It is usually sufficient to set the number of trees in the forest (n_{tree}) to a high value; 500 was selected in this case.

III.3.2.3 Predictor variable selection

Predictor variable selection can be achieved in different ways. Here, we chose forward feature (variable) selection as implemented in the package "CAST" (Meyer et al., 2018). The algorithm first trained the models based on all possible combinations of two predictor variables. The best combination was retained and tested for the best performance with a third variable. Additional variables are added until the performance stops to increase. The model performance was calculated as R^2 using a spatial cross-validation scheme. Processing time increased with the number of predictors and response data points. The number of observations in the ^{210}Pb dataset was sufficiently small to run the forward feature selection on all predictor variables. However, it was decided to run a predictor variable pre-selection in the case of the porosity model. This pre-selection process first only retained important variables that performed better than random variables using the Boruta algorithm (Kursa and Rudnicki, 2010). In a second step, a de-correlation analysis was carried out to limit the collinearity. This was achieved with the "vifcor" function of the package "usdm" (Naimi et al., 2014). The function required a correlation threshold and the predictor variables as input to

calculate variance inflation factors (VIF) of the predictors. The correlation threshold was stepwise decreased from 1 with a step size of 0.01 and predictors with a VIF ≥ 5 were removed. This process was repeated until the VIFs of all predictors were below 5 to avoid a problematic amount of collinearity (James et al., 2013).

A full list of the predictor variables that were selected by the models is provided in Table III1.

III.3.2.4 Spatial cross-validation

The estimation of model performance was based on k-fold cross-validation, whereby the response data were split into k folds. The model was built on k - 1 folds and validated against the fold which was not used for model building. This process was repeated k times, where k was set to 3. In the case of spatially clustered data, spatial autocorrelation might lead to inflated estimates of model performance (Roberts et al., 2017; Ploton et al., 2020). Folds therefore needed to be spatially separated and this was achieved with the function "cv_spatial" of the package "blockCV" (Valavi et al., 2019). The block size was initially determined by estimating the spatial autocorrelation range of the response data with the "automap package" (Hiemstra et al., 2009). The distance functions of the sample-to-sample, prediction-to-sample, and cross-validation distances were plotted with the "plot_geodist" function of "CAST" (Meyer and Pebesma, 2021) and the block size was altered by applying a multiplier to the spatial autocorrelation range until there was a visual agreement between the distance functions of the prediction-to-sample and cross-validation distances.

The performances of the final models were assessed based on the explained variance (R^2) and the root mean square error (RMSE). Correlation plots between measured and predicted data are shown in the supplement (Fig. IIIS1, IIIS2).

III.3.2.5 Area of applicability

We estimate the area of applicability (AOA) of the two models with the "aoa" function of the package "CAST" (Meyer and Pebesma, 2020). The spatial predictions and areawide quantifications presented in this study refer to the joint AOA of both the porosity and ^{210}Pb rain rate models, which spans an area of 21,270 km^2.

III.3.3 Calculation of MAR

In each grid cell of the model, predicted porosities were multiplied with existing spatial data of sedimentation rates (Diesing et al., 2021) to determine the spatial distribution of MAR:

$$\mathrm{MAR} = \rho_{\mathrm{DB}} \cdot \mathrm{SR} \quad \text{(III4)}$$

where ρ_{DB} is the dry bulk density (Eq. III2) and SR is the sedimentation rate.

Uncertainties for MAR (u(MAR)) were propagated by the uncertainties of ρ_{DB} and sedimentation rate from the literature (Diesing et al., 2021):

$$u(\rho_{DB}) = \rho_{DB} \cdot \left(\frac{u(\phi)}{1-\phi}\right) \quad \text{(III5)}$$

$$u(MAR) = MAR \cdot \sqrt{\left(\frac{u(\rho_{DB})}{\rho_{DB}}\right)^2 + \left(\frac{u(SR)}{SR}\right)^2} \quad \text{(III6)}$$

where $u(\rho_{DB})$, $u(\phi)$ and u(SR) are the uncertainties for dry bulk density, porosity, and sedimentation rates. The uncertainty of ds was assumed to be 0 g cm^{-3}. We note that the uncertainty calculation of porosity in this study differs from the approach for sedimentation rates in Diesing et al. (2021).

III.4 Results

III.4.1 Porosity

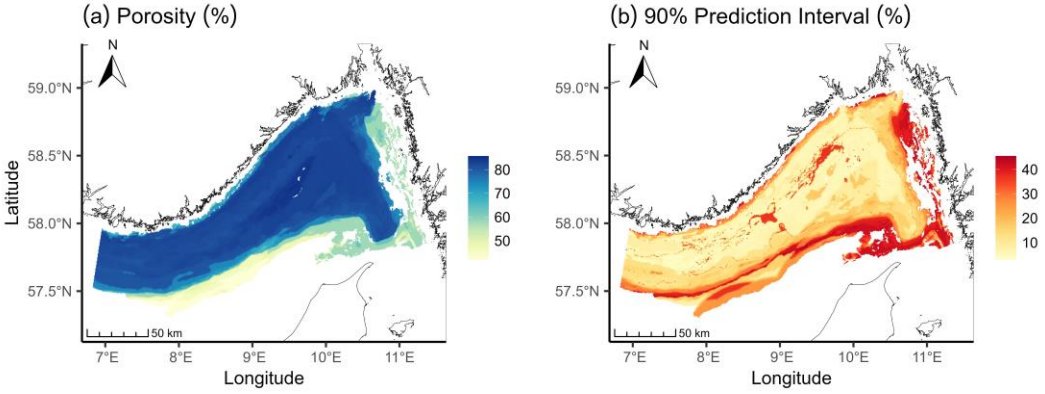

Figure III3. (a) Predicted spatial distribution of porosity and (b) associated uncertainty of the prediction.

The four predictor variables for porosity selected by the model were the content of silt and clay in surface sediments, the distance to shoreline, mean bottom water temperatures and concentrations of suspended particulate matter during summer (Tab. III1). Predicted porosities varied between 42 and 86 %, while the uncertainty ranged from 3 to 47 % (Fig. III3). The RMSE of the model was 5.1 % and the R^2 was 0.8 (Fig. IIIS1). High porosities were observed in the basin below approximately 400 m water depth and low values along the coastlines at shallower water depths.

III.4.2 Mass accumulation rate

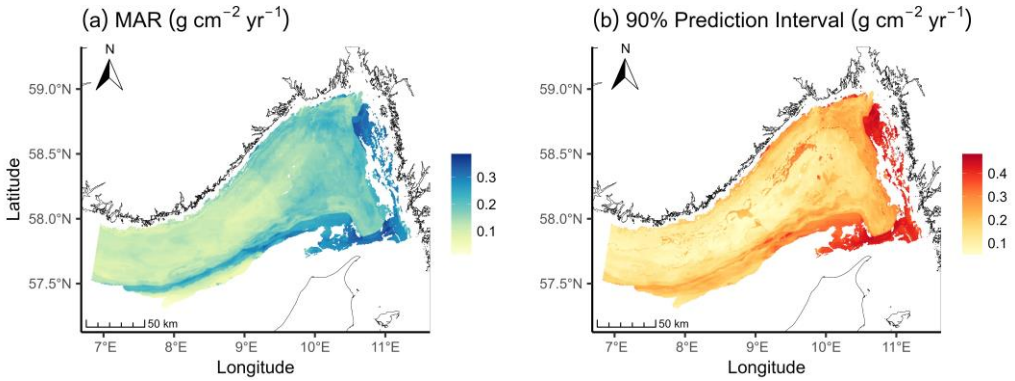

Figure III4. (a) Calculated spatial distribution of MAR and (b) associated uncertainty of the prediction.

Total MAR within the joint AOA of 21,270 km^2 was 34.7 Mt yr^{-1} with an uncertainty of 39.8 Mt yr^{-1} (Fig. III4). The MAR varied between 0.01 and 0.38 g cm^{-2} yr^{-1} with the uncertainty ranging from 0.05 to 0.51 g cm^{-2} yr^{-1}. High MARs were observed in a narrow belt between 300 and 350 m water depth in the southwestern part. The belt widens as it extends towards the northeastern part to up to 130 m water depth. Intermediate MAR occurred in the central Skagerrak basin, while lowest MAR were found in the southwestern part of the Skagerrak basin and along the Danish coastline at shallow water depth.

III.4.3 ^{210}Pb rain rate

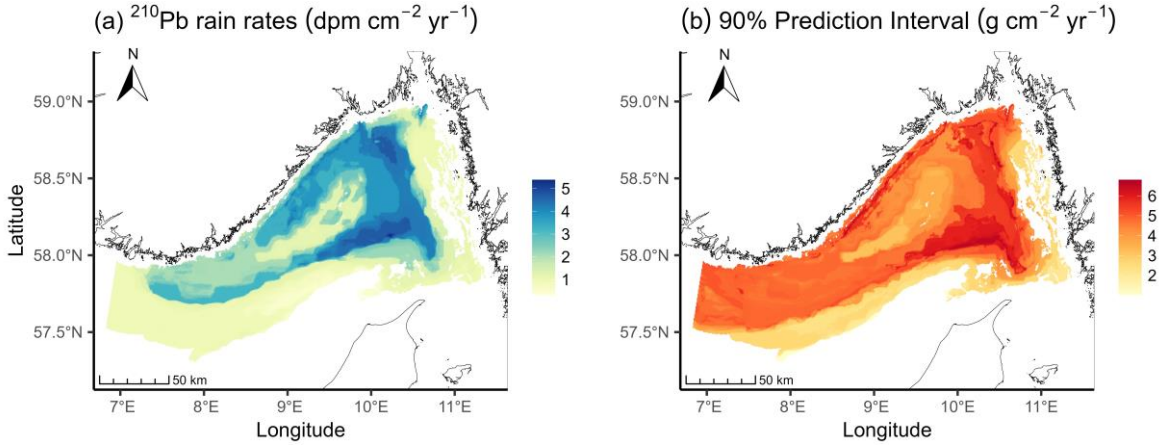

Figure III5. (a) Predicted spatial distribution of ^{210}Pb rain rates and (b) associated uncertainty of the prediction.

The predictor variables for the ^{210}Pb rain rate selected by the model were bathymetry, minimum and maximum surface current velocity and temperature, tidal current velocity at the seafloor, the ratio of tidal boundary layer thickness to water depth and minimum, maximum, as well as mean bottom and surface salinity. The predicted total ^{210}Pb rain rate in the joint AOA was $4.7 \cdot 10^{14}$ dpm yr^{-1} with an uncertainty of $9.3 \cdot 10^{14}$ dpm yr^{-1} (Fig. III5). The ^{210}Pb rain rates varied between 0.3 and 5.4 dpm cm^{-2} yr^{-1} with uncertainties ranging from 1.0 to 6.8 dpm cm^{-2} yr^{-1}. The model had an RMSE of 1.4 dpm cm^{-2} yr^{-1} and an R^2 of 0.41 (Fig. IIIS2). The highest rates were found in a belt structure along the basin between approximately 120 and 600 m water depth. Intermediate ^{210}Pb rain rates were predicted at the flanks of the high accumulation belt and in the central Skagerrak basin. The lowest rates were found along the Danish coastline at shallower water depths.

III.5 Discussion

III.5.1 Spatial distribution of porosity, MAR and ^{210}Pb rain rates

Certain patterns in the spatial variability of porosity, MAR, and ^{210}Pb rain rates can be explained by the hydrographic regime, indicating that the sediment transport broadly follows the general water circulation in the Skagerrak. Towards the northeastern part of the Skagerrak the current velocities decrease (van Weering et al., 1987, 1993), which promotes particle settling and contributes to the formation of belts characterized by high MAR and ^{210}Pb rain rates. In the case of MAR, the belt is located closer towards the coast at shallower water depths of up to 130 m. Since the MAR is a function of sedimentation rates and porosity (Eq. III5), where lower porosities lead to higher MAR, the shift of the belt towards the coastline can be explained by the spatial variability of the porosity (Fig. III3). Lower porosities close to the coastlines are indicative of coarser particle settling as a result of a more energetic hydrodynamic regime preventing the deposition of fine sediments. This relationship is consistent with the spatial grain size data in the Skagerrak (Stevens et al., 1996; Mitchell et al., 2019). Conversely, high porosities found at greater water depths reflect the dominance of finer particles at the seafloor that settle due to reduced current velocities. The belt of elevated ^{210}Pb rain rates is situated in the area of high porosity and extends along the basin between 120 and 600 m water depth. The close relationship between ^{210}Pb rain rate and sediment transport is reflected in similar spatial patterns of the ^{210}Pb rain rates compared to previously published sedimentation rates (Diesing et al., 2021). Intermediate to high ^{210}Pb rain rates, sedimentation rates, and high porosities in large parts of the region suggest a substantial input of fine particles that may be delivered by lateral transport into the Skagerrak (see section III5.3).

In some areas along the coastlines at shallow water depths, the ^{210}Pb rain rates are comparable to, or lower than, the atmospheric ^{210}Pb input of 0.52 dpm cm^{-2} yr^{-1} (Peirson et al., 1966; Beks et al., 1998;

Baskaran, 2011), indicating no lateral sediment input or net seafloor erosion in these areas (Fig. III5). A possible explanation is the physical disturbance by waves and currents, leading to the resuspension of surface sediments at the seafloor. Given the exponential shape of a ^{210}Pb activity profile, continuous resuspension and subsequent relocation of ^{210}Pb-rich surface sediments could explain the depleted ^{210}Pb inventories at these sites. Considering the fishery activities in shallow waters and their impact on the seafloor in the North Sea and Skagerrak (ICES, 2020; Zhang et al., 2023), relocation of surface sediments by bottom trawling is another potential reason behind the ^{210}Pb loss. Supporting this hypothesis, disturbed ^{210}Pb profiles (Fig. III2b) that may be indicative of bottom trawling (Spiegel et al., 2023) exclusively occur at shallow water depths < 400 m in line with the footprint of bottom trawling on the seafloor of the Skagerrak.

III.5.2 Total MAR and ^{210}Pb rain rates in the Skagerrak

The spatial distributions predicted by the machine learning models allowed for an estimate of the total MAR and ^{210}Pb rain rates in the Skagerrak. When integrating the rates across the joint AOA of the two models of 21270 km^2, the Skagerrak exhibits a MAR of 34.7 ± 39.8 Mt yr^{-1} and a ^{210}Pb rain rate of $4.7 \cdot 10^{14} \pm 9.3 \cdot 10^{14}$ dpm yr^{-1}. The presented rates are applicable for the last ~ 100 years, as the ^{210}Pb rain rates and the sedimentation rates used to calculate the MAR depend on ^{210}Pb activities in the sediment, of which roughly 97% is decayed after five times the half-life of ^{210}Pb (22.3 years). Hence, the results are representative as average values since the beginning of extensive human activities in the Skagerrak and North Sea (ICES, 2018, 2019, 2020; OSPAR, 2023) and can be used for comparisons with the sediment system of pre-industrial times. The presented MAR is comparable to previous estimates of 28 Mt yr^{-1} and 46 Mt yr^{-1} for the same area slightly differing in size (van Weering et al., 1987; De Haas and van Weering, 1997) and 19 Mt yr^{-1} in the Norwegian part of the Skagerrak (Bøe et al., 1996). Their results were based on averaging sedimentation rate data and either assuming or measuring values for the porosity and density of dry solids to calculate area-wide MAR. Hence, the difference in the estimates is likely due to utilizing different data sets and upscaling methods.

III.5.3 Proportions of local and lateral ^{210}Pb and sediment inputs

By comparing ^{210}Pb rain rates at the seafloor with the atmospheric ^{210}Pb flux, it is possible to estimate the proportions of local and lateral ^{210}Pb inputs (DeMaster et al., 1986; Biscaye and Anderson, 1994), where the atmospheric flux is considered as the local source for ^{210}Pb. Assuming a constant spatial and temporal atmospheric ^{210}Pb flux of 0.52 dpm cm^{-2} yr^{-1} (Peirson et al., 1966; Beks et al., 1998; Baskaran, 2011) across the Skagerrak, the ^{210}Pb input by the atmosphere was calculated to be 1.1 ·

10^{14} dpm yr^{-1}. Hence, the total ^{210}Pb rain rate of $4.7 \cdot 10^{14}$ dpm yr^{-1} is about 4 times the atmospheric input. The relative proportions of the local and lateral inputs are 24% and 76%, respectively. Consequently, lateral transport from outside the study area is the main source of ^{210}Pb in the Skagerrak. No details on the provenance of the lateral load can be derived from our evaluation. However, it is likely that a substantial portion stems from the southern and central North Sea as proposed by previous studies (Zöllmer and Irion, 1993; Bengtsson and Stevens, 1998; Irion and Zöllmer, 1999; Lepland et al., 2000).

De Haas and van Weering (1997) presented proportions of local and lateral organic matter inputs in the Skagerrak based on total organic carbon accumulation rates and primary production rates. They proposed that primary production only contributes about 10% to the total organic carbon accumulation rate, while the remaining 90% is transported laterally into the Skagerrak. We argue that the high affinity for particles and the otherwise conservative behavior make ^{210}Pb a favorable indicator for separating the lateral and local inputs of MAR. Despite its high particle reactivity, ^{210}Pb activities in deposits can be further affected by TOC contents (Xu et al., 2011; Anjum et al., 2017), the grain-size distribution (He and Walling, 1996) and sediment redistribution, making the assumption of a proportional relationship between ^{210}Pb and sediment fluxes in a natural system uncertain (Sanchez-Cabeza and Ruiz-Fernández, 2012). Such effects may become even more pronounced when considering that particle transport from the North Sea to the Skagerrak requires about two years (Hainbucher et al., 1987; Dahlgaard et al., 1995; Salomon et al., 1995). For instance, during transport from the North Sea, resuspension might introduce buried and already decayed ^{210}Pb to the lateral particle load. Conversely, the lateral load could be continuously recharged by fresh ^{210}Pb from the atmosphere. Decay during the transit is unlikely to significantly affect ^{210}Pb activities given the travel times and a ^{210}Pb half-life of 22.3 years. Since a detailed understanding of the relationship between long transit times, resuspension, and their impact on ^{210}Pb activities is unknown, the local and lateral sediment inputs we obtained represent a rough estimate. Assuming that the proportions of the local and lateral inputs derived from ^{210}Pb can be applied to the MAR, we calculated local and lateral sediment inputs of 8.2 and 26.5 Mt yr^{-1}, respectively. Local sediment sources usually constitute aeolian input and primary production. Considering primary production rate estimates of 90 - 190 g m^{-2} yr^{-1} in the Skagerrak (Anton et al., 1993; Meyenburg and Liebezeit, 1993; Heilmann et al., 1994; Richardson and Heilmann, 1995; Skogen et al., 1995; De Haas and van Weering, 1997; Skogen and Søiland, 2006), multiplication with the AOA yields a primary production of 1.9 - 4.0 Mt yr^{-1} in the research area. Hence, our results indicate that aeolian inputs account for a significant fraction of the local input. However, there exist significant uncertainties in both the earlier estimates and in our ^{210}Pb-based calculations. Furthermore, previous studies indicated substantial temporal variability of primary production rates in the Skagerrak (Binczewska et al., 2018; Louchart et al., 2022). Hence, a more comprehensive approach, such as the application of organic carbon

diagenetic modeling, is required to constrain the role of primary production in the local sediment input.

III.5.4 Tentative sediment budget of the North Sea

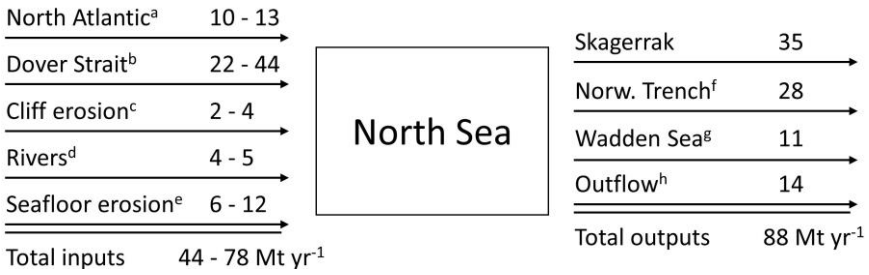

Figure III6. Tentative sediment budget for the North Sea. The major contributors to the sediment input include transport from (a) the North Atlantic (Eisma and Irion, 1988; Puls et al., 1997; Eisma, 2009) and (b) the Dover Strait (McManus and Prandle, 1997; Fettweis et al., 2007; Eisma, 2009), (c) cliff erosion (Eisma and Irion, 1988), (d) riverine input (Eisma and Irion, 1988) and (e) seafloor erosion (Eisma and Irion, 1988; Van Alphen, 1990; ICONA, 1992). Sediment outputs include deposition in the Skagerrak (this study), (f) the Norwegian Trench (De Haas et al., 1996) and (g) the Wadden Sea (Oost et al., 2021) and (h) outflow towards the North Atlantic (Eisma, 2009). All numbers are given in million tons of sediment per year.

Based on our updated estimate on MAR and the existing literature, we derived a tentative sediment budget for the North Sea (Fig. III6). Minor contributors to the sediment budget (< 3 Mt yr^{-1}) such as the Baltic Current input or sediment extraction were not considered in this budget, as their sum constituted only a small fraction of the overall sediment budget and sources and sinks of these minor contributors mostly balance out (Oost et al., 2021). Total sediment input into the North Sea amounts to 44 - 78 Mt yr^{-1}. The main contributors include sediment transport via the North Atlantic (Eisma and Irion, 1988; Puls et al., 1997; Eisma, 2009), the Dover Strait (McManus and Prandle, 1997; Fettweis et al., 2007; Eisma, 2009), cliff erosion along the UK coastline (Eisma and Irion, 1988; Puls et al., 1997), riverine inputs (Eisma and Irion, 1988) and seafloor erosion (Eisma and Irion, 1988; Van Alphen, 1990; ICONA, 1992). Total sediment outputs at depocenters in the North Sea and by the outflow to the North Atlantic are 88 Mt yr^{-1}. Of that, 35 Mt yr^{-1} are deposited in the Skagerrak, supporting the notion that this region is the main depocenter for sediments from the North Sea. The Wadden Sea, in the southern and central North Sea, acts as another major sediment sink and traps approximately 11 Mt of the total sediment input annually (Oost et al., 2021). Furthermore, substantial MAR on the order of 28 Mt yr^{-1} has been previously reported in the Norwegian Trench (De Haas et al., 1996). The remainder of 14 Mt yr^{-1} that is not deposited at the seafloor leaves the North Sea through the Norwegian Coastal Current (Eisma, 2009). The overview reveals an imbalance between sedimentary sources and sinks in the North Sea, with sinks exceeding the sources. It is important to note the substantial uncertainties associated with the presented estimates, which may explain the

observed imbalance. However, we further emphasize that the riverine inputs play a relatively minor role, while the particle transport through the northern Atlantic entrance and the Dover Straight are the major sediment sources for the North Sea. Most of the suspended load carried by both of these channels is probably supplied by erosion at coastlines surrounding the North Sea region. Recent studies have demonstrated that coastal erosion is a more dominant source than previously thought in the European seas (Regard et al., 2022) including the Baltic Sea (Wallmann et al., 2022). Hence, we suggest that current estimates of the channel inputs might be underestimated and could potentially close the sediment budget in the North Sea. The tentative North Sea sediment budget demonstrates the need to constrain the quantities of the different major sediment pathways for a comprehensive sediment budget in the North Sea.

III.5.5 Model appraisal, limitations, and future directions

We applied a machine learning approach to spatially predict sediment porosity and ^{210}Pb rain rates in the Skagerrak, while previous studies employed averaging to scale up individual data points in the Skagerrak (van Weering et al., 1987; Bøe et al., 1996; de Haas et al., 1996; de Haas and van Weering, 1997). We opted for machine learning as it has been previously demonstrated to be successful in predicting sedimentation rates and organic carbon densities in the same region (Diesing et al., 2021). Moreover, the machine learning approach shows principal advantages over averaging: (1) Machine learning yields spatially explicit results that can be displayed as maps. This allowed us to identify differences in the spatial patterns of MAR and ^{210}Pb rain rate, which were presented in section III5.1. In contrast, upscaling by averaging would yield one value applicable to the whole area, but without information about spatial variability. (2) The uncertainty of the predictions was assessed in a robust and spatially explicit way. Previous studies, as cited above, have provided estimates of the sediment accumulation, but no uncertainty has been given. (3) Although not investigated here, it is generally possible to explore the relationships between the response variable and the predictor variables with tools like variable importance and partial dependence plots (Hastie et al., 2009). This might help improve model building and understanding of the driving forces of the spatial patterns of the variable under consideration.

Although high uncertainties were calculated, it is important to keep in mind the definition of uncertainty we used (Eq. III3). The PI90 gives the range of values within which the true value is expected to occur in 90% percent of the cases. Other studies have used the standard deviation (Diesing et al., 2021), a conformal prediction methodology (Restreppo et al., 2021) or none (Mitchell et al., 2021), leading to lower estimated uncertainties. Additionally, the propagation of uncertainties when calculating MAR (Eq. III6) has increased the associated uncertainty estimates. This could be

alleviated by directly predicting the MAR. However, this would require sufficient stations where sedimentation rates and dry bulk density or porosity have been measured.

General difficulties associated with sediment budgeting have been discussed in the literature (Brown et al., 2009; Parsons, 2012; Walton et al., 2012). Uncertainties include data availability, data quality and the applied upscaling approach. In our study, it was not possible to quantitatively address uncertainties owing to the data quality of the predictor and response variables, as measurement errors were rarely reported, and different sampling strategies and measurement techniques were applied in the complied literature. Therefore, improving the model performance and reducing the uncertainties was largely dependent on the available amount of response data and how the stations are distributed in space. Ideally, one should design a sampling survey prior to modeling in a way that optimizes the coverage of the samples in the study area. This could be achieved by, e.g., a simple random design (Meyer and Pebesma, 2022). However, data collection at sea is time and resource-consuming, and not making use of existing datasets would be a wasteful practice. We therefore followed the advice of Meyer and Pebesma (2021) and estimated the AOA of our models. The AOA results could be used for directing future sampling surveys to areas where the environment has not been sufficiently captured (Fig. III2). Such a strategy would allow collecting additional data in an informed way to reduce uncertainties in the spatial distributions.

Predictor variables affected the performance based on their predictive capability, data quality and spatial resolution. A wide set of spatial data was available in the Skagerrak, enabling us to test their potential as predictors and ultimately providing a sufficient amount for the machine learning model. However, most of these predictors originate from the Bio-ORACLE global dataset (Tyberghein et al., 2012; Assis et al., 2018) with a spatial resolution of 5 arcmin, limiting the resolution of the model's grid and its ability to consider fine-scale heterogeneities below the resolution of the raster stack. Hence, additional high-quality data on predictor variables could improve the predictive capability of the machine learning models to constrain the presented spatial distributions of porosity, MAR and ^{210}Pb rain rates.

III.6 Conclusion

In this study, we present the spatial distributions of porosity, ^{210}Pb rain rates and mass accumulation rates (MAR) in the Skagerrak based on machine learning. High MAR and ^{210}Pb rain rates are observed within two similar belt structures. The MAR belt is situated at shallower water depths given lower porosities towards the coast, while the ^{210}Pb belt extends along the basin. The calculated areawide MAR is 34.7 ± 39.8 Mt yr^{-1} and ^{210}Pb rain rate is $4.7 \cdot 10^{14} \pm 9.3 \cdot 10^{14}$ dpm yr^{-1}. By comparing the total ^{210}Pb rain rate to the atmospheric ^{210}Pb input, we calculate that 24 % of the ^{210}Pb

stems from the atmosphere, with the remainder of 76 % being transported laterally into the Skagerrak. Considering the high particle reactivity of ^{210}Pb, these proportions are applied to the MAR to broadly estimate the local and lateral sediment inputs of 8.2 and 26.5 Mt yr^{-1}, respectively. We further present a tentative sediment budget for the North Sea, which reveals sedimentary sinks to be higher compared to the sources. Large uncertainties in the budget estimates may explain the imbalance. We further suggest that sediment inputs through the northern North Atlantic entrance and the Dover Straight could be underestimated. Although the machine learning approach currently represents one of the state-of-the-art methods for upscaling, large uncertainties in the predicted quantities persist. Incorporating more response data in areas that lie outside the AOA of the models could improve the predicted spatial distributions. The findings of this study contribute to the characterization of the Skagerrak region, particularly in terms of sediment mass balances and its role as the major depocenter for sediments from the North Sea. The spatial distributions can be used to validate ecosystem models and vice versa and provide a knowledge basis for resource management plans. Furthermore, the presented machine learning method for spatial upscaling can be applied to other regions to gain insights into areawide distribution patterns.

Acknowledgements

We thank the captain and crew of RV Alkor for supporting our research at sea, as well as our colleagues Bettina Domeyer, Anke Bleyer, Regina Surberg, Matthias Türk and Asmus Petersen for their help onboard during the cruise AL561 and in the GEOMAR laboratories. We further wish to thank Andreas Neumann from the Helmholtz-Zentrum Hereon for providing sediment samples of the RV Alkor cruise AL557. We would also like to acknowledge Matthias Moros from the Leibniz-Institut für Ostseeforschung Warnemünde, Bernd Kopka and Marvin Blaue from the Laboratory for Radioisotopes at the University of Göttingen, Christian Kunze and Robert Arndt from the IAF Dresden and Hendrik Wolschke from the Helmholtz-Zentrum Hereon for the ^{210}Pb analyses. Funding for this study was provided by the Federal Ministry of Education and Research, Germany, via the APOC project (03F0874B) – "Anthropogenic impacts on particulate organic carbon cycling in the North Sea".

Literature

Alperin, M.J., Suayah, I.B., Benninger, L.K., Martens, C.S., 2002. Modern organic carbon burial fluxes, recent sedimentation rates, and particle mixing rates from the upper continental slope near Cape Hatteras, North Carolina (USA). Deep Sea Res. Part II Top. Stud. Oceanogr. 49, 4645–4665. https://doi.org/10.1016/S0967-0645(02)00133-9

Anjum, R., Gao, J., Tang, Q., He, X., Zhang, X., Long, Y., Shi, Z., Wang, M., 2017. Linking sedimentary total organic carbon to 210 Pb ex chronology from Changshou Lake in the Three Gorges Reservoir Region, China. Chemosphere 174, 243–252. https://doi.org/10.1016/j.chemosphere.2017.01.060

Anton, K.K., Liebezeit, G., Rudolph, C., Wirth, H., 1993. Origin, distribution and accumulation of organic carbon in the Skagerrak. Mar. Geol. 111, 287–297. https://doi.org/10.1016/0025-3227(93)90136-J

Arrouays, D., Grundy, M.G., Hartemink, A.E., Hempel, J.W., Heuvelink, G.B.M., Hong, S.Y., Lagacherie, P., Lelyk, G., McBratney, A.B., McKenzie, N.J., Mendonca-Santos, M. d.L., Minasny, B., Montanarella, L., Odeh, I.O.A., Sanchez, P.A., Thompson, J.A., Zhang, G.-L., 2014. GlobalSoilMap, in: Advances in Agronomy. Elsevier, pp. 93–134. https://doi.org/10.1016/B978-0-12-800137-0.00003-0

Assis, J., Tyberghein, L., Bosch, S., Verbruggen, H., Serrão, E.A., De Clerck, O., Tittensor, D., 2018. Bio-ORACLE v2.0: Extending marine data layers for bioclimatic modelling. Glob. Ecol. Biogeogr. 27, 277–284. https://doi.org/10.1111/geb.12693

Baskaran, M., 2011. Po-210 and Pb-210 as atmospheric tracers and global atmospheric Pb-210 fallout: a Review. J. Environ. Radioact. 102, 500–513. https://doi.org/10.1016/j.jenvrad.2010.10.007

Beks, J.P., 2000. Storage and distribution of plutonium, 241Am, 137Cs and 210Pbxs in North Sea sediments. Cont. Shelf Res. 20, 1941–1964. https://doi.org/10.1016/S0278-4343(00)00057-1

Beks, J.P., Eisma, D., Van Der Plicht, J., 1998. A record of atmospheric 210Pb deposition in The Netherlands. Sci. Total Environ. 222, 35–44. https://doi.org/10.1016/S0048-9697(98)00289-7

Bengtsson, H., Stevens, R.L., 1998. Source and grain-size influences upon the clay mineral distribution in the Skagerrak and northern Kattegat. Clay Miner. 33, 3–13. https://doi.org/10.1180/000985598545381

Binczewska, A., Risebrobakken, B., Polovodova Asteman, I., Moros, M., Tisserand, A., Jansen, E., Witkowski, A., 2018. Coastal primary productivity changes over the last millennium: a case study from the Skagerrak (North Sea). Biogeosciences 15, 5909–5928. https://doi.org/10.5194/bg-15-5909-2018

Biscaye, P.E., Anderson, R.F., 1994. Fluxes of particulate matter on the slope of the southern Middle Atlantic Bight: SEEP-II. Deep Sea Res. Part II Top. Stud. Oceanogr. 41, 459–509. https://doi.org/10.1016/0967-0645(94)90032-9

Biswas, A., Zhang, Y., 2018. Sampling Designs for Validating Digital Soil Maps: A Review. Pedosphere 28, 1–15. https://doi.org/10.1016/S1002-0160(18)60001-3

Bivand, R.S., Pebesma, E.J., Gómez-Rubio, 2008. Applied Spatial Data Analysis with R. Springer New York, New York, NY. https://doi.org/10.1007/978-0-387-78171-6

Bøe, R., Rise, L., Thorsnes, T., De Haas, H., Saether, O.M., Kunzendortf, H., 1996. Sea-bed sediments and sediment accumulation rates in the Norwegian part of the Skagerrak. Geol Bull 430, 75–84.

Breiman, L., 2001. Random Forests. Mach. Learn. 45, 5–32. https://doi.org/10.1023/A:1010933404324

Brown, A.G., Carey, C., Erkens, G., Fuchs, M., Hoffmann, T., Macaire, J.-J., Moldenhauer, K.-M., Walling, D.E., 2009. From sedimentary records to sediment budgets: Multiple approaches to

catchment sediment flux. Geomorphology 108, 35–47. https://doi.org/10.1016/j.geomorph.2008.01.021

Cochran, J.K., McKibbin-Vaughan, T., Dornblaser, M.M., Hirschberg, D., Livingston, H.D., Buesseler, K.O., 1990. 210Pb scavenging in the North Atlantic and North Pacific Oceans. Earth Planet. Sci. Lett. 97, 332–352. https://doi.org/10.1016/0012-821X(90)90050-8

Cutler, D.R., Edwards, T.C., Beard, K.H., Cutler, A., Hess, K.T., Gibson, J., Lawler, J.J., 2007. RANDOM FORESTS FOR CLASSIFICATION IN ECOLOGY. Ecology 88, 2783–2792. https://doi.org/10.1890/07-0539.1

Dahlgaard, H., Herrmann, J., Salomon, J.C., 1995. A tracer study of the transport of coastal water from the English Channel through the German Bight to the Kattegat. J. Mar. Syst. 6, 415–425. https://doi.org/10.1016/0924-7963(95)00017-J

De Groot, S.J., 1986. Marine sand and gravel extraction in the North Atlantic and its potential environmental impact, with emphasis on the North Sea. Ocean Manag. 10, 21–36. https://doi.org/10.1016/0302-184X(86)90004-1

De Haas, H., Okkels, E., De Haas, van Weering, 1996. Recent sediment accumulation in the Norwegian Channel, North Sea. Geol Bull 430, 57–65.

De Haas, H., van Weering, T.C.E., 1997. Recent sediment accumulation, organic carbon burial and transport in the northeastern North Sea. Mar. Geol. 136, 173–187. https://doi.org/10.1016/S0025-3227(96)00072-2

DeMaster, D.J., Kuehl, S.A., Nittrouer, C.A., 1986. Effects of suspended sediments on geochemical processes near the mouth of the Amazon River: examination of biological silica uptake and the fate of particle-reactive elements. Cont. Shelf Res. 6, 107–125. https://doi.org/10.1016/0278-4343(86)90056-7

Deng, L., Bölsterli, D., Kristensen, E., Meile, C., Su, C.-C., Bernasconi, S.M., Seidenkrantz, M.-S., Glombitza, C., Lagostina, L., Han, X., Jørgensen, B.B., Røy, H., Lever, M.A., 2020. Macrofaunal control of microbial community structure in continental margin sediments. Proc. Natl. Acad. Sci. 117, 15911–15922. https://doi.org/10.1073/pnas.1917494117

Diesing, M., 2020. Deep-sea sediments of the global ocean. Earth Syst. Sci. Data 12, 3367–3381. https://doi.org/10.5194/essd-12-3367-2020

Diesing, M., Thorsnes, T., Bjarnadóttir, L.R., 2021. Organic carbon densities and accumulation rates in surface sediments of the North Sea and Skagerrak. Biogeosciences 18, 2139–2160. https://doi.org/10.5194/bg-18-2139-2021

Eisma, D., 2009. Supply and Deposition of Suspended Matter in the North Sea, in: Nio, S.-D., Shüttenhelm, R.T.E., Van Weering, Tj.C.E. (Eds.), Holocene Marine Sedimentation in the North Sea Basin. Blackwell Publishing Ltd., Oxford, UK, pp. 415–428. https://doi.org/10.1002/9781444303759.ch29

Eisma, D., Irion, G., 1988. Suspended Matter and Sediment Transport, in: Salomons, W., Bayne, B.L., Duursma, E.K., Förstner, U. (Eds.), Pollution of the North Sea. Springer Berlin Heidelberg, Berlin, Heidelberg, pp. 20–35. https://doi.org/10.1007/978-3-642-73709-1_2

EMODnet Bathymetry Consortium, 2018. EMODnet Digital Bathymetry (DTM 2018). https://doi.org/10.12770/18FF0D48-B203-4A65-94A9-5FD8B0EC35F6

Erlenkeuser, H., 1985. Distribution of 210Pb with depth in core GIK 15530-4 from the Skagerrak. Nor. Geol. Tidsskr. 65, 27–34.

Erlenkeuser, H., Pederstad, K., 1984. Recent sediment accumulation in Skagerrak as depicted by 210pb-dating. Nor. Geol. Tidsskr. 18.

Ferdelman, T.G., 2005a. Radionuclides of caesium, potassium, lead and radium of sediment core GT03-71RL. https://doi.org/10.1594/PANGAEA.319835

Ferdelman, T.G., 2005b. Radionuclides of caesium, potassium, lead and radium of sediment core GT03-71RL. https://doi.org/10.1594/PANGAEA.319835

Ferdelman, T.G., 2005c. Radionuclides of caesium, potassium, lead and radium of sediment core GT03-68RL. https://doi.org/10.1594/PANGAEA.319834

Fettweis, M., Nechad, B., Van Den Eynde, D., 2007. An estimate of the suspended particulate matter (SPM) transport in the southern North Sea using SeaWiFS images, in situ measurements and numerical model results. Cont. Shelf Res. 27, 1568–1583. https://doi.org/10.1016/j.csr.2007.01.017

Guisan, A., Zimmermann, N.E., 2000. Predictive habitat distribution models in ecology. Ecol. Model. 135, 147–186. https://doi.org/10.1016/S0304-3800(00)00354-9

Guyon, I., Elisseeff, A., 2003. An Introduction to Variable and Feature Selection. J. Mach. Learn. Res. 3, 1157–1182.

Hainbucher, D., Pohlmann, T., Backhaus, J., 1987. Transport of conservative passive tracers in the North Sea: first results of a circulation and transport model. Cont. Shelf Res. 7, 1161–1179. https://doi.org/10.1016/0278-4343(87)90083-5

Hastie, T., Tibshirani, R., Friedman, J., 2009. The Elements of Statistical Learning, Springer Series in Statistics. Springer New York, New York, NY. https://doi.org/10.1007/978-0-387-84858-7

He, Q., Walling, D.E., 1996. Interpreting particle size effects in the adsorption of 137Cs and unsupported 210Pb by mineral soils and sediments. J. Environ. Radioact. 30, 117–137. https://doi.org/10.1016/0265-931X(96)89275-7

Heilmann, J.P., Richardson, K., Ærtebjerg, G., 1994. Annual distribution and activity of phytoplankton in the Skagerrak/Kattegat frontal region. Mar. Ecol. Prog. Ser. 112, 213–223.

Heinatz, K., Scheffold, M.I.E., 2023. A first estimate of the effect of offshore wind farms on sedimentary organic carbon stocks in the Southern North Sea. Front. Mar. Sci. 9, 1068967. https://doi.org/10.3389/fmars.2022.1068967

Heuvelink, G., 2014. Uncertainty quantification of GlobalSoilMap products, in: Arrouays, D., McKenzie, N., Hempel, J., De Forges, A., McBratney, A. (Eds.), GlobalSoilMap. CRC Press, pp. 335–340. https://doi.org/10.1201/b16500-62

Hiemstra, P.H., Pebesma, E.J., Twenhöfel, C.J.W., Heuvelink, G.B.M., 2009. Real-time automatic interpolation of ambient gamma dose rates from the Dutch radioactivity monitoring network. Comput. Geosci. 35, 1711–1721. https://doi.org/10.1016/j.cageo.2008.10.011

Huang, Z., Siwabessy, J., Nichol, S.L., Brooke, B.P., 2014. Predictive mapping of seabed substrata using high-resolution multibeam sonar data: A case study from a shelf with complex geomorphology. Mar. Geol. 357, 37–52. https://doi.org/10.1016/j.margeo.2014.07.012

Hughes, G., 1968. On the mean accuracy of statistical pattern recognizers. IEEE Trans. Inf. Theory 14, 55–63. https://doi.org/10.1109/TIT.1968.1054102

ICES, 2020. Greater North Sea ecoregion ? Fisheries overview, including mixed-fisheries considerations. https://doi.org/10.17895/ICES.ADVICE.7605

ICES, 2019. Working Group on the Effects of Extraction of Marine Sediments on the Marine Ecosystem (WGEXT). https://doi.org/10.17895/ICES.PUB.5733

ICES, 2018. Greater North Sea Ecoregion ? Ecosystem overview. https://doi.org/10.17895/ICES.PUB.4670

ICONA (Ed.), 1992. North Sea atlas: for Netherlands policy and management. Stadsuitgeverij Amsterdam, Amsterdam.

Irion, G., Zöllmer, V., 1999. Clay mineral associations in fine-grained surface sediments of the North Sea. J. Sea Res. 41, 119–128. https://doi.org/10.1016/S1385-1101(98)00041-0

James, G., Witten, D., Hastie, T., Tibshirani, R., 2013. An Introduction to Statistical Learning, Springer Texts in Statistics. Springer New York, New York, NY. https://doi.org/10.1007/978-1-4614-7138-7

Krishnaswamy, S., Lal, D., Martin, J.M., Meybeck, M., 1971. Geochronology of lake sediments. Earth Planet. Sci. Lett. 11, 407–414. https://doi.org/10.1016/0012-821X(71)90202-0

Kristiansen, T., Aas, E., 2015. Water type quantification in the Skagerrak, the Kattegat and off the Jutland west coast. Oceanologia 57, 177–195. https://doi.org/10.1016/j.oceano.2014.11.002

Kursa, M.B., Rudnicki, W.R., 2010. Feature Selection with the **Boruta** Package. J. Stat. Softw. 36. https://doi.org/10.18637/jss.v036.i11

Lepland, A., Sæther, O., Thorsnes, T., 2000. Accumulation of barium in recent Skagerrak sediments: sources and distribution controls. Mar. Geol. 163, 13–26. https://doi.org/10.1016/S0025-3227(99)00104-8

Louchart, A., Lizon, F., Claquin, P., Artigas, L.F., Tilstone, G., Land, P., 2022. Pilot assessment on primary production. In: OSPAR, 2023: The 2023 Quality Status Report for the North-East Atlantic. OSPAR Commission, London.

Lyons, M.B., Keith, D.A., Phinn, S.R., Mason, T.J., Elith, J., 2018. A comparison of resampling methods for remote sensing classification and accuracy assessment. Remote Sens. Environ. 208, 145–153. https://doi.org/10.1016/j.rse.2018.02.026

McManus, J.P., Prandle, D., 1997. Development of a model to reproduce observed suspended sediment distributions in the southern North Sea using Principal Component Analysis and Multiple Linear Regression. Cont. Shelf Res. 17, 761–778. https://doi.org/10.1016/S0278-4343(96)00057-X

Meinshausen, N., 2006. Quantile Regression Forests. J Mach Learn Res 7, 983–999.

Meyenburg, G., Liebezeit, G., 1993. Mineralogy and geochemistry of a core from the Skagerrak/Kattegat boundary. Mar. Geol. 111, 337–344. https://doi.org/10.1016/0025-3227(93)90139-M

Meyer, H., Pebesma, E., 2022. Machine learning-based global maps of ecological variables and the challenge of assessing them. Nat. Commun. 13, 2208. https://doi.org/10.1038/s41467-022-29838-9

Meyer, H., Pebesma, E., 2021. Predicting into unknown space? Estimating the area of applicability of spatial prediction models. Methods Ecol. Evol. 12, 1620–1633. https://doi.org/10.1111/2041-210X.13650

Meyer, H., Pebesma, E., 2020. Mapping (un)certainty of machine learning-based spatial prediction models based on predictor space distances (other). oral. https://doi.org/10.5194/egusphere-egu2020-8492

Meyer, H., Reudenbach, C., Hengl, T., Katurji, M., Nauss, T., 2018. Improving performance of spatio-temporal machine learning models using forward feature selection and target-oriented validation. Environ. Model. Softw. 101, 1–9. https://doi.org/10.1016/j.envsoft.2017.12.001

Mielck, F., Hass, H.C., Michaelis, R., Sander, L., Papenmeier, S., Wiltshire, K.H., 2019. Morphological changes due to marine aggregate extraction for beach nourishment in the German Bight (SE North Sea). Geo-Mar. Lett. 39, 47–58. https://doi.org/10.1007/s00367-018-0556-4

Mitchell, P., Aldridge, J., Diesing, M., 2019a. Predictor variables and groundtruth samples for north-west European continental shelf quantitative sediment analysis. https://doi.org/10.14466/CEFASDATAHUB.62

Mitchell, P., Aldridge, J., Diesing, M., 2019b. Quantitative sediment composition predictions for the north-west European continental shelf. https://doi.org/10.14466/CEFASDATAHUB.63

Mitchell, P.J., Aldridge, J., Diesing, M., 2019. Legacy Data: How Decades of Seabed Sampling can Produce Robust Predictions and Versatile Products. Geosciences 9, 182. https://doi.org/10.3390/geosciences9040182

Mitchell, P.J., Spence, M.A., Aldridge, J., Kotilainen, A.T., Diesing, M., 2021. Sedimentation rates in the Baltic Sea: A machine learning approach. Cont. Shelf Res. 214, 104325. https://doi.org/10.1016/j.csr.2020.104325

Morang, A., Waters, J.P., Khalil, S.M., 2012. Gulf of Mexico Regional Sediment Budget. J. Coast. Res. 60, 14–29. https://doi.org/10.2112/SI_60_3

Mutanga, O., Adam, E., Cho, M.A., 2012. High density biomass estimation for wetland vegetation using WorldView-2 imagery and random forest regression algorithm. Int. J. Appl. Earth Obs. Geoinformation 18, 399–406. https://doi.org/10.1016/j.jag.2012.03.012

Naimi, B., Hamm, N.A.S., Groen, T.A., Skidmore, A.K., Toxopeus, A.G., 2014. Where is positional uncertainty a problem for species distribution modelling? Ecography 37, 191–203. https://doi.org/10.1111/j.1600-0587.2013.00205.x

Nittrouer, C.A., Sternberg, R.W., Carpenter, R., Bennett, J.T., 1979. The use of Pb-210 geochronology as a sedimentological tool: Application to the Washington continental shelf. Mar. Geol. 31, 297–316. https://doi.org/10.1016/0025-3227(79)90039-2

Nozaki, Y., Tsubota, H., Kasemsupaya, V., Yashima, M., Naoko, I., 1991. Residence times of surface water and particle-reactive 210Pb and 210Po in the East China and Yellow seas. Geochim. Cosmochim. Acta 55, 1265–1272. https://doi.org/10.1016/0016-7037(91)90305-O

Oliveira, S., Oehler, F., San-Miguel-Ayanz, J., Camia, A., Pereira, J.M.C., 2012. Modeling spatial patterns of fire occurrence in Mediterranean Europe using Multiple Regression and Random Forest. For. Ecol. Manag. 275, 117–129. https://doi.org/10.1016/j.foreco.2012.03.003

Oost, A., Colina Alonso, A., Esselink, P., Wang, Z.B., Kessel, T. van, Maren, B. van, 2021. Where mud matters: towards a mud balance for the trilateral Wadden Sea Area: mud supply, transport and deposition. Wadden Academy, Leeuwarden.

OSPAR, 2023. OSPAR Quality Status Synthesis Report 2023. oap.ospar.org.

Otto, L., Zimmerman, J.T.F., Furnes, G.K., Mork, M., Saetre, R., Becker, G., 1990. Review of the physical oceanography of the North Sea. Neth. J. Sea Res. 26, 161–238. https://doi.org/10.1016/0077-7579(90)90091-T

Paetzel, M., Schrader, H., Bjerkli, K., 1994. Do decreased trace metal concentrations in surficial skagerrak sediments over the last 15–30 years indicate decreased pollution? Environ. Pollut. 84, 213–226. https://doi.org/10.1016/0269-7491(94)90132-5

Parsons, A.J., 2012. How useful are catchment sediment budgets? Prog. Phys. Geogr. Earth Environ. 36, 60–71. https://doi.org/10.1177/0309133311424591

Peirson, D.H., Cambray, R.S., Spicer, G.S., 1966. Lead-210 and polonium-210 in the atmosphere. Tellus 18, 427–433. https://doi.org/10.1111/j.2153-3490.1966.tb00254.x

Ploton, P., Mortier, F., Réjou-Méchain, M., Barbier, N., Picard, N., Rossi, V., Dormann, C., Cornu, G., Viennois, G., Bayol, N., Lyapustin, A., Gourlet-Fleury, S., Pélissier, R., 2020. Spatial validation reveals poor predictive performance of large-scale ecological mapping models. Nat. Commun. 11, 4540. https://doi.org/10.1038/s41467-020-18321-y

Prasad, A.M., Iverson, L.R., Liaw, A., 2006. Newer Classification and Regression Tree Techniques: Bagging and Random Forests for Ecological Prediction. Ecosystems 9, 181–199. https://doi.org/10.1007/s10021-005-0054-1

Puls, W., Heinrich, H., Mayer, B., 1997. Suspended particulate matter budget for the German Bight. Mar. Pollut. Bull. 34, 398–409. https://doi.org/10.1016/S0025-326X(96)00161-0

R Core Team, 2022. R: A language and environment for statistical computing. R Foundation for Statistical Computing, Vienna, Austria. URL https://www.R-project.org/.

Regard, V., Prémaillon, M., Dewez, T.J.B., Carretier, S., Jeandel, C., Godderis, Y., Bonnet, S., Schott, J., Pedoja, K., Martinod, J., Viers, J., Fabre, S., 2022. Rock coast erosion: An overlooked source of sediments to the ocean. Europe as an example. Earth Planet. Sci. Lett. 579, 117356. https://doi.org/10.1016/j.epsl.2021.117356

Restreppo, G.A., Wood, W.T., Graw, J.H., Phrampus, B.J., 2021. A machine-learning derived model of seafloor sediment accumulation. Mar. Geol. 440, 106577. https://doi.org/10.1016/j.margeo.2021.106577

Richardson, K., Heilmann, J.P., 1995. Primary production in the Kattegat: Past and present. Ophelia 41, 317–328. https://doi.org/10.1080/00785236.1995.10422050

Richardson, M.D., Jackson, D.R., 2017. The Seafloor, in: Applied Underwater Acoustics. Elsevier, pp. 469–552. https://doi.org/10.1016/B978-0-12-811240-3.00008-4

Roberts, D.R., Bahn, V., Ciuti, S., Boyce, M.S., Elith, J., Guillera-Arroita, G., Hauenstein, S., Lahoz-Monfort, J.J., Schröder, B., Thuiller, W., Warton, D.I., Wintle, B.A., Hartig, F., Dormann, C.F., 2017. Cross-validation strategies for data with temporal, spatial, hierarchical, or phylogenetic structure. Ecography 40, 913–929. https://doi.org/10.1111/ecog.02881

Salomon, J.C., Breton, M., Guegueniat, P., 1995. A 2D long term advection—dispersion model for the Channel and southern North Sea Part B: Transit time and transfer function from Cap de La Hague. J. Mar. Syst. 6, 515–527. https://doi.org/10.1016/0924-7963(95)00021-G

Sanchez-Cabeza, J.A., Ruiz-Fernández, A.C., 2012. 210Pb sediment radiochronology: An integrated formulation and classification of dating models. Geochim. Cosmochim. Acta 82, 183–200. https://doi.org/10.1016/j.gca.2010.12.024

Schmidt, M., 2021. Dynamics and variability of POC burial in depocenters of the North Sea (Skagerrak), Cruise No. AL561, 2.08.2021 – 13.08.2021, Kiel – Kiel, APOC. GEOMAR Helmholtz Centre for Ocean Research Kiel. https://doi.org/10.3289/CR_AL561

Skogen, M.D., Søiland, H., 2006. Environmental status of the Skagerrak and North Sea 2004.

Skogen, M.D., Svendsen, E., Berntsen, J., Aksnes, D., Ulvestad, K.B., 1995. Modelling the primary production in the North Sea using a coupled three-dimensional physical-chemical-biological ocean model. Estuar. Coast. Shelf Sci. 41, 545–565. https://doi.org/10.1016/0272-7714(95)90026-8

Spiegel, T., Dale, A.W., Lenz, N., Schmidt, M., Sommer, S., Kalapurakkal, H.T., Przibilla, A., Lindhorst, S., Wallmann, K., 2023. Biogenic silica cycling in the Skagerrak. Front. Mar. Sci. 10, 1141448. https://doi.org/10.3389/fmars.2023.1141448

Ståhl, H., Tengberg, A., Brunnegård, J., Bjørnbom, E., Forbes, T.L., Josefson, A.B., Kaberi, H.G., Hassellöv, I.M.K., Olsgard, F., Roos, P., Hall, P.O.J., 2004. Factors influencing organic carbon recycling and burial in Skagerrak sediments. J. Mar. Res. 62, 867–907. https://doi.org/10.1357/0022240042880873

Stevens, R.L., Bengtsson, H., Lepland, A., 1996. Textural provinces and transport interpretations with fine-grained sediments in the Skagerrak. J. Sea Res. 35, 99–110. https://doi.org/10.1016/S1385-1101(96)90739-X

Tyberghein, L., Verbruggen, H., Pauly, K., Troupin, C., Mineur, F., De Clerck, O., 2012. Bio-ORACLE: a global environmental dataset for marine species distribution modelling: Bio-ORACLE marine environmental data rasters. Glob. Ecol. Biogeogr. 21, 272–281. https://doi.org/10.1111/j.1466-8238.2011.00656.x

Valavi, R., Elith, J., Lahoz-Monfort, J.J., Guillera-Arroita, G., 2019. BlockCV: An r package for generating spatially or environmentally separated folds for k-fold cross-validation of species distribution models. Methods Ecol. Evol. 10, 225–232. https://doi.org/10.1111/2041-210X.13107

Van Alphen, J.S.L.J., 1990. A mud balance for Belgian-Dutch coastal waters between 1969 and 1986. Neth. J. Sea Res. 25, 19–30. https://doi.org/10.1016/0077-7579(90)90005-2

van Weering, T.C.E., Berger, G.W., Kalf, J., 1987. Recent sediment accumulation in the Skagerrak, Northeastern North Sea. Neth. J. Sea Res. 21, 177–189. https://doi.org/10.1016/0077-7579(87)90011-1

van Weering, T.C.E., Berger, G.W., Okkels, E., 1993. Sediment transport, resuspension and accumulation rates in the northeastern Skagerrak. Mar. Geol. 111, 269–285. https://doi.org/10.1016/0025-3227(93)90135-I

Walling, D.E., Collins, A.L., 2008. The catchment sediment budget as a management tool. Environ. Sci. Policy 11, 136–143. https://doi.org/10.1016/j.envsci.2007.10.004

Wallmann, K., Diesing, M., Scholz, F., Rehder, G., Dale, A.W., Fuhr, M., Suess, E., 2022. Erosion of carbonate-bearing sedimentary rocks may close the alkalinity budget of the Baltic Sea and support atmospheric CO2 uptake in coastal seas. Front. Mar. Sci. 9, 968069. https://doi.org/10.3389/fmars.2022.968069

Walton, T.L., Dean, R.G., Rosati, J.D., 2012. Sediment budget possibilities and improbabilities. Coast. Eng. 60, 323–325. https://doi.org/10.1016/j.coastaleng.2011.08.008

Wilken, M., Anton, K.K., Liebezeit, G., 1990. Porewater chemistry of inorganic nitrogen compounds in the eastern Skagerrak (NE North Sea). Hydrobiologia 207, 179–186. https://doi.org/10.1007/BF00041455

Williams, M.E., Amoudry, L.O., Brown, J.M., Thompson, C.E.L., 2019. Fine particle retention and deposition in regions of cyclonic tidal current rotation. Mar. Geol. 410, 122–134. https://doi.org/10.1016/j.margeo.2019.01.006

Wilson, R.J., Speirs, D.C., Sabatino, A., Heath, M.R., 2018. A synthetic map of the north-west European Shelf sedimentary environment for applications in marine science. Earth Syst. Sci. Data 10, 109–130. https://doi.org/10.5194/essd-10-109-2018

Xu, L., Wu, F., Wan, G., Liao, H., Zhao, X., Xing, B., 2011. Relationship between 210Pbex activity and sedimentary organic carbon in sediments of 3 Chinese lakes. Environ. Pollut. 159, 3462–3467. https://doi.org/10.1016/j.envpol.2011.08.020

Zhang, W., Porz, L., Yilmaz, R., Wallmann, K., Spiegel, T., Neumann, A., Holtappels, M., Kasten, S., Kuhlmann, J., Ziebarth, N., Taylor, B., Ha Ho-Hagemann1, Daewel, U., Schrum, C., 2023. Intense and persistent bottom trawling impairs long-term carbon storage in shelf sea sediments (preprint). In Review. https://doi.org/10.21203/rs.3.rs-3313118/v1

Zöllmer, V., Irion, G., 1993. Clay mineral and heavy metal distributions in the northeastern North Sea. Mar. Geol. 111, 223–230. https://doi.org/10.1016/0025-3227(93)90132-F

Biogenic silica cycling in the Skagerrak

Timo Spiegel[1*], Andrew W. Dale[1], Nina Lenz[1], Mark Schmidt[1], Stefan Sommer[1], Habeeb Thanveer Kalapurakkal[1], Anna Przibilla[2], Sebastian Lindhorst[3], Klaus Wallmann[1]

[1]GEOMAR Helmholtz Centre for Ocean Research Kiel, Wischhofstrasse 1–3, 24148 Kiel, Germany

[2]Helmholtz-Zentrum Hereon, Max-Planck Straße 1, 21502 Geesthacht, Germany

[3]Universität Hamburg, Bundesstraße 55, 20146 Hamburg, Germany

***Correspondence:**
Timo Spiegel
tspiegel@geomar.de

Keywords: Biogenic silica, Dissolved silicate, In situ measurement, Burial, Marine cycling, Diagenetic model, Sedimentation rate, Skagerrak.

Abstract

Dissolved silicate (H_4SiO_4) is essential for the formation of the opaline skeletal structures of diatoms and other siliceous plankton. A fraction of particulate biogenic silica (bSi) formed in surface waters sinks to the seabed, where it either dissolves and returns to the water column or is permanently buried. Global silica budgets are still poorly constrained since data on benthic bSi cycling are lacking, especially on continental margins. This study describes benthic bSi cycling in the Skagerrak, a sedimentary depocenter for particles from the North Sea. Biogenic silica burial fluxes, benthic H_4SiO_4 fluxes to the water column and bSi burial efficiencies are reported for nine stations by evaluating data from in-situ benthic landers and sediment cores with a diagenetic reaction-transport model. The model simulates bSi contents and H_4SiO_4 concentrations at all sites using a novel power law to describe bSi dissolution kinetics with a small number of adjustable parameters. Our results show that, on average, 1100 mmol m^{-2} yr^{-1} of bSi rains down to the Skagerrak basin seafloor, of which 50% is released back to overlying waters, with the remainder being buried. Biogenic silica cycling in the Skagerrak is generally consistent with previously reported global trends, showing higher Si fluxes and burial efficiencies than deep-sea sites and similar values compared to other continental margins. A significant finding of this work is a molar bSi-to-organic carbon burial ratio of 0.22 in Skagerrak sediments, which is distinctively lower compared to other continental margins. We suggest that the continuous dissolution of bSi in suspended sediments transported over long distances from the North Sea leads to the apparent decoupling between bSi and organic carbon in Skagerrak sediments.

IV.1 Introduction

Global marine biogeochemical cycling of dissolved silicate (H_4SiO_4) and biogenic silica (bSi) is mainly controlled by riverine inputs and by outputs via burial at the seafloor (Wollast, 1974; DeMaster, 1981, 2002, 2019; Nelson et al., 1995; Ragueneau et al., 2000; Rahman et al., 2017; Tréguer et al., 1995; Tréguer and De La Rocha, 2013). Silicon (Si) is an essential nutrient in the ocean for a number of siliceous organisms such as diatoms, silicoflagellates, siliceous sponges and radiolaria (DeMaster, 2002). The bSi and carbon (C) cycles are coupled via biomineralization in the surface ocean and subsequent dissolution of detritus in the water column and burial in sediments. The tightness of this coupling is thus important for the sequestration of atmospheric CO_2 (Dugdale et al., 1995; Ragueneau et al., 2006; Tréguer et al., 2018, 2021; Tréguer and De La Rocha, 2013).

The global ocean is undersaturated with respect to Si (Hurd, 1973; Nelson et al., 1995; Ragueneau et al., 2000; Tréguer and De La Rocha, 2013). Biogenic siliceous material dissolves as it sinks through the water column and only a fraction of the bSi exported from the surface ocean reaches the seafloor (Wollast and Mackenzie, 1983; Nelson et al., 1995, 1991; Nelson and Gordon, 1982; Tréguer et al., 1995). Upon sedimentation, bSi is subject to further dissolution, although the regenerated dissolved H_4SiO_4 can reprecipitate into authigenic minerals (Mackenzie et al., 1981; Mackenzie and Kump, 1995; Michalopoulos and Aller, 1995; Loucaides et al., 2010; Ehlert et al., 2016) or adsorb to mineral surfaces (Huang, 1975; Sigg and Stumm, 1981; Swedlund, 1999; Davis et al., 2001, 2002). The competition between these processes determines the proportion of bSi that is reintroduced to the water column via a benthic flux of H_4SiO_4 and the proportion that is permanently buried. Tréguer and De La Rocha (2013) underlined the importance of the benthic bSi cycle by showing that most of the marine bSi dissolves at the sediment-water interface rather than during the sinking of silica particles.

Based on molar bSi:C ratios and particulate organic carbon (POC) burial rates, DeMaster (2002) updated global estimates of bSi burial on continental margins and demonstrated that the contribution of these regions to the global Si budget is more important than previously thought. Since then, more studies have focused on the margins, e.g. in the North Atlantic (Schlüter and Sauter, 2000; Schmidt et al., 2001; Oehler et al., 2015b). Yet, current global Si budgets still lack sufficient data, especially with regard to benthic fluxes and burial efficiencies, to accurately constrain bSi burial and dissolution on continental margins.

To our knowledge, no comprehensive study on bSi cycling has been published for the Skagerrak; a continental margin representing the largest depocenter for sediments transported from the North Sea (Eisma and Kalf, 1987; Van Weering et al., 1987; Van Weering et al., 1993). Here, we present a

dataset on bSi cycling for the Skagerrak and quantify benthic fluxes of H_4SiO_4, bSi rain rates to the seafloor, burial fluxes and burial efficiencies using a combination of geochemical observations and modelling. We propose a novel model for bSi cycling in Skagerrak sediments with potential broader applicability. We compare our results with other regions to highlight bSi cycling in the Skagerrak in a global context.

IV.2 Study area

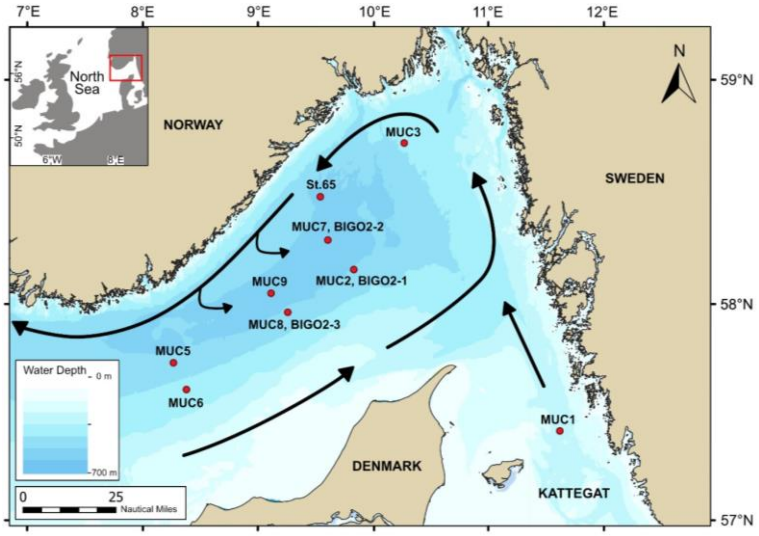

Figure IV1. Study area and sampling sites of MUCs and BIGOs within the Skagerrak. Black arrows indicate the surface water circulation.

The Skagerrak strait is located between Denmark, Norway and Sweden and links the North Sea and the Kattegat with maximum water depths of approximately 700 m (Fig. IV1). Surface waters in the Skagerrak circulate anticlockwise. Water from the North Sea enters the Skagerrak via the Jutland Current from the south, which, together with the Baltic Current, results in the outflowing Norwegian Coastal Current leaving the Skagerrak to the north (Van Weering et al., 1987; Otto et al., 1990). Annual total sediment deposition in the Skagerrak is $46 \cdot 10^6$ tons yr^{-1} (de Haas and Van Weering, 1997). Sediment composition varies between sand (<40% clay), mainly along the Danish coast, and fine-grained silt and clay sediments in the deeper parts (Stevens et al., 1996). Substantial animal burrows are present in the upper 10 - 20 cm in the fine-grained areas (Canfield et al., 1993; Kristensen et al., 2018). Skagerrak sediments are characterized by a large lateral input of mostly lithogenic material from the North Sea (Van Weering et al., 1993; De Haas and Van Weering, 1997). Nutrient supply from external waters and local rivers support an annual primary productivity of 130 g C_{org} m^{-2} yr^{-1} (Beckmann and Liebezeit, 1988). Both siliceous (diatoms) and carbonate (haptophytes)

frustule-building phytoplankton are present in the Skagerrak, with diatoms being dominant during the early bloom in February-March and a second bloom in May-June (Gran-Stadniczeñko et al., 2019).

IV.3 Material and methods

Data are presented from nine stations (65 to 677 m water depth) visited over two sampling campaigns, AL557 and AL561, with R/V Alkor in June and August 2021, respectively (Schmidt et al., 2021, Thomas et al., 2022). Only data from St. 65 are from June 2021 (Fig. IV1, Tab. IV1). At each station, a short sediment core was recovered (<50cm) using a multiple-corer (MUC). Sediments at these sites were dominated by fine-grained material except MUC6, which was taken from a more sandy area (Tab. IV1). At three stations during AL561, autonomous benthic landers (Biogeochemical Observatories, BIGO) were deployed to determine benthic H_4SiO_4 fluxes.

Table IV1. Summary of sampling sites and general information on multicorer (MUC) and biogeochemical observatory (BIGO) stations.

Station	Latitude N	Longitude E	Water depth (m)	Porosity [a]	Grain sizes [b] D_{50} (µm)	bSi [a] (%)	TOC [a] (%)	$CaCO_3$ [a] (%)	Lithogenic [c] material (%)
MUC1	57º 27.030'	11º 30.480'	65	0.75	11	3.2	1.7	12.0	80
MUC6	57º 38.086'	08º 23.998'	185	0.50	94	0.6	0.6	6.3	91
MUC3	58º 44.876'	10º 13.437'	215	0.77	11	2.5	2.0	14.1	78
MUC5	57º 45.191'	08º 17.173'	434	0.77	9	2.6	2.1	13.8	78
MUC8	57º 59.286'	09º 14.305'	490	0.77	14	2.0	2.5	14.0	77
MUC2	58º 10.884'	09º 47.624'	500	0.78	9	2.5	2.5	13.4	77
St. 65	58° 30.068'	09° 29.887'	530	0.79		2.1	2.2	12.5	79
MUC9	58º 04.352'	09º 05.736'	604	0.80	8	2.2	2.1	11.4	80
MUC7	58º 18.785'	09º 34.335'	677	0.82	7	2.3	2.1	11.4	81
BIGO-2-1	58º 10.969'	09º 47.423'	502						
BIGO-2-2	58º 18.778'	09º 34.362'	678						
BIGO-2-3	57º 59.220'	09º 14.300'	490						

[a] Porosity, and contents of bSi (as wt% SiO_2), total organic carbon (TOC) and $CaCO_3$ represent mean values for the whole core. [b] Grain sizes are given as D_{50} (50% of particles are smaller than this value), provided as average of all samples from the core. [c] Lithogenic material was calculated as: Lithogenic material = 100 – (bSi + $CaCO_3$ + 2.8 · TOC), where the factor 2.8 converts the mass of TOC to total particulate organic matter (Sayles et al., 2001).

IV.3.1 Sampling

Sediment samples for porosity and solid phase analyses from the MUC were taken every centimetre and subsequently stored refrigerated at 4 °C. An additional core from each station was subsampled

at the same resolution for ^{210}Pb radionuclide and grain size analyses. From a third core, sediment for porewater analysis was sampled in an argon-filled glove bag in a refrigerated laboratory adjusted to bottom water temperatures (ca. 7 °C). The samples were centrifuged at 4000 rpm at 8 °C for 20 min to separate porewater from the solid phase. Subsequently, the supernatant water was filtered through a 0.2 µm cellulose-acetate syringe filter inside the glove bag. Porewater from St. 65 (AL557) was sampled with syringes and rhizones (0.15 µm pore size).

IV.3.2 In-situ flux measurements

For the measurement of total solute fluxes, the GEOMAR BIGO type lander (Biogeochemical Observatory) was deployed as described in detail by (Sommer et al. (2009). BIGO-2 contained two circular flux chambers (internal diameter 28.8 cm area 651.4 cm^2). A TV-guided launching system allowed smooth placement of the observatory on the sea floor. Approximately 2 hours (BIGO-2-1) or 4 hours (BIGO-2-2 & -3) after the observatories were placed on the seabed, the chambers were slowly driven into the sediment (~30 cm h^{-1}). During this initial period, where the bottom of the chambers was not closed by the sediment, the water inside the flux chamber was periodically replaced with ambient bottom water. The water body inside the chamber was replaced once more with ambient bottom water after the chamber had been driven into the sediment to flush out solutes that might have been released from the sediment during chamber insertion. To determine fluxes of H_4SiO_4, eight sequential water samples were removed with glass syringes (volume ~ 47 ml) using syringe water samplers. The syringes were connected to the chamber using 1 m long Vygon tubes with a dead volume of 5.2 ml. Prior to deployment, these tubes were filled with distilled water.

IV.3.3 Analytical methods

Porewater H_4SiO_4 analysis was done onboard immediately after filtering using standard methods (Grasshoff et al., 1999) with a Hitachi U-2001 spectrophotometer. The analytical precision of the analysis was better than 2 µmol L^{-1}. The porewater samples from St. 65 (AL557) were stored frozen until they were analyzed for H_4SiO_4 six months after sampling with a TECAN infinite 200 plate reader at 810 nm according to the method by Ringuet et al. (2011). Porewater sub-samples for total dissolved iron (Fe), potassium (K) and lithium (Li) were acidified with 10 µL of suprapure concentrated HNO_3^- per mL of sample and stored refrigerated at 4 °C in the dark for later analyses at GEOMAR by inductively coupled plasma optical emission spectroscopy (ICP-OES, Varian ICP 720-ES). A seawater standard (IAPSO) was used for quality control. The analytical accuracy was better than 2%.

Porosity was determined from the loss of water after freeze-drying. Biogenic silica contents were analyzed on freeze-dried and homogenized sediment by a wet-leaching procedure based on the method of Müller and Schneider (1993) using 1 M NaOH as the leaching solution. An internal sediment standard was used for quality control and the analytical accuracy was better than 7%. The presented bSi contents are given as wt% SiO_2. This method may underestimate bSi content if particles are coated with metal oxides that protect bSi from dissolution or if bSi is incorporated into authigenic clay minerals (Michalopoulos and Aller, 2004; Rahman et al., 2017). Biogenic silica may also be overestimated if coexisting non-biogenic compounds are extracted by the alkaline leach (DeMaster, 1991; Kamatani and Oku, 2000). In particular, for sediments with high contents of lithogenic silica, alkaline leaching of lithogenic silica can interfere with the measured bSi content (Ragueneau and Tréguer, 1994; Zhu et al., 2023). Total carbon (TC) and total organic carbon (TOC) were analyzed on freeze-dried and homogenized sediment using a EuroEA 3000 element analyzer. For TOC analysis, sediments were first decarbonized with 0.25 N HCl on a hotplate at ~70 °C. Total inorganic carbon (TIC) was calculated by subtracting TOC from TC. TIC values are reported as weight percent $CaCO_3$ assuming that all TIC occurs as calcium carbonate. The analytical accuracy was better than 5% for TOC and TC based on repeated analyses of certified reference material BSTD1 (soil standard).

Analysis of ^{210}Pb was carried out at stations MUC1, MUC3, MUC5, MUC9 and St.65. Freeze-dried and homogenized sediment was embedded into containers sealed with a two-component epoxy resin. Samples were left standing for two weeks to ensure steady state equilibration between ^{226}Ra and ^{214}Bi. Activities of total ^{210}Pb were measured via its peak intensity at 46.5 keV by gamma spectrometry on n-type planar or coaxial Canberra Ge-detectors at GEOMAR (MUC5), Göttingen (St.65) and IAF Dresden (MUC1, MUC3, MUC9). Total ^{210}Pb activities were corrected for the natural background decay of ^{226}Ra at 295 keV in marine sediments to obtain excess ^{210}Pb ($^{210}Pb_{ex}$) values.

IV.3.4 Grain size determination

Bulk grain size distributions were determined for each station except St. 65. Samples were treated with 10% - 30% hydrogen peroxide and 60% acetic acid to dissolve organic and carbonate compounds. Subsequently, samples were dispersed in water using tetra-sodium diphosphate decahydrate. Grain size distributions were determined at the CEN, University of Hamburg, with a laser-diffraction particle-sizer (Sympatec HELOS/KF Magic; range 0.5/18 to 3500 µm). Accuracy of measurements and absence of a long-term instrumental drift is ensured by regular analysis of an in-house standard (standard deviation for mean grain size and D_{50} over the analysis period was < 1.1

µm). Statistical evaluation of the grain size distribution is based on the graphical method (Folk and Ward, 1957), calculated using GRADISTAT software (Blott and Pye, 2001).

IV.3.5 Steady-state calculations

Biogenic silica burial fluxes (bSi_{bur}) were calculated as follows:

$$bSi_{bur} = ds\ (1-\phi)\ SR\ bSi \quad (IV1)$$

Where ds is the density of dry solids, ϕ is the mean porosity of the whole sediment core, bSi is the mean bSi content of each sediment core in wt% SiO_2 and SR is the sediment accumulation or sedimentation rate in compacted sediments. Mean bSi contents were used due to scattering of bSi and an absence of clear trends with sediment depth. SR was either determined from $^{210}Pb_{ex}$ data (Eq. IV7) or taken from literature values close to the station (Tab. IV2).

At BIGO stations, benthic fluxes of H_4SiO_4 (J_{Si}) were calculated from least-square linear regression fits of concentration versus time plots of the data obtained by benthic chamber in-situ measurements and the height of overlying water in the benthic chamber (Dale et al., 2021). The H_4SiO_4 benthic fluxes represent the mean flux of both benthic chambers at each station. At non-BIGO stations, porewater gradients of H_4SiO_4 were used to calculate H_4SiO_4 benthic fluxes by applying Fick's First Law. This approach only considers diffusive transport and does not account for additional non-local transport by bioirrigation, in contrast to in-situ BIGO measurements that provide the total flux. The enhancement of solute transport via bioturbation and bioirrigation was obtained by calculating a correction factor, α (Ståhl et al., 2004). The factor (mean $\alpha = 2.2$) was calculated as the ratio between benthic fluxes determined from in-situ measurements and porewater gradients at the three BIGO stations. The correction factor was then applied to the diffusive flux at non-BIGO stations to obtain H_4SiO_4 benthic fluxes:

$$J_{Si} = -\ \phi\ D_{sed}\ \frac{d[C]}{dx}\ \alpha \quad (IV2)$$

Where J_{Si} is the H_4SiO_4 benthic flux, ϕ is porosity, d[C]/dx is the concentration gradient between porewater (taken at 0.5cm) and bottom water (taken from overlying water of the MUCs), and D_{sed} is the molecular diffusion coefficient of H_4SiO_4 corrected for tortuosity ($0.58 \cdot 10^{-5}$ $cm^2\ s^{-1}$) and bottom water temperatures (7 °C) taken from Rebreanu et al. (2008). H_4SiO_4 fluxes were always directed out of the sediment. In this study, they are reported as positive numbers.

Rain rates of bSi (bSi_{rr}) were then calculated as the sum of bSi burial fluxes and H_4SiO_4 benthic fluxes:

$$bSi_{rr} = bSi_{bur} + J_{Si} \quad (IV3)$$

The percent bSi burial efficiency (bSi_{be}) was then calculated as follows:

$$bSi_{be} = \frac{bSi_{bur}}{bSi_{rr}}\ 100\% \quad (IV4)$$

IV.3.6 Model description

To simulate bSi turnover, we used a steady-state numerical transport-reaction model for dissolved H_4SiO_4 and particulate bSi and $^{210}Pb_{ex}$. The following one-dimensional partial differential equations (Berner, 1980) were applied to solve for the concentration profiles of H_4SiO_4 and bSi:

$$ds\ (1\text{-}\phi)\ \frac{\delta bSi}{\delta t} = \frac{\delta}{\delta x}\left(ds\ (1\text{-}\phi)\ D_B \frac{\delta BSi}{\delta x} - ds\ (1\text{-}\phi)\ us\ BSi\right) - ds\ (1\text{-}\phi)\ RbSi \quad (IV5)$$

$$\phi\ \frac{\delta H_4SiO_4}{\delta t} = \frac{\delta}{\delta x}\left(\phi\ D_s \frac{\delta H_4SiO_4}{\delta x} - \phi\ upw\ H_4SiO_4\right) + \phi\ D_I\ (BW\text{-}H_4SiO_4)\ + \phi\ RbSi \quad (IV6)$$

where x is sediment depth, t is time, ds is the density of dry solids (= 2.5 g cm^{-3}), ϕ is porosity, D_s is the tortuosity-corrected molecular diffusion coefficient, D_B is the bioturbation coefficient, D_I is the bioirrigation coefficient, BW denotes the concentration of H_4SiO_4 in ambient bottom water, us and upw are burial velocities for solids and porewater, respectively, and RbSi is the rate of bSi dissolution.

The following equation was used to simulate particle-bound $^{210}Pb_{ex}$ and derive burial velocities and bioturbation rates:

$$ds\ (1\text{-}\phi)\frac{\delta\ Pb_{ex}}{\delta t} = \frac{\delta}{\delta x}\left(ds\ (1\text{-}\phi)\ D_B \frac{\delta\ Pb_{ex}}{\delta x} - ds\ (1\text{-}\phi)\ us\ Pb_{ex}\right) - ds\ (1\text{-}\phi)\ \lambda\ Pb_{ex} \quad (IV7)$$

where Pb_{ex} is the excess activity of ^{210}Pb in sediments and λ is the ^{210}Pb decay constant (0.031 yr^{-1}).

Sediment compaction was considered in the model by fitting the following function to the porosity data at each station:

$$\phi = \phi_c + (\phi_0\text{-}\phi_c)^{\left(-\frac{x}{px}\right)} \quad (IV8)$$

where ϕ_0 is the porosity at the sediment surface, ϕ_c is the porosity in compacted sediment and px is the attenuation coefficient. Burial velocities of solids and solutes were then described as:

$$us = \frac{SR\ (1\text{-}\phi_c)}{(1\text{-}\phi)} \quad (IV9)$$

$$upw = \frac{SR\ \phi_c}{(1-\phi)} \quad (IV10)$$

The distribution of $^{210}Pb_{ex}$ in surface sediments was used to constrain bioturbation rates:

$$D_B = D_{B0}\ \exp\left(-\frac{x^2}{2\ x_B{}^2}\right) \quad (IV11)$$

where D_{B0} is the bioturbation coefficient at the sediment-water interface and x_B controls the bioturbation mixing depth.

Flushing of animal burrows by bioirrigation was mathematically described as:

$$D_I = D_{I0}\ \exp\left(-\frac{x^2}{2\ x_I{}^2}\right) \quad (IV12)$$

where D_{I0} is the bioirrigation coefficient at the sediment-water interface and x_I controls the bioirrigation depth. Bioirrigation rates were constrained from porewater H_4SiO_4 concentrations.

Most models that simulate bSi dissolution use a rate that decreases rapidly with sediment depth to simulate porewater H_4SiO_4 concentrations (e.g. McManus et al., 1995; Rabouille et al., 1997; Khalil et al., 2007). Three different explanations have been put forward to explain the decrease in bSi dissolution; (i) saturation control by high porewater H_4SiO_4 levels (McManus et al., 1995; Rabouille et al., 1997), (ii) different phases of bSi undergoing dissolution, each with its own reactivity (Boudreau, 1990, Archer et al., 1993, McManus et al., 1995), and (iii) retardance of dissolution due to progressive coating of particle surfaces by Al-containing minerals (Kamatani et al., 1988; McManus et al., 1995). Since the underlying mechanisms are unknown in Skagerrak sediments, we made no attempt to resolve the different factors controlling the rate decline with depth. Instead, we applied an empirical power law model to simulate the combined effect of these processes, which implicitly includes dissolution, reprecipitation and adsorption, and which we refer to as the depth-dependent net bSi dissolution rate (RbSi). Thus, true bSi dissolution rates may be higher if large amounts of H_4SiO_4 are removed from porewaters by adsorption or reprecipitation.

Based on previous modelling work (Middelburg, 1989; Boudreau and Ruddick, 1991; Boudreau et al., 2008), Stolpovsky et al. (2015) proposed a depth-dependent power function to simulate POC degradation in bioturbated sediments:

$$RPOC = B_0\ (x + B_1)^{B_2} \quad (IV13)$$

where RPOC is the rate of POC degradation with sediment depth (mmol cm^{-3} yr^{-1}) and B_0 (mmol cm^{-3-B2} yr^{-1}), B_1 (cm) and B_2 (dimensionless) are parameters defining the decrease in POC degradation rate. Given that the rates of both bSi dissolution and POC degradation decrease with sediment depth,

we assumed that the power law from Stolpovsky et al. (2015) is applicable to describe bSi dissolution kinetics:

$$\mathrm{RbSi} = \mathrm{B_0}\ (\mathrm{x} + \mathrm{B_1})^{\mathrm{B_2}} \quad \text{(IV14)}$$

where RbSi is the depth-dependent net rate of bSi dissolution (mmol cm^{-3} yr^{-1}). The values of B_0, B_1 and B_2 for bSi dissolution are expected to be different to those for POC degradation that were constrained from a global database of benthic oxygen and nitrate fluxes (Stolpovsky et al., 2015). Following Stolpovsky et al. (2015), we assume that the rain rate of bSi to the seafloor provides an upper limit of the total amount of bSi available for dissolution and that its burial efficiency describes the limit of bSi preservation. Consequently, bSi rain rates and burial efficiencies are model input parameters. If bSi_{rr} and bSi_{be} are known, the value of one of the parameters B_0, B_1 or B_2 can be determined from the other two, i.e. for B_0:

$$\mathrm{B_0} = \frac{((1 + \mathrm{B_2})\ (-100 + \mathrm{bSi_{be}})\ \mathrm{bSi_{rr}})}{\left(100\ \left(\mathrm{B_2}^{1+\mathrm{B_2}} - \mathrm{B_1}\ (\mathrm{B_1} + \mathrm{L})^{\mathrm{B_2}} - \mathrm{L}\ (\mathrm{B_1} + \mathrm{L})^{\mathrm{B_2}}\right)\right)} \quad \text{(IV15)}$$

where L is the depth at which bSi no longer dissolves. Since the depth profiles of bSi and H_4SiO_4 indicate that bSi dissolution stops near the bottom of the sediment core, we assumed L to be 50 cm.

Two adjustable parameters, B_1 and B_2, are required to simulate net bSi dissolution. These were constrained from the measured bSi and H_4SiO_4 data. In total, 10 parameters (B_1, B_2, SR, ϕ_0, ϕ_c, px, D_{I0}, x_I, D_{B0}, x_B) were adjusted to fit the porosity, $^{210}Pb_{ex}$, H_4SiO_4 and bSi data. The parameters SR, D_{B0} and x_B were evaluated by a Monte Carlo procedure (2000 runs) after Dale et al. (2021). For each model run, the parameters were randomly varied from 0.05 to 4 cm yr^{-1} for SR, 1 to 30 cm^2 yr^{-1} for D_{B0} and 1 to 3 cm for x_B. These ranges were chosen based on literature values and visual identification of the bioturbation layer in the $^{210}Pb_{ex}$ data. At stations MUC1 and MUC3, no clear bioturbation layer was observed. Here, ranges of D_{B0} and x_B for the Monte Carlo runs were extended to 1 - 150 cm^2 yr^{-1} and 1 - 30 cm, respectively.

Upper boundary conditions were set as constant concentrations for H_4SiO_4 and constant particulate fluxes to the seafloor for bSi. For $^{210}Pb_{ex}$, a constant rate of supply was set at the upper boundary from the measured integrated $^{210}Pb_{ex}$ activity in the sediment and the decay constant λ:

$$\mathrm{FPb_{ex}} = \lambda\ \mathrm{ds}\ (1\text{-}\phi_0) \int_0^{\infty} \mathrm{Pb_{ex}}\ \mathrm{dx} \quad \text{(IV16)}$$

where FPb_{ex} is the flux of $^{210}Pb_{ex}$ to the seafloor. At the lower boundary at 50 cm, a zero gradient condition was imposed for all model variables.

Model input data for each station are summarized in Table IV2. The model was run to steady-state using the partial differential equation solver implemented in Mathematica 12.2. Mass conservation

> 99 % was achieved in all model runs. Mean deviations between the model and measured H_4SiO_4, bSi and $^{210}Pb_{ex}$ data, expressed as root mean square errors, were 27 μmol L^{-1}, 0.4 wt% and 0.6 dpm g^{-1}, respectively.

Table IV2. Measured and modelled results for bSi cycling. Stations are arranged with increasing water depth. Si fluxes in the table are rounded to two significant figures.

Measured and modelled data	MUC1 65m	MUC6 185m	MUC3 215m	MUC5 434m	MUC8 490m	MUC2 500m	St.65 530m	MUC9 604m	MUC7 677m
H_4SiO_4 bottom water (μmol L^{-1})	7.5	0.0	7.1	15.0	12.5	10.5	22.6 [a]	20.2	22.6
bSi content (wt%) [b]	3.2	0.6	2.5	2.6	2	2.5	2.1	2.2	2.3
Sedimentation rate, SR (cm yr^{-1})	0.14	0.12 [c]	0.14	0.32	0.21 [c]	0.38 [c]	0.26	0.19	0.24 [c]
bSi burial flux (mmol m^{-2} yr^{-1})	460	150	340	790	390	850	490	360	410
H_4SiO_4 benthic flux (mmol m^{-2} yr^{-1})	670 [d]	30 [d]	600 [d]	500 [d]	660	420	510 [d]	450 [d]	590
Bioirrigation (%) [e]	43	33	43	42	45	43	41	49	42
bSi rain rate, bSi_{rr} (mmol m^{-2} yr^{-1}) [f]	1130	180	940	1290	1060	1270	1070	1000	1000
bSi burial efficiency, bSi_{be} (%) [f]	41	83	36	61	37	67	49	44	41
Integrated bSi dissolution (mmol m^{-2} yr^{-1}) [f]	670	30	600	500	660	420	510	450	590
Kinetic constant, B_0 (mmol cm^{-3-B2} yr^{-1})	0.40	0.06	0.28	0.26	0.35	0.26	0.32	0.27	0.42
Kinetic constant, B_1 (cm)	2.3	2.7	2.3	2.3	2.3	2.3	2.4	2.5	2.4
Kinetic constant, B_2 (-)	-2.6	-1.5	-2.4	-2.5	-2.5	-2.3	-2.4	-2.5	-2.6
Bioturbation coefficient, D_{B0} (cm^2 yr^{-1})	50	26	52	6	20	25	5	13	15
Bioturbation coefficient, x_B (cm)	20.0	4.0	19.5	3.0	2.5	2.3	1.5	3.0	3.0
Bioirrigation coefficient, D_{I0} (yr^{-1})	39	24	33	22	33	19	17	32	23
Bioirrigation coefficient, x_I (cm)	4.1	1.5	4.3	6.0	5.7	6.3	6.9	6.9	8.0
Porosity at sediment-water interface, ϕ_0 (-)	0.85	0.50	0.86	0.87	0.89	0.89	0.90	0.88	0.89
Porosity in compacted sediment, ϕ_c (-)	0.73	0.49	0.76	0.74	0.75	0.77	0.76	0.78	0.80
Attenuation coefficient, px (cm)	0.12	0.10	0.11	0.10	0.14	0.17	0.15	0.13	0.11

[a] Bottom water H_4SiO_4 concentration at St. 65 was taken from the adjacent station MUC7. [b] Biogenic silica contents are given as mean values for the whole sediment core. [c] Sedimentation rates were taken from reported values measured in cores close to our stations: MUC2: Van Weering et al. (1993); MUC6: Van Weering et al. (1987); MUC7: Paetzel et al. (1994); MUC8: Erlenkeuser and Pederstad (1984). [d] H_4SiO_4 benthic fluxes were calculated by the diffusive fluxes and the correction factor α (Eq. IV2). [e] Bioirrigation contribution to total H_4SiO_4 benthic fluxes. [f] In the model, bSi rain rates and burial efficiencies were prescribed using field data (Eq. IV14, IV15). Consequently, depth-integrated net bSi dissolution rates were also predefined and equal to the H_4SiO_4 benthic flux.

IV.4 Results

IV.4.1 $^{210}Pb_{ex}$ activities, sedimentation rates and mixing

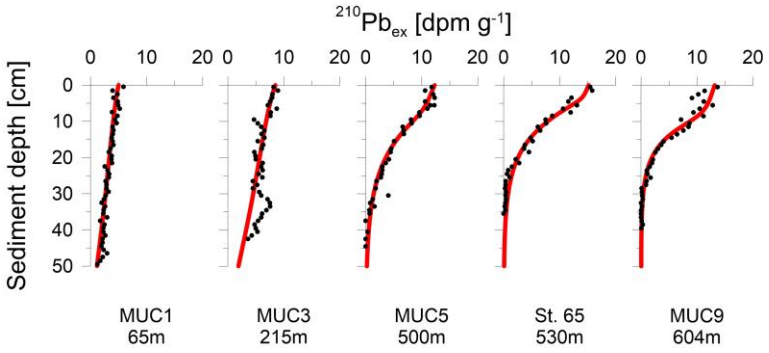

Figure IV2. Measured data (symbols) and model simulations (curves) of $^{210}Pb_{ex}$.

At stations MUC5, MUC9 and St.65, $^{210}Pb_{ex}$ activities decreased exponentially below the upper centimetres where $^{210}Pb_{ex}$ activities tended to be more constant (Fig. IV2). In contrast, stations MUC1 and MUC3 showed an almost linear $^{210}Pb_{ex}$ decrease throughout the whole core. Sedimentation rates determined by the model ranged from 0.14 to 0.32 cm yr^{-1} (Tab. IV2) and varied with water depth, but no clear trend was observed.

Sediment mixing via bioturbation was limited to the upper 5 - 10 cm at most sites (Fig. IV3c, Eq. IV11) with bioturbation coefficients (D_{B0}) and mixing coefficients (x_B) of 5 - 26 cm^2 yr^{-1} and 1.5 - 4.0 cm, respectively (Tab. IV2). In contrast, bioturbation was predicted to proceed throughout the whole sediment core at stations MUC1 and MUC3. At these sites, extreme DB_0 and x_B values in the range of 50 cm^2 yr^{-1} and 20 cm, respectively, were required to simulate the measured $^{210}Pb_{ex}$ data. Bioirrigation was most intense in the upper layers and extended up to 5 - 20 cm depth, with deeper bioirrigation observed with increasing water depth (Fig. IV3c).

IV.4.2 Dissolved and solid phase geochemistry

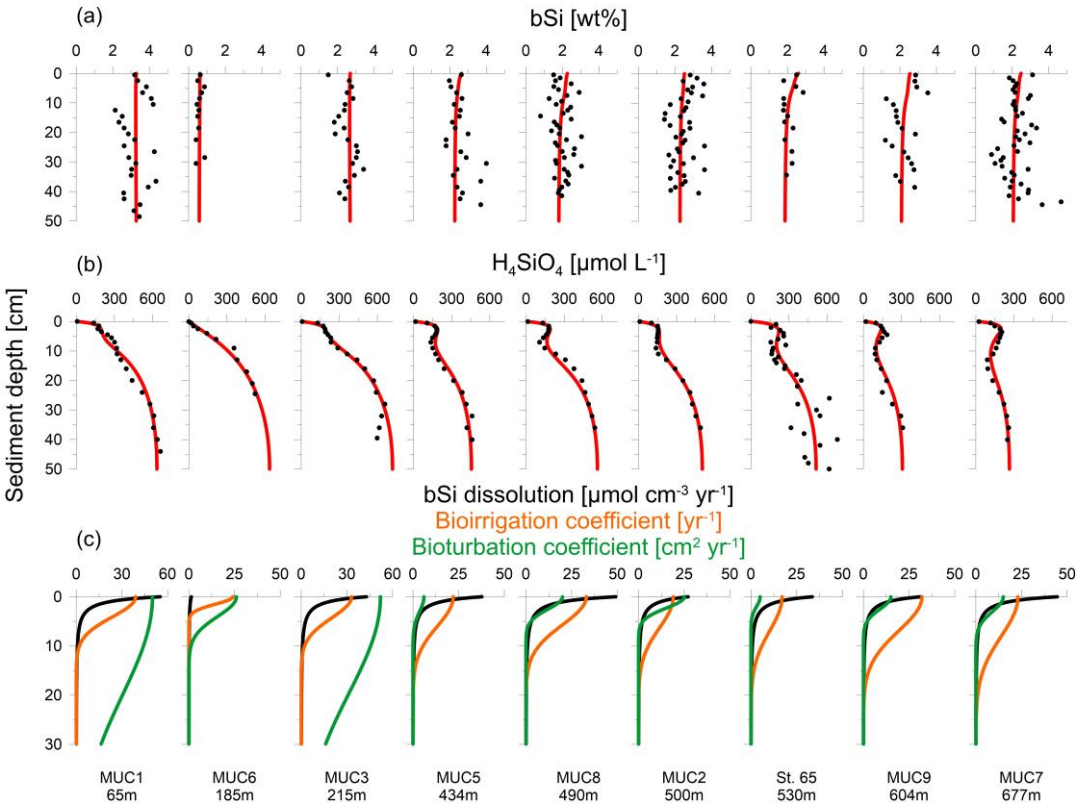

Figure IV3. Measured data (symbols) and model simulations (curves) of (a) H_4SiO_4 concentration, (b) bSi content and (c) net bSi dissolution rates (black), bioirrigation coefficient (orange) and bioturbation (green). Note different depth scale in (c).

Sediments were generally fine-grained with mean D_{50} values ranging from 7 to 14 µm (Tab. IV1). MUC6 contained a higher proportion of sand with a D_{50} of 94 µm. Solid phase bSi contents varied between 1 and 5 wt%, except for the sandy station MUC6, where lower values of 0.4 - 0.9 wt% were observed (Fig. IV3a). Biogenic silica showed no clear trend with sediment depth. $CaCO_3$ varied from ca. 6 – 13 % and lithogenic material from 77 - 91 % (Tab. IV1).

H_4SiO_4 concentrations in the Skagerrak generally increased with sediment depth up to asymptotic concentrations of 300 - 660 µmol L^{-1} (Fig. IV3b). Although asymptotic values were not reached at every station, the data indicate that the maximum asymptotic concentrations decreased with water depth. Furthermore, concentration plateaus, or local minima, were observed between 2 - 15 cm and were most pronounced at the deeper stations (>400 m).

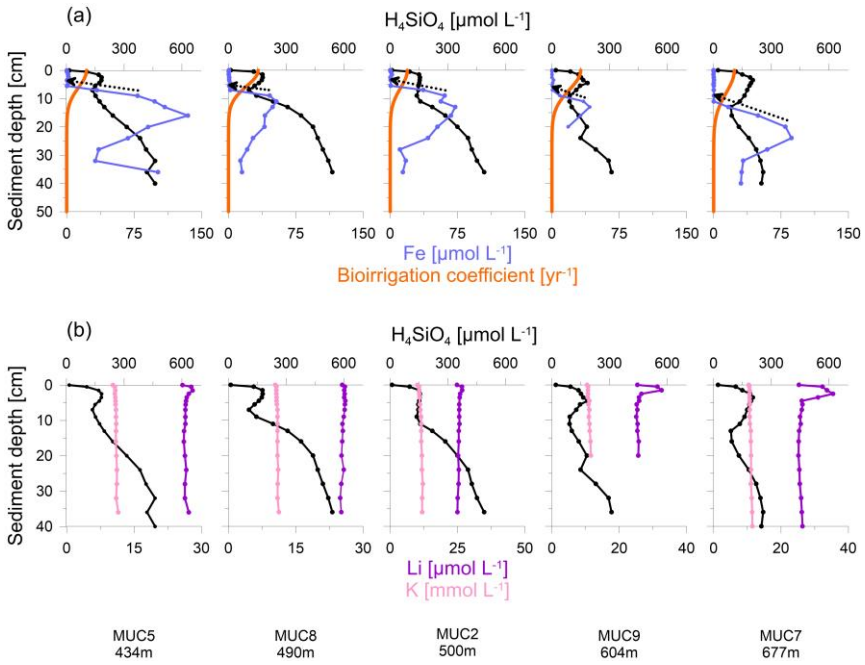

Figure IV4. (a) Porewater concentrations of H_4SiO_4, total dissolved Fe and model simulations of bioirrigation (orange curves). Dashed arrows indicate the gradient used to calculate diffusive Fe fluxes; and (b) Porewater concentrations of H_4SiO_4, K and Li at deep-water stations with distinct H_4SiO_4-minima. Note different scales in Li and K concentrations.

Total dissolved Fe concentrations were below the detection limit in the upper 5 - 10 cm, followed by an increase up to a maximum concentration of 40 - 135 µmol L^{-1} (Fig. IV4a). Thereafter, dissolved Fe concentrations tended to decrease. The zone of increasing dissolved Fe concentrations coincided with the concentration plateaus of H_4SiO_4 at the deeper sites. Dissolved K and Li concentrations showed near-constant concentrations with sediment depth, ranging between 10 and 12 mmol L^{-1} and 24 and 36 µmol L^{-1}, respectively, across the different sites (Fig. IV4b).

IV.4.3 Si fluxes and burial efficiencies

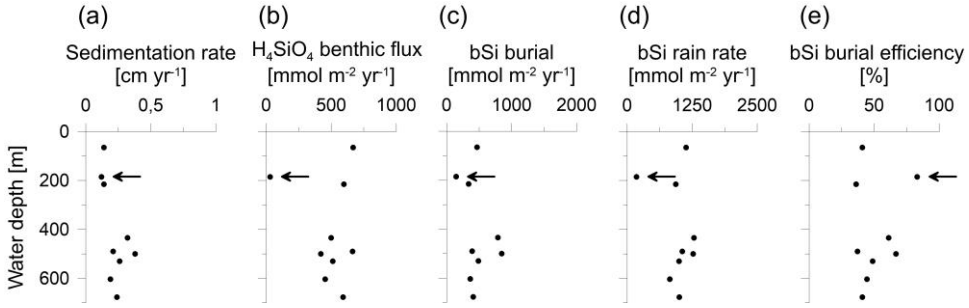

Figure IV5. (a) Sedimentation rate, (b) H_4SiO_4 benthic flux, (c) bSi burial flux, (d) bSi rain rate and (e) burial efficiency plotted against water depth. Data at 185 m water depths correspond to the sandy station MUC6 (indicated by the arrow).

Burial fluxes varied between 150 and 850 mmol m^{-2} yr^{-1}. (Tab. IV2). H_4SiO_4 fluxes at the three BIGO stations ranged between 420 and 660 mmol m^{-2} yr^{-1}, which is similar to reported in-situ flux measurements of 360 - 609 mmol m^{-2} yr^{-1} in the Skagerrak basin between 411 - 682 m water depth (Hall et al., 1996). Benthic fluxes at stations that were calculated based on porewater gradients and the correction factor α for non-diffusive transport (Eq. IV2) were between 450 - 670 mmol m^{-2} yr^{-1}, except for the sandy station MUC6 that showed a lower rate of 30 mmol m^{-2} yr^{-1}. Bioirrigation accounted for 33 - 49 % of the total benthic H_4SiO_4 flux. Biogenic silica rain rates varied between 180 and 1290 mmol m^{-2} yr^{-1} with burial efficiencies of 36 - 83 %. Fluxes and burial efficiencies varied between the different stations, but no clear trend was observed with water depth (Fig. IV5).

IV.4.4 Modelled bSi dissolution

The model predicted that most of the net bSi dissolution takes place within the top sediment layer (Fig. IV3c). The adjustable parameters B_1 and B_2 that describe bSi dissolution varied between 2.3 and 2.5 cm, and -2.3 and -2.6 (dimensionless), respectively, excluding sandy station MUC6 (Tab. IV2). At this station, B_1 and B_2 were 2.7 and -1.5, respectively. There were no clear trends in B_0, B_1 and B_2 across different sites.

IV.5 Discussion

IV.5.1 Biogenic silica cycling

The major fluxes of bSi in Skagerrak sediments are investigated in this study through numerical interpretation of the geochemical data. In our approach, the down-core decrease in net bSi dissolution, bioirrigation and bioturbation can be quantified with our novel kinetic bSi dissolution model with reasonable confidence. The two adjustable parameters needed to describe bSi dissolution, B_1 and B_2, show consistent values across the stations with fine-grained material, demonstrating the potential to apply the model elsewhere in comparable environments. Our kinetic description of bSi dissolution represents an alternative to previous approaches. It is especially applicable for regions where bSi dissolution rates and underlying mechanisms that control dissolution rates are unknown but where data for bSi rain rate and burial are available.

Biogenic silica burial fluxes were calculated based on ^{210}Pb derived sedimentation rates that are in the range of reported values from nearby locations (Erlenkeuser and Pederstad, 1984; Van Weering et al., 1993; Deng et al., 2020). A mean bSi burial efficiency of 50% in fine-grained sediments in the

Skagerrak basin indicates that about half of the annual bSi raining onto the seafloor, on average ca. 1100 mmol m^{-2} yr^{-1}, is buried in the sediment. The other half dissolves and is subsequently returned to the water column. This calculation excludes the sandy station MUC6 and shallow stations MUC1 and MUC3, where non-exponential $^{210}Pb_{ex}$ profiles indicate substantial sediment mixing and more uncertainty in calculated bSi rain rates. The unusually intense and deep mixing rates required to simulate the data at MUC1 and MUC3 compared to other sites could be attributed to bottom trawling, which is frequent in the MUC1 region at water depths <200 m (Sköld et al., 2018). Piles of sediment alongside furrows created by dragging trawl doors through the sediment can reach 1 to 2 dm in height (Bradshaw et al., 2021) and it may be that sediment cores taken at stations MUC1 and MUC3 penetrated such sediment piles during sampling. We find this explanation more convincing than deep bioturbation since no visual evidence of macrofauna was observed below ca. 10 cm depth during the slicing of the sediment cores. Furthermore, if the bioturbation parameters were set to values similar to those predicted for the undisturbed sites, sedimentation rates of 1 to 2 cm yr^{-1} would be required to fit the $^{210}Pb_{ex}$ data (results not shown); a magnitude that seems unlikely for the Skagerrak. For a seafloor surface area of the Skagerrak basin below 200 m of about 10700 km^2, and assuming a mean bSi burial flux of 550 mmol m^{-2} yr^{-1}, we calculated a mean annual bSi burial flux of $6 \cdot 10^9$ mol yr^{-1}.

Ongoing dissolution of bSi leads to the accumulation of H_4SiO_4 in porewaters and drives H_4SiO_4 fluxes to the bottom water. Scanning electron micrographs have revealed evidence of chemical erosion of bSi in Skagerrak sediments (Meyenburg and Liebezeit, 1993). According to our model, the bulk of net bSi dissolution occurs in the upper 5 centimetres (Fig. IV3c). A steep down-core decline in the dissolution rate is mirrored by the steep increase in H_4SiO_4 concentrations below the sediment-water interface. This is not evident in the bSi profiles that show high variability, possibly due to interannual changes in bulk sediment supply and/or bSi rain rate. Our bSi contents are lower than ca. 6 wt% measured in a single sediment sample from the top 50 cm at 325 m water depth in the Skagerrak (Bohrmann, 1986). Meyenburg and Liebezeit (1993) and Fengler et al. (1994) reported 0.1 - 0.6 wt% bSi at water depths of 80 and 183 m, which is similar to the sandy station MUC6, although the sediment type in their data was not reported.

No obvious trends between Si fluxes and individual environmental factors were observed at our stations, despite sizeable differences in water depth. Aside from H_4SiO_4 concentration and pH in the water column, water depth typically controls the amount of bSi that reaches the seafloor (Nelson et al., 1995; Ragueneau et al., 2000; Tréguer and De La Rocha, 2013), with lower fluxes expected at deeper stations. However, apart from the sandy station MUC6, our data reveal relatively little variability in Si fluxes across stations (Fig. IV5, Tab. IV2). Additional input of bSi to the deeper sites from the North Sea may partly explain this observation (see section IV5.3). We observed a higher bSi burial efficiency at MUC6 where the sediment was coarser, which could point toward an additional control by grain size (Tab. IV1, Fig. IV5e). Similar trends of burial efficiency and grain

size were reported in sediments of the Helgoland mud area (Oehler et al., 2015b); a sedimentary depocenter in the southern North Sea.

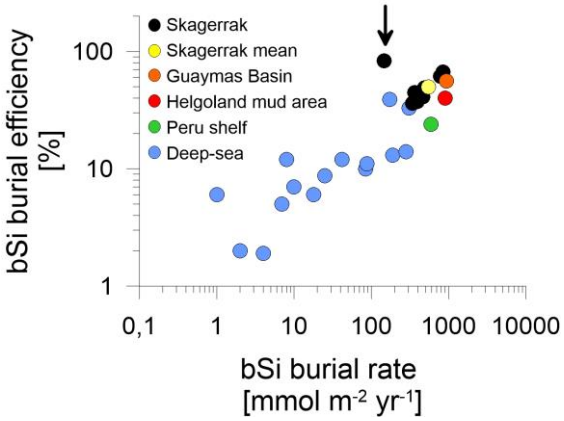

Figure IV6. Log-log plot of regional mean bSi data adapted from the compiled dataset presented by Dale et al. (2021). Biogenic silica burial rates are plotted against bSi burial efficiencies. Individual Skagerrak stations (black) and a Skagerrak mean value of stations > 400 m water depth (yellow) are compared to deep-sea regions at >3000 m water depth (blue), the Peru shelf (green) by Froelich et al. (1988), the Helgoland mud area (red) by Oehler et al. (2015b) and the Guaymas Basin (orange) by Geilert et al. (2020). Data indicated by the arrow corresponds to sandy station MUC6.

To frame bSi cycling in the Skagerrak in a global context, we compared our bulk fluxes to sites compiled by Dale et al. (2021), most of which are from the deep-sea (>3000 m water depth). In general, the Skagerrak bSi burial data aligns well with the global trend (Fig. IV6) and extends the existing database towards continental margin sites of higher burial efficiencies and burial fluxes. The Skagerrak data is in the range of other continental margins, such as the Peru shelf (Froelich et al., 1988), the Helgoland mud area (Oehler et al., 2015b) and the Guaymas Basin (Geilert et al., 2020). Variations in bSi cycling among continental margins likely stem from a combination of different regional settings, i.e. water depth, surface productivity, sedimentation rates and sediment composition.

IV.5.2 Controls on H_4SiO_4 porewater concentrations

The rapid downcore increase in H_4SiO_4 to a constant asymptotic concentration observed in the Skagerrak is typical for fine-grained marine sediments (Hurd, 1973; Schink et al., 1974; McManus et al., 1995; Rabouille et al., 1997; Khalil et al., 2007; Oehler et al., 2015b; Ehlert et al., 2016). The tendency for a decrease in the maximum concentration with increasing water depth has been attributed to the proportion of lithogenic material present in the sediment, whereby the release of

dissolved aluminium from clay minerals and subsequent adsorption or incorporation into the particulate silica phase lowers bSi solubility (Van Beusekom et al., 1997; Van Cappellen and Qiu, 1997; Dixit et al., 2001; Dixit and Van Cappellen, 2003). At our sites, lithogenic material changed only slightly with water depth (Tab. IV1). Consequently, inhibition of bSi dissolution by aluminium may not be a major control on H_4SiO_4 distributions in our sediment cores, although this conclusion would be strengthened with data on dissolved aluminium concentrations.

Especially at the deeper stations (>400 m), H_4SiO_4 porewater profiles were characterized by decreases or local minima of H_4SiO_4 concentrations between 2 - 15 cm (Fig. IV3b). The model predicts that the H_4SiO_4 minima are caused by more intense removal of H_4SiO_4 in discrete sediment layers by bioirrigation versus H_4SiO_4 added by bSi dissolution. It further predicts more intense bioirrigation at the deeper stations where the minima are more pronounced (Fig. IV3c). This is supported by reports that deep-water Skagerrak sediments are preferably colonized by deeply penetrating deposit feeders, whereas suspension and interface feeders are more abundant at shallower depths (Rosenberg et al., 1996; Dauwe et al., 1998). However, our results differ from Kristensen et al. (2018), who observed decreasing bioirrigation intensity with water depth. In addition, our modelled bioirrigation extends deeper than the zone where dissolved Fe is below the detection limit (Fig. IV4a). Given that bioirrigation enhances the transport of oxidants into the sediment, and that dissolved Fe is rapidly oxidized, this may indicate that our model overestimates the depth of bioirrigation. Hence, it might be possible that the H_4SiO_4 minima observed at deeper sites are not caused by deep-reaching bioirrigation. Instead, high rates of H_4SiO_4 removal by adsorption or precipitation might lower H_4SiO_4 concentrations in distinct sediment layers.

High sedimentary manganese and iron oxide contents have been reported for the Skagerrak, especially in deep waters (Canfield et al., 1993; Thamdrup et al., 1994). Experimental studies have demonstrated that H_4SiO_4 can adsorb to iron oxides (Huang, 1975; Sigg and Stumm, 1981; Swedlund, 1999; Davis et al., 2001, 2002), suggesting that this process is a potential sink for H_4SiO_4 in Skagerrak sediments. Since the depths of local H_4SiO_4 minima and dissolved iron removal coincide (Fig. IV4a), this sink may be relevant for the formation of observed H_4SiO_4 minima. In order to estimate the significance of this process, potential H_4SiO_4 adsorption fluxes were calculated from the diffusive flux of Fe and then compared to H_4SiO_4 removal by bioirrigation integrated over the depth interval centred on the H_4SiO_4 minima, typically spanning 5 cm (Fig. IV4a). Under the assumption that all dissolved Fe is consumed by iron oxide formation, the diffusive flux of Fe (Eq. IV2) was calculated at the depth where Fe increases. With a diffusion coefficient (D_{sed}) of 121 cm^2 yr^{-1} (Schulz and Zabel, 2006), dissolved Fe removal fluxes of 6 - 14 mmol m^{-2} yr^{-1} were calculated for the stations shown in Fig. IV4. Given mean H_4SiO_4 concentrations at the depth of H_4SiO_4 minima of ca. 150 µmol L^{-1} and assuming a pH value of 8, a molar Si/Fe sorption density on iron oxides of 0.2 is expected (Davis et al., 2002). Multiplying the Fe flux by the molar Si/Fe ratio yields potential

H_4SiO_4 adsorption fluxes of 1 - 3 mmol m^{-2} yr^{-1}. This corresponds to only 2 - 6 % of bioirrigation fluxes integrated over the depth of H_4SiO_4 minima. It illustrates that H_4SiO_4 adsorption to iron oxides may be a feasible but probably not a dominant pathway of local H_4SiO_4 removal in Skagerrak sediments.

During authigenic clay formation, H_4SiO_4 is consumed in the presence of dissolved cations (e.g. K and Li) and weathered clay minerals, a process referred to as reverse weathering (Mackenzie et al., 1981; Mackenzie and Kump, 1995; Loucaides et al., 2010; Ehlert et al., 2016). Reverse weathering occurs in anoxic marine sediments rich in biogenic opal and metal hydroxides (Michalopoulos and Aller, 1995; Michalopoulos et al., 2000) but has not been investigated in the Skagerrak. Previous studies have demonstrated reverse weathering to be a dominant process altering H_4SiO_4 porewater profiles on continental margins (Michalopoulos and Aller, 1995, 2004; Wallmann et al., 2008; Ehlert et al., 2016; Spiegel et al., 2021). Furthermore, the competition between bSi dissolution and reprecipitation during reverse weathering can create features similar to the H_4SiO_4 minima in our dataset (Spiegel et al., 2021). Since dissolved cations are consumed during reverse weathering, we compared the porewater distribution of H_4SiO_4 to dissolved K and Li concentrations (Fig. IV4b). The concentration profiles of K and Li are near-constant with sediment depth and, thus, do not show obvious indications for reverse weathering, i.e. uptake in the same horizon as H_4SiO_4 minima. However, we note that the effect of reverse weathering on dissolved cation concentrations, especially for K (~10 mM), might be too low relative to bulk porewater concentrations to result in distinct porewater signatures.

Since our model describes a continuous decline in net bSi dissolution with sediment depth, we are currently unable to resolve processes that operate in narrow depth intervals where the H_4SiO_4 porewater plateaus are observed. Hence, explicitly describing adsorption, precipitation and aluminium inhibition could lead to a better fit to the data and consequently to a more detailed description of the benthic bSi cycle in the Skagerrak. A model that includes these additional sinks may also be able to reproduce the data using shallower penetration depths of bioirrigation that are more consistent with those that have been previously reported by Kristensen et al. (2018). Further work on the parameterization of these processes in Skagerrak sediments and elsewhere would benefit future bSi model descriptions. Since the parameterization of these processes is uncertain on the basis of our dataset and yet to be investigated in the Skagerrak, we reiterate that our simple model currently only provides net bSi dissolution rates.

IV.5.3 Effect of lateral sediment supply on bSi/TOC ratios

DeMaster (2002) calculated global bSi burial on continental margins of 1.8 - 2.8 · 10^{12} mol yr^{-1} based on organic carbon burial and a mean molar bSi/TOC burial ratio of 0.6. However, DeMaster (2002) and subsequent budgets (Tréguer and De La Rocha, 2013; DeMaster, 2019) excluded continental margins dominated by high lithogenic loads, such as the Skagerrak, in their calculations. Rahman et al. (2016, 2017) reported bSi burial fluxes based on ^{32}Si isotopes in tropical and subtropical deltaic regions dominated by significant lithogenic inputs. Their results, when incorporated into more recent global Si budgets, point toward a greater significance of margins in total bSi burial (Tréguer et al., 2021). Since we have no ^{32}Si data, we compared our findings to previous approaches utilizing sedimentary bSi/TOC molar ratios. Based on our field data (Tab. IV1), we calculated a mean bSi/TOC molar ratio of 0.22 in Skagerrak sediments, which is distinctively lower than the mean ratio of 0.6 applied by DeMaster (2002). Other continental margin settings with high lithogenic inputs and where bSi was determined by the same method (Müller and Schneider, 1993) showed molar ratios of 1.0 for the Guaymas basin (Geilert et al., 2020), 0.52 for the Helgoland mud area (Oehler et al., 2015a, 2015b) and 0.55 for the Amazon shelf (Spiegel et al., 2021). Dale et al. (2021) reported much lower ratios of 0.14 for the Peruvian oxygen minimum zone, which was attributed to a lack of bioturbation and enhanced bSi dissolution in undersaturated surface sediment layers. Tréguer et al. (2021) reported ratios between 2.4 and 11 in tropical and subtropical deltaic systems. The wide range in molar bSi/TOC ratios, presumably related to the differing diagenetic regimes, emphasizes the need to further study continental margins to better constrain global bSi burial.

Low bSi/TOC ratios in the Skagerrak may be confounded by the long transit time of sediments on the order of several months from the central North Sea and 1 - 2 years from the southern North Sea to the Skagerrak (Hainbucher et al., 1987; Dahlgaard et al., 1995; Salomon et al., 1995). Since seawater is undersaturated with respect to bSi, we hypothesize repeated resuspension and deposition during particle transport leads to more extensive bSi dissolution relative to POC. This may set the Skagerrak apart from most other continental margins with regard to the coupling between bSi and TOC. Similar regions need to be investigated in order to determine whether the Skagerrak is a unique environment with regards to bSi cycling or is emblematic of continental margins exhibiting protracted transport pathways.

IV.6 Conclusions

In this study, we present bSi cycling in Skagerrak sediments based on geochemical data and modelling. Approximately 1100 mmol m^{-2} yr^{-1} of bSi annually rains onto the seafloor at the sites investigated, of which half dissolves in sediments and is reintroduced into the water column and half

is permanently buried. Biogenic silica cycling shows some spatial variability across stations, which can probably be explained by differences in water depth, sedimentation rate and sediment grain size. At deep-water sites, we observed distinct minima or plateaus in the porewater profiles of H_4SiO_4 that are likely caused by deep-reaching bioirrigation rather than H_4SiO_4 removal by adsorption to iron oxide minerals. The contribution of reverse weathering to these minima remains uncertain. Biogenic silica cycling in the Skagerrak generally aligns with the global trends and shows comparable burial fluxes and burial efficiencies to other margins. However, Skagerrak sediments are characterized by distinctively lower molar bSi/TOC ratios compared to most other continental margins, which we suggest is due to decoupling between bSi and organic carbon during the long travel time of suspended matter transported from the North Sea. It is currently unclear whether Si cycling in the Skagerrak behaves similarly to other depocenters where sediment is first transported over large distances before it finally accumulates on the seafloor. The model presented here simulates bSi cycling and quantifies net bSi dissolution, bioirrigation and bioturbation in Skagerrak sediments with few adjustable parameters but does not yet fully resolve the mechanisms behind H_4SiO_4 release and removal that operate in distinct and narrow depth intervals. Further work on the parameterization of bSi adsorption, reprecipitation and inhibition of bSi dissolution via aluminium would improve the predicted bSi kinetics. Our results contribute to the global dataset on bSi cycling and demonstrate the importance of continuing investigations in different regions, especially on continental margins, to better understand regional variability in bSi cycling and to constrain global Si budgets.

Acknowledgements

We wish to thank the captain and crew of RV Alkor for supporting our research at sea, as well as our colleagues Regina Surberg, Bettina Domeyer, Anke Bleyer, Matthias Türk, Asmus Petersen and Christoph Böttner for their help onboard during the cruise and in the GEOMAR laboratories. We thank Andreas Neumann from the Helmholtz-Zentrum Hereon (Geesthacht, Germany) for providing sediment samples from RV Alkor cruise Al557. We would also like to acknowledge Bernd Kopka and Marvin Blaue from the Laboratory for Radioisotopes at the University of Göttingen and Christian Kunze and Robert Arndt from the IAF Dresden for the ^{210}Pb analyses. Funding for this study was provided by the Federal Ministry of Education and Research, Germany, via the APOC project (03F0874B) – "Anthropogenic impacts on particulate organic carbon cycling in the North Sea".

Literature

Beckmann, M., Liebezeit, G., 1988. Organic carbon in the North Sea in May/June 1986: Distribution and controlling factors. Mitt. Geol.-Palaontol. Inst. Univ. Hamburg 65, 99-l 16

Berner, R.A., 1980. Early diagenesis: a theoretical approach, Princeton series in geochemistry. Princeton University Press, Princeton, N.J.

Blott, S.J., Pye, K., 2001. GRADISTAT: a grain size distribution and statistics package for the analysis of unconsolidated sediments. Earth Surf. Process. Landf. 26, 1237–1248. https://doi.org/10.1002/esp.261

Bohrmann, G., 1986. Accumulation of biogenie silica and opal dissolution in upper quaternary skagerrak sediments. Geo-Mar. Lett. 6, 165–172. https://doi.org/10.1007/BF02238088

Boudreau, B.P., Arnosti, C., Jørgensen, B.B., Canfield, D.E., 2008. Comment on "Physical Model for the Decay and Preservation of Marine Organic Carbon." Science 319, 1616–1616. https://doi.org/10.1126/science.1148589

Boudreau, B.P., Ruddick, B.R., 1991. On a reactive continuum representation of organic matter diagenesis. Am. J. Sci. 291, 507–538. https://doi.org/10.2475/ajs.291.5.507

Bradshaw, C., Jakobsson, M., Brüchert, V., Bonaglia, S., Mörth, C.-M., Muchowski, J., Stranne, C., Sköld, M., 2021. Physical Disturbance by Bottom Trawling Suspends Particulate Matter and Alters Biogeochemical Processes on and Near the Seafloor. Front. Mar. Sci. 8, 683331. https://doi.org/10.3389/fmars.2021.683331

Canfield, D.E, Jørgensen, B.B., Fossing, H., Glud, R., Gundersen, J., Ramsing, N.B., Thamdrup, B., Hansen, J.W., Nielsen, L.P., Hall, P.O.J., 1993. Pathways of organic carbon oxidation in three continental margin sediments. Mar. Geol. 113, 27–40. https://doi.org/10.1016/0025-3227(93)90147-N

Canfield, Donald E., Thamdrup, B., Hansen, J.W., 1993. The anaerobic degradation of organic matter in Danish coastal sediments: Iron reduction, manganese reduction, and sulfate reduction. Geochim. Cosmochim. Acta 57, 3867–3883. https://doi.org/10.1016/0016-7037(93)90340-3

Dahlgaard, H., Herrmann, J., Salomon, J.C., 1995. A tracer study of the transport of coastal water from the English Channel through the German Bight to the Kattegat. J. Mar. Syst. 6, 415–425. https://doi.org/10.1016/0924-7963(95)00017-J

Dale, A.W., Paul, K.M., Clemens, D., Scholz, F., Schroller-Lomnitz, U., Wallmann, K., Geilert, S., Hensen, C., Plass, A., Liebetrau, V., Grasse, P., Sommer, S., 2021. Recycling and Burial of Biogenic Silica in an Open Margin Oxygen Minimum Zone. Glob. Biogeochem. Cycles 35. https://doi.org/10.1029/2020GB006583

Dauwe, B., Herman, P., Heip, C., 1998. Community structure and bioturbation potential of macrofauna at four North Sea stations with contrasting food supply. Mar. Ecol. Prog. Ser. 173, 67–83. https://doi.org/10.3354/meps173067

Davis, C.C., Chen, H.-W., Edwards, M., 2002. Modeling Silica Sorption to Iron Hydroxide. Environ. Sci. Technol. 36, 582–587. https://doi.org/10.1021/es010996t

Davis, C.C., Knocke, W.R., Edwards, M., 2001. Implications of Aqueous Silica Sorption to Iron Hydroxide: Mobilization of Iron Colloids and Interference with Sorption of Arsenate and Humic Substances. Environ. Sci. Technol. 35, 3158–3162. https://doi.org/10.1021/es0018421

De Haas, H., Van Weering, T.C.E., 1997. Recent sediment accumulation, organic carbon burial and transport in the northeastern North Sea. Mar. Geol. 136, 173–187. https://doi.org/10.1016/S0025-3227(96)00072-2

DeMaster, D. J., 2019. The global marine silica budget: Sources and sinks. In K. Cochran, H. Bokuniewicz, & P. Yager (Eds.), Encyclopedia of ocean sciences 3, 473–483. Elsevier Academic Press

DeMaster, D.J., 2002. The accumulation and cycling of biogenic silica in the Southern Ocean: revisiting the marine silica budget. Deep Sea Res. Part II Top. Stud. Oceanogr. 49, 3155–3167. https://doi.org/10.1016/S0967-0645(02)00076-0

DeMaster, D.J., 1991. Measuring Biogenic Silica in Marine Sediments and Suspended Matter, in: Hurd, D.C., Spencer, D.W. (Eds.), Geophysical Monograph Series. American Geophysical Union, Washington, D. C., pp. 363–367. https://doi.org/10.1029/GM063p0363

DeMaster, D.J., 1981. The supply and accumulation of silica in the marine environment. Geochim. Cosmochim. Acta 45, 1715–1732. https://doi.org/10.1016/0016-7037(81)90006-5

Deng, L., Bölsterli, D., Kristensen, E., Meile, C., Su, C.-C., Bernasconi, S.M., Seidenkrantz, M.-S., Glombitza, C., Lagostina, L., Han, X., Jørgensen, B.B., Røy, H., Lever, M.A., 2020. Macrofaunal control of microbial community structure in continental margin sediments. Proc. Natl. Acad. Sci. 117, 15911–15922. https://doi.org/10.1073/pnas.1917494117

Dixit, S., Van Cappellen, P., 2003. Predicting benthic fluxes of silicic acid from deep-sea sediments. J. Geophys. Res. 108, 3334. https://doi.org/10.1029/2002JC001309

Dixit, S., Van Cappellen, P., van Bennekom, A.J., 2001. Processes controlling solubility of biogenic silica and pore water build-up of silicic acid in marine sediments. Mar. Chem. 73, 333–352. https://doi.org/10.1016/S0304-4203(00)00118-3

Dugdale, R.C., Wilkerson, F.P., Minas, H.J., 1995. The role of a silicate pump in driving new production. Deep Sea Res. Part Oceanogr. Res. Pap. 42, 697–719. https://doi.org/10.1016/0967-0637(95)00015-X

Ehlert, C., Doering, K., Wallmann, K., Scholz, F., Sommer, S., Grasse, P., Geilert, S., Frank, M., 2016. Stable silicon isotope signatures of marine pore waters – Biogenic opal dissolution versus authigenic clay mineral formation. Geochim. Cosmochim. Acta 191, 102–117. https://doi.org/10.1016/j.gca.2016.07.022

Eisma, D., Kalf, J., 1987. Dispersal, concentration and deposition of suspended matter in the North Sea. J. Geol. Soc. 144, 161–178. https://doi.org/10.1144/gsjgs.144.1.0161

Erlenkeuser, H., Pederstad, K., 1984. Recent sediment accumulation in Skagerrak as depicted by 210pb-dating. Nor. Geol. Tidsskr. 64, 135–152.

Fengler, G., Grossman, D., Kersten, M., Liebezeit, G., 1994. Trace metals in humic acids from recent Skagerrak sediments. Mar. Pollut. Bull. 28, 143–147. https://doi.org/10.1016/0025-326X(94)90389-1

Folk, R.L., Ward, W.C., 1957. Brazos River bar [Texas]; a study in the significance of grain size parameters. J. Sediment. Res. 27, 3–26. https://doi.org/10.1306/74D70646-2B21-11D7-8648000102C1865D

Froelich, P.N., Arthur, M.A., Burnett, W.C., Deakin, M., Hensley, V., Jahnke, R., Kaul, L., Kim, K.-H., Roe, K., Soutar, A., Vathakanon, C., 1988. Early diagenesis of organic matter in Peru continental margin sediments: Phosphorite precipitation. Mar. Geol. 80, 309–343. https://doi.org/10.1016/0025-3227(88)90095-3

Geilert, S., Grasse, P., Doering, K., Wallmann, K., Ehlert, C., Scholz, F., Frank, M., Schmidt, M., Hensen, C., 2020. Impact of ambient conditions on the Si isotope fractionation in marine pore fluids during early diagenesis. Biogeosciences 17, 1745–1763. https://doi.org/10.5194/bg-17-1745-2020

Gran-Stadniczeñko, S., Egge, E., Hostyeva, V., Logares, R., Eikrem, W., Edvardsen, B., 2019. Protist Diversity and Seasonal Dynamics in Skagerrak Plankton Communities as Revealed by Metabarcoding and Microscopy. J. Eukaryot. Microbiol. 66, 494–513. https://doi.org/10.1111/jeu.12700

Grasshoff, K., Kremling, K., Ehrhardt, M. (Eds.), 1999. Methods of Seawater Analysis, 1st ed. Wiley. https://doi.org/10.1002/9783527613984

Hainbucher, D., Pohlmann, T., Backhaus, J., 1987. Transport of conservative passive tracers in the North Sea: first results of a circulation and transport model. Cont. Shelf Res. 7, 1161–1179. https://doi.org/10.1016/0278-4343(87)90083-5

Hall, P.O.J., Hulth, S., Hulthe, G., Landén, A., Tengberg, A., 1996. Benthic nutrient fluxes on a basin-wide scale in the Skagerrak (North-Eastern North Sea). J. Sea Res. 35, 123–137. https://doi.org/10.1016/S1385-1101(96)90741-8

Huang, C.P., 1975. The removal of aqueous silica from dilute aqueous solution. Earth Planet. Sci. Lett. 27, 265–274. https://doi.org/10.1016/0012-821X(75)90038-2

Hurd, D.C., 1973. Interactions of biogenic opal, sediment and seawater in the Central Equatorial Pacific. Geochim. Cosmochim. Acta 37, 2257–2282. https://doi.org/10.1016/0016-7037(73)90103-8

Kamatani, A., Ejiri, N., Treguer, P., 1988. The dissolution kinetics of diatom ooze from the Antarctic area. Deep Sea Res. Part Oceanogr. Res. Pap. 35, 1195–1203. https://doi.org/10.1016/0198-0149(88)90010-6

Kamatani, A., Oku, O., 2000. Measuring biogenic silica in marine sediments. Mar. Chem. 68, 219–229. https://doi.org/10.1016/S0304-4203(99)00079-1

Khalil, K., Rabouille, C., Gallinari, M., Soetaert, K., DeMaster, D.J., Ragueneau, O., 2007. Constraining biogenic silica dissolution in marine sediments: A comparison between diagenetic models and experimental dissolution rates. Mar. Chem. 106, 223–238. https://doi.org/10.1016/j.marchem.2006.12.004

Kristensen, E., Røy, H., Debrabant, K., Valdemarsen, T., 2018. Carbon oxidation and bioirrigation in sediments along a Skagerrak-Kattegat-Belt Sea depth transect. Mar. Ecol. Prog. Ser. 604, 33–50. https://doi.org/10.3354/meps12734

Loucaides, S., Michalopoulos, P., Presti, M., Koning, E., Behrends, T., Van Cappellen, P., 2010. Seawater-mediated interactions between diatomaceous silica and terrigenous sediments: Results from long-term incubation experiments. Chem. Geol. 270, 68–79. https://doi.org/10.1016/j.chemgeo.2009.11.006

Mackenzie, F.T., Kump, L.R., 1995. Reverse Weathering, Clay Mineral Formation, and Oceanic Element Cycles. Science 270, 586–586. https://doi.org/10.1126/science.270.5236.586

Mackenzie, F.T., Ristvet, B.L., Thorstenson, C.D., Lerman, A., Leeper, R.H., 1981. Reverse weathering and chemical mass balance in a coastal environment. In: River Inputs from Ocean Systems, 152–187

McManus, J., Hammond, D.E., Berelson, W.M., Kilgore, T.E., Demaster, D.J., Ragueneau, O.G., Collier, R.W., 1995. Early diagenesis of biogenic opal: Dissolution rates, kinetics, and paleoceanographic implications. Deep Sea Res. Part II Top. Stud. Oceanogr. 42, 871–903. https://doi.org/10.1016/0967-0645(95)00035-O

Meyenburg, G., Liebezeit, G., 1993. Mineralogy and geochemistry of a core from the Skagerrak/Kattegat boundary. Mar. Geol. 111, 337–344. https://doi.org/10.1016/0025-3227(93)90139-M

Michalopoulos, P., Aller, R.C., 2004. Early diagenesis of biogenic silica in the Amazon delta: alteration, authigenic clay formation, and storage. Geochim. Cosmochim. Acta 68, 1061–1085. https://doi.org/10.1016/j.gca.2003.07.018

Michalopoulos, P., Aller, R.C., 1995. Rapid Clay Mineral Formation in Amazon Delta Sediments: Reverse Weathering and Oceanic Elemental Cycles. Sci. New Ser. 270, 614–617.

Michalopoulos, P., Aller, R.C., Reeder, R.J., 2000. Conversion of diatoms to clays during early diagenesis in tropical, continental shelf muds. Geology 28, 1095. https://doi.org/10.1130/0091-7613(2000)28<1095:CODTCD>2.0.CO;2

Middelburg, J.J., 1989. A simple rate model for organic matter decomposition in marine sediments. Geochim. Cosmochim. Acta 53, 1577–1581. https://doi.org/10.1016/0016-7037(89)90239-1

Müller, P.J., Schneider, R., 1993. An automated leaching method for the determination of opal in sediments and particulate matter. Deep Sea Res. Part Oceanogr. Res. Pap. 40, 425–444. https://doi.org/10.1016/0967-0637(93)90140-X

Nelson, D.M., Ahern, J.A., Herlihy, L.J., 1991. Cycling of biogenic silica within the upper water column of the Ross Sea. Mar. Chem. 35, 461–476. https://doi.org/10.1016/S0304-4203(09)90037-8

Nelson, D.M., Gordon, L.I., 1982. Production and pelagic dissolution of biogenic silica in the Southern Ocean. Geochim. Cosmochim. Acta 46, 491–501. https://doi.org/10.1016/0016-7037(82)90153-3

Nelson, D.M., Tréguer, P., Brzezinski, M.A., Leynaert, A., Quéguiner, B., 1995. Production and dissolution of biogenic silica in the ocean: Revised global estimates, comparison with regional data and relationship to biogenic sedimentation. Glob. Biogeochem. Cycles 9, 359–372. https://doi.org/10.1029/95GB01070

Oehler, T., Martinez, R., Schückel, U., Winter, C., Kröncke, I., Schlüter, M., 2015a. Seasonal and spatial variations of benthic oxygen and nitrogen fluxes in the Helgoland Mud Area (southern North Sea). Cont. Shelf Res. 106, 118–129. https://doi.org/10.1016/j.csr.2015.06.009

Oehler, T., Schlüter, M., Schückel, U., 2015b. Seasonal dynamics of the biogenic silica cycle in surface sediments of the Helgoland Mud Area (southern North Sea). Cont. Shelf Res. 107, 103–114. https://doi.org/10.1016/j.csr.2015.07.016

Otto, L., Zimmerman, J.T.F., Furnes, G.K., Mork, M., Saetre, R., Becker, G., 1990. Review of the physical oceanography of the North Sea. Neth. J. Sea Res. 26, 161–238. https://doi.org/10.1016/0077-7579(90)90091-T

Paetzel, M., Schrader, H., Bjerkli, K., 1994. Do decreased trace metal concentrations in surficial skagerrak sediments over the last 15–30 years indicate decreased pollution? Environ. Pollut. 84, 213–226. https://doi.org/10.1016/0269-7491(94)90132-5

Rabouille, C., Gaillard, J.-F., Tréguer, P., Vincendeau, M.-A., 1997. Biogenic silica recycling in surficial sediments across the Polar Front of the Southern Ocean (Indian Sector). Deep Sea Res. Part II Top. Stud. Oceanogr. 44, 1151–1176. https://doi.org/10.1016/S0967-0645(96)00108-7

Ragueneau, O., Schultes, S., Bidle, K., Claquin, P., Moriceau, B., 2006. Si and C interactions in the world ocean: Importance of ecological processes and implications for the role of diatoms in the biological pump: Si AND C INTERACTIONS IN THE OCEAN. Glob. Biogeochem. Cycles 20, n/a-n/a. https://doi.org/10.1029/2006GB002688

Ragueneau, O., Tréguer, P., 1994. Determination of biogenic silica in coastal waters: applicability and limits of the alkaline digestion method. Mar. Chem. 45, 43–51. https://doi.org/10.1016/0304-4203(94)90090-6

Ragueneau, O., Tréguer, P., Leynaert, A., Anderson, R.F., Brzezinski, M.A., DeMaster, D.J., Dugdale, R.C., Dymond, J., Fischer, G., François, R., Heinze, C., Maier-Reimer, E., Martin-Jézéquel, V., Nelson, D.M., Quéguiner, B., 2000. A review of the Si cycle in the modern ocean: recent progress and missing gaps in the application of biogenic opal as a paleoproductivity proxy. Glob. Planet. Change 26, 317–365. https://doi.org/10.1016/S0921-8181(00)00052-7

Rahman, S., Aller, R.C., Cochran, J.K., 2017. The Missing Silica Sink: Revisiting the Marine Sedimentary Si Cycle Using Cosmogenic ^{32} Si: The Missing Sedimentary Silica Sink. Glob. Biogeochem. Cycles 31, 1559–1578. https://doi.org/10.1002/2017GB005746

Rahman, S., Aller, R.C., Cochran, J.K., 2016. Cosmogenic ^{32} Si as a tracer of biogenic silica burial and diagenesis: Major deltaic sinks in the silica cycle. Geophys. Res. Lett. 43, 7124–7132. https://doi.org/10.1002/2016GL069929

Rebreanu, L., Vanderborght, J.-P., Chou, L., 2008. The diffusion coefficient of dissolved silica revisited. Mar. Chem. 112, 230–233. https://doi.org/10.1016/j.marchem.2008.08.004

Ringuet, S., Sassano, L., Johnson, Z.I., 2011. A suite of microplate reader-based colorimetric methods to quantify ammonium, nitrate, orthophosphate and silicate concentrations for aquatic nutrient monitoring. J Env. Monit 13, 370–376. https://doi.org/10.1039/C0EM00290A

Rosenberg, R., Hellman, B., Lundberg, A., 1996. Benthic macrofaunal community structure in the Norwegian Trench, deep skagerrak. J. Sea Res. 35, 181–188. https://doi.org/10.1016/S1385-1101(96)90745-5

Salomon, J.C., Breton, M., Guegueniat, P., 1995. A 2D long term advection—dispersion model for the Channel and southern North Sea Part B: Transit time and transfer function from Cap de La Hague. J. Mar. Syst. 6, 515–527. https://doi.org/10.1016/0924-7963(95)00021-G

Sayles, F.L., Martin, W.R., Chase, Z., Anderson, R.F., 2001. Benthic remineralization and burial of biogenic SiO2, CaCO3, organic carbon, and detrital material in the Southern Ocean along a transect at 170° West. Deep Sea Res. Part II Top. Stud. Oceanogr. 48, 4323–4383. https://doi.org/10.1016/S0967-0645(01)00091-1

Schink, D.R., Fanning, K.A., Pilson, M.E.Q., 1974. Dissolved silica in the upper pore waters of the Atlantic Ocean floor. J. Geophys. Res. 79, 2243–2250. https://doi.org/10.1029/JC079i015p02243

Schlüter, M., Sauter, E., 2000. Biogenic silica cycle in surface sediments of the Greenland Sea. J. Mar. Syst. 23, 333–342. https://doi.org/10.1016/S0924-7963(99)00070-6

Schmidt, M., 2021. Dynamics and variability of POC burial in depocenters of the North Sea (Skagerrak), Cruise No. AL561, 2.08.2021 – 13.08.2021, Kiel – Kiel, APOC. GEOMAR Helmholtz Centre for Ocean Research Kiel. https://doi.org/10.3289/CR_AL561

Schmidt, M., Botz, R., Rickert, D., Bohrmann, G., Hall, S.R., Mann, S., 2001. Oxygen isotopes of marine diatoms and relations to opal-A maturation. Geochim. Cosmochim. Acta 65, 201–211. https://doi.org/10.1016/S0016-7037(00)00534-2

Schulz, H.D., Zabel, M. (Eds.), 2006. Marine Geochemistry. Springer-Verlag, Berlin/Heidelberg. https://doi.org/10.1007/3-540-32144-6

Sigg, L., Stumm, W., 1981. The interaction of anions and weak acids with the hydrous goethite (α-FeOOH) surface. Colloids Surf. 2, 101–117. https://doi.org/10.1016/0166-6622(81)80001-7

Sköld, M., Göransson, P., Jonsson, P., Bastardie, F., Blomqvist, M., Agrenius, S., Hiddink, J., Nilsson, H., Bartolino, V., 2018. Effects of chronic bottom trawling on soft-seafloor macrofauna in the Kattegat. Mar. Ecol. Prog. Ser. 586, 41–55. https://doi.org/10.3354/meps12434

Sommer, S., Linke, P., Pfannkuche, O., Schleicher, T., Schneider v. D, D., Reitz, A., Haeckel, M., Flögel, S., Hensen, C., 2009. Seabed methane emissions and the habitat of frenulate tubeworms on the Captain Arutyunov mud volcano (Gulf of Cadiz). Mar. Ecol. Prog. Ser. 382, 69–86. https://doi.org/10.3354/meps07956

Spiegel, T., Vosteen, P., Wallmann, K., Paul, S.A.L., Gledhill, M., Scholz, F., 2021. Updated estimates of sedimentary potassium sequestration and phosphorus release on the Amazon shelf. Chem. Geol. 560, 120017. https://doi.org/10.1016/j.chemgeo.2020.120017

Ståhl, H., Tengberg, A., Brunnegård, J., Bjørnbom, E., Forbes, T.L., Josefson, A.B., Kaberi, H.G., Hassellöv, I.M.K., Olsgard, F., Roos, P., Hall, P.O.J., 2004. Factors influencing organic carbon recycling and burial in Skagerrak sediments. J. Mar. Res. 62, 867–907. https://doi.org/10.1357/0022240042880873

Stevens, R.L., Bengtsson, H., Lepland, A., 1996. Textural provinces and transport interpretations with fine-grained sediments in the Skagerrak. J. Sea Res. 35, 99–110. https://doi.org/10.1016/S1385-1101(96)90739-X

Stolpovsky, K., Dale, A.W., Wallmann, K., 2015. Toward a parameterization of global-scale organic carbon mineralization kinetics in surface marine sediments: Benthic carbon mineralization. Glob. Biogeochem. Cycles 29, 812–829. https://doi.org/10.1002/2015GB005087

Swedlund, P., 1999. Adsorption and polymerisation of silicic acid on ferrihydrite, and its effect on arsenic adsorption. Water Res. 33, 3413–3422. https://doi.org/10.1016/S0043-1354(99)00055-X

Thamdrup, B., Fossing, H., Jørgensen, B.B., 1994. Manganese, iron and sulfur cycling in a coastal marine sediment, Aarhus bay, Denmark. Geochim. Cosmochim. Acta 58, 5115–5129. https://doi.org/10.1016/0016-7037(94)90298-4

Thomas, H., Freund, W., Mears, C., Meckel, E., Minutolo, F., Nantke, C., Neumann, A., Seidel, M., Van Dam, B., 2022. ALKOR Scientific Cruise Report. The Ocean's Alkalinity - Connecting geological and metabolic processes and time-scales: mechanisms and magnitude of metabolic alkalinity generation in the North Sea Cruise No. AL557. Open Access. Alkor-Berichte, AL557. GEOMAR Helmholtz-Zentrum für Ozeanforschung Kiel, Kiel, Germany, 22 pp

Tréguer, P., Bowler, C., Moriceau, B., Dutkiewicz, S., Gehlen, M., Aumont, O., Bittner, L., Dugdale, R., Finkel, Z., Iudicone, D., Jahn, O., Guidi, L., Lasbleiz, M., Leblanc, K., Levy, M., Pondaven, P., 2018. Influence of diatom diversity on the ocean biological carbon pump. Nat. Geosci. 11, 27–37. https://doi.org/10.1038/s41561-017-0028-x

Tréguer, P., Nelson, D.M., Van Bennekom, A.J., DeMaster, D.J., Leynaert, A., Quéguiner, B., 1995. The Silica Balance in the World Ocean: A Reestimate. Science 268, 375–379. https://doi.org/10.1126/science.268.5209.375

Tréguer, P.J., De La Rocha, C.L., 2013. The World Ocean Silica Cycle. Annu. Rev. Mar. Sci. 5, 477–501. https://doi.org/10.1146/annurev-marine-121211-172346

Tréguer, P.J., Sutton, J.N., Brzezinski, M., Charette, M.A., Devries, T., Dutkiewicz, S., Ehlert, C., Hawkings, J., Leynaert, A., Liu, S.M., Llopis Monferrer, N., López-Acosta, M., Maldonado, M., Rahman, S., Ran, L., Rouxel, O., 2021. Reviews and syntheses: The biogeochemical cycle of silicon in the modern ocean. Biogeosciences 18, 1269–1289. https://doi.org/10.5194/bg-18-1269-2021

Van Beusekom, J.E.E., Van Bennekom, A.J., Tréguer, P., Morvan, J., 1997. Aluminium and silicic acid in water and sediments of the Enderby and Crozet Basins. Deep Sea Res. Part II Top. Stud. Oceanogr. 44, 987–1003. https://doi.org/10.1016/S0967-0645(96)00105-1

Van Weering, T.C.E., Berger, G.W., Kalf, J., 1987. Recent sediment accumulation in the Skagerrak, Northeastern North Sea. Neth. J. Sea Res. 21, 177–189. https://doi.org/10.1016/0077-7579(87)90011-1

Van Weering, T.C.E., Berger, G.W., Okkels, E., 1993. Sediment transport, resuspension and accumulation rates in the northeastern Skagerrak. Mar. Geol. 111, 269–285. https://doi.org/10.1016/0025-3227(93)90135-I

Wallmann, K., Aloisi, G., Haeckel, M., Tishchenko, P., Pavlova, G., Greinert, J., Kutterolf, S., Eisenhauer, A., 2008. Silicate weathering in anoxic marine sediments. Geochim. Cosmochim. Acta 72, 2895–2918. https://doi.org/10.1016/j.gca.2008.03.026

Zhu, D., Sutton, J.N., Leynaert, A., Tréguer, P.J., Schoelynck, J., Gallinari, M., Ma, Y., Liu, S.M., 2023. Revisiting the biogenic silica burial flux determinations: A case study for the East China seas. Front. Mar. Sci. 9, 1058730. https://doi.org/10.3389/fmars.2022.1058730

Wollast R., 1974. The silica problem. In: The Sea, ed. ED Goldberg 5, 365–81. New York: Wiley-Interscience

Wollast, R., Mackenzie, F.T., 1983. The global cycle of silica, in Silicon Geochemistry and Biogeochemistry, edited by S.R. Aston, 39-76. Academic, San Diego, Calif.

Benthic POC cycling in the Skagerrak

V.1 Introduction

Extensive research has been conducted on the global marine cycling and budgeting of sedimentary organic carbon (Berner, 1980, 1982, 1989; Hedges and Keil, 1995; Hedges et al., 1997; Duarte et al., 2005; Wallmann and Aloisi, 2012; Middelburg, 2019). Although continental shelfs cover less than 10% of the total ocean seafloor area, these environments account for ~30 % of total primary production (Berger et al., 1989) and for ~75 - 80% of long-term carbon burial (Walsh, 1991; Liu et al., 2000). Particulate organic carbon (POC) in the ocean primarily originates from riverine input and from primary production in the surface ocean, where phytoplankton takes up carbon dioxide (CO_2) and nutrients to synthesize organic material during photosynthesis (Hedges and Keil, 1995; Behrenfeld et al., 2006). As the POC sinks through the water column, it is partly remineralized to dissolved inorganic carbon (DIC). Hence, only a fraction of the POC exported from the surface ocean reaches the seafloor (Suess, 1980; Buesseler, 1998; Schlitzer, 2000; De La Rocha and Passow, 2007). On continental shelfs, between 25 - 50% of the primary production reaches the seafloor (Wollast, 1991). Upon sedimentation, the POC is subject to microbial degradation and part of the remineralized POC is recycled back to the overlying water column as DIC (benthic DIC flux). The remaining POC is permanently buried in marine sediments (POC burial flux), effectively removing it from the marine carbon cycle (Berner, 1980).

Hence, quantifying the efficiency at which organic carbon is preserved and buried in marine sediments (POC burial efficiency) represents a prerequisite for constraining global POC budgets and assessing the key role of POC burial in climate regulation (IPCC, 2023). Major driving factors for POC preservation in marine sediments involve the primary production rate, sedimentation rate, oxygen levels in ambient waters, particle sizes, the quality of organic material and bacterial activity (Aller and Mackin, 1984; Pedersen and Calvert, 1990; Canfield, 1994; Mayer, 1994; Hedges and Keil, 1995; Hartnett et al., 1998; Ståhl et al., 2004; Burdige, 2007; Arndt et al., 2013; Dale et al., 2015). However, it is important to note that burial efficiencies can substantially vary between different marine regions depending on the relative importance of individual driving factors in the respective setting. Hence, it is essential to investigate benthic POC cycling among different marine regions.

Here, we examine the benthic POC cycle in the Skagerrak, a continental margin and the largest depocenter for sediments and POC in the North Sea (De Haas et al., 1997; De Haas and van Weering, 1997; Diesing et al., 2021; Spiegel et al., 2024). The Skagerrak and North Sea areas act as substantial sinks for atmospheric CO_2 with uptake rates of 1.2 and 1.38 mol m^{-2} yr^{-1}, respectively (Thomas et al., 2005; Hjalmarsson et al., 2010). Previous studies presented POC burial fluxes (Jørgensen et al.,

1990; Anton et al., 1993; Bakker and Helder, 1993; Meyenburg and Liebezeit, 1993; De Haas and van Weering, 1997; Ståhl et al., 2004; Diesing et al., 2021) and benthic DIC and O_2 fluxes (Jørgensen et al., 1990; Bakker and Helder, 1993; Canfield et al., 1993; Van Cappellen and Wang, 1996; Wang and Van Cappellen, 1996) based on solid phase and porewater measurements, sediment core incubations and modeling. However, in-situ investigations on benthic POC recycling fluxes are yet scarce in the Skagerrak (Ståhl et al., 2004). Sedimentary POC in the Skagerrak partly originates from local primary production of 11 mol C m^{-2} yr^{-1} (Beckmann and Liebezeit, 1988). However, the bulk (~50 - 90%) of the POC deposited in the Skagerrak consists of refractory material from the North Sea (Liebezeit, 1988; Anton et al., 1993; Meyenburg and Liebezeit, 1993; De Haas and van Weering, 1997). This is the result of continuous POC degradation during particle transit, which takes several months from the central North Sea and 1 - 2 years from the southern North Sea (Hainbucher et al., 1987; Dahlgaard et al., 1995; Salomon et al., 1995). Since industrial times, the POC cycle in the North Sea has been subject to intense human and natural alterations including bottom trawling (Eigaard et al., 2017; ICES, 2020; Rijnsdorp et al., 2020), wind park construction (Baeye and Fettweis, 2015; Slavik et al., 2019; Daewel et al., 2022; Heinatz and Scheffold, 2023), coastal protection and land reclamation (Kelletat, 1992; Hoeksema, 2007; Hofstede, 2008), dredging and sediment extraction (De Groot, 1986; ICES, 2019; Mielck et al., 2019), river damming (IKSE, 2005, 2012; Lange et al., 2008; Hübner and Schwandt, 2018) and changes in circulation patterns, river discharge, coastal erosion and frequent storm events (Stride, 1982; Eisma and Irion, 1988; Green et al., 1995; Elliott et al., 1998; Holland and Elmore, 2008; Stanev et al., 2009; Fettweis et al., 2010; Dangendorf et al., 2014). Hence, the Skagerrak provides a characteristic setting to investigate benthic POC cycling derived from both local and transported sources under changing environmental conditions.

In this study, we aim to extend the existing database by presenting POC burial fluxes, benthic DIC fluxes and burial efficiencies based on sediment, porewater and in-situ benthic lander data to describe benthic POC cycling in the Skagerrak. Given its relevance in the Skagerrak setting, we assess different approaches to estimate the proportion between locally produced and laterally transported POC and discuss previous estimates. Furthermore, we determine average POC burial fluxes before and after 1963 based on a reported temporal shift of sedimentation rates (Spiegel et al., 2024 - in rev.) to explore decadal changes of POC cycling in the Skagerrak and North Sea. Finally, we compare the results in the Skagerrak to global data on burial efficiencies in different marine environments.

V.2 Study area

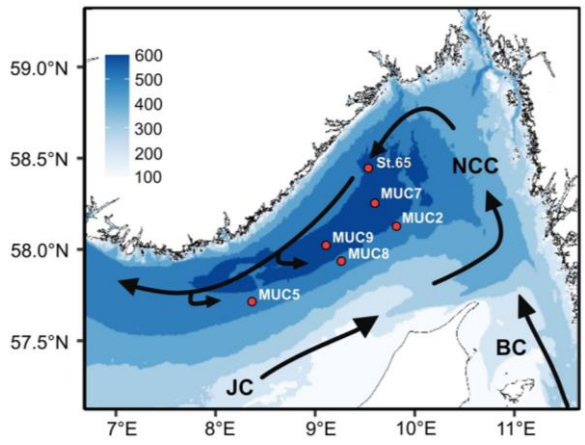

Figure V1. Study area with information on sampling stations and water depth. Black arrows indicate the surface water circulation of the Jutland Current (JC), the Baltic Current (BC) and the Norwegian Coastal Current (NCC).

The Skagerrak is a continental margin sea, which is located between Denmark, Norway and Sweden and is the water straight that connects the North Sea and the Kattegat (Fig. V1). Water depths extend to approximately 700 m in the central Skagerrak basin. Surface water enters the Skagerrak through the Jutland Current from the south, which then circulates anticlockwise until leaving the Skagerrak to the northwest via the Norwegian Coastal Current (Van Weering et al., 1987; Otto et al., 1990). Total sediment deposition in the Skagerrak amounts to 35 - 46 Mt yr^{-1} (Van Weering et al., 1987; De Haas and van Weering, 1997; Spiegel et al., 2024). Along the basin, sediment composition is dominated by fine-grained silt and clay, while sediments are composed of sand (<40% clay) at shallower water depths along the Danish coastline (Stevens et al., 1996).

V.3 Material and Methods

We present data from six stations taken during two sampling campaigns with RV Alkor, AL557 and AL561, in June and August 2021, respectively (Schmidt, 2021; Thomas et al., 2022). The stations were located in the central Skagerrak basin at water depths between 434 and 677 m (Tab. V1). At each station a short sediment core (<50cm) was retrieved using a multiple-corer (MUC). At the stations MUC2, MUC7 and MUC8 autonomous benthic landers (Biogeochemical Observatories, BIGO) were deployed adjacent to the MUC sites to determine benthic DIC fluxes at the sediment-water interface.

Table V1. Summary of Multicorer (MUC) and Biogeochemical Observatory (BIGO) sampling sites.

Station	Latitude	Longitude	Water depth (m)	Sediment type [a]
MUC2	58º 10.884'	09º 47.624'	500	Silt, Clay
MUC5	57º 45.191'	08º 17.173'	434	Silt, Clay
MUC7	58º 18.785'	09º 34.335'	677	Silt, Clay
MUC8	57º 59.286'	09º 14.305'	490	Silt, Clay
MUC9	58º 04.352'	09º 05.736'	604	Silt, Clay
St. 65	58° 30.068'	09° 29.887'	530	Silt, Clay
BIGO2-1	58º 10.969'	09º 47.423'	502	Silt, Clay
BIGO2-2	58º 18.778'	09º 34.362'	678	Silt, Clay
BIGO2-3	57º 59.220'	09º 14.300'	490	Silt, Clay

[a] Sediment type description is based on grain size compositions presented in previous studies (Spiegel et al., 2023).

V.3.1 Sampling

Sediment samples for solid phase analysis were taken at every centimeter of the sediment cores and subsequently stored refrigerated at 4°C. Sediment for pore water analysis was sampled from an additional core in an argon-filled glove bag in a cooled laboratory adjusted to bottom water temperatures (~7°C). Subsequently, the sediment samples were centrifuged at 4000 rpm at 8°C for 20 min to separate the porewater from the solid phase. The supernatant water was filtered through a 0.2 μm cellulose-acetate syringe filter inside the glove bag and subsequently stored refrigerated until further home-based analysis. From the same core, a water sample of the overlying water was taken and filtered for bottom water analysis.

For the measurement of benthic DIC fluxes, the GEOMAR BIGO (Biogeochemical Observatory) lander was deployed as described in detail by Sommer et al. (2008, 2009). The BIGO contained two circular flux chambers (internal diameter 28.8 cm, area 651.4 cm^2) that were smoothly placed on the sea floor using a TV-guided launching system. During an initial period of approximately 2 hours (BIGO-2-1) and 4 hours (BIGO-2-2 & -3), the water inside the flux chambers was periodically replaced with ambient bottom water. Subsequently, the chambers were slowly driven into the sediment (~30 cm h^{-1}). After insertion, the water inside the benthic chambers was replaced once more with ambient bottom water to flush out solutes that might have been released from the sediment during this process. To determine benthic DIC fluxes, eight sequential water samples were taken with glass syringes (~47 ml) using syringe water samplers. The syringes were connected to the chamber using 1 m long Vygon tubes with a volume of 5.2 ml. Before deployment, these tubes were filled with distilled water. After 35 hours (BIGO-2-1) or 28 hours (BIGO-2-2, -3), the BIGO landers were recovered and the water samples were stored refrigerated until DIC analysis at GEOMAR laboratories.

V.3.2 Analytical techniques

Total alkalinity (TA) was determined directly onboard by titration of 1 ml porewater or bottom water with 0.02 M hydrochloric acid (HCl) and using methyl red and methylene blue as indicators for the colour shift. During titration, argon gas was constantly added to the solution to remove CO_2. The analysis was calibrated using an IAPSO seawater standard with an analytical precision better than 0.4%. Water samples taken with the BIGO were analysed for DIC concentrations immediately after the cruise by flow injection (Hall and Aller, 1992). The water samples were injected into a steady flow of 0.03 M HCl. The produced CO_2 was carried along a Teflon membrane into a 0.01 M NaOH solution and subsequently measured by a conductivity detector (VWR scientific, model 1054). The solid phase analytics for the determination of porosity and POC contents at the six stations were described in Spiegel et al. (2023).

V.3.3 Calculating the benthic POC system

Mass accumulation rates (MAR) were calculated as follows:

$$\mathrm{MAR} = \mathrm{ds} \cdot (1\text{-}\phi_c) \cdot \mathrm{SR} \quad \text{(V1)}$$

Where ds is the density of dry solids (2.5 g cm^{-3}), ϕ_c is the porosity in compacted sediment and SR is the sedimentation rate in compacted sediments. The SR was adopted from a previous study reporting average sedimentation rates before and after 1963 in compacted sediments in the same sediment cores (Spiegel et al., 2024 - in rev.). Burial fluxes of POC before and after 1963 were then described as:

$$\text{POC burial flux} = \mathrm{MAR} \cdot \mathrm{POC}_{10\mathrm{cm}} \quad \text{(V2)}$$

Where POC_{10cm} is the POC content at 10 cm sediment depth, which is the depth below the bioturbated layer (Spiegel et al., 2024 - in rev.). Recent POC burial fluxes were calculated using the sedimentation rate after 1963. The sedimentation rate before 1963 was used to estimate temporal variability in POC burial fluxes, assuming that POC contents at 10 cm were constant over time.

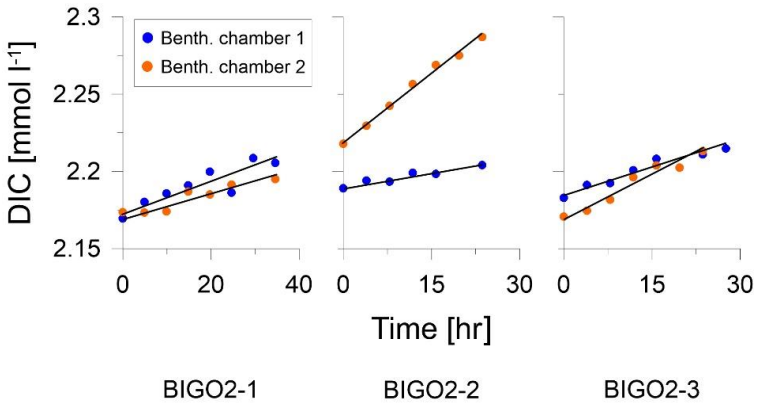

Figure V2. DIC concentrations over time in the benthic chambers at the three BIGO stations. The solid lines indicate linear regression used for calculating the benthic DIC fluxes. The R^2 were 0.79 and 0.88 for BIGO-2-1, 0.92 and 0.99 for BIGO-2-2, and 0.95 and 0.95 for BIGO-2-3.

At the three BIGO stations, benthic DIC fluxes were calculated by least-square linear regression of the DIC concentration increase over time and the height of the overlying water in the benthic chamber (Fig. V2). The benthic DIC fluxes presented in this study represent the mean of both benthic chambers. At non-BIGO stations, TA porewater gradients were used to calculate benthic DIC fluxes by applying Fick's First Law:

$$\text{Benthic DIC flux} = -\phi D_{sed} \cdot \frac{d[C]}{dx} \cdot \alpha \quad \text{(V3)}$$

Where ϕ is porosity in the upper most sediment layer, d[C]/dx is the TA concentration gradient between the porewater (at 0.5cm) and bottom water, D_{sed} is the effective molecular diffusion coefficient of bicarbonate (HCO_3^-) in sediments calculated by the free water molecular diffusion coefficient of $0.66 \cdot 10^{-5}$ cm^2 s^{-1} at ambient water conditions of 7°C, 50 bar and 35 PSU (Boudreau, 1997) and the tortuosity of the sediment, and α is a correction factor for the enhancement of solute transport by bioirrigation (Ståhl et al., 2004). We thereby assumed that the diffusive TA flux is governed by HCO_3^- and that the contributions of CO_2 and carbonate (CO_3^{2-}) are minor. The tortuosity was determined following the empirical relationship with porosity presented by (Iversen and Jørgensen, 1993). The correction factor α was calculated as the ratio between fluxes determined from in-situ measurements and porewater gradients at the three BIGO stations. Bioirrigation at these stations accounted for 35 - 66 % of the total benthic DIC fluxes. The mean correction factor of the three BIGO stations (α = 2.1) was then applied to the diffusive TA flux at non-BIGO stations to obtain total benthic DIC fluxes. Sedimentary $CaCO_3$ dissolution can contribute to the benthic DIC and diffusive TA fluxes. Following the approach of Ståhl et al. (2004) based on previous studies (Anderson et al., 1986; Jørgensen, 1996; Hulthe et al., 1998), we assumed that 10% of the benthic DIC and diffusive TA fluxes originates from $CaCO_3$ dissolution and corrected for this fraction accordingly.

Rain rates of POC were calculated as the sum of POC burial fluxes and benthic DIC fluxes:

$$\text{POC rain rate} = \text{POC burial flux} + \text{Benthic DIC flux} \quad \text{(V4)}$$

The POC burial efficiency was then calculated as follows:

$$\text{POC burial efficiency} = \frac{\text{POC burial flux}}{\text{POC rain rate}} \cdot 100\% \quad \text{(V5)}$$

Table V2. POC cycling in the Skagerrak.

Model data	MUC2 500m	MUC5 434m	MUC7 677m	MUC8 490m	MUC9 604m	St.65 530m
Mass accumulation rate (g cm^{-2} yr^{-1}) [a]	0.10	0.08	0.08	0.14	0.06	0.07
POC content at 10 cm (wt%) [b]	2.7	2.0	2.4	2.5	2.3	2.3
POC burial flux (mol m^{-2} yr^{-1}) [a]	2.3	1.4	1.5	2.9	1.2	1.4
Benthic DIC flux (mol m^{-2} yr^{-1}) [c]	1.4	1.2	2.8	2.5	4.1	-
POC rain rate (mol m^{-2} yr^{-1})	3.6	2.7	4.3	5.4	5.3	-
POC burial efficiency (%)	63	54	35	54	22	-

[a] Mass accumulation rates and POC burial fluxes refer to sedimentation rates after the year 1963 (Eq. V1). [b] POC contents at 10 cm refer to the depth below the bioturbation zone (Spiegel et al., 2024 - in rev.). [c] Benthic DIC fluxes were corrected for $CaCO_3$ dissolution assuming a contribution of 10% (Source). Benthic DIC fluxes at stations MUC5 and MUC9 were calculated by diffusive TA fluxes and a correction factor for faunal activity (Eq. V3).

V.4 Results

V.4.1 Solid phase and dissolved geochemistry

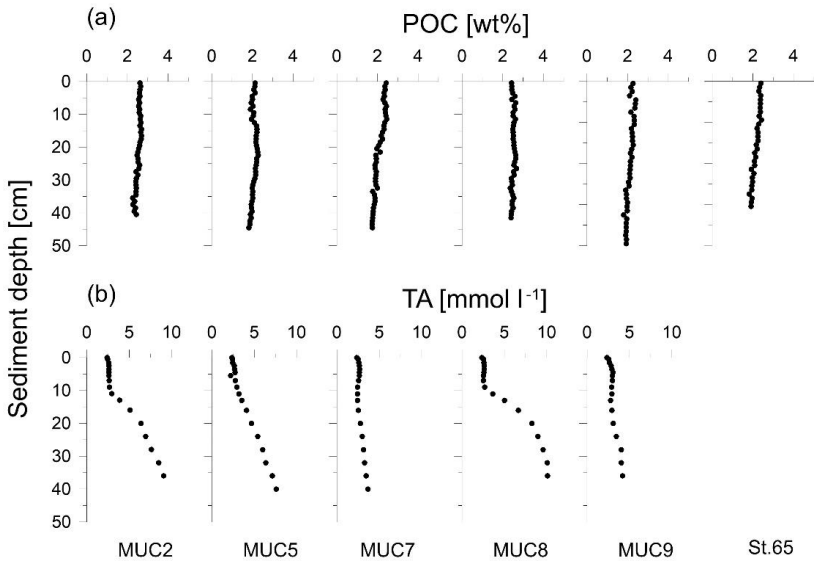

Figure V3. (a) Solid phase POC content and (b) dissolved TA concentration with sediment depth. The measurement at 0 cm in the TA profiles refers to the bottom water sample. No TA measurements were conducted at St. 65.

POC contents varied between 1.6 and 2.8 wt% and generally decreased with sediment depth (Fig. V3a). In the upper ~10 - 20 cm of the sediment cores, POC contents scattered but stayed nearly constant on average. Below this depth, POC contents showed a decreasing trend. Dissolved TA concentrations ranged between 2.3 and 10.2 mmol l^{-1} (Fig. V3b). Concentrations were nearly constant in the upper ~5 - 10 cm of the sediment cores and increased thereafter with sediment depth. Benthic chamber DIC concentrations varied between 2.17 and 2.29 mmol l^{-1} and showed an increasing trend over time.

V.4.2 POC fluxes and burial efficiencies

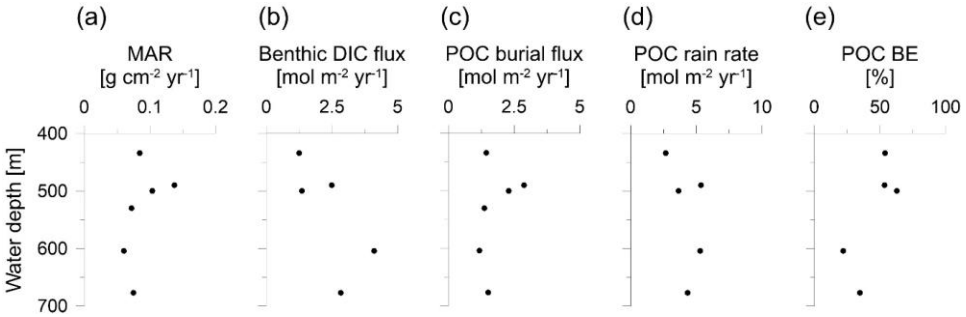

Figure V4. (a) Mass accumulation rate, (b) benthic DIC flux, (c) POC burial flux, (d) POC rain rate and (e) POC burial efficiency plotted against water depth.

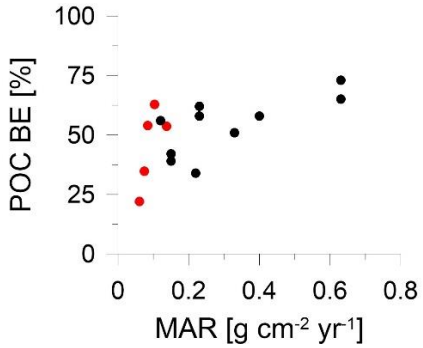

Figure V5. POC burial efficiencies plotted against mass accumulation rates of this study (red dots) and from Ståhl et al. (2004) in the Skagerrak (black dots).

Burial fluxes of POC varied between 1.2 and 2.9 mol m^{-2} yr^{-1} (Tab. V2, Fig. V4) while benthic DIC fluxes ranged between 1.2 and 4.1 mol m^{-2} yr^{-1}. The resulting POC rain rates varied between 2.7 and 5.4 mol m^{-2} yr^{-1} and burial efficiencies between 22 - 63 %. While benthic DIC fluxes increased with

water depth, POC burial efficiencies decreased across the different stations. Mass accumulation rates, POC burial fluxes and POC rain rates varied between the stations, but no clear trend was observed with water depth (Fig. V4, Fig. V5). Average POC burial fluxes before 1963 ranged from 2.6 to 9.4 mol m^{-2} yr^{-1} and after 1963 from 1.2 to 2.9 mol m^{-2} yr^{-1} (Fig. V6). On average across all stations, POC burial fluxes decreased from 4.3 to 1.8 mol m^{-2} yr^{-1}.

V.5 Discussion

V.5.1 POC cycling in the Skagerrak

Given average POC burial fluxes of 1.9 mol m^{-2} yr^{-1} and benthic DIC fluxes of 2.3 mol m^{-2} yr^{-1}, roughly 56 % of the POC that settles on the seafloor is recycled back to the overlaying water column. The other 44 % is permanently buried in Skagerrak sediments. The presented numbers are in the range of previously reported burial fluxes of 0.2 - 10.8 mol m^{-2} yr^{-1} (Jørgensen et al., 1990; Anton et al., 1993; Bakker and Helder, 1993; Meyenburg and Liebezeit, 1993; De Haas and van Weering, 1997; Ståhl et al., 2004; Diesing et al., 2021), in-situ benthic DIC or O_2 fluxes of 1.9 - 5.3 mol m^{-2} yr^{-1} (Ståhl et al., 2004) and ex-situ benthic DIC or O_2 fluxes of 0.7 - 13.7 mol m^{-2} yr^{-1} (Jørgensen et al., 1990; Bakker and Helder, 1993; Canfield et al., 1993; Van Cappellen and Wang, 1996; Wang and Van Cappellen, 1996). Hence, our dataset further extends the existing literature in the Skagerrak, in particular towards in-situ measurements. In addition to DIC, we determined in-situ O_2 fluxes in the benthic chambers (Fig. VS1) showing comparable values of 1.8 - 2.5 mol m^{-2} yr^{-1} to the benthic DIC fluxes with a mean DIC:O_2 ratio of 1.2:1. Benthic O_2 uptake and benthic DIC release are both commonly used as representatives for POC recycling in marine sediments. However, the use of O_2 is limited by not accounting for the anaerobic degradation of POC in the sediment, while benthic DIC fluxes need to be corrected for the dissolution of $CaCO_3$ in sediments. Considering that aerobic respiration only represents a fraction of the POC degradation in Skagerrak sediments (Bakker and Helder, 1993; Canfield et al., 1993; Van Cappellen and Wang, 1996; Wang and Van Cappellen, 1996; Rysgaard et al., 2001), we opted for DIC fluxes to describe sedimentary POC recycling and accounted for $CaCO_3$ dissolution by subtracting 10% from the total benthic DIC flux (Eq. V3). On average, in-situ benthic DIC fluxes were roughly two times higher than diffusive TA fluxes, indicating a strong effect of faunal activity on benthic fluxes in the Skagerrak. Combining POC burial fluxes and benthic DIC fluxes yields average POC rain rates of 4.1 mol m^{-2} yr^{-1}, which is in good agreement with earlier studies (Ståhl et al., 2004). It should be noted that POC burial fluxes in this study represent values integrated over decades, while benthic fluxes may vary seasonally or daily depending on the faunal activity. Hence, combining the two measures is associated with uncertainty. Dissolved organic carbon fluxes were not considered in this study, which have been estimated to contribute ~3% to total POC rain rates in the Skagerrak (Ståhl et al., 2004).

Despite the small dataset, the positive correlation between MAR and POC burial efficiencies (Fig. V5) suggests that bulk sediment deposition controls the variability of burial efficiencies in the Skagerrak. However, it is important to note that this relationship might arise since MAR is used to calculate POC burial efficiencies (Eq. V2, V5). The quality of the deposited POC might also affect POC cycling in the Skagerrak as indicated by decreasing POC burial efficiencies and increasing DIC recycling fluxes with water depth (Fig. V4). While fresher material is deposited in the central deep basin below 600 meters water depth (MUC7 and MUC9), more refractory material is deposited between 400 and 500 meters water depth (MUC2, MUC5, MUC8). Previous studies showed that sedimentation rates and MAR are elevated in belt-like structures between 120 and 600 meters following the general circulation pattern (Fig. V1) and widening towards the northeastern Skagerrak (Diesing et al., 2021; Spiegel et al., 2024). Given that a large part of the POC input is likely to be transported from the North Sea (Liebezeit, 1988; Anton et al., 1993; Meyenburg and Liebezeit, 1993; De Haas and van Weering, 1997), POC deposition at intermediate water depths in the Skagerrak might be dominated by the lateral input of refractory material, resulting in lower benthic DIC recycling fluxes and higher POC burial efficiencies at these sites. This is consistent with an earlier study that found lower-quality POC settling in the northeastern Skagerrak and less lateral transport in the central deep Skagerrak (Ståhl et al., 2004).

V.5.2 Disentangling the sources of POC

Based on POC burial fluxes and primary production rates, previous studies proposed that 50-90% of the sedimentary POC is of allochthonous origin (Liebezeit, 1988; Anton et al., 1993; Meyenburg and Liebezeit, 1993; De Haas and van Weering, 1997). In order to constrain these numbers, we present three approaches to differentiate between locally produced and laterally transported POC (Tab. V3).

Suess (1980) introduced an empirical function of POC fluxes with water depth based on surface ocean primary production rates:

$$\text{POC flux (z)} = \frac{\text{Primary production rate}}{0.0238 \cdot \text{z} + 0.212} \quad \text{(V6)}$$

Where z is the water depth. Applying a primary production of 11 mol m^{-2} yr^{-1} (Beckmann and Liebezeit, 1988) yields 0.6 - 1.0 mol m^{-2} yr^{-1} of locally produced POC raining onto the seafloor using the respective water depths at each station (Tab. V1). These values compare well with sediment trap data of 1.1 mol m^{-2} yr^{-1} at 263 meters (Kempe and Jennerjahn, 1988) and 0.2 - 1.1 mol m^{-2} yr^{-1} between 266 and 562 meters water depth based on Chlorophyll-a measurements representative of locally produced POC (Ståhl et al., 2004). This approach results in an average contribution of 24±6 % of locally produced POC to total POC rain rates.

Since siliceous phytoplankton (diatoms) are seasonally dominant in the Skagerrak (Gran-Stadniczeñko et al., 2019) and biogenic silica (bSi) is depleted in the laterally transported material (Spiegel et al., 2023), bSi rain rates might represent a reasonable proxy for locally produced POC rain rates. Ragueneau et al. (2002) proposed a function for Si:C flux ratios with water depth:

$$\text{Si: C flux ratio (z)} = \text{Si: C flux ratio (0)} \cdot z^{0.41} \quad \text{(V7)}$$

Where z is the water depth. Assuming a bSi:C ratio of 0.13 in surface water diatoms (Brzezinski, 1985), resulting bSi:C flux ratios vary from 1.6 to 1.9 at the different sites. This is slightly higher compared to sediment trap data of 0.1 - 1.7 (Kempe and Jennerjahn, 1988) and 0.1 - 0.5 (Petersson and Floderus, 2001). The reason for the discrepancy could be bSi depletion relative to POC during the lateral transport of material from the North Sea (Spiegel et al., 2023) diluting bSi in the sediment traps. Hence, we opted for the bSi:C flux ratios of 1.6 - 1.9 (Eq. V7). Multiplication of the bSi:C flux ratios and bSi rain rates reported at the same stations (Spiegel et al., 2023) then yields locally produced POC rain rates of 0.5 - 0.8 mol m^{-2} yr^{-1}. Averaged across the stations, this represents 19±4 % of total POC rain rates. Despite the depleted bSi content relative to POC in the lateral transport, it is important to note that the reported bSi rain rates by Spiegel et al. (2023) partly comprise lateral bSi inputs. Hence, the derived local POC rain rates likely represent an upper limit.

A previous study differentiated between locally produced and laterally transported bulk sediment inputs by comparing ^{210}Pb rain rates at the seafloor with the atmospheric ^{210}Pb input in the Skagerrak at the sites presented in this study (Spiegel et al., 2024). Considering that ^{210}Pb and POC are both particle reactive and transported alongside bulk sediment fluxes, the proportions based on ^{210}Pb might be representative of POC fluxes. Applying the ^{210}Pb-derived proportions at the individual sites to total POC rain rates (Tab. V2) results in local and lateral POC rain rates of 0.4 - 1 and 2.1 - 4.2 mol m^{-2} yr^{-1}, respectively. This approach yields 15±4 % of locally produced and 85±4 % of laterally transported POC contributions to total POC rain rates. However, the local material probably contains more POC than the lateral material given the continuous degradation during the transit from the North Sea. Since ^{210}Pb variability over the transit is unknown (Spiegel et al., 2024), the POC fluxes derived from ^{210}Pb rain rates are associated with uncertainty.

The summary shows that, on average, 19±6 % of the total POC rain rate stems from local primary production, with the remainder of 81±6% being transported laterally into the Skagerrak (Tab. V3). This is in good agreement with the previous estimates of 50 - 90% (Liebezeit, 1988; Anton et al., 1993; Meyenburg and Liebezeit, 1993; De Haas and van Weering, 1997).

Table V3. Summary of methods used to differentiate between locally produced and laterally transported POC in Skagerrak sediments.

Local and lateral POC rain rates (mol m^{-2} yr^{-1}) [a]	MUC7		MUC8		MUC7		MUC8		MUC9	
	Loc	Lat	Loc	Lat	Loc	Lat	Loc	Lat	Loc	Lat
POC flux at a given water depth [b]	0.9 (24%)	2.8 (76%)	1.0 (40%)	1.5 (60%)	0.7 (21%)	2.5 (79%)	0.9 (19%)	3.8 (81%)	0.7 (16%)	3.9 (84%)
Biogenic silica proxy [c]	0.8 (21%)	2.9 (79%)	0.8 (32%)	1.7 (68%)	0.5 (17%)	2.7 (83%)	0.6 (14%)	4.1 (86%)	0.5 (10%)	4.2 (90%)
^{210}Pb rain rate proxy [d]	0.4 (11%)	3.3 (89%)	0.4 (16%)	2.1 (84%)	0.4 (14%)	2.8 (86%)	0.5 (10%)	4.2 (90%)	1.0 (22%)	3.7 (78%)

[a] Proportions refer to locally produced (Loc) and laterally transported (Lat) POC rain rates and their relative percentage in brackets. The sum of both equals the total POC rain rate (Tab. V2). [b] POC flux at a given water depth is based on a function predicting the POC flux at any given water depth based on surface ocean primary production (Suess, 1980) and the water depths at the respective stations. [c] The biogenic silica proxy calculates locally produced POC based on Si:C ratios in particles raining onto the seafloor multiplied by biogenic silica rain rates (Spiegel et al., 2023). Si:C ratios in particles raining onto the seafloor were calculated using a function describing Si:C variations with water depth (Ragueneau et al., 2002) and surface ocean Si:C ratios in diatoms (Brzezinski, 1985). [d] ^{210}Pb rain rate proxy applies the proportions between atmospheric (local) ^{210}Pb inputs and total ^{210}Pb rain rates at the seafloor to calculate local and lateral POC inputs.

V.5.3 Temporal variability of POC burial fluxes

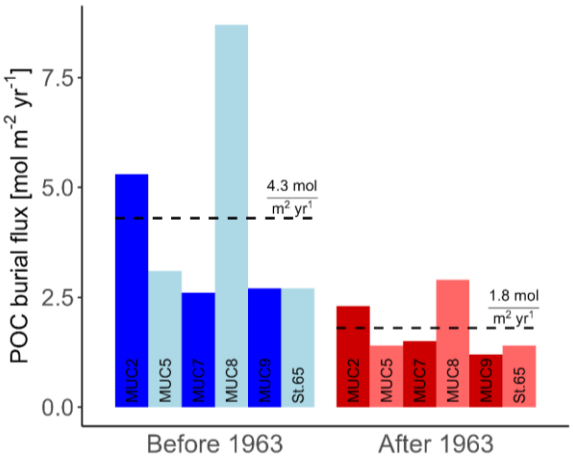

Figure V6. POC burial fluxes before (blue) and after 1963 (red). The dashed lines indicate average POC burial fluxes across the six stations.

Average POC burial fluxes before and after the year 1963 suggest substantial temporal variability of POC cycling in the Skagerrak, with decreasing POC burial fluxes in the Skagerrak over the last ~100 years (Fig. V6). Since the POC burial fluxes are based on the decline in sedimentation rates reported by Spiegel et al. (2024 - in rev.), our calculations share the uncertainties and assumption discussed therein. In short, the shift in the presented POC burial fluxes before and after 1963 represents a

general trend rather than describing the actual temporal evolution of POC burial in the natural system, which is likely more complex. Additionally, we assumed a constant POC content at 10 cm sediment depth over time (Eq. V2). Considering that POC burial efficiencies correlate with MAR in the Skagerrak (Fig. V5), this assumption likely introduces further uncertainty. Nevertheless, the consistent and substantial decrease from 4.3 to 1.8 mol m^{-2} yr^{-1} across stations suggests that the general trend of declining POC burial fluxes in the Skagerrak remains valid.

Spiegel et al. (2024 - in rev.) qualitatively assessed major driving factors for the decrease in sedimentation rates in the Skagerrak based on the relative contributions of individual processes to the overall North Sea sediment budget. They concluded that a shift in the North Sea circulation pattern at ~1960 (Mathis et al., 2015; Daewel and Schrum, 2017) and increased deposition in neighbouring depocenters, such as the Wadden Sea (Cahoon et al., 2000; van Wijnen and Bakker, 2001; Flemming, 2002; Madsen et al., 2007; Bartholdy et al., 2010; Lodder et al., 2019), could be responsible for the decline in sedimentation rates. Since POC is transported alongside the bulk sediment, these processes may also explain the decrease in Skagerrak POC burial fluxes. Concerning POC cycling, another reason might be temporal variability in primary production rates in the Skagerrak and North Sea. Phytoplankton growth may have been affected by extensive eutrophication since ~1900 followed by reduced riverine nutrient loads since 1985 and decreased eutrophication observed in the North Sea since 1990 (Axe et al., 2017, 2022). A similar shift was reported for the year 1975 in the Oslofjord (Dale et al., 1999). Furthermore, Binczewska et al. (2018) found a species shift from B. Skagerrakensis to S. Fusiform in the Skagerrak between 1948 and 2018, indicating a relative increase in labile organic matter accumulation and more degradation in sediments. Hence, reduced surface water production rates in the Skagerrak and North Sea since 1975 - 1990 and the deposition of more labile material since 1948 might have resulted in lower POC burial fluxes over time in the Skagerrak. Conversely, other studies reported increased primary production rates in the North Sea and Skagerrak since 1950 (Brückner and Mackensen, 2008) and between 1980 and 2000 (Reid et al., 1998; McQuatters-Gollop et al., 2007). Furthermore, despite lower nutrient inputs, higher POC concentrations were reported in the Skagerrak since 1998 (Frigstad et al., 2013) in response to a positive North Atlantic Oscillation (NAO) phase and its influence on sea surface temperature, wind systems and circulation patterns in the North Sea (Edwards, 2001; Reid et al., 2003; Beaugrand, 2004; Alheit et al., 2005; Mathis et al., 2015; Daewel and Schrum, 2017). Therefore, it is unclear whether productivity shifts in the North Sea and Skagerrak could account for the observed trend in POC burial fluxes in the Skagerrak. To unravel the underlying mechanisms that lead to the decline in POC burial fluxes, we recommend combining a more detailed description of the organic material with temporally resolved provenance and large-scale particle transport studies in the North Sea and Skagerrak.

V.5.4 Global context

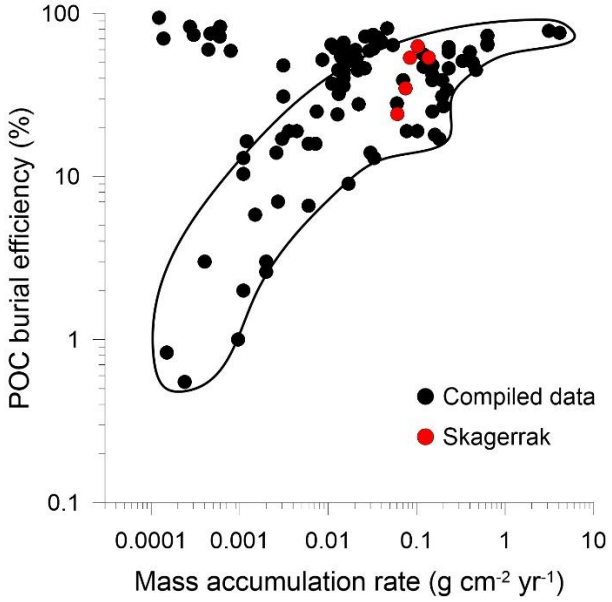

Figure V7. Log-log plot of POC burial efficiencies plotted against mass accumulation rates. The solid line represents normal marine conditions, datapoints outside this area were taken in low oxygen environments (euxinic and < 20µM O_2). Skagerrak data from this study (red dots) are compared to compiled literature data (black dots) in coastal to continental margin sediments at the Danish coast (Jørgensen et al., 1990), the Baltic Sea (Balzer et al., 1986), the northwest Atlantic (Heggie et al., 1987), California basins (Berelson et al., 1987, 1996; Bender et al., 1989; Jahnke, 1990), North Carolina (Martens and Klump, 1984), Svalbad (Glud et al., 1998), the Southern Weddell Sea (Hulth et al., 1997), the Peru continental margin (Reimers and Suess, 1983; Dale et al., 2015) and other Skagerrak sites (Ståhl et al., 2004), in deep sea sediments in the northeast pacific (Bender and Heggie, 1984), the Southern Weddell Sea (Hulth et al., 1997) and the Pacific-Antarctic Ridge (Reimers and Suess, 1983) and in sediments under low oxygen or euxinic conditions in the Black Sea (Canfield, 1989; Li et al., 2023), the Baltic Sea (Boesen and Postma, 1988), British Columbia (Ahmed et al., 1984), Long Island Sound (Krom and Bennett, 1985) and the Skan Bay Alaska (Alperin et al., 1992).

In order to evaluate POC burial efficiencies in the Skagerrak in a global context, we compare our results to other marine settings including continental margin, shelf and deep-sea environments under oxic or anoxic/euxinic conditions (Fig. V7). The Skagerrak generally aligns well with the global trend. Within the oxic environments, our stations show comparably high MAR and burial efficiencies. This could be explained by the large lateral sediment (Spiegel et al., 2024) and POC (Tab. V3) input of mostly refractory material increasing the burial efficiency in Skagerrak deposits relative to other sites.

Literature

Ahmed, S.I., King, S.L., Clayton, J.R., 1984. Organic matter diagenesis in the anoxic sediments of saanich inlet, British Columbia, Canada: a case for highly evolved community interactions. Mar. Chem. 14, 233–252. https://doi.org/10.1016/0304-4203(84)90044-6

Alheit, J., Möllmann, C., Dutz, J., Kornilovs, G., Loewe, P., Mohrholz, V., Wasmund, N., 2005. Synchronous ecological regime shifts in the central Baltic and the North Sea in the late 1980s. ICES J. Mar. Sci. 62, 1205–1215. https://doi.org/10.1016/j.icesjms.2005.04.024

Aller, R.C., Mackin, J.E., 1984. Preservation of reactive organic matter in marine sediments. Earth Planet. Sci. Lett. 70, 260–266. https://doi.org/10.1016/0012-821X(84)90010-4

Alperin, M.J., Reeburgh, W.S., Devol, A.H., 1992. Organic carbon remineralization and preservation in sediments of Skan Bay, Alaska. Product. Accumul. Preserv. Org. Matter Recent Anc. Sediments Pp 99-122.

Anderson, L.G., Hall, P.O.J., Iverfeldt, A., Rutgers Van Der Loejf, M.M., Sundby, B., Westerlund, S.F.G., 1986. Benthic respiration measured by total carbonate production. Limnol. Oceanogr. 31, 319–329. https://doi.org/10.4319/lo.1986.31.2.0319

Anton, K.K., Liebezeit, G., Rudolph, C., Wirth, H., 1993. Origin, distribution and accumulation of organic carbon in the Skagerrak. Mar. Geol. 111, 287–297. https://doi.org/10.1016/0025-3227(93)90136-J

Arndt, S., Jørgensen, B.B., LaRowe, D.E., Middelburg, J.J., Pancost, R.D., Regnier, P., 2013. Quantifying the degradation of organic matter in marine sediments: A review and synthesis. Earth-Sci. Rev. 123, 53–86. https://doi.org/10.1016/j.earscirev.2013.02.008

Axe, P., Clausen, U., Leujak, W., Malcolm, S., Ruiter, H., Prins, T., Harvey, E.T., 2017. Eutrophication Status of the OSPAR Maritime Area. Third Integrated Report on the Eutrophication Status of the OSPAR Maritime Area.

Axe, P., Sonesten, L., Skarbövik, E., Leujak, W., Nielsen, L., 2022. Inputs of Nutrients to the OSPAR Maritime Area. In OSPAR, 2023: The 2023 Quality Status Report for the North-East Atlantic. OSPAR Commission, London. Available at: https://oap.ospar.org/en/ospar-assessments/quality-status-reports/qsr-2023/indicator-assessments/inputs-nutrients/.

Baeye, M., Fettweis, M., 2015. In situ observations of suspended particulate matter plumes at an offshore wind farm, southern North Sea. Geo-Mar. Lett. 35, 247–255. https://doi.org/10.1007/s00367-015-0404-8

Bakker, J.F., Helder, W., 1993. Skagerrak (northeastern North Sea) oxygen microprofiles and porewater chemistry in sediments. Mar. Geol. 111, 299–321. https://doi.org/10.1016/0025-3227(93)90137-K

Balzer, W., Pollehne, F., Erlenkeuser, H., 1986. Cycling of Organic Carbon in a Coastal Marine System, in: Sly, P.G. (Ed.), Sediments and Water Interactions. Springer New York, New York, NY, pp. 325–330. https://doi.org/10.1007/978-1-4612-4932-0_27

Bartholdy, A.T., Bartholdy, J., Kroon, A., 2010. Salt marsh stability and patterns of sedimentation across a backbarrier platform. Mar. Geol. 278, 31–42. https://doi.org/10.1016/j.margeo.2010.09.001

Beaugrand, G., 2004. The North Sea regime shift: Evidence, causes, mechanisms and consequences. Prog. Oceanogr. 60, 245–262. https://doi.org/10.1016/j.pocean.2004.02.018

Beckmann, M., Liebezeit, G., 1988. Organic carbon in the North Sea in May/June 1986: Distribution and controlling factors. Mitt. Geol.-Palaontol. Inst. Univ. Hamburg 65, 99-l 16.

Behrenfeld, M.J., O'Malley, R.T., Siegel, D.A., McClain, C.R., Sarmiento, J.L., Feldman, G.C., Milligan, A.J., Falkowski, P.G., Letelier, R.M., Boss, E.S., 2006. Climate-driven trends in contemporary ocean productivity. Nature 444, 752–755. https://doi.org/10.1038/nature05317

Bender, M., Jahnke, R., Ray, W., Martin, W., Heggie, D.T., Orchardo, J., Sowers, T., 1989. Organic carbon oxidation and benthic nitrogen and silica dynamics in San Clemente Basin, a continental borderland site. Geochim. Cosmochim. Acta 53, 685–697. https://doi.org/10.1016/0016-7037(89)90011-2

Bender, M.L., Heggie, D.T., 1984. Fate of organic carbon reaching the deep sea floor: a status report. Geochim. Cosmochim. Acta 48, 977–986. https://doi.org/10.1016/0016-7037(84)90189-3

Berelson, W.M., Hammond, D.E., Johnson, K.S., 1987. Benthic fluxes and the cycling of biogenic silica and carbon in two southern California borderland basins. Geochim. Cosmochim. Acta 51, 1345–1363. https://doi.org/10.1016/0016-7037(87)90320-6

Berelson, W.M., McManus, J., Coale, K.H., Johnson, K.S., Kilgore, T., Burdige, D., Pilskaln, C., 1996. Biogenic matter diagenesis on the sea floor: A comparison between two continental margin transects. J. Mar. Res. 54, 731–762. https://doi.org/10.1357/0022240963213673

Berger, W., Smetacek, V., Wefer, G., 1989. Ocean productivity and paleoproductivity - An overview. pp. 1–34.

Berner, R.A., 1989. Biogeochemical cycles of carbon and sulfur and their effect on atmospheric oxygen over phanerozoic time. Glob. Planet. Change 1, 97–122. https://doi.org/10.1016/0921-8181(89)90018-0

Berner, R.A., 1982. Burial of organic carbon and pyrite sulfur in the modern ocean; its geochemical and environmental significance. Am. J. Sci. 282, 451–473. https://doi.org/10.2475/ajs.282.4.451

Berner, R.A., 1980. Early diagenesis: a theoret. approach, Princeton series in geochemistry. Princeton University Press, Princeton, N.J.

Binczewska, A., Risebrobakken, B., Polovodova Asteman, I., Moros, M., Tisserand, A., Jansen, E., Witkowski, A., 2018. Coastal primary productivity changes over the last millennium: a case study from the Skagerrak (North Sea). Biogeosciences 15, 5909–5928. https://doi.org/10.5194/bg-15-5909-2018

Boesen, C., Postma, D., 1988. Pyrite formation in anoxic environments of the Baltic. Am. J. Sci. 288, 575–603. https://doi.org/10.2475/ajs.288.6.575

Boudreau, B.P., 1997. Diagenetic Models and Their Implementation: Modelling Transport and Reactions in Aquatic Sediments. Springer Berlin Heidelberg, Berlin, Heidelberg.

Brückner, S., Mackensen, A., 2008. Organic matter rain rates, oxygen availability, and vital effects from benthic foraminiferal δ13C in the historic Skagerrak, North Sea. Mar. Micropaleontol. 66, 192–207. https://doi.org/10.1016/j.marmicro.2007.09.002

Brzezinski, M.A., 1985. THE Si:C:N RATIO OF MARINE DIATOMS: INTERSPECIFIC VARIABILITY AND THE EFFECT OF SOME ENVIRONMENTAL VARIABLES [1]. J. Phycol. 21, 347–357. https://doi.org/10.1111/j.0022-3646.1985.00347.x

Buesseler, K.O., 1998. The decoupling of production and particulate export in the surface ocean. Glob. Biogeochem. Cycles 12, 297–310. https://doi.org/10.1029/97GB03366

Burdige, D.J., 2007. Preservation of Organic Matter in Marine Sediments: Controls, Mechanisms, and an Imbalance in Sediment Organic Carbon Budgets? Chem. Rev. 107, 467–485. https://doi.org/10.1021/cr050347q

Cahoon, D.R., French, J.R., Spencer, T., Reed, D., Möller, I., 2000. Vertical accretion versus elevational adjustment in UK saltmarshes: an evaluation of alternative methodologies. Geol. Soc. Lond. Spec. Publ. 175, 223–238. https://doi.org/10.1144/GSL.SP.2000.175.01.17

Canfield, D.E., 1994. Factors influencing organic carbon preservation in marine sediments. Chem. Geol. 114, 315–329. https://doi.org/10.1016/0009-2541(94)90061-2

Canfield, D.E., 1989. Sulfate reduction and oxic respiration in marine sediments: implications for organic carbon preservation in euxinic environments. Deep Sea Res. Part Oceanogr. Res. Pap. 36, 121–138. https://doi.org/10.1016/0198-0149(89)90022-8

Canfield, D.E., Jørgensen, B.B., Fossing, H., Glud, R., Gundersen, J., Ramsing, N.B., Thamdrup, B., Hansen, J.W., Nielsen, L.P., Hall, P.O.J., 1993. Pathways of organic carbon oxidation in three continental margin sediments. Mar. Geol. 113, 27–40. https://doi.org/10.1016/0025-3227(93)90147-N

Daewel, U., Akhtar, N., Christiansen, N., Schrum, C., 2022. Offshore wind farms are projected to impact primary production and bottom water deoxygenation in the North Sea. Commun. Earth Environ. 3, 292. https://doi.org/10.1038/s43247-022-00625-0

Daewel, U., Schrum, C., 2017. Low-frequency variability in North Sea and Baltic Sea identified through simulations with the 3-D coupled physical–biogeochemical model ECOSMO. Earth Syst. Dyn. 8, 801–815. https://doi.org/10.5194/esd-8-801-2017

Dahlgaard, H., Herrmann, J., Salomon, J.C., 1995. A tracer study of the transport of coastal water from the English Channel through the German Bight to the Kattegat. J. Mar. Syst. 6, 415–425. https://doi.org/10.1016/0924-7963(95)00017-J

Dale, A.W., Sommer, S., Lomnitz, U., Montes, I., Treude, T., Liebetrau, V., Gier, J., Hensen, C., Dengler, M., Stolpovsky, K., Bryant, L.D., Wallmann, K., 2015. Organic carbon production, mineralisation and preservation on the Peruvian margin. Biogeosciences 12, 1537–1559. https://doi.org/10.5194/bg-12-1537-2015

Dale, B., Thorsen, T.A., Fjellsa, A., 1999. Dinoflagellate Cysts as Indicators of Cultural Eutrophication in the Oslofjord, Norway. Estuar. Coast. Shelf Sci. 48, 371–382. https://doi.org/10.1006/ecss.1999.0427

Dangendorf, S., Müller-Navarra, S., Jensen, J., Schenk, F., Wahl, T., Weisse, R., 2014. North Sea Storminess from a Novel Storm Surge Record since AD 1843*. J. Clim. 27, 3582–3595. https://doi.org/10.1175/JCLI-D-13-00427.1

De Groot, S.J., 1986. Marine sand and gravel extraction in the North Atlantic and its potential environmental impact, with emphasis on the North Sea. Ocean Manag. 10, 21–36. https://doi.org/10.1016/0302-184X(86)90004-1

De Haas, H., Boer, W., van Weering, T.C.E., 1997. Recent sedimentation and organic carbon burial in a shelf sea: the North Sea. Mar. Geol. 144, 131–146. https://doi.org/10.1016/S0025-3227(97)00082-0

De Haas, H., van Weering, T.C.E., 1997. Recent sediment accumulation, organic carbon burial and transport in the northeastern North Sea. Mar. Geol. 136, 173–187. https://doi.org/10.1016/S0025-3227(96)00072-2

De La Rocha, C.L., Passow, U., 2007. Factors influencing the sinking of POC and the efficiency of the biological carbon pump. Deep Sea Res. Part II Top. Stud. Oceanogr. 54, 639–658. https://doi.org/10.1016/j.dsr2.2007.01.004

Diesing, M., Thorsnes, T., Bjarnadóttir, L.R., 2021. Organic carbon densities and accumulation rates in surface sediments of the North Sea and Skagerrak. Biogeosciences 18, 2139–2160. https://doi.org/10.5194/bg-18-2139-2021

Duarte, C.M., Middelburg, J.J., Caraco, N., 2005. Major role of marine vegetation on the oceanic carbon cycle. Biogeosciences 2, 1–8. https://doi.org/10.5194/bg-2-1-2005

Edwards, M., 2001. Long-term and regional variability of phytoplankton biomass in the Northeast Atlantic (1960–1995). ICES J. Mar. Sci. 58, 39–49. https://doi.org/10.1006/jmsc.2000.0987

Eigaard, O.R., Bastardie, F., Hintzen, N.T., Buhl-Mortensen, L., Buhl-Mortensen, P., Catarino, R., Dinesen, G.E., Egekvist, J., Fock, H.O., Geitner, K., Gerritsen, H.D., González, M.M., Jonsson, P., Kavadas, S., Laffargue, P., Lundy, M., Gonzalez-Mirelis, G., Nielsen, J.R., Papadopoulou, N., Posen, P.E., Pulcinella, J., Russo, T., Sala, A., Silva, C., Smith, C.J., Vanelslander, B., Rijnsdorp, A.D., 2017. The footprint of bottom trawling in European waters: distribution, intensity, and seabed integrity. ICES J. Mar. Sci. 74, 847–865. https://doi.org/10.1093/icesjms/fsw194

Eisma, D., Irion, G., 1988. Suspended Matter and Sediment Transport, in: Salomons, W., Bayne, B.L., Duursma, E.K., Förstner, U. (Eds.), Pollution of the North Sea. Springer Berlin Heidelberg, Berlin, Heidelberg, pp. 20–35. https://doi.org/10.1007/978-3-642-73709-1_2

Elliott, M., Nedwell, S., Jones, N.V., Read, S.J., Cutts, N.D., Hemingway, K.L., 1998. Intertidal Sand and Mudflats & Subtidal Mobile Sandbanks (volume II). An overview of dynamic and sensitivity characteristics for conservation management of marine SACs. Scott. Assoc. Mar. Sci. UK Mar. SACs Proj.

Fettweis, M., Francken, F., Van Den Eynde, D., Verwaest, T., Janssens, J., Van Lancker, V., 2010. Storm influence on SPM concentrations in a coastal turbidity maximum area with high anthropogenic impact (southern North Sea). Cont. Shelf Res. 30, 1417–1427. https://doi.org/10.1016/j.csr.2010.05.001

Flemming, B.W., 2002. Effects of Climate and Human Interventions on the Evolution of the Wadden Sea Depositional System (Southern North Sea), in: Wefer, G., Berger, W.H., Behre, K.-E., Jansen, E. (Eds.), Climate Development and History of the North Atlantic Realm. Springer Berlin Heidelberg, Berlin, Heidelberg, pp. 399–413. https://doi.org/10.1007/978-3-662-04965-5_26

Frigstad, H., Andersen, T., Hessen, D.O., Jeansson, E., Skogen, M., Naustvoll, L.-J., Miles, M.W., Johannessen, T., Bellerby, R.G.J., 2013. Long-term trends in carbon, nutrients and stoichiometry in Norwegian coastal waters: Evidence of a regime shift. Prog. Oceanogr. 111, 113–124. https://doi.org/10.1016/j.pocean.2013.01.006

Glud, R., Holby, O., Hoffmann, F., Canfield, D., 1998. Benthic mineralization and exchange in Arctic sediments (Svalbard, Norway). Mar. Ecol. Prog. Ser. 173, 237–251. https://doi.org/10.3354/meps173237

Gran-Stadniczeñko, S., Egge, E., Hostyeva, V., Logares, R., Eikrem, W., Edvardsen, B., 2019. Protist Diversity and Seasonal Dynamics in Skagerrak Plankton Communities as Revealed by Metabarcoding and Microscopy. J. Eukaryot. Microbiol. 66, 494–513. https://doi.org/10.1111/jeu.12700

Green, M.O., Vincent, C.E., McCave, I.N., Dickson, R.R., Rees, J.M., Pearsons, N.D., 1995. Storm sediment transport: observations from the British North Sea shelf. Cont. Shelf Res. 15, 889–912. https://doi.org/10.1016/0278-4343(95)80001-T

Hainbucher, D., Pohlmann, T., Backhaus, J., 1987. Transport of conservative passive tracers in the North Sea: first results of a circulation and transport model. Cont. Shelf Res. 7, 1161–1179. https://doi.org/10.1016/0278-4343(87)90083-5

Hall, P.. J., Aller, R.C., 1992. Rapid, small-volume, flow injection analysis for SCO2, and NH4+ in marine and freshwaters. Limnol. Oceanogr. 37, 1113–1119. https://doi.org/10.4319/lo.1992.37.5.1113

Hartnett, H.E., Keil, R.G., Hedges, J.I., Devol, A.H., 1998. Influence of oxygen exposure time on organic carbon preservation in continental margin sediments. Nature 391, 572–575. https://doi.org/10.1038/35351

Hedges, J.I., Keil, R.G., 1995. Sedimentary organic matter preservation: an assessment and speculative synthesis. Mar. Chem. 49, 81–115. https://doi.org/10.1016/0304-4203(95)00008-F

Hedges, J.I., Keil, R.G., Benner, R., 1997. What happens to terrestrial organic matter in the ocean? Org. Geochem. 27, 195–212. https://doi.org/10.1016/S0146-6380(97)00066-1

Heggie, D., Maris, C., Hudson, A., Dymond, J., Beach, R., Cullen, J., 1987. Organic carbon oxidation and preservation in NW Atlantic continental margin sediments. Geol. Soc. Lond. Spec. Publ. 31, 215–236. https://doi.org/10.1144/GSL.SP.1987.031.01.15

Heinatz, K., Scheffold, M.I.E., 2023. A first estimate of the effect of offshore wind farms on sedimentary organic carbon stocks in the Southern North Sea. Front. Mar. Sci. 9, 1068967. https://doi.org/10.3389/fmars.2022.1068967

Hjalmarsson, S., Anderson, L.G., She, J., 2010. The exchange of dissolved inorganic carbon between the Baltic Sea and the North Sea in 2006 based on measured data and water transport estimates from a 3D model. Mar. Chem. 121, 200–205. https://doi.org/10.1016/j.marchem.2010.04.008

Hoeksema, R.J., 2007. Three stages in the history of land reclamation in the Netherlands. Irrig. Drain. 56, S113–S126. https://doi.org/10.1002/ird.340

Hofstede, J., 2008. Coastal Flood Defence and Coastal Protection along the North Sea Coast of Schleswig-Holstein. Küste 134–142.

Holland, K.T., Elmore, P.A., 2008. A review of heterogeneous sediments in coastal environments. Earth-Sci. Rev. 89, 116–134. https://doi.org/10.1016/j.earscirev.2008.03.003

Hübner, G., Schwandt, D., 2018. EXTREME LOW FLOW AND WATER QUALITY – A LONG-TERM VIEW ON THE RIVER ELBE. Erdkunde 72, 235–252.

Hulth, S., Tengberg, A., Landén, A., Hall, P.O.J., 1997. Mineralization and burial of organic carbon in sediments of the southern Weddell Sea (Antarctica). Deep Sea Res. Part Oceanogr. Res. Pap. 44, 955–981. https://doi.org/10.1016/S0967-0637(96)00114-8

Hulthe, G., Hulth, S., Hall, P.O.J., 1998. Effect of oxygen on degradation rate of refractory and labile organic matter in continental margin sediments. Geochim. Cosmochim. Acta 62, 1319–1328. https://doi.org/10.1016/S0016-7037(98)00044-1

ICES, 2020. Greater North Sea ecoregion ? Fisheries overview, including mixed-fisheries considerations. https://doi.org/10.17895/ICES.ADVICE.7605

ICES, 2019. Working Group on the Effects of Extraction of Marine Sediments on the Marine Ecosystem (WGEXT). https://doi.org/10.17895/ICES.PUB.5733

IKSE, 2012. Abschlussbericht über die Erfüllung des „Aktionsplans Hochwasserschutz Elbe“ im Zeitraum 2003–2011.

IKSE, 2005. Die Elbe und ihr Einzugsgebiet – Ein geographisch-hydrologischer und wasserwirtschaftlicher Überblick.

IPCC, 2023. Climate Change 2021 – The Physical Science Basis: Working Group I Contribution to the Sixth Assessment Report of the Intergovernmental Panel on Climate Change, 1st ed. Cambridge University Press. https://doi.org/10.1017/9781009157896

Iversen, N., Jørgensen, B.B., 1993. Diffusion coefficients of sulfate and methane in marine sediments: Influence of porosity. Geochim. Cosmochim. Acta 57, 571–578. https://doi.org/10.1016/0016-7037(93)90368-7

Jahnke, R.A., 1990. Early diagenesis and recycling of biogenic debris at the seafloor, Santa Monica Basin, California. Journal of Marine Research 48, (2). https://elischolar.library.yale.edu/journal_of_marine_research/1975.

Jørgensen, B.B., 1996. Case study — Aarhus Bay, in: Jørgensen, B.B., Richardson, K. (Eds.), Coastal and Estuarine Studies. American Geophysical Union, Washington, D. C., pp. 137–154. https://doi.org/10.1029/CE052p0137

Jørgensen, B.B., Bang, M., Blackburn, T.H., 1990. Anaerobic mineralization in marine sediments from the Baltic Sea-North Sea transition. Mar. Ecol. Prog. Ser. 59, 39–54.

Kelletat, D., 1992. Coastal Erosion and Protection Measures at the German North Sea Coast. J. Coast. Res. 8, 699–711.

Kempe, S., Jennerjahn, T.C., 1988. The vertical particle flux in the northern North Sea, its seasonality and composition. Biogeochem. Distrib. Suspended Matter North Sea Implic. Fish. Biol. 65, 229–268.

Krom, M.D., Bennett, J.T., 1985. Sources, deposition rates and decomposition of organic carbon in recent sediment of Sachem Head Harbor, Long Island Sound. Estuar. Coast. Shelf Sci. 21, 325–336. https://doi.org/10.1016/0272-7714(85)90014-9

Lange, D., Müller, H., Piechotta, F., Schubert, R., 2008. The Weser Estuary. Küste 275–287.

Li, J., Haeckel, M., Dale, A.W., Wallmann, K., 2023. Degradation and accumulation of organic matter in euxinic surface sediments. Geochim. Cosmochim. Acta S0016703723006506. https://doi.org/10.1016/j.gca.2023.12.030

Liebezeit, G., 1988. Early diagenesis of carbohydrates in the marine environment—II. Composition and origin of carbohydrates in Skagerrak sediments, in: Organic Geochemistry In Petroleum Exploration. Elsevier, pp. 387–391. https://doi.org/10.1016/B978-0-08-037236-5.50046-4

Liu, K. -K., Atkinson, L., Chen, C.T.A., Gao, S., Hall, J., MacDonald, R.W., McManus, L.T., Quiñones, R., 2000. Exploring continental margin carbon fluxes on a global scale. Eos Trans. Am. Geophys. Union 81, 641–644. https://doi.org/10.1029/EO081i052p00641-01

Lodder, Wang, Elias, Van Der Spek, De Looff, Townend, 2019. Future Response of the Wadden Sea Tidal Basins to Relative Sea-Level rise—An Aggregated Modelling Approach. Water 11, 2198. https://doi.org/10.3390/w11102198

Madsen, A.T., Murray, A.S., Andersen, T.J., Pejrup, M., 2007. Temporal changes of accretion rates on an estuarine salt marsh during the late Holocene — Reflection of local sea level changes? The Wadden Sea, Denmark. Mar. Geol. 242, 221–233. https://doi.org/10.1016/j.margeo.2007.03.001

Martens, C.S., Klump, V.J., 1984. Biogeochemical cycling in an organic-rich coastal marine basin 4. An organic carbon budget for sediments dominated by sulfate reduction and methanogenesis. Geochim. Cosmochim. Acta 48, 1987–2004. https://doi.org/10.1016/0016-7037(84)90380-6

Mathis, M., Elizalde, A., Mikolajewicz, U., Pohlmann, T., 2015. Variability patterns of the general circulation and sea water temperature in the North Sea. Prog. Oceanogr. 135, 91–112. https://doi.org/10.1016/j.pocean.2015.04.009

Mayer, L.M., 1994. Surface area control of organic carbon accumulation in continental shelf sediments. Geochim. Cosmochim. Acta 58, 1271–1284. https://doi.org/10.1016/0016-7037(94)90381-6

McQuatters-Gollop, A., Raitsos, D.E., Edwards, M., Pradhan, Y., Mee, L.D., Lavender, S.J., Attrill, M.J., 2007. A long-term chlorophyll dataset reveals regime shift in North Sea phytoplankton biomass unconnected to nutrient levels. Limnol. Oceanogr. 52, 635–648. https://doi.org/10.4319/lo.2007.52.2.0635

Meyenburg, G., Liebezeit, G., 1993. Mineralogy and geochemistry of a core from the Skagerrak/Kattegat boundary. Mar. Geol. 111, 337–344. https://doi.org/10.1016/0025-3227(93)90139-M

Middelburg, J.J., 2019. Carbon Processing at the Seafloor, in: Marine Carbon Biogeochemistry, SpringerBriefs in Earth System Sciences. Springer International Publishing, Cham, pp. 57–75. https://doi.org/10.1007/978-3-030-10822-9_4

Mielck, F., Hass, H.C., Michaelis, R., Sander, L., Papenmeier, S., Wiltshire, K.H., 2019. Morphological changes due to marine aggregate extraction for beach nourishment in the German Bight (SE North Sea). Geo-Mar. Lett. 39, 47–58. https://doi.org/10.1007/s00367-018-0556-4

Otto, L., Zimmerman, J.T.F., Furnes, G.K., Mork, M., Saetre, R., Becker, G., 1990. Review of the physical oceanography of the North Sea. Neth. J. Sea Res. 26, 161–238. https://doi.org/10.1016/0077-7579(90)90091-T

Pedersen, T.F., Calvert, S.E., 1990. Anoxia vs. Productivity: What Controls the Formation of Organic-Carbon-Rich Sediments and Sedimentary Rocks? AAPG Bull. 74. https://doi.org/10.1306/0C9B232B-1710-11D7-8645000102C1865D

Petersson, M., Floderus, S., 2001. Use of amino acid composition to investigate settling and resuspension of a spring bloom in the southern Skagerrak. Limnol. Oceanogr. 46, 1111–1120. https://doi.org/10.4319/lo.2001.46.5.1111

Ragueneau, O., Dittert, N., Pondaven, P., Tréguer, P., Corrin, L., 2002. Si/C decoupling in the world ocean: is the Southern Ocean different? Deep Sea Res. Part II Top. Stud. Oceanogr. 49, 3127–3154. https://doi.org/10.1016/S0967-0645(02)00075-9

Reid, P.C., Edwards, M., Beaugrand, G., Skogen, M., Stevens, D., 2003. Periodic changes in the zooplankton of the North Sea during the twentieth century linked to oceanic inflow. Fish. Oceanogr. 12, 260–269. https://doi.org/10.1046/j.1365-2419.2003.00252.x

Reid, P.C., Edwards, M., Hunt, H.G., Warner, A.J., 1998. Phytoplankton change in the North Atlantic. Nature 391, 546–546. https://doi.org/10.1038/35290

Reimers, C.E., Suess, E., 1983. The partitioning of organic carbon fluxes and sedimentary organic matter decomposition rates in the ocean. Mar. Chem. 13, 141–168. https://doi.org/10.1016/0304-4203(83)90022-1

Rijnsdorp, A.D., Boute, P., Tiano, J., Lankheet, M., Soetaert, K., Beier, U., de Borger, E., Hintzen, N.T., Molenaar, P., Polet, H., Poos, J.J., Schram, E., Soetaert, M., van Overzee, H., van De Wolfshaar, K., van Kooten, T., 2020. The implications of a transition from tickler chain beam trawl to electric pulse trawl on the sustainability and ecosystem effects of the fishery for North Sea sole: an impact assessment. Wageningen Marine Research, IJmuiden,. https://doi.org/10.18174/519729

Rysgaard, S., Fossing, H., Jensen, M.M., 2001. Organic matter degradation through oxygen respiration, denitrification, and manganese, iron, and sulfate reduction in marine sediments (the Kattegat and the Skagerrak). Ophelia 55, 77–91. https://doi.org/10.1080/00785236.2001.10409475

Salomon, J.C., Breton, M., Guegueniat, P., 1995. A 2D long term advection—dispersion model for the Channel and southern North Sea Part B: Transit time and transfer function from Cap de La Hague. J. Mar. Syst. 6, 515–527. https://doi.org/10.1016/0924-7963(95)00021-G

Schlitzer, R., 2000. Applying the adjoint method for biogeochemical modeling: Export of particulate organic matter in the World Ocean , Inverse methods in biogeochemical cycles (P Kasibhata, ed). AGU Monogr. 114, 107–124.

Schmidt, M., 2021. Dynamics and variability of POC burial in depocenters of the North Sea (Skagerrak), Cruise No. AL561, 2.08.2021 – 13.08.2021, Kiel – Kiel, APOC. GEOMAR Helmholtz Centre for Ocean Research Kiel. https://doi.org/10.3289/CR_AL561

Slavik, K., Lemmen, C., Zhang, W., Kerimoglu, O., Klingbeil, K., Wirtz, K.W., 2019. The large-scale impact of offshore wind farm structures on pelagic primary productivity in the southern North Sea. Hydrobiologia 845, 35–53. https://doi.org/10.1007/s10750-018-3653-5

Sommer, S., Linke, P., Pfannkuche, O., Schleicher, T., Schneider v. D, D., Reitz, A., Haeckel, M., Flögel, S., Hensen, C., 2009. Seabed methane emissions and the habitat of frenulate tubeworms on the Captain Arutyunov mud volcano (Gulf of Cadiz). Mar. Ecol. Prog. Ser. 382, 69–86. https://doi.org/10.3354/meps07956

Sommer, S., Türk, M., Kriwanek, S., Pfannkuche, O., 2008. Gas exchange system for extended in situ benthic chamber flux measurements under controlled oxygen conditions: First application-Sea bed methane emission measurements at Captain Arutyunov mud volcano: Oxygen controlled benthic flux measurements. Limnol. Oceanogr. Methods 6, 23–33. https://doi.org/10.4319/lom.2008.6.23

Spiegel, T., Dale, A.W., Lenz, N., Schmidt, M., Moros, M., Lindhorst, S., Wolschke, H., Müller, D., Butzin, M., Fuhr, M., Kalapurakkal, H.T., Kasten, S., Wallmann, K., 2024a. A look into the temporal variability of sedimentation rates in the Skagerrak to track human and natural impacts in the North Sea - In review.

Spiegel, T., Dale, A.W., Lenz, N., Schmidt, M., Sommer, S., Kalapurakkal, H.T., Przibilla, A., Lindhorst, S., Wallmann, K., 2023. Biogenic silica cycling in the Skagerrak. Front. Mar. Sci. 10, 1141448. https://doi.org/10.3389/fmars.2023.1141448

Spiegel, T., Diesing, M., Dale, A.W., Lenz, N., Schmidt, M., Sommer, S., Böttner, C., Fuhr, M., Kalapurakkal, H.T., Schulze, C.-S., Wallmann, K., 2024b. Modelling mass accumulation rates and 210Pb rain rates in the Skagerrak: lateral sediment transport dominates the sediment input. Front. Mar. Sci. 11, 1331102. https://doi.org/10.3389/fmars.2024.1331102

Ståhl, H., Tengberg, A., Brunnegård, J., Bjørnbom, E., Forbes, T.L., Josefson, A.B., Kaberi, H.G., Hassellöv, I.M.K., Olsgard, F., Roos, P., Hall, P.O.J., 2004. Factors influencing organic carbon recycling and burial in Skagerrak sediments. J. Mar. Res. 62, 867–907. https://doi.org/10.1357/0022240042880873

Stanev, E.V., Dobrynin, M., Pleskachevsky, A., Grayek, S., Günther, H., 2009. Bed shear stress in the southern North Sea as an important driver for suspended sediment dynamics. Ocean Dyn. 59, 183–194. https://doi.org/10.1007/s10236-008-0171-4

Stevens, R.L., Bengtsson, H., Lepland, A., 1996. Textural provinces and transport interpretations with fine-grained sediments in the Skagerrak. J. Sea Res. 35, 99–110. https://doi.org/10.1016/S1385-1101(96)90739-X

Stride, A.H. (Ed.), 1982. Offshore tidal sands: processes and deposits. Chapman and Hall, London ; New York.

Suess, E., 1980. Particulate organic carbon flux in the oceans—surface productivity and oxygen utilization. Nature 288, 260–263. https://doi.org/10.1038/288260a0

Thomas, H., Bozec, Y., De Baar, H.J.W., Elkalay, K., Frankignoulle, M., Schiettecatte, L.-S., Kattner, G., Borges, A.V., 2005. The carbon budget of the North Sea. Biogeosciences 2, 87–96. https://doi.org/10.5194/bg-2-87-2005

Thomas, H., Freund, W., Mears, C., Meckel, E., Minutolo, F., Nantke, C., Neumann, A., Seidel, M., Van Dam, B., 2022. ALKOR Scientific Cruise Report. The Ocean's Alkalinity - Connecting geological and metabolic processes and time-scales: mechanisms and magnitude of metabolic alkalinity generation in the North Sea Cruise No. AL557. Open Access. Alkor-Berichte, AL557. GEOMAR Helmholtz-Zentrum für Ozeanforschung Kiel, Kiel, Germany, 22 pp.

Van Cappellen, P., Wang, Y., 1996. Cycling of iron and manganese in surface sediments; a general theory for the coupled transport and reaction of carbon, oxygen, nitrogen, sulfur, iron, and manganese. Am. J. Sci. 296, 197–243. https://doi.org/10.2475/ajs.296.3.197

Van Weering, T.C.E., Berger, G.W., Kalf, J., 1987. Recent sediment accumulation in the Skagerrak, Northeastern North Sea. Neth. J. Sea Res. 21, 177–189. https://doi.org/10.1016/0077-7579(87)90011-1

van Wijnen, H.J., Bakker, J.P., 2001. Long-term Surface Elevation Change in Salt Marshes: a Prediction of Marsh Response to Future Sea-Level Rise. Estuar. Coast. Shelf Sci. 52, 381–390. https://doi.org/10.1006/ecss.2000.0744

Wallmann, K., Aloisi, G., 2012. The Global Carbon Cycle: Geological Processes, in: Knoll, A.H., Canfield, D.E., Konhauser, K.O. (Eds.), Fundamentals of Geobiology. Wiley, pp. 20–35. https://doi.org/10.1002/9781118280874.ch3

Walsh, J.J., 1991. Importance of continental margins in the marine biogeochemical cycling of carbon and nitrogen. Nature 350, 53–55. https://doi.org/10.1038/350053a0

Wang, Y., Van Cappellen, P., 1996. A multicomponent reactive transport model of early diagenesis: Application to redox cycling in coastal marine sediments. Geochim. Cosmochim. Acta 60, 2993–3014. https://doi.org/10.1016/0016-7037(96)00140-8

Wollast, R., 1991. The coastal organic carbon cycle: Fluxes, sources, and sinks. In: Mantoura, R.F.C., Martin, J.M. and Wollast, R. Eds., Ocean Margin Processes in Global Change, Wiley, Chichester, 365-381.

VI. General conclusion and outlook

VI.1 Progress and limitations of the main objective of this thesis

The main objective of this thesis was to quantify the temporal variability in the lateral POC transport from the North Sea to the Skagerrak. Combining highly resolved age-depth models and sedimentary POC contents revealed a decrease in sedimentation rates and POC burial fluxes over time in the Skagerrak (Fig. II3, Fig. V6). However, deriving temporal trends in the lateral POC transport from the described POC burial fluxes requires two crucial assumptions. Firstly, the presented benthic DIC fluxes have been constant over the last century. Under this assumption, the trend in POC burial fluxes can be applied to total POC rain rates. However, various mechanisms have likely affected the benthic POC cycle in the Skagerrak over time. They include the sedimentation rate, which has been shown to change over time (Fig. II3), oxygen levels in the water column, the quality of organic material and bacterial activity (Aller and Mackin, 1984; Pedersen and Calvert, 1990; Canfield, 1994; Hedges and Keil, 1995; Hartnett et al., 1998; Ståhl et al., 2004; Burdige, 2007; Arndt et al., 2013; Dale et al., 2015). Hence, assuming a steady-state benthic DIC flux is likely not accurate and introduces unknown uncertainty and further investigations are recommended to fill this knowledge gap. For instance, long-term time series investigations of benthic DIC fluxes could improve our understanding of temporal changes in POC rain rates in the Skagerrak. The second assumption is that the contributions of local and lateral POC inputs to the Skagerrak deposits (Tab. V3) have been constant over the last century. If applicable, the temporal variability in the lateral POC input can be calculated from the change in POC rain rates over time and the relative contribution of laterally transported POC into the Skagerrak. However, the temporal variability in sedimentation rates in the Skagerrak indicates that the proportional input of the two POC sources has likely changed over time. Furthermore, previous studies showed that the eutrophication status and primary production rates in the North Sea and Skagerrak varied over time (Reid et al., 1998; Dale et al., 1999; McQuatters-Gollop et al., 2007; Brückner and Mackensen, 2008; Frigstad et al., 2013; Axe et al., 2017, 2022; Binczewska et al., 2018). Comparing the detailed characteristics of POC in suspended particles along a transect from the Skagerrak entrance to the basin with downcore POC characteristics in sediments, coupled with early diagenetic modeling, could help to distinguish between the local and lateral quantities of POC settling at the Skagerrak seafloor over time.

The temporal trends in the Skagerrak allow an estimation of the net effect of combined natural and human processes on the North Sea sediment and POC systems. This enables a qualitative evaluation of the possible causes for the observed decline in sediment and POC deposition in the Skagerrak. Preliminary results of the provenance study carried out by colleagues at GEOMAR reveal that the seafloor erosion at the northern Atlantic entrance into the North Sea is a currently underestimated sediment source to the Skagerrak deposits. This agrees well with the hypothesis presented in Chapter

I, which suggests that the North Atlantic entrance plays a crucial role in the decline of the sedimentation rate in the Skagerrak. Quantifying the downcore contributions of different source areas to the Skagerrak is currently in progress. However, it is recommended to verify the reasons behind the temporal variability in the Skagerrak resulting from this thesis and the provenance study with further independent methods. This could for example be achieved with the ensemble empirical mode decomposition method (EEMD) and the nonparametric Mann-Kendall test that have shown the capability to separate human and natural impacts on sedimentation processes (Liu et al., 2016; Li et al., 2020).

Ultimately, a large-scale reaction-transport model across the North Sea and Skagerrak regions is required to resolve the temporal evolution of lateral sediment and POC inputs into the Skagerrak and to quantify the impact of human activities on the POC cycle of the North Sea. The patterns and dynamics of sedimentation and biogeochemical processes in the Skagerrak region presented in this thesis can be used to feed and validate such a sophisticated model. Hence, this work represents a significant accomplishment of the APOC project.

VI.2 Outlook and further work

Following the work outlined in this study, the next step involves collecting additional data to finalize the preliminary draft presented in Chapter V. Therefore, the results of chlorophyll-a and lipid analysis of suspended and sedimentary material will be used to better characterize the quality of the POC. In addition, we will use the results of the 3d biophysical ecosystem model ECOMSO II (Daewel and Schrum, 2013) provided by colleagues at UHH and HEREON to investigate the POC transport across the boundaries of the Skagerrak region and to constrain the POC rain rates presented in this study. The model results may also offer an additional tool to quantify the contributions of locally and laterally derived POC to the total POC rain rates. The study will be further complemented by porewater data to identify the various pathways of microbial POC degradation in sediments. Finally, the complete dataset will be integrated into a sophisticated transport-reaction model simulating the benthic POC cycle in the Skagerrak. The model should ideally simulate the temporal trends observed at the individual stations in the Skagerrak and distinguish between the two distinct sources of POC, each with its own reactivity.

Literature

Aller, R.C., Mackin, J.E., 1984. Preservation of reactive organic matter in marine sediments. Earth Planet. Sci. Lett. 70, 260–266. https://doi.org/10.1016/0012-821X(84)90010-4

Anton, K.K., Liebezeit, G., Rudolph, C., Wirth, H., 1993. Origin, distribution and accumulation of organic carbon in the Skagerrak. Mar. Geol. 111, 287–297. https://doi.org/10.1016/0025-3227(93)90136-J

Arndt, S., Jørgensen, B.B., LaRowe, D.E., Middelburg, J.J., Pancost, R.D., Regnier, P., 2013. Quantifying the degradation of organic matter in marine sediments: A review and synthesis. Earth-Sci. Rev. 123, 53–86. https://doi.org/10.1016/j.earscirev.2013.02.008

Axe, P., Clausen, U., Leujak, W., Malcolm, S., Ruiter, H., Prins, T., Harvey, E.T., 2017. Eutrophication Status of the OSPAR Maritime Area. Third Integrated Report on the Eutrophication Status of the OSPAR Maritime Area.

Axe, P., Sonesten, L., Skarbövik, E., Leujak, W., Nielsen, L., 2022. Inputs of Nutrients to the OSPAR Maritime Area. In OSPAR, 2023: The 2023 Quality Status Report for the North-East Atlantic. OSPAR Commission, London. Available at: https://oap.ospar.org/en/ospar-assessments/quality-status-reports/qsr-2023/indicator-assessments/inputs-nutrients/.

Baeye, M., Fettweis, M., 2015. In situ observations of suspended particulate matter plumes at an offshore wind farm, southern North Sea. Geo-Mar. Lett. 35, 247–255. https://doi.org/10.1007/s00367-015-0404-8

Berner, R.A., 1982. Burial of organic carbon and pyrite sulfur in the modern ocean; its geochemical and environmental significance. Am. J. Sci. 282, 451–473. https://doi.org/10.2475/ajs.282.4.451

Berner, R.A., 1980. Early diagenesis: a theoret. approach, Princeton series in geochemistry. Princeton University Press, Princeton, N.J.

Binczewska, A., Risebrobakken, B., Polovodova Asteman, I., Moros, M., Tisserand, A., Jansen, E., Witkowski, A., 2018. Coastal primary productivity changes over the last millennium: a case study from the Skagerrak (North Sea). Biogeosciences 15, 5909–5928. https://doi.org/10.5194/bg-15-5909-2018

Bradshaw, C., Jakobsson, M., Brüchert, V., Bonaglia, S., Mörth, C.-M., Muchowski, J., Stranne, C., Sköld, M., 2021. Physical Disturbance by Bottom Trawling Suspends Particulate Matter and Alters Biogeochemical Processes on and Near the Seafloor. Front. Mar. Sci. 8, 683331. https://doi.org/10.3389/fmars.2021.683331

Brückner, S., Mackensen, A., 2008. Organic matter rain rates, oxygen availability, and vital effects from benthic foraminiferal δ13C in the historic Skagerrak, North Sea. Mar. Micropaleontol. 66, 192–207. https://doi.org/10.1016/j.marmicro.2007.09.002

Burdige, D.J., 2007. Preservation of Organic Matter in Marine Sediments: Controls, Mechanisms, and an Imbalance in Sediment Organic Carbon Budgets? Chem. Rev. 107, 467–485. https://doi.org/10.1021/cr050347q

Canfield, D.E., 1994. Factors influencing organic carbon preservation in marine sediments. Chem. Geol. 114, 315–329. https://doi.org/10.1016/0009-2541(94)90061-2

Daewel, U., Akhtar, N., Christiansen, N., Schrum, C., 2022. Offshore wind farms are projected to impact primary production and bottom water deoxygenation in the North Sea. Commun. Earth Environ. 3, 292. https://doi.org/10.1038/s43247-022-00625-0

Daewel, U., Schrum, C., 2013. Simulating long-term dynamics of the coupled North Sea and Baltic Sea ecosystem with ECOSMO II: Model description and validation. J. Mar. Syst. 119–120, 30–49. https://doi.org/10.1016/j.jmarsys.2013.03.008

Dale, A.W., Sommer, S., Lomnitz, U., Montes, I., Treude, T., Liebetrau, V., Gier, J., Hensen, C., Dengler, M., Stolpovsky, K., Bryant, L.D., Wallmann, K., 2015. Organic carbon production, mineralisation and preservation on the Peruvian margin. Biogeosciences 12, 1537–1559. https://doi.org/10.5194/bg-12-1537-2015

Dale, B., Thorsen, T.A., Fjellsa, A., 1999. Dinoflagellate Cysts as Indicators of Cultural Eutrophication in the Oslofjord, Norway. Estuar. Coast. Shelf Sci. 48, 371–382. https://doi.org/10.1006/ecss.1999.0427

De Groot, S.J., 1986. Marine sand and gravel extraction in the North Atlantic and its potential environmental impact, with emphasis on the North Sea. Ocean Manag. 10, 21–36. https://doi.org/10.1016/0302-184X(86)90004-1

De Haas, H., van Weering, T.C.E., 1997. Recent sediment accumulation, organic carbon burial and transport in the northeastern North Sea. Mar. Geol. 136, 173–187. https://doi.org/10.1016/S0025-3227(96)00072-2

De La Rocha, C.L., Passow, U., 2014. The Biological Pump, in: Treatise on Geochemistry. Elsevier, pp. 93–122. https://doi.org/10.1016/B978-0-08-095975-7.00604-5

Deng, L., Bölsterli, D., Kristensen, E., Meile, C., Su, C.-C., Bernasconi, S.M., Seidenkrantz, M.-S., Glombitza, C., Lagostina, L., Han, X., Jørgensen, B.B., Røy, H., Lever, M.A., 2020. Macrofaunal control of microbial community structure in continental margin sediments. Proc. Natl. Acad. Sci. 117, 15911–15922. https://doi.org/10.1073/pnas.1917494117

DeVries, T., 2022. The Ocean Carbon Cycle. Annu. Rev. Environ. Resour. 47, 317–341. https://doi.org/10.1146/annurev-environ-120920-111307

Diesing, M., Thorsnes, T., Bjarnadóttir, L.R., 2021. Organic carbon densities and accumulation rates in surface sediments of the North Sea and Skagerrak. Biogeosciences 18, 2139–2160. https://doi.org/10.5194/bg-18-2139-2021

Duan, Z., Sun, R., 2003. An improved model calculating CO2 solubility in pure water and aqueous NaCl solutions from 273 to 533 K and from 0 to 2000 bar. Chem. Geol. 193, 257–271. https://doi.org/10.1016/S0009-2541(02)00263-2

Eigaard, O.R., Bastardie, F., Hintzen, N.T., Buhl-Mortensen, L., Buhl-Mortensen, P., Catarino, R., Dinesen, G.E., Egekvist, J., Fock, H.O., Geitner, K., Gerritsen, H.D., González, M.M., Jonsson, P., Kavadas, S., Laffargue, P., Lundy, M., Gonzalez-Mirelis, G., Nielsen, J.R., Papadopoulou, N., Posen, P.E., Pulcinella, J., Russo, T., Sala, A., Silva, C., Smith, C.J., Vanelslander, B., Rijnsdorp, A.D., 2017. The footprint of bottom trawling in European waters: distribution, intensity, and seabed integrity. ICES J. Mar. Sci. 74, 847–865. https://doi.org/10.1093/icesjms/fsw194

Emerson, S., Hedges, J., 2008. Chemical Oceanography and the Marine Carbon Cycle, 1st ed. Cambridge University Press. https://doi.org/10.1017/CBO9780511793202

Friedlingstein et al., 2023. Global Carbon Budget 2023. Earth Syst. Sci. Data 15, 5301–5369. https://doi.org/10.5194/essd-15-5301-2023

Frigstad, H., Andersen, T., Hessen, D.O., Jeansson, E., Skogen, M., Naustvoll, L.-J., Miles, M.W., Johannessen, T., Bellerby, R.G.J., 2013. Long-term trends in carbon, nutrients and stoichiometry in Norwegian coastal waters: Evidence of a regime shift. Prog. Oceanogr. 111, 113–124. https://doi.org/10.1016/j.pocean.2013.01.006

Gran-Stadniczeñko, S., Egge, E., Hostyeva, V., Logares, R., Eikrem, W., Edvardsen, B., 2019. Protist Diversity and Seasonal Dynamics in Skagerrak Plankton Communities as Revealed by Metabarcoding and Microscopy. J. Eukaryot. Microbiol. 66, 494–513. https://doi.org/10.1111/jeu.12700

Hartnett, H.E., Keil, R.G., Hedges, J.I., Devol, A.H., 1998. Influence of oxygen exposure time on organic carbon preservation in continental margin sediments. Nature 391, 572–575. https://doi.org/10.1038/35351

Hedges, J.I., Keil, R.G., 1995. Sedimentary organic matter preservation: an assessment and speculative synthesis. Mar. Chem. 49, 81–115. https://doi.org/10.1016/0304-4203(95)00008-F

Heinatz, K., Scheffold, M.I.E., 2023. A first estimate of the effect of offshore wind farms on sedimentary organic carbon stocks in the Southern North Sea. Front. Mar. Sci. 9, 1068967. https://doi.org/10.3389/fmars.2022.1068967

Hiddink, J.G., Van De Velde, S.J., McConnaughey, R.A., De Borger, E., Tiano, J., Kaiser, M.J., Sweetman, A.K., Sciberras, M., 2023. Quantifying the carbon benefits of ending bottom trawling. Nature 617, E1–E2. https://doi.org/10.1038/s41586-023-06014-7

Hoeksema, R.J., 2007. Three stages in the history of land reclamation in the Netherlands. Irrig. Drain. 56, S113–S126. https://doi.org/10.1002/ird.340

Hofstede, J., 2008. Coastal Flood Defence and Coastal Protection along the North Sea Coast of Schleswig-Holstein. Küste 134–142.

Holland, H.D., 1984. The chemical evolution of the atmosphere and oceans, Princeton series in geochemistry. Princeton University Press, Princeton, N.J.

Hübner, G., Schwandt, D., 2018. EXTREME LOW FLOW AND WATER QUALITY – A LONG-TERM VIEW ON THE RIVER ELBE. Erdkunde 72, 235–252.

ICES, 2020. Greater North Sea ecoregion ? Fisheries overview, including mixed-fisheries considerations. https://doi.org/10.17895/ICES.ADVICE.7605

ICES, 2019. Working Group on the Effects of Extraction of Marine Sediments on the Marine Ecosystem (WGEXT). https://doi.org/10.17895/ICES.PUB.5733

ICES, 2018. Greater North Sea Ecoregion ? Ecosystem overview. https://doi.org/10.17895/ICES.PUB.4670

IKSE, 2012. Abschlussbericht über die Erfüllung des „Aktionsplans Hochwasserschutz Elbe“ im Zeitraum 2003–2011.

IKSE, 2005. Die Elbe und ihr Einzugsgebiet – Ein geographisch-hydrologischer und wasserwirtschaftlicher Überblick.

IPCC, 2023. Sections. In: Climate Change 2023: Synthesis Report. Contribution of Working Groups I, II and III to the Sixth Assessment Report of the Intergovernmental Panel on Climate

Change [Core Writing Team, H. Lee and J. Romero (eds.)]. IPCC, Geneva, Switzerland, pp. 35-115, doi: 10.59327/IPCC/AR6-9789291691647.

Kelletat, D., 1992. Coastal Erosion and Protection Measures at the German North Sea Coast. J. Coast. Res. 8, 699–711.

Lange, D., Müller, H., Piechotta, F., Schubert, R., 2008. The Weser Estuary. Küste 275–287.

LaRowe, D.E., Arndt, S., Bradley, J.A., Burwicz, E., Dale, A.W., Amend, J.P., 2020. Organic carbon and microbial activity in marine sediments on a global scale throughout the Quaternary. Geochim. Cosmochim. Acta 286, 227–247. https://doi.org/10.1016/j.gca.2020.07.017

Leipe, T., Moros, M., Kotilainen, A., Vallius, H., Kabel, K., Endler, M., Kowalski, N., 2013. Mercury in Baltic Sea sediments—Natural background and anthropogenic impact. Geochemistry 73, 249–259. https://doi.org/10.1016/j.chemer.2013.06.005

Li, B., Shi, X., Lian, L., Chen, Y., Chen, Z., Sun, X., 2020. Quantifying the effects of climate variability, direct and indirect land use change, and human activities on runoff. J. Hydrol. 584, 124684. https://doi.org/10.1016/j.jhydrol.2020.124684

Liebezeit, G., 1988. Early diagenesis of carbohydrates in the marine environment—II. Composition and origin of carbohydrates in Skagerrak sediments, in: Organic Geochemistry In Petroleum Exploration. Elsevier, pp. 387–391. https://doi.org/10.1016/B978-0-08-037236-5.50046-4

Liu, H., Xu, X., Lin, Z., Zhang, M., Mi, Y., Huang, C., Yang, H., 2016. Climatic and human impacts on quasi-periodic and abrupt changes of sedimentation rate at multiple time scales in Lake Taihu, China. J. Hydrol. 543, 739–748. https://doi.org/10.1016/j.jhydrol.2016.10.046

Longhurst, A.R., 1991. Role of the marine biosphere in the global carbon cycle. Limnol. Oceanogr. 36, 1507–1526. https://doi.org/10.4319/lo.1991.36.8.1507

Longhurst, A.R., Glen Harrison, W., 1989. The biological pump: Profiles of plankton production and consumption in the upper ocean. Prog. Oceanogr. 22, 47–123. https://doi.org/10.1016/0079-6611(89)90010-4

McQuatters-Gollop, A., Raitsos, D.E., Edwards, M., Pradhan, Y., Mee, L.D., Lavender, S.J., Attrill, M.J., 2007. A long-term chlorophyll dataset reveals regime shift in North Sea phytoplankton biomass unconnected to nutrient levels. Limnol. Oceanogr. 52, 635–648. https://doi.org/10.4319/lo.2007.52.2.0635

Meyenburg, G., Liebezeit, G., 1993. Mineralogy and geochemistry of a core from the Skagerrak/Kattegat boundary. Mar. Geol. 111, 337–344. https://doi.org/10.1016/0025-3227(93)90139-M

Middelburg, J.J., 2019. Marine Carbon Biogeochemistry: A Primer for Earth System Scientists, SpringerBriefs in Earth System Sciences. Springer International Publishing, Cham. https://doi.org/10.1007/978-3-030-10822-9

Mielck, F., Hass, H.C., Michaelis, R., Sander, L., Papenmeier, S., Wiltshire, K.H., 2019. Morphological changes due to marine aggregate extraction for beach nourishment in the German Bight (SE North Sea). Geo-Mar. Lett. 39, 47–58. https://doi.org/10.1007/s00367-018-0556-4

Millero, F.J., 2007. The Marine Inorganic Carbon Cycle. Chem. Rev. 107, 308–341. https://doi.org/10.1021/cr0503557

Moros, M., Andersen, T.J., Schulz-Bull, D., Häusler, K., Bunke, D., Snowball, I., Kotilainen, A., Zillén, L., Jensen, J.B., Kabel, K., Hand, I., Leipe, T., Lougheed, B.C., Wagner, B., Arz, H.W., 2017. Towards an event stratigraphy for Baltic Sea sediments deposited since AD 1900: approaches and challenges. Boreas 46, 129–142. https://doi.org/10.1111/bor.12193

Oost, A., Colina Alonso, A., Esselink, P., Wang, Z.B., Kessel, T. van, Maren, B. van, 2021. Where mud matters: towards a mud balance for the trilateral Wadden Sea Area: mud supply, transport and deposition. Wadden Academy, Leeuwarden.

OSPAR, 2023. OSPAR Quality Status Synthesis Report 2023. oap.ospar.org.

Pätsch, J., Lorkowski, I., Kühn, W., Moll, A., Serna, A., 2010. 150 years of ecosystem evolution in the North Sea-from pristine conditions to acidification. Eur. Geophys. Union Gen. Assem. 2010 Vienna Austria 2010 12291.

Pedersen, T.F., Calvert, S.E., 1990. Anoxia vs. Productivity: What Controls the Formation of Organic-Carbon-Rich Sediments and Sedimentary Rocks? AAPG Bull. 74. https://doi.org/10.1306/0C9B232B-1710-11D7-8645000102C1865D

Polovodova Asteman, I., Risebrobakken, B., Moros, M., Binczewska, A., Dobosz, S., Jansen, E., Sławińska, J., Bąk, M., 2018. Late Holocene palaeoproductivity changes: a multi-proxy study in the Norwegian Trench and the Skagerrak, North Sea. Boreas 47, 238–255. https://doi.org/10.1111/bor.12264

Reid, P.C., Edwards, M., Hunt, H.G., Warner, A.J., 1998. Phytoplankton change in the North Atlantic. Nature 391, 546–546. https://doi.org/10.1038/35290

Rijnsdorp, A.D., Boute, P., Tiano, J., Lankheet, M., Soetaert, K., Beier, U., de Borger, E., Hintzen, N.T., Molenaar, P., Polet, H., Poos, J.J., Schram, E., Soetaert, M., van Overzee, H., van De Wolfshaar, K., van Kooten, T., 2020. The implications of a transition from tickler chain beam trawl to electric pulse trawl on the sustainability and ecosystem effects of the fishery for North Sea sole: an impact assessment. Wageningen Marine Research, IJmuiden,. https://doi.org/10.18174/519729

Sala, E., Mayorga, J., Bradley, D., Cabral, R.B., Atwood, T.B., Auber, A., Cheung, W., Costello, C., Ferretti, F., Friedlander, A.M., Gaines, S.D., Garilao, C., Goodell, W., Halpern, B.S., Hinson, A., Kaschner, K., Kesner-Reyes, K., Leprieur, F., McGowan, J., Morgan, L.E., Mouillot, D., Palacios-Abrantes, J., Possingham, H.P., Rechberger, K.D., Worm, B., Lubchenco, J., 2021. Protecting the global ocean for biodiversity, food and climate. Nature 592, 397–402. https://doi.org/10.1038/s41586-021-03371-z

Schmidt, M., 2021. Dynamics and variability of POC burial in depocenters of the North Sea (Skagerrak), Cruise No. AL561, 2.08.2021 – 13.08.2021, Kiel – Kiel, APOC. GEOMAR Helmholtz Centre for Ocean Research Kiel. https://doi.org/10.3289/CR_AL561

Skogen, M.D., Eilola, K., Hansen, J.L.S., Meier, H.E.M., Molchanov, M.S., Ryabchenko, V.A., 2014. Eutrophication status of the North Sea, Skagerrak, Kattegat and the Baltic Sea in present and future climates: A model study. J. Mar. Syst. 132, 174–184. https://doi.org/10.1016/j.jmarsys.2014.02.004

Sköld, M., Göransson, P., Jonsson, P., Bastardie, F., Blomqvist, M., Agrenius, S., Hiddink, J., Nilsson, H., Bartolino, V., 2018. Effects of chronic bottom trawling on soft-seafloor macrofauna in the Kattegat. Mar. Ecol. Prog. Ser. 586, 41–55. https://doi.org/10.3354/meps12434

Slavik, K., Lemmen, C., Zhang, W., Kerimoglu, O., Klingbeil, K., Wirtz, K.W., 2019. The large-scale impact of offshore wind farm structures on pelagic primary productivity in the southern North Sea. Hydrobiologia 845, 35–53. https://doi.org/10.1007/s10750-018-3653-5

Spiegel, T., Diesing, M., Dale, A.W., Lenz, N., Schmidt, M., Sommer, S., Böttner, C., Fuhr, M., Kalapurakkal, H.T., Wallmann, K., 2024. Modelling mass accumulation rates and 210 Pb rain rates in the Skagerrak: lateral sediment transport dominates the sediment input. Front. Mar. Sci. 11. https://doi.org/10.3389/fmars.2023.1141448

Ståhl, H., Tengberg, A., Brunnegård, J., Bjørnbom, E., Forbes, T.L., Josefson, A.B., Kaberi, H.G., Hassellöv, I.M.K., Olsgard, F., Roos, P., Hall, P.O.J., 2004. Factors influencing organic carbon recycling and burial in Skagerrak sediments. J. Mar. Res. 62, 867–907. https://doi.org/10.1357/0022240042880873

Thomas, H., Bozec, Y., De Baar, H.J.W., Elkalay, K., Frankignoulle, M., Schiettecatte, L.-S., Kattner, G., Borges, A.V., 2005. The carbon budget of the North Sea. Biogeosciences 2, 87–96. https://doi.org/10.5194/bg-2-87-2005

Thomas, H., Freund, W., Mears, C., Meckel, E., Minutolo, F., Nantke, C., Neumann, A., Seidel, M., Van Dam, B., 2022. ALKOR Scientific Cruise Report. The Ocean's Alkalinity - Connecting geological and metabolic processes and time-scales: mechanisms and magnitude of metabolic alkalinity generation in the North Sea Cruise No. AL557. Open Access. Alkor-Berichte, AL557. GEOMAR Helmholtz-Zentrum für Ozeanforschung Kiel, Kiel, Germany, 22 pp.

Turner, J.T., 2015. Zooplankton fecal pellets, marine snow, phytodetritus and the ocean's biological pump. Prog. Oceanogr. 130, 205–248. https://doi.org/10.1016/j.pocean.2014.08.005

van Weering, T.C.E., Berger, G.W., Okkels, E., 1993. Sediment transport, resuspension and accumulation rates in the northeastern Skagerrak. Mar. Geol. 111, 269–285. https://doi.org/10.1016/0025-3227(93)90135-I

Volk, T., Hoffert, M.I., 2013. Ocean Carbon Pumps: Analysis of Relative Strengths and Efficiencies in Ocean-Driven Atmospheric CO_2 Changes, in: Sundquist, E.T., Broecker, W.S. (Eds.), Geophysical Monograph Series. American Geophysical Union, Washington, D. C., pp. 99–110. https://doi.org/10.1029/GM032p0099

Zarate-Barrera, T.G., Maldonado, J.H., 2015. Valuing Blue Carbon: Carbon Sequestration Benefits Provided by the Marine Protected Areas in Colombia. PLOS ONE 10, e0126627. https://doi.org/10.1371/journal.pone.0126627

Acknowledgments

This thesis was conducted under the supervision of Prof. Dr. Klaus Wallmann and Dr. Andrew W. Dale. Firstly, I am grateful for the support of Klaus Wallmann, who introduced me to the world of biogeochemistry and helped me as a mentor during my first steps in sciences. His patient and humble approach to supervision and the frequent discussions about scientific and common topics made the three years an enjoyable journey. Next, I wish to thank Andrew W. Dale for providing support with long and detailed discussions that granted me insights into various scientific topics, especially into modeling, and for creating a positive and welcoming environment. Furthermore, I would like to give sincere thanks to Prof. Dr. Mark Schmidt for acting as a referee, for planning the research cruise AL561 and for providing guidance at GEOMAR, during AL561 and past research cruises. I further wish to thank my office mates Habeeb Thanveer Kalapurakkal, Michael Fuhr and Jannes Kowalski for the pleasant time in the office and for the many memorable moments complementary to the scientific work. Furthermore, this study greatly benefited from the close collaboration in the project with Nina Lenz and I wish to thank her for her various supports. I further sincerely thank Stefan Sommer for coordinating the benthic lander deployments during AL561 and the subsequent interpretation of the lander data. A special thanks is addressed to the GEOMAR technicians for their enduring support during the cruise and the laboratory work. In particular, I would like to thank Bettina Domeyer, Anke Bleyer, Regina Surberg, Antje Beck, Assmuss Petersson, Matthias Türk, Sebastian Fessler and their team of HIWI's, without whom much of the work would not have been possible. Furthermore, this work greatly benefited from the review and editing of the Co-Authors and I would like to thank each of them for the helpful discussions and suggestions during the preparation of the manuscripts. Finally, I want to thank all my colleagues and friends at GEOMAR and the collaborating institutes of the APOC project for the pleasant time throughout the past three years.

Appendix

Tables

Table IIS1. Initial $^{210}Pb_{ex}$ activities (Pb_0) determined by extrapolations to the surface (Sanchez-Cabeza and Ruiz-Fernández, 2012). Values were obtained by applying an exponential regression function to the $^{210}Pb_{ex}$ data below the bioturbated zone (Bioturbation rate < 0.2 cm^2 yr^{-1}) using "R".

Station	Initial $^{210}Pb_{ex}$ activity, Pb_0 (dpm g^{-1})
MUC2	30
MUC5	18
MUC7	38
MUC8	24
MUC9	34
St.65	30

Table IIIS1. List of data used to predict the spatial distribution of ^{210}Pb rain rates.

Station	**Latitude N**	**Longitude E**	**Water depth (m)**	**^{210}Pb rain rate[a] (dpm cm^{-2} yr^{-1})**	**Source**
RO 3.2	57.863	8.180	522	2.1	Erlenkeuser and Pederstad, 1984
1	57.915	9.247	239	0.6	Erlenkeuser and Pederstad, 1984
2	57.997	9.333	454	1.2	Erlenkeuser and Pederstad, 1984
SII-2	58.772	10.143	230	5.4	Erlenkeuser and Pederstad, 1984
AU1	58.049	9.125	586	2.2	Deng et al., 2020
AU2	58.104	9.822	318	5.4	Deng et al., 2020
AU3	57.807	11.053	46	1.1	Deng et al., 2020
A	58.367	9.617	645	1.3	Paetzel and Schrader, 1993
84-4	57.852	8.250	530	0.9	Van Weering et al., 1987
84-5	57.735	8.333	387	0.9	Van Weering et al., 1987
84-6	57.635	8.400	184	0.9	Van Weering et al., 1987
84-7	57.500	8.500	73	1.2	Van Weering et al., 1987
84-22	57.783	9.100	117	0.2	Van Weering et al., 1987
84-24	58.068	8.883	631	0.7	Van Weering et al., 1987
84-25	58.135	8.833	421	1.3	Van Weering et al., 1987
84-9	57.951	9.818	100	0.3	Van Weering et al., 1987
84-10	58.035	9.668	318	1.0	Van Weering et al., 1987
84-11	58.218	9.333	677	0.9	Van Weering et al., 1987
84-12	58.301	9.200	428	2.1	Van Weering et al., 1987
84-13	58.333	9.800	621	1.0	Van Weering et al., 1987
84-14	58.333	10.300	409	3.8	Van Weering et al., 1987
84-16	58.333	10.817	146	0.3	Van Weering et al., 1987
84-19	57.900	11.292	74	1.0	Van Weering et al., 1987
84-20	57.800	11.019	47	0.3	Van Weering et al., 1987

9001	57.820	9.485	100	0.2	Van Weering et al., 1993
9002	57.919	9.318	234	0.5	Van Weering et al., 1993
9003	58.078	9.147	630	1.2	Van Weering et al., 1993
9004	58.187	8.976	425	3.3	Van Weering et al., 1993
9005	58.587	9.597	500	3.8	Van Weering et al., 1993
9006	58.591	9.933	560	4.3	Van Weering et al., 1993
9007	58.596	10.418	310	1.4	Van Weering et al., 1993
9008	58.605	10.589	200	1.0	Van Weering et al., 1993
9009	58.300	10.704	180	1.3	Van Weering et al., 1993
9010	58.260	10.446	260	6.5	Van Weering et al., 1993
9011	58.235	10.090	375	4.2	Van Weering et al., 1993
9012	57.948	10.211	280	1.2	Van Weering et al., 1993
9013	57.972	10.434	295	2.9	Van Weering et al., 1993
9014	58.033	10.721	290	4.2	Van Weering et al., 1993
9015	58.086	10.994	250	2.4	Van Weering et al., 1993
9016	57.840	10.936	93	0.3	Van Weering et al., 1993
9017	57.937	11.197	112	2.2	Van Weering et al., 1993
GT03-68RL	57.802	11.053	46	0.7	Ferdelmann, 2005 (Pangaea)
GT03-71RL	57.850	11.278	90	1.3	Ferdelmann, 2005 (Pangaea)
GT03-72RL	57.855	11.298	98	1.0	Ferdelmann, 2005 (Pangaea)
VA 57/10-2	58.030	10.012	150	2.2	Wilken et al., 1990
10	58.498	9.171	362	3.3	Beks, 1999
11	58.249	8.998	406	4.8	Beks, 1999
12	58.035	9.050	590	5.5	Beks, 1999
13	57.834	7.985	522	3.5	Beks, 1999
33	58.167	10.250	270	7.1	Beks, 1999
34	58.585	10.497	180	4.3	Beks, 1999
35	58.038	9.635	297	4.4	Beks, 1999
K1	58.750	10.622	112	0.8	Stahl et al., 2004
H2	58.025	9.597	302	3.1	Stahl et al., 2004
K3	58.657	10.260	259	5.1	Stahl et al., 2004
H1	58.008	9.615	266	2.6	Stahl et al., 2004
GIK 15530-4	57.667	7.092	325	0.7	Erlenkeuser, 1985
MUC2	58.181	9.794	500	4.7	Own data
MUC3	58.748	10.224	215	4.7	Own data
MUC5	57.753	8.286	434	3.2	Own data
MUC6	57.635	8.400	185	1.1	Own data
MUC7	58.313	9.572	677	3.8	Own data
MUC8	57.988	9.238	490	5.4	Own data
MUC9	58.073	9.096	604	2.4	Own data
St.65	58.501	9.498	530	2.7	Own data

[a] Calculation of ^{210}Pb rain rates is explained in the method section (Eq 1).

Table IIIS2. List of data used to predict the spatial distribution of porosity. The porosity data were sourced from the PANGAEA database (pangaea.de).

Latitude N	Longitude E	Porosity (%)
58.996	10.676	85.8
58.965	10.376	75.3
58.917	10.479	83.9
58.853	10.586	84.5
58.888	10.062	81.8
58.876	9.847	84.0
58.812	10.250	82.4
58.808	9.961	68.3
58.750	10.348	80.0
58.803	9.722	83.9
58.749	10.221	86.0
58.747	10.094	82.2
58.698	10.483	80.0
58.739	9.846	82.7
58.687	10.226	83.2
58.683	9.981	83.6
58.627	10.350	84.2
58.675	9.725	82.4
58.619	10.104	82.3
58.665	9.479	85.8
58.614	9.858	83.9
58.556	10.252	83.0
58.610	9.613	86.2
58.554	9.991	82.8
58.551	9.730	82.7
58.494	10.115	82.7
58.541	9.492	85.7
58.491	9.862	81.5
58.534	9.264	82.9
58.503	9.497	49.0
58.481	9.625	82.0
58.426	9.993	83.1
58.474	9.397	86.9
58.480	9.131	79.1
58.422	9.749	84.1
58.417	9.505	80.6
58.357	9.880	82.5

58.410	9.278	83.8
58.409	9.028	81.6
58.358	9.380	82.0
58.284	10.040	81.2
58.298	9.753	82.6
58.311	9.574	86.0
58.340	9.158	82.0
58.293	9.511	85.1
58.329	8.914	84.8
58.282	9.275	80.0
58.219	9.929	78.1
58.234	9.634	82.0
58.275	9.048	82.6
58.223	9.399	84.3
58.272	8.815	83.2
58.181	9.793	87.0
58.158	9.786	83.2
58.211	9.180	80.3
58.165	9.515	82.6
58.208	8.947	82.3
58.153	9.288	85.3
58.201	8.713	83.7
58.108	9.663	81.1
58.150	9.063	84.6
58.099	9.413	83.4
58.143	8.830	81.7
58.092	9.179	86.4
58.142	8.574	83.1
58.046	9.521	79.9
58.085	8.946	83.3
58.071	9.099	85.0
57.837	11.360	62.9
57.837	11.277	58.1
58.034	9.303	82.5
58.077	8.721	80.0
58.031	9.072	82.0
58.080	8.475	81.8
57.991	9.406	68.9
57.987	9.240	86.0
58.020	8.838	84.9
58.022	8.592	81.5
57.969	9.186	80.2

58.014	8.359	80.2
57.962	8.954	81.8
57.933	9.266	70.0
57.959	8.723	78.6
58.005	8.127	81.7
58.005	7.897	65.6
57.956	8.484	81.2
57.949	8.236	82.5
57.898	8.608	81.1
57.943	8.021	83.2
57.843	8.962	70.3
57.890	8.369	80.0
57.934	7.782	80.6
57.835	8.731	81.1
57.928	7.551	81.2
57.882	8.129	79.5
57.796	9.056	47.3
57.921	7.329	81.8
57.876	7.907	81.9
57.829	8.484	83.4
57.778	8.838	77.6
57.824	8.262	80.9
57.866	7.676	81.9
57.864	7.455	82.5
57.820	8.024	80.0
57.726	8.947	46.2
57.854	7.216	77.7
57.809	7.801	81.6
57.750	8.406	80.6
57.762	8.149	82.1
57.751	8.284	83.0
57.804	7.572	81.6
57.707	8.738	46.5
57.798	7.342	81.0
57.753	7.918	80.5
57.704	8.501	74.2
57.747	7.697	83.8
57.786	7.112	82.3
57.678	8.315	79.9
57.742	7.460	80.0
57.646	8.624	47.5
57.691	8.042	73.0

57.691	7.814	81.5
57.642	8.395	59.4
57.732	7.206	80.2
57.637	8.402	87.0
57.680	7.584	80.3
57.391	10.622	42.3
57.616	8.202	72.4
57.674	7.355	80.8
57.629	7.937	73.8
57.624	7.701	72.9
57.577	8.281	50.3
57.618	7.472	82.1
57.640	7.048	80.5
57.560	8.083	65.2
57.562	7.824	81.4
57.532	8.133	56.2
57.557	7.596	81.5
57.568	7.194	80.6
57.500	7.955	45.3
57.496	7.711	56.3
57.512	7.311	74.5
57.456	7.436	40.1
57.394	7.559	42.0
57.407	7.143	41.9
57.347	7.259	41.5

Table VS1. In-situ benthic chamber DIC concentrations.

Station	Benthic chamber	DIC	Time	Water height in the benthic chamber
		mmol/l	h	m
BIGO2-1	K1-1	2.17	0.0	0.20
	K1-2	2.18	4.9	
	K1-3	2.19	9.9	
	K1-4	2.19	14.8	
	K1-5	2.20	19.7	
	K1-6	2.19	24.7	
	K1-7	2.21	29.6	
	K1-8	2.21	34.5	
	K2-1	2.17	0.0	0.20
	K2-2	2.17	4.9	
	K2-3	2.17	9.9	
	K2-4	2.19	14.8	
	K2-5	2.19	19.7	

	K2-6	2.19	24.7	
	K2-7	2.16	29.6	
	K2-8	2.20	34.5	
BIGO2-2	K1-1	2.19	0.0	0.23
	K1-2	2.19	3.9	
	K1-3	2.19	7.9	
	K1-4	2.20	11.8	
	K1-5	2.20	15.7	
	K1-6	2.16	19.7	
	K1-7	2.20	23.6	
	K1-8	2.20	27.5	
	K2-1	2.22	0.0	0.20
	K2-2	2.23	3.9	
	K2-3	2.24	7.9	
	K2-4	2.26	11.8	
	K2-5	2.27	15.7	
	K2-6	2.28	19.7	
	K2-7	2.29	23.6	
	K2-8	2.25	27.5	
BIGO2-3	K1-1	2.18	0.0	0.20
	K1-2	2.19	3.9	
	K1-3	2.19	7.9	
	K1-4	2.20	11.8	
	K1-5	2.21	15.8	
	K1-6	2.10	19.7	
	K1-7	2.21	23.6	
	K1-8	2.21	27.5	
	K2-1	2.17	0.0	0.22
	K2-2	2.17	3.9	
	K2-3	2.18	7.9	
	K2-4	2.20	11.8	
	K2-5	2.20	15.8	
	K2-6	2.20	19.7	
	K2-7	2.21	23.6	
	K2-8	2.10	27.5	

Figures

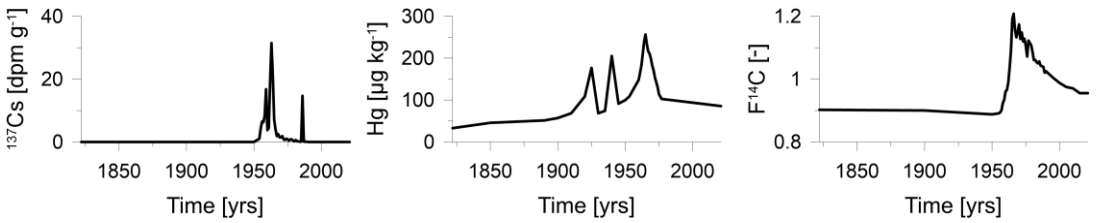

Figure IIS1. Temporal variability of $C_0(t)$ values of ^{137}Cs (Garcia Agudo, 1998), Hg (Hylander and Meili, 2003; Streets et al., 2011) and $F^{14}C$ (see method section) for the calculation of upper boundary fluxes in the model.

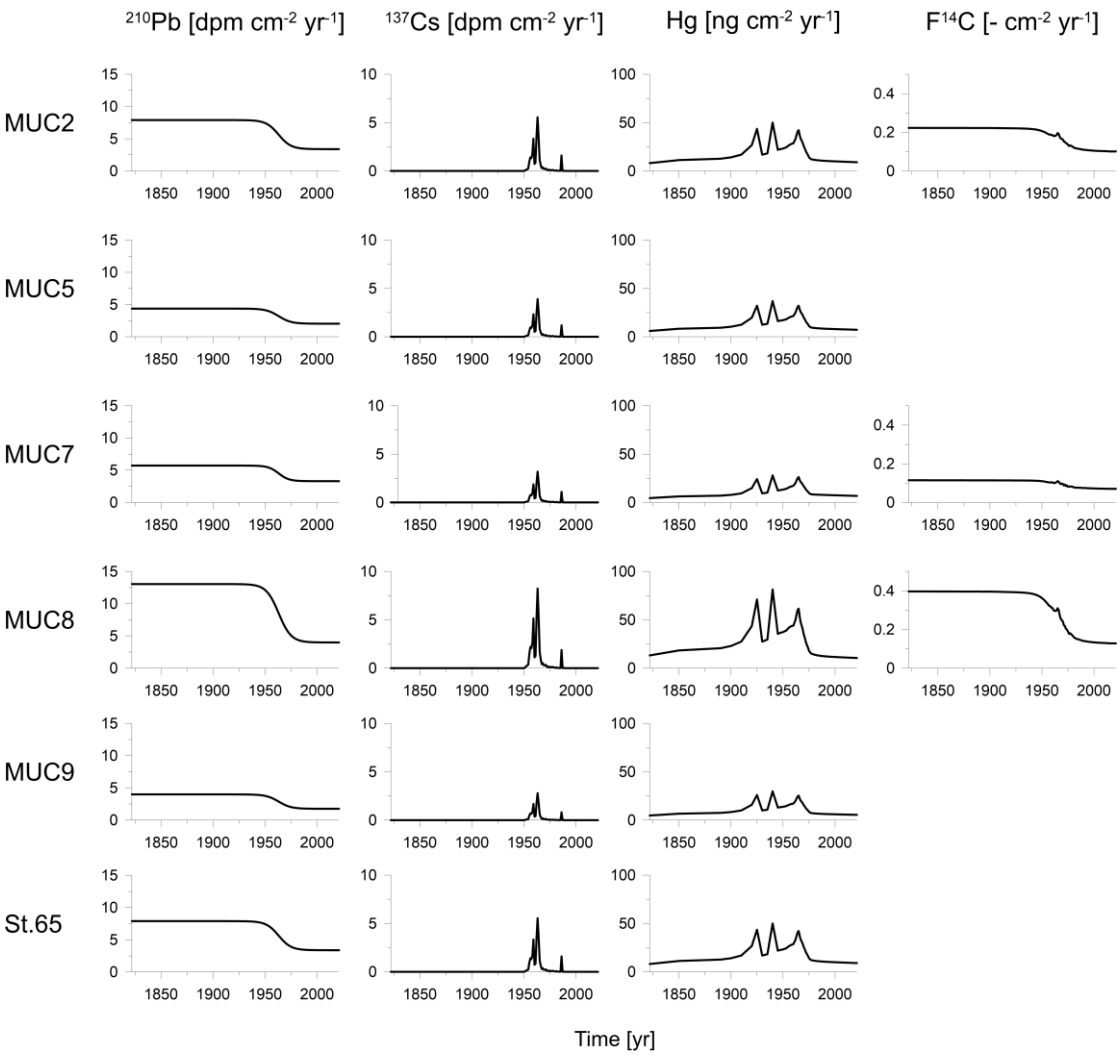

Figure IIS2. Temporal variability of upper boundary fluxes of ^{210}Pb, ^{137}Cs, Hg and $F^{14}C$.

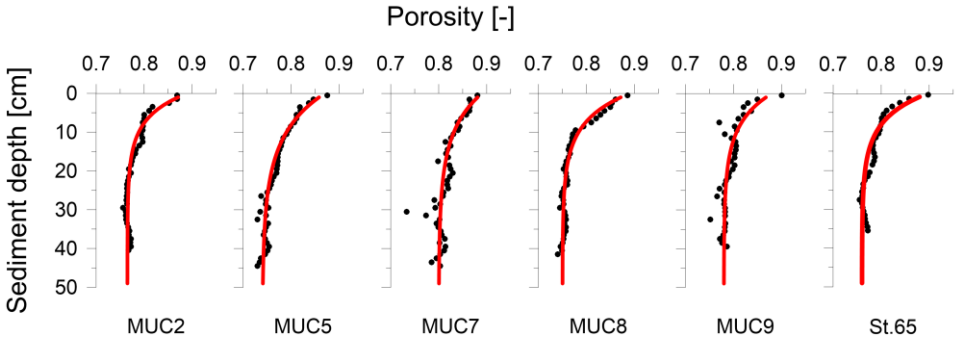

Figure IIS3. Measured data (symbols) and model simulations (curves) of porosity.

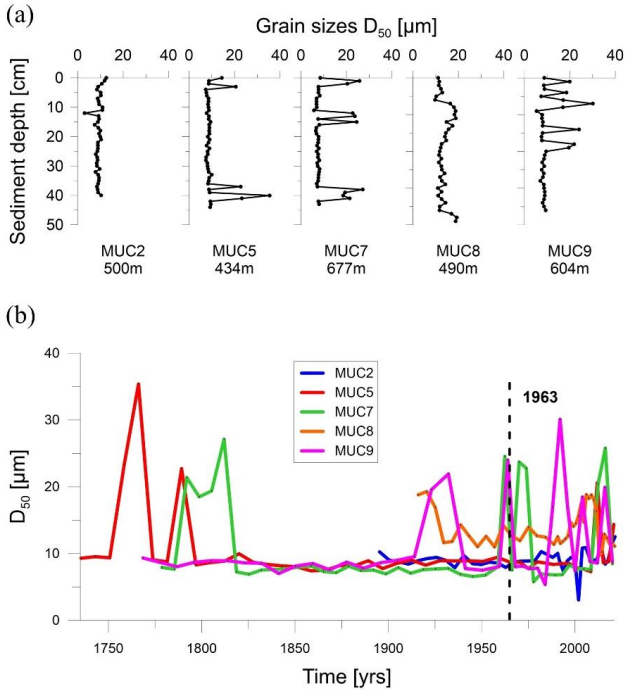

Figure IIS4. Median grain sizes (D_{50}) as a function of sediment depth (a) and time (b). The temporal grain size distribution is based on the sedimentation rates calculated in this study and the dashed line indicates the year 1963.

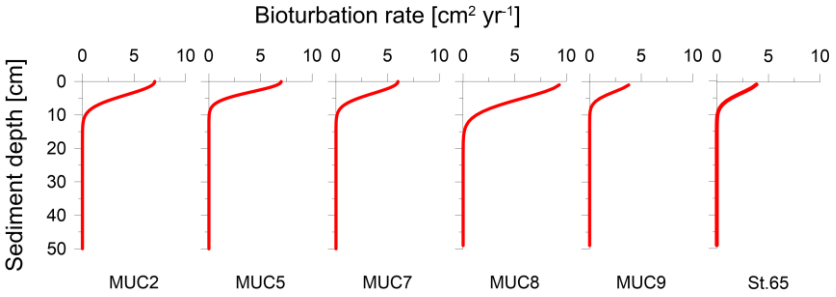

Figure IIS5. Model simulations of bioturbation rates.

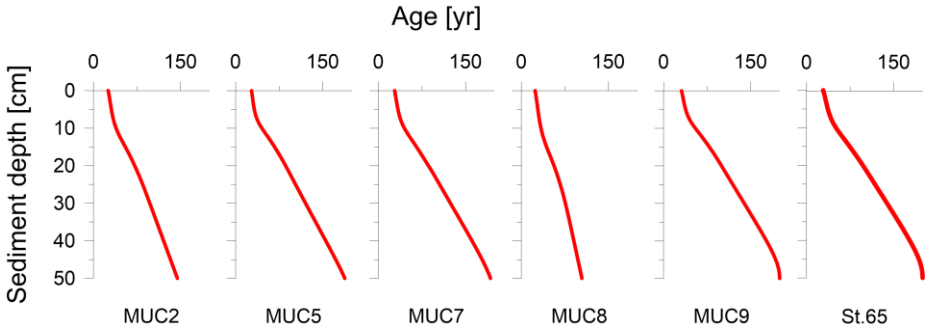

Figure IIS6. Model simulations of age with sediment depth. Down-core distributions of age were calculated following Eq. 1, where C is the age and λ_C is the rate term set to 1 yr yr^{-1}. Upper boundary conditions were set to "0" and a zero gradient condition was set at the lower model boundary at 50 cm.

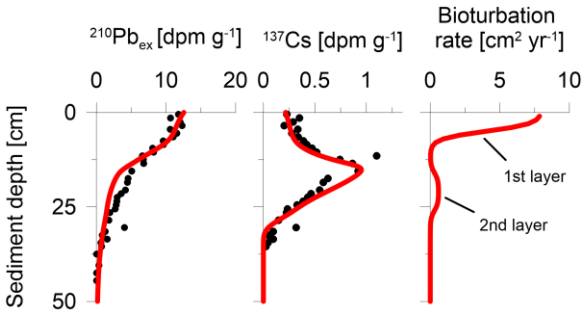

Figure IIS7. Measured data (symbols) and model simulations (curves) of $^{210}Pb_{ex}$, ^{137}Cs and bioturbation rates. Two separate bioturbation layers are indicated.

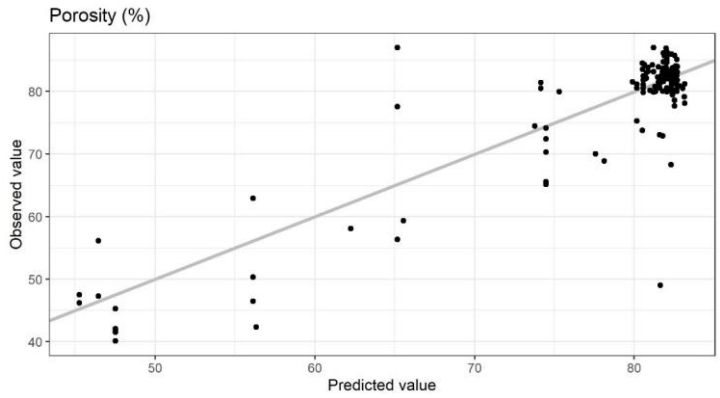

Figure IIIS1. Predicted versus observed values of porosity. The diagonal line indicates the 1:1 slope. The RMSE of the model is 5.1 % and the R^2 is 0.8.

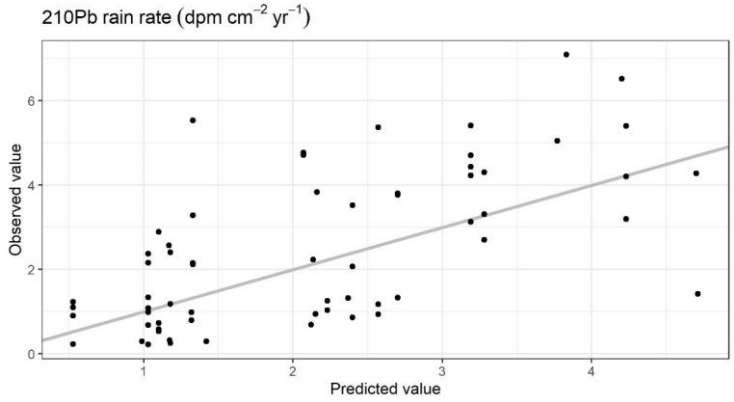

Figure IIIS2. Predicted versus observed values of ^{210}Pb rain rates. The diagonal line indicates the 1:1 slope. The RMSE of the model is 1.4 dpm cm^{-2} yr^{-1} and the R^2 is 0.41.

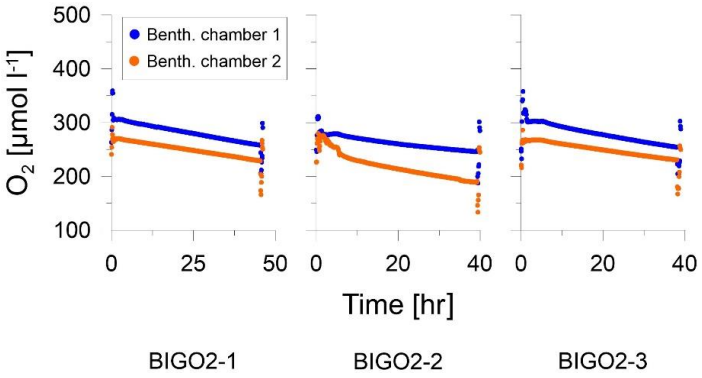

Figure VS1. Benthic O_2 concentrations over time in the benthic chambers. The BIGO landers were equipped with optodes to measure dissolved O_2 concentrations as explained in detail in Sommer et al. (2008, 2009).